Connections by Adhesion, Interlocking and Friction for Steel-Concrete Composite Bridges under Static and Cyclic Loading

THÈSE N^{O} 5301 (2012)

PRÉSENTÉE LE 24 FÉVRIER 2012

À LA FACULTÉ DE L'ENVIRONNEMENT NATUREL, ARCHITECTURAL ET CONSTRUIT

LABORATOIRE DE LA CONSTRUCTION MÉTALLIQUE

PROGRAMME DOCTORAL EN STRUCTURES

ÉCOLE POLYTECHNIQUE FÉDÉRALE DE LAUSANNE

POUR L'OBTENTION DU GRADE DE DOCTEUR ÈS SCIENCES

PAR

Dimitrios PAPASTERGIOU

acceptée sur proposition du jury:

Prof. A. Muttoni, président du jury
Prof. J.-P. Lebet, directeur de thèse
Prof. E. Brühwiler, rapporteur
Prof. J. Raoul, rapporteur
Dr M. Thomann, rapporteur

ÉCOLE POLYTECHNIQUE
FÉDÉRALE DE LAUSANNE

Suisse
2012

Πᾶσα δόσις ἀγαθὴ καὶ πᾶν δώρημα τέλειον ἄνωθέν ἐστιν, καταβαῖνον ἀπὸ τοῦ πατρὸς τῶν φώτων, παρ’ ᾧ οὐκ ἔνι παραλλαγὴ ἢ τροπῆς ἀποσκίασμα.

ΙΑΚΩΒΟΥ 1:17

Tout bienfait et tout don parfait viennent d'en haut; ils descendent du Père des lumières, en qui il n'y a ni changement ni l’ombre d’une variation.

Jacques 1:17

Every good gift and every perfect gift is from above, coming down from the Father of lights with whom there is no variation or shadow due to change.

James 1:17

Alle gute Gabe und alle vollkommene Gabe kommt von obenherab, von dem Vater des Lichts, bei welchem ist keine Veränderung noch Wechsel des Lichtes und der Finsternis.

Jakobus 1:17

Acknowledgements

I would first like to express thanks to my supervisor Prof. Dr. Jean-Paul Lebet for the opportunity to conduct research at the Steel Structures Laboratory, for his valuable suggestions and our excellent cooperation. I express my acknowledgements also to members of the jury, Prof. Joël Raoul, Prof. Eugen Brühwiler and Dr. Michel Thomann for reviewing my work and for their remarks, and to the chairman of the jury Prof. Aurelio Muttoni for the coordination of the private defense.

I strongly appreciate the feedback from the members of the committee that followed my work, Mrs. Farida Salamé, Dr. Emmanuel Denarié and Dr. Michel Thomann. I am also thankful to Prof. Alain Nussbaumer for his scientific advice and to Prof. Manfred Hirt and Mr. Michel Crisinel for their comments to my initial work.

This research was financially supported by the Swiss National Science Foundation (SNF). Donation of materials for the specimen fabrication from the Swiss Federal Roads Office (OFROU) and the VSL Company is highly acknowledged.

Special thanks to Gary Prinz for reviewing long parts of this thesis for the use of English. I express my thanks also to Pia Hannewald, Claire Acevedo and Manuel Santarsiero for the German, French and Italian, correspondingly translation of the abstract. Special thanks to Prof. Katrin Beyer for the always interesting discussions and for her encouragement.

The quite extensive experimental investigation performed during this project could not have been realized without the excellent cooperation of the technical staff. I express my thanks to Sylvain Demierre and Gilles Guignet for their help on the test set up and execution. I also thank all the rest of the technical team, Gerald Rouge, Patrice Gallay, Frédérique Dubugnon and François Perrin for their important contribution. I appreciate also the help from Qian Wang concerning the specimen preparation.

I also appreciate all help from our secretary, Esther Von Arx, for all the administrative issues and the help from Nicolas Dubois and Stefano Nepa for their support concerning informatics. I am also thankful to Gustavo Cortes and Farshid Zamiri for the suggestions concerning the use of FEA software.

Lots of thanks to all my friends and colleagues at ICOM and all over the EPFL, for their friendship all these years; from the warm welcoming of the first days to the support at the final stages.

One thousand thanks to my father for contaminating me with the science of civil engineering, to my mother for having taught me to aim the progress in my life, and to my twin sister Maria for her encouragement in all my decisions.

Finally, I express my gratitude to my wife Eleni for recognizing my love of research and encouraging me to apply for a PhD. I truly thank her also for her love, devotion, support, understanding, and for encouraging me always to chase higher goals.

ABSTRACT

Steel-concrete composite bridges with twin-I steel girders and prefabricated slabs constitute an economical and competitive solution for small and medium bridge spans. In recent years they have started to gain their share in the construction market. However, the current slab-to-girder connection with groups of headed shear stud connectors is not well adapted for prefabrication and fast erection, and does not respond successfully to the durability of the construction. New types of connections by adhesion, interlocking and friction constitute a conception that aims to answer these demands. The resistance of these connections is based on the development of longitudinal shear stresses in the interfaces which form the connection.

The goals of this study are to complete the existing research in this field by proposing scientific tools in order to predict the connection's structural performance, i.e. prediction of the connection's ultimate resistance and deformation capacity, including the post-failure behaviour. In addition, the behaviour of the connection under cyclic loading is also investigated to assess the connection's resistance to fatigue and to propose a design method for composite bridges under fatigue loading.

To fulfill theses goals a combinational methodology was applied which included:

- study of the state of the art: a) in composite bridges so as to define the requirements and b) in interface behaviour in order to emphasize the parameters which are responsible for the resistance and obtain information for the nature of cyclic loading damage mechanisms,
- experimental investigations: a) to reveal the laws describing the interfaces and the connection's behaviour for static and cyclic loading, and provide data for development of analytical expressions and model validation and b) demonstrate the capacity of a composite beam under cyclic loading and the extent of its remaining resistance at ultimate limit state,
- analytical studies: a) to produce the laws describing the interface behaviour under static and cyclic loading and b) to evaluate the impact of the cyclic loading to the slip in the interfaces and in the connection and thus propose a damage factor for cyclic loading,
- finite element analysis in order to enable an analytical description of the confinement effect, caused by the reinforced concrete slab, which contributes to the resistance,
- the development of a numerical model to predict the connection's structural performance and to propose a design method for composite bridges fabricated with the new connection.

Application of the mentioned methodology resulted in several useful conclusions:

- The interface behaviour can be described by analytical laws. The post failure behaviour of the interfaces was explained by accounting for the kinematics of the failed surface and basic notions of fracture mechanics.
- The damage due to cyclic loading on the interfaces and on the connection is expressed by the accumulation of a residual slip. Provided that the shear stresses remain lower than an elastic limit and the accumulated slip does not exceed the failure slip for static loading, fatigue failure is avoided.
- The confinement effect was incorporated, analytically, together with the laws of the interface behaviour in a numerical model to predict the connection's structural performance and allow a parametrical study.
- A design method for the verification of composite beams under static and cyclic loading was developed.

Keywords: *steel-concrete connections, longitudinal shear, interfaces, softening behaviour, confinement effect, cyclic loading, residual slip, fatigue limit*

EPFL Thesis 5301

RÉSUMÉ

Les ponts mixtes acier-béton composés de poutres en acier en double T et de dalles préfabriquées constituent une solution économique et très compétitive pour des ponts des petites et moyennes portées. Ces dernières années ils gagnent des places de marché. Cependant, la connexion acier-béton courante par groupe de goujons s'avère mal adaptée à la préfabrication, au montage rapide et ne garanti pas une durabilité suffisante de la construction. De nouveaux types de connexions par adhérence, « interlocking » et frottement répondent mieux à ces demandes. La résistance de ces connexions est basée sur le développement de contraintes de cisaillement longitudinales dans les interfaces qui forment la connexion.

Les objectifs de cette étude sont de compléter la recherche existante dans ce domaine en proposant des outils scientifiques pour prévoir la performance structurelle de la connexion, i.e. la prédiction de la résistance ultime de la connexion et sa capacité de déformation, y compris le comportement post-rupture. En outre, le comportement de la connexion sous chargement cyclique est également étudié pour évaluer la résistance de la connexion à la fatigue et proposer une méthode de dimensionnement de la connexion pour des ponts mixtes sous chargement de fatigue.

Pour atteindre ces objectifs la méthodologie suivante a été appliquée:

- étude de l'état de l'art, a) pour les ponts mixtes afin de définir les exigences et b) pour le comportement des interfaces afin de souligner les paramètres qui sont responsables de la résistance et obtenir des informations sur la nature des mécanismes d'endommagement sous sollicitations cycliques,
- études expérimentales a) pour révéler les lois décrivant les interfaces et le comportement de la connexion dans le cas de chargement statique et cyclique pour fournir des données pour le développement des expressions analytiques et la validation des modèles, et b) pour démontrer la capacité portante d'une poutre mixte sous chargement cyclique ainsi que sa résistance résiduelle à l'état limite ultime,
- études analytiques a) pour définir des lois décrivant le comportement des interfaces sous sollicitations statiques et cycliques, et b) pour évaluer l'influence de la sollicitation cyclique sur le glissement au niveau des interfaces et de la connexion et, par suite, de proposer un facteur d'endommagement pour les sollicitations cycliques,
- analyse par éléments finis, afin de permettre une description analytique de l'effet de confinement causée par la dalle en béton armé qui contribue à la résistance,
- utilisation des ces résultats dans un modèle numérique pour prédire la performance structurelle de la connexion, et proposition d'une méthode de conception des ponts mixtes fabriqués avec la nouvelle connexion.

L'application de la méthodologie mentionnée aboutit à plusieurs conclusions utiles :

- Le comportement des interfaces peut être décrit par les lois analytiques. Le comportement post-rupture des interfaces a été expliqué par la cinématique de la surface de rupture et les lois fondamentales de mécanique de la rupture.
- L'endommagement dû aux charges cycliques sur les interfaces et sur la connexion est exprimé par l'accumulation du glissement résiduel. Tant que les contraintes de cisaillement restent inférieures la limite de l'élasticité de l'interface et que le glissement accumulé ne dépasse pas la valeur du glissement correspondant à la rupture statique, la rupture par fatigue est évitée.
- L'effet de confinement a été déterminé analytiquement, puis appliqué en interaction avec les lois de comportement des interfaces dans un modèle numérique. Ce modèle a permis de prédire la performance structurelle de la connexion et d'effectuer une étude paramétrique.

– Une méthode de dimensionnement pour la vérification des poutres mixtes sous sollicitations statiques et cycliques a été développée.

Mots-clés: *connexion acier-béton, cisaillement longitudinal, interfaces, comportement d'adoucissement, effet de confinement, chargement cyclique, glissement résiduelle, limite de fatigue*

Zusammenfassung

Verbundbrücken mit I-Profilen aus Stahl und vorfabrizierten Stahlbetonplatten stellen eine ökonomische und sehr konkurrenzfähige Lösung für Brücken mit kleiner und mittlerer Spannweite dar und haben während der letzten Jahre einen gewissen Marktanteil erobert. Allerdings ist die momentan übliche Ausführung mit gruppierten Kopfbolzendübeln nicht gut für die Vorfabrikation und schnelle Konstruktion geeignet und genügt nicht den Dauerhaftigkeitsanforderungen an eine Brücke. Aus diesem Grund wurden neuere Typen von Verbindungen, die durch Haftung, Verzahnung und Reibung wirken, entwickelt, um diesen Anforderungen zu genügen. Der Tragwiderstand dieser Verbindungen basiert auf der Entwicklung der Längsschubspannungen entlang der Kontaktfläche der Verbindung.

Das Ziel dieser Arbeit ist es, die bestehende Forschung auf diesem Gebiet, durch das Entwickeln von wissenschaftlichen Werkzeugen zur Vorhersage des Tragverhaltens zu komplettieren, mit denen die Tragfähigkeit der Verbindung sowie ihre Verformungskapazität inklusive des Verhaltens nach Versagen vorhergesagt werden können. Desweiteren wird das Verhalten der Verbindung under zyklischer Belastung untersucht, um die Dauerstandfestigkeit zu beurteilen und eine Bemessungsmethode für Verbundbrücken unter Ermüdungslasten vorzuschlagen.

Um diese Ziele zu erreichen wurden folgende Fragestellungen bearbeitet:

- Studium des Stands der Technik bei a) Verbundbrücken, um die Anforderungen zu identifizieren und b) hinsichtlich des Verhaltens der Kontaktfläche, um die Parameter zu identifizieren, die zum Widerstand beitragen, und Informationen über die Art der Schädigungsmechanismen bei zyklischer Belastung zu erhalten.
- Experimentelle Untersuchungen a) um die Gesetzmässigkeiten, mit denen sich das Verhalten der Kontaktflächen und der Verbindung unter statischer und dynamischer Belastung beschreiben lässt, aufzudecken und Versuchsdaten zur Entwicklung und Validierung von Modellen bereit zu stellen und b) um die Kapazität eines Verbundbalkens unter zyklischer Belastung und die Grössenordnung des verbleibenden Widerstandes im Grenzzustand der Tragfähigkeit aufzuzeigen.
- Analytische Studien, a) um Gesetzmässigkeiten aufzustellen, die das Verhalten der Kontaktfläche unter statischer und dynamischer Belastung beschreiben, und b) um den Einfluss der zyklischen Belastung auf den Schlupf der Kontaktflächen und der Verbindung zu evaluieren und einen Schädigungsfaktor für zyklische Belastung vorzuschlagen.
- Finite-Elemente Analyse, um eine analytische Beschreibung des durch die Stahlbetonplatte ausgelösten Umschnürungseffektes zu ermöglichen, der zum Tragwiderstand beiträgt.
- Entwickeln eines numerischen Models um das Tragverhalten der Verbindung vorherzusagen und einer Design Methode für Verbundbrücken, die mit der neuen Verbindung ausgeführt wurden.

Die folgenden Schlussfolgerungen können nach dem Anwenden dieser Methodik gezogen werden:

– Das Verhalten der Kontaktfläche kann mit analytischen Gesetzmässigkeiten beschrieben werden. Nach dem Versagen wurde das Verhalten durch Berücksichtigung der Kinematik entlang der Kontaktfläche und Grundprinzipien der Bruchmechanik beschrieben.

- Die Schädigung der Kontaktfläche und der Verbindung durch zyklische Belastung wird durch die Summierung des verbleibenden Schlupfes ausgedrückt. Unter der Voraussetzung, dass die Schubspannungen unter einem elastischen Limit bleiben, wird Ermüdungsversagen durch eine Stabilisierung des kumulierten Schlupfes, welcher den Schlupfwert nicht überschreitet, der unter statischer Belastung zum Versagen führt, vermieden.
- Der Umschnürungseffekt wurde analytisch, zusammen mit den Gesetzmässigkeiten, die das Verhalten der Kontaktflächen beschreiben, im numerischen Modell eingebunden um das Tragverhalten der Verbindung zu beschreiben und eine Parameterstudie zu ermöglichen.
- Eine Bemessungsmethode zur Verifikation von Verbundbalken unter statischer und dynamischer Belastung wurde entwickelt.

Schlüsselwörter: Stahl-Beton Verbindungen, Längsschubspannung, Kontaktfläche, Ermüdungsgrenze, Entfestigungsverhalten, Umschnürungseffekt, zyklische Belastung, verbleibender Schlupf.

Riassunto

La tipologia di ponte in struttura mista, con due travi longitudinali in carpenteria metallica e soletta prefabbricata in cemento armato, rappresenta sicuramente una delle soluzioni più economicamente vantaggiose per ponti di media e piccola luce. Negli ultimi anni ha infatti guadagnato una considerevole aliquota del mercato delle costruzioni. Tuttavia, le attuali connessioni soletta-trave realizzate con gruppi di connettori metallici non rispondono in maniera soddisfacente ai necessari requisiti prestazionali, sia in termini di prefabbricazione e posa in opera, sia in termini di durabilità. Una nuova tipologia di connessione, basata sui fenomeni di adesione, ingranamento e attrito, ha l'obiettivo di rispondere a tali tipi di requisiti prestazionali. La resistenza di queste connessioni si basa sullo sviluppo di sforzi di taglio longitudinali in prossimità dell'interfaccia tra connessione metallica e soletta.

Gli obbiettivi del presente studio sono quelli di completare una ricerca già esistente in questo campo, mediante la formulazione di strumenti scientifici atti a predire le prestazioni strutturali della connessione, con particolare interesse nel calcolo della resistenza ultima della connessione e della sua capacità di deformazione, tenendo in conto del comportamento post-rottura.

Con lo scopo di soddisfare i succitati obbiettivi, è stata adottata una strategia di ricerca che ha incluso:

- Uno studio dello stato dell'arte su: a) in ponti in struttura mista con lo scopo di definire gli obbiettivi e i requisiti e b) il comportamento dell'interfaccia con lo scopo di mettere in evidenza i parametri che maggiormente influenzano la resistenza della connessione e ottenere informazioni sul meccanismo di danneggiamento per carichi ciclici,
- Campagna sperimentale: a) per scoprire le leggi che descrivono il comportamento dell'interfaccia e della connessione per carichi statici e dinamici, per fornire dati utili allo sviluppo di espressioni analitiche e alla validazione del modello che verrà in seguito sviluppato,
- Studi analitici: a) con lo scopo di definire delle leggi costitutive atte a descrivere il comportamento dell'interfaccia sottoposta a carichi statici e dinamici e b) per valutare l'influenza dei carichi ciclici sullo scorrimento relativo delle interfacce e della connessione e quindi di proporre un "fattore di danno" per carichi ciclici,
- Analisi agli elementi finiti atti a definire una descrizione analitica dell'effetto di confinamento, causato dalle armature della soletta in cemento armato, che contribuisce in maniera significativamente alla resistenza della connessione,

- Lo sviluppo di un modello numerico capace di predire le prestazioni strutturali della connessione e di una metodologia per la progettazione e la verifica di ponti in struttura mista realizzati mediate questo innovativo tipo di connessione.

L'applicazione della succitata metodologia ha avuto come risultato le seguenti conclusioni:

- Il comportamento dell'interfaccia può essere descritta da leggi costitutive analitiche. Il comportamento post-rottura dell'interfaccia è stato spiegato tenendo in conto della cinematica della superficie di scorrimento in condizioni di post-rottua e delle basilari nozioni di meccanica della frattura,
- Il danno indotto all'interfaccia e alla connessione dai carichi ciclici è espressa dall'accumulazione di scorrimento relativo residuo,
- È stato analiticamente implementato l'effetto di confinamento con un modello numerico, insieme alla legge costitutiva dell'interfaccia, con lo scopo di prevedere le prestazioni della connessione e di permettere uno studio parametrico della risposta strutturale,
- È stata compiutamente sviluppata una metodologia di verifica per le travi in struttura mista sottoposta a carico statico e dinamico.

Keywords: connessione acciaio-cemento armato, taglio longitudinale, interfaccia, comportamento softening, effetto di confinamento, carico ciclico, scorrimento relativo residuo, limite di fatica.

ΣΥΝΟΨΗ

Η τυπολογία των σύμμικτων γεφυρών αποτελούμενων από ένα ζεύγος μεταλλικών δοκών και το κατάστρωμα ωπλισμένου σκυροδέματος συνιστά μία εξόχως οικονομική και ανταγωνιστική λύση για μικρά και μεσαία ανοίγματα. Τα τελευταία χρόνια ειδικότερα η τυπολογία αυτή έχει αρχίσει να κατακτά το μερίδιό της στην αγορά. Εντούτοις, η τρέχουσα και συνήθως εφαρμοζόμενη διατμητική σύνδεση μεταξύ μεταλλικής δοκού και προκατασκευασμένου καταστρώματος μέσω διατμητικών ήλων δεν είναι κατάλληλη για προκατασκευή με γρήγορη εκτέλεση παρουσιάζοντας παράλληλα και τρωτότητα όσον αφορά την ανθεκτικότητα στο χρόνο. Καινοτόμες συνδέσεις βασιζόμενες στην συνάφεια, την αλληλεμπλοκή και την τριβή συνιστούν εναλλακτικές λύσεις που ανταποκρίνονται στις απαιτήσεις. Η αντοχή αυτών τον συνδέσεων σχετίζεται με την ανάπτυξη διατμητικών τάσεων κατά μήκος των σχηματιζόμενων διεπιφανειών.

Η παρούσα σπουδή αποσκοπεί να ολοκληρώσει την ήδη διεξαχθείσα έρευνα στον τομέα αυτό προτείνοντας επιστημονικά εργαλεία για την πρόβλεψη της απόκρισης της διατμητικής σύνδεσης, ήτοι της φέρουσας ικανότητας και της παραμορφωσιμότητας, συμπεριλαμβανόμενης και της συμπεριφοράς μετά την αστοχία. Ερευνάται επιπλέον η συμπεριφορά της σύνδεσης υπό κυκλική φόρτιση με σκοπό την εκτίμηση της αντοχής της σύνδεσης στην κόπωση και τη δημιουργία μιας μεθόδου διαστασιολόγησης της σύνδεσης για χρήση σε σύμμικτες γέφυρες.

Για την επίτευξη των στόχων αυτών ακολουθείται η ακόλουθη μεθοδολογία:

- βιβλιογραφική επισκόπηση: α) περί φορτίσεων σύμμικτων γεφυρών και β) περί συμπεριφοράς διεπιφανειών, με σκοπό να δοθεί έμφαση στις παραμέτρους που είναι υπεύθυνοι για την αντοχή των διεπιφανειών και να διερευνηθεί η φύση της φθοράς λόγω κυκλικής φόρτισης,
- πειραματική διερεύνηση: α) με σκοπό να ανακαλυφθούν οι νόμοι της συμπεριφοράς τόσο των διεπιφανειών όσο και της διατμητικής σύνδεσης για στατική και για κυκλική φόρτιση και να παραχθούν πειραματικά δεδομένα αφενός για τη δημιουργία αναλυτικών σχέσεων και αφετέρου για την επαλήθευση μηχανικών προσομοιωμάτων, β) με σκοπό να αποκαλυφθεί η

αντοχή των σύμμικτων δοκών -με τη νέα σύνδεση- σε κυκλική φόρτιση καθώς και η απομένουσα αντοχή σε οριακή κατάσταση αστοχίας,

- αναλυτική σπουδή με σκοπό: α) τη δημιουργία αναλυτικών μαθηματικών εκφράσεων για την προσομοίωση της συμπεριφοράς των διεπιφανειών υπό στατική και κυκλική φόρτιση και β) τη δημιουργία αναλυτικών μαθηματικών εκφράσεων για την εκτίμηση της φθοράς λόγω κυκλικής επιπόνησης, εκφραζόμενης μέσω της συσσώρευσης ολίσθησης, τόσο για τις διεπιφάνειες όσο και για τη διατμητική σύνδεση,
- εφαρμογή της μέθοδου των πεπερασμένων στοιχείων αποσκοπώντας στην δημιουργία αναλυτικών εκφράσεων για το φαινόμενο της περίσφυξης που παρέχει η πλάκα ωπλισμένου σκυροδέματος στις διεπιφάνειες και που συνεισφέρει ουσιωδώς στην αντοχή,
- ανάπτυξη ενός αλγορίθμου-προσομοίωματος για την πρόβλεψη της απόκρισης της διατμητικής σύνδεσης και για τη δημιουργία μιας μεθόδου διαστασιολόγησης της διατμητικής σύνδεσης για χρήση σε σύμμικτες γέφυρες.

Η εφορμογή της ως άνω μεθοδολογίας καταλήγει στα ακόλουθα συμπεράσματα :

- Η συμπεριφορά των διεπιφανειών μπορεί να προσομοιωθεί με αναλυτικές σχέσεις. Η απόκριση μετά την αστοχία μπορεί να προσομοιωθεί με βάση την κινηματική των διεπιφανειών και τις αρχές της θραυστομηχανικής.
- Η φθορά λόγω ανακυκλικής διατμητικής φόρτισης των διεπιφανειών καθώς και της διατμητικής συνδέσεως μπορεί να εκφραστεί με τη συσσώρευση της ολίσθησης. Ενόσο οι διατμητικές τάσεις παραμένουν χαμηλότερες του ελαστικού διατμητικού ορίου διαρροής των διεπιφανειών και η συσσωρευμένη ολίσθηση δεν υπερβαίνει την ολίσθηση αστοχίας για μονοτονική φόρτιση, αποφεύγεται η αστοχία σε κόπωση.
- Η αλληλεπίδραση της περίσφυξης, των καταστατικών νόμων συμπεριφοράς και των κριτηρίων αστοχίας των διεπιφανείων καθώς και της κινηματικής τους προσμοιώνεται μέσω ενός αριθμητικού αλγορίθμου. Το μοντέλο αυτό προβλέπει την απόκριση της διατμητικής συνδέσεως και εκ τούτου την πραματοποίηση παραμετρικής ανάλυσης.
- Εντέλει, μια μέθοδος διαστασιολόγησης της διατμητικής σύνδεσης προτείνεται για εφαρμογή σε σύμμικτες γέφυρες.

Λέξεις κλειδιά: *σύμμικτες συνδέσεις, διαμήκης διάτμηση, διεπιφάνειες, απομειούμενη απόκριση, περίσφυξη, κυκλική φόρτιση, παραμένουσα ολίσθηση, όριο κόπωσης*

Table of contents

Chapter 3-Experimental investigation

Chapter 4-Analytical study

Chapter 5-Numerical model to predict the connection resistance

Chapter 6-Design method

Chapter 7-Conclusions

Notations

Capital english letters

A : area of an interface
A_a : area of steel section (in a composite beam)
A_b : equivalent area of the composite action, $A_b = A_a + A_c/n_0$
A_c : area of concrete section in a composite beam for width equal to b_{eff}
A_j : area of joint interface
A_s : area of steel reinforcement
A_{vf} : area of shear friction rebars
E_{cm} : modulus of elasticity of concrete
G_f : fracture energy for concrete
G_F^I : normal fracture energy release rate (interface opening)
G_F^{II} : fracture energy release rate (interface slipping)
$I_{b,i}$: second moment of inertia of the composite section calculated with the corresponding modular ratio $n_{el,i}$
$M_{a,Ed}$: bending moment for loads acting in the steel section only
$M_{\Delta T}$: bending moment to composite section due to thermal gradient ΔT
M_{Ed} : design bending moment
$M_{el,Rd}$: design elastic moment of the composite section
$M_{pl,Rd}$: design plastic moment of the composite section
N : number of cycles
N_f : number of cycles to failure
$N_{c,d}$: normal force acting to the slab on the position of maximum moment
$N_{c,el}$: normal force acting to the slab on the position where the plastification initiates
$N_{c,Rd}$: normal force acting in the slab when section is fully plastified
$N_{\Delta T}$: normal force to the composite section due to thermal gradient ΔT
Q_{fat} : traffic load considered in a load model of a code
R^2 : coefficient of determination
R_{max} : maximum peak to valley height of a longitudinal surface profile
S : spacing of steel reinforcement
$S_{c,i}$: first moment of inertia of the slab calculated from the neutral axis of the composite section
$V_{Ed,i}$: shear force due to load i acting after the realization of connection
V_{max} : maximum cyclic shear force
V_{min} : minimum cyclic shear force
V_u : ultimate shear at ULS following after a cyclic loading
$V_{u,stat}$: ultimate shear at ULS for static loading

Small english letters

b : power index for accumulated slip under load for an interface
b_{con} : power index for accumulated slip under load for the connection
$b_{con,res}$: power index for the residual accumulated slip for the connection
b_{res} : power index for the residual accumulated slip for an interface
c : cohesion, adhesion/interlocking stress, multiplication factor of f_{ctd} for adhesion-interlocking stress for joint resistance according to EC2, covering of steel rebars

d : multiplication factor of normal stress in the interface failure criterion proposed by Thomann

d_i : damage factor corresponding to cyclic loading under the load $V_{max,i}$

f_c : concrete compressive strength, cement grout compressive strength

f_{cd} : design concrete compressive strength, design cement grout compressive strength

f_{ck} : concrete characteristic compressive strength, cement grout characteristic compressive strength

f_{cm} : mean concrete compressive strength, mean cement grout compressive strength

$f_{lct,d}$: design tensile strength of pumice lightweight concrete

f_{lck} : characteristic compressive strength of lightweight concrete

f_{ctd} : design tensile strength of concrete

f_y : limit of elasticity of steel, yield stress of steel reinforcement

f_{yd} : design yield strength of steel reinforcement

h : height of the slab

h_{mid} : distance of the middle reinforcement from the upper edge of the inner rib of the slab

h_{rib} : height of the inner rib of the slab (equal also to the height of the connector)

k_a,k_b,k_c : slopes of the law of the confinement effect

k_{con} : stiffness of the connection

k_{des} : stiffness of the descending part of the constitutive law (unloading)

k_{el} : elastic stiffness of an interface constitutive law

k_i : secant stiffness of an interface constitutive law

k_n : characteristic fractile factor (5% fractile factor)

k_{pl} : plastic stiffness of an interface constitutive law

k_{sec} : secant stiffness related to failure point in an interface constitutive law

k_{slab} : translational stiffness of a reinforced concrete slab enclosing a connection by adhesion, interlocking and friction

l : length, distance

$n_{el,i}$: elastic modular ratio for load i

n_v : conversion factor for the resistance in longitudinal shear force per unit length

$n_{v,el}$: conversion factor for the fatigue limit of the longitudinal shear force per unit length

n_0 : modular ratio for short term loads

r : coefficient with units in mm used in the expression of the kinematic law

s : slip

s_a : coefficient with units in mm used in the expression of the kinematic and the constitutive law

s_{res} : residual slip

s_{Vmax} : slip under maximum cyclic load

$s_{Vmax,N}$: slip under maximum cyclic load at the N^{th} cycle

s_u : slip at failure point in an interface constitutive law, slip at failure point for connection

s_X : estimated standard deviation

t : time interval, in days, from fabrication day till the day of application of the load for a static test after a cyclic loading

t_0 : time interval, in days, from fabrication till application of the load for a static test

u : uplift

u_a,u_b : characteristic values of uplift used in the curve of the confinement effect

u_{max} : ultimate uplift in an interface when shear stress is reduced to a constant frictional resistance

$u_{max,0}$: ultimate uplift in an interface when shear stress is reduced to a constant frictional resistance for zero normal stress on the interface

u_{Su} : uplift at failure point in an interface constitutive law, uplift at failure point for connection

w : vertical deflection

Capital greek letters

Δ : variation of a magnitude

ΔT : thermal gradient

Δv : variation of longitudinal shear force per unit length

Δv_C : fatigue resistance to longitudinal shear force per unit length for 2 million cycles (concerns connections with shear studs)

Δv_D : constant amplitude fatigue limit for longitudinal shear force per unit length

Δv_{E2} : equivalent longitudinal shear force range per unit length for 2 million cycles (concerns connections with shear studs)

$\Delta v(Q_{fat})$: variation of longitudinal shear force per unit length due to traffic load Q_{fat}

Φ : dynamic amplification factor

Small greek letters

a : ratio of elastic shear stress versus ultimate shear stress in an interface, factor for dowel action in fib Model Code 2010

$a_{0.05}$: 5% fractile values of the ratio of the elastic shear stress versus the ultimate shear stress in an interface

γ_c : partial safety factor of concrete

γ_{fat} : partial factor for fatigue strength

γ_g : partial factor for gravity loads

γ_v : partial factor for resistance of connection, γ_v = 1.25 [SIA-264 2003]

z_a : position of centre of gravity of steel section

z_b : position of centre of gravity of composite section

z_c : position of centre of gravity of concrete section

κ : interaction factor (bending –tension)

λ : correction load factor, constant accounting for density of concrete in Loov's equation

μ : coefficient of friction

μ_r : remaining friction coefficient (kinetic friction coefficient)

ρ : density in kg/m^3, area of reinforcement crossing the joint versus the area A_j of the joint

ρ_v : steel ratio

ρ_w : steel ratio

v : longitudinal shear force per unit length, strength reduction factor

$v_{\Delta T}$: longitudinal shear force per unit length due to thermal gradient ΔT

v_{Ed} : design value of longitudinal shear force per unit length

v_{el} : longitudinal shear force per unit length at the end of the elastic behaviour (fatigue limit)

v_{long} : the design longitudinal shear force per unit length due to permanent loads acting in the connection after the realization of the connection, calculated with a partial factor γ_v

v_{min} : minimum cyclic longitudinal shear force per unit length

v_{max} : maximum cyclic longitudinal shear force per unit length

v_{Rd} : design value of the resistance to longitudinal shear force per unit length

v_{Rk} : characteristic value of the resistance to longitudinal shear force per unit length

$v_{Rk,fat}$: characteristic value of the fatigue limit of the longitudinal shear force per unit length
v_u : ultimate resistance to longitudinal shear force per unit length
σ : normal stress
$\sigma_{ext,i}$: normal stress on interface from transversal bending of the slab, for loads applied after the realization of the connection
τ : shear stress
τ_{adh} : shear stress in a bonded joint by means of epoxy adhesive layer
τ_c : adhesion, interlocking stress in fib Model Code 2010
τ_{el} : elastic shear stress
τ_{fr} : frictional shear stress
τ_{fu} : shear resistance of pumice lightweight aggregate concrete-UHPFRC joints
τ_{max} : maximum cyclic shear stress, ultimate shear stress in interface failure criterion proposed by Thomann
τ_{min} : minimum cyclic shear stress
τ_u : ultimate shear stress (failure shear stress)
τ_{Rdj} : design shear resistance of joint for equation proposed by EC2
x_{pl} : length of the beam from the position where plastification initiates till the position of the maximum moment.
ψ_0 : reduction factor for the occasional (rare) value of a load

Abbreviations

FEA : finite element analysis
FLS : fatigue limit state
SLS : serviceability limit state
ULS : ultimate limit state

1. Introduction

1.1 Context and motivation

Steel-concrete composite bridges have known a success since their appearance in Europe in the 80's and much earlier in Switzerland [Badoux 1985]. The simplified version, i.e. the case of a twin steel I-girder with reinforced concrete deck, is quite often an economical solution and very competitive compared to prestressed and reinforced bridges [Brozzetti 2000]. In Europe this design is deemed safe enough although the fact that if one girder fails the whole bridge will fall down. In the US twin-girder are allowed but the safety factors are higher, which makes twin girder bridge less competitive. The distribution of the French new road and railway bridges in 2004, according to the main span length, shows the high competiveness of composite bridges, for spans between 40 m to 80 m (figure 1.1).

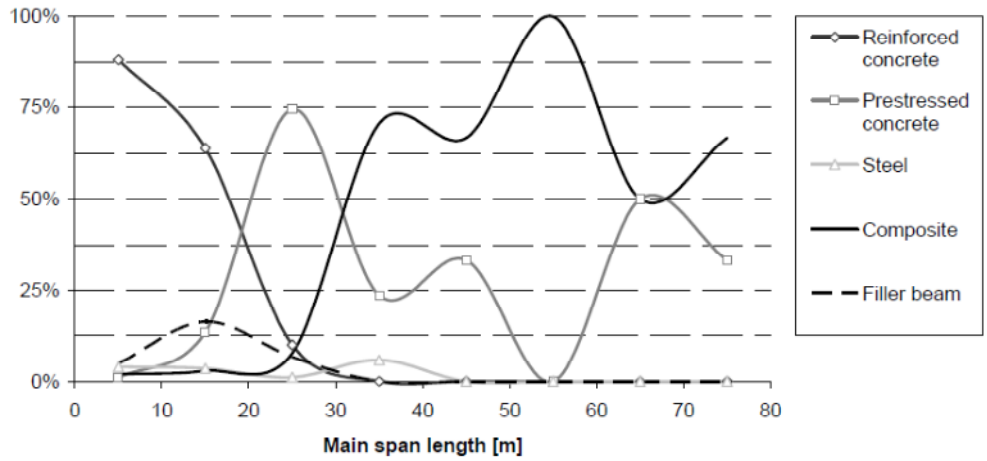

Fig. 1.1: Distribution of new bridges in France in 2004 according to the main span length [COMBRI 2008].

In Germany despite the domination of prestressed concrete in bridges, lately, steel concrete composite bridges start to gain their share in the market. As illustrated in figure 1.2, from the overall new highway bridges with bridge lengths between 30 to 60 m, constructed in 2005 in Germany, composite bridges reach up to 54.6 % [COMBRI 2008].

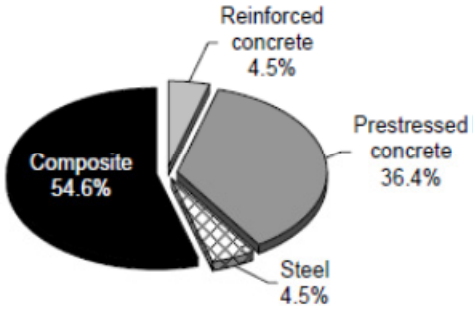

Fig. 1.2: Distribution of types of highway bridges with lengths referenced between 30 to 60 m, built in 2005 in Germany [COMBRI 2008]

In order to keep and increase their competiveness compared to other types of bridges, composite bridges, need also to have a high level of prefabrication. This is easily done for the steel I-girders and box girders which can be fabricated in the factory and then transported and assembled in situ. The

deck slabs can also be prefabricated, consisting of reinforced concrete slab segments fabricated in the factory. The segments are equipped with shear pockets, i.e. openings. The positioning of segments is done usually by cranes (figure 1.3), in such a way that the shear pockets encircle the groups of the shear studs which are welded to the steel girders in advance in the factory. When the positioning of the segments is accomplished by the launching method, shear pockets allow the welding of shear studs to the steel structure by means of specific gun on site (figure 1.4).

Fig. 1.3: Positioning of prefabricated segments over steel girders [Artéfac 2008]

Fig. 1.4: In situ welding of shear studs inside the pockets of prefabricated deck
[Japan Highway administration]

The prefabricated slab segments are connected to the rest of the structure by concreting the rectangular openings and the transverse joints, followed by longitudinal prestressing (figure 1.5).

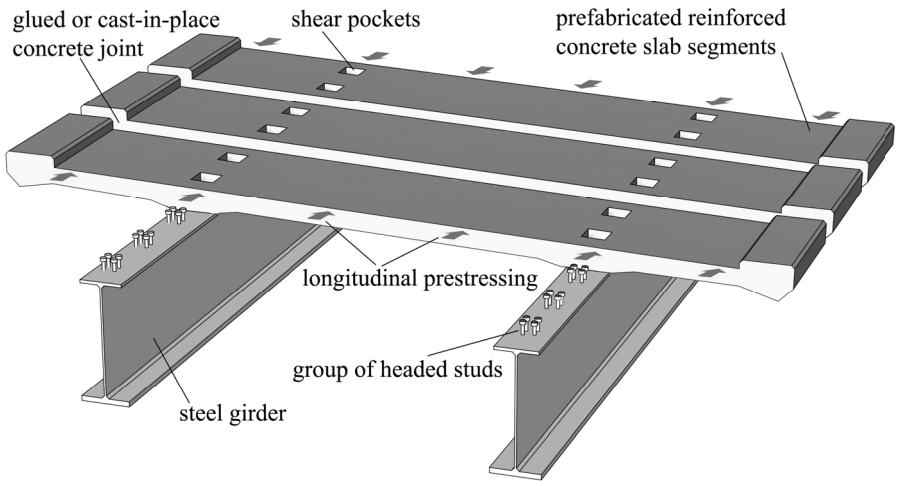

Fig. 1.5: Composite bridge with prefabricated deck and shear pockets [Lebet and Hirt 2009]

Recent advances in technology [Collin et al. 2002], [Hieber et al. 2005], [Dauner 2006], propose an alternative to the concreting of the transverse joints of the deck. Instead of concreting, transverse joints, formed with shear keys, are glued together with epoxy raisin. Longitudinal prestressing of the deck follows.

Fig.1.6: Trowel application of the adhering joint to prefabricated deck slab segments with sealing rings for the cable troughs [Dauner 2006]

Despite these advances, the realization of the connection between prefabricated deck slabs and the steel girders is still done by concreting the shear pockets, inside which lay the shear studs that are welded to the upper steel flange. This construction method presents several disadvantages:

- Due to concreting at two stages and hence different development of shrinkage in time, cracks appear both at the corners of the pockets, related also to stress concentration, and in the perimeter of the pockets as well. Cracking results, in long term, to degradation of the deck, and most important, it menaces the connection itself.
- When the supplementary concreting is executed after the longitudinal prestressing, the concrete of the pockets does not benefit of the prestressing, whereas when the application of the longitudinal prestressing is executed after the supplementary concreting of the pockets, the prestressing force has to be increased, because forces are applied to the composite structure in the whole.
- All supplementary work in situ results to the increase of the overall time construction and thus to the increase of the cost of the project together with the other consequences in the economic activities and the quality of life which are influenced by traffic diversion, noise, and other disturbance.

For this reason new connections have to be developed, keeping the advantages of prefabrication, minimizing the construction time and guarantee a long term durability of the engineering product. Several connections, which are being developed lately in Europe and presented in the second chapter, constitute solutions with prefabricated elements and linear connectors with increased resistance in fatigue of the connection, but they do not avoid supplementary concreting. Another solution proposed is that of connecting concrete decks to the steel girder by means of epoxy glue. This method that avoids supplementary on site work but its execution is questionable both due to increased demand for accuracy of execution work and the behaviour in long term of the glued connection.

The Steel Structures Laboratory together with the engineering bureau DIC Engineers [Dauner 2002] has developed an innovative connection which fulfills the criteria for fast and entire prefabrication and long term durability. The connection was studied experimentally and analytically by Thomann [Thomann 2005]. The following figure presents this new connection.

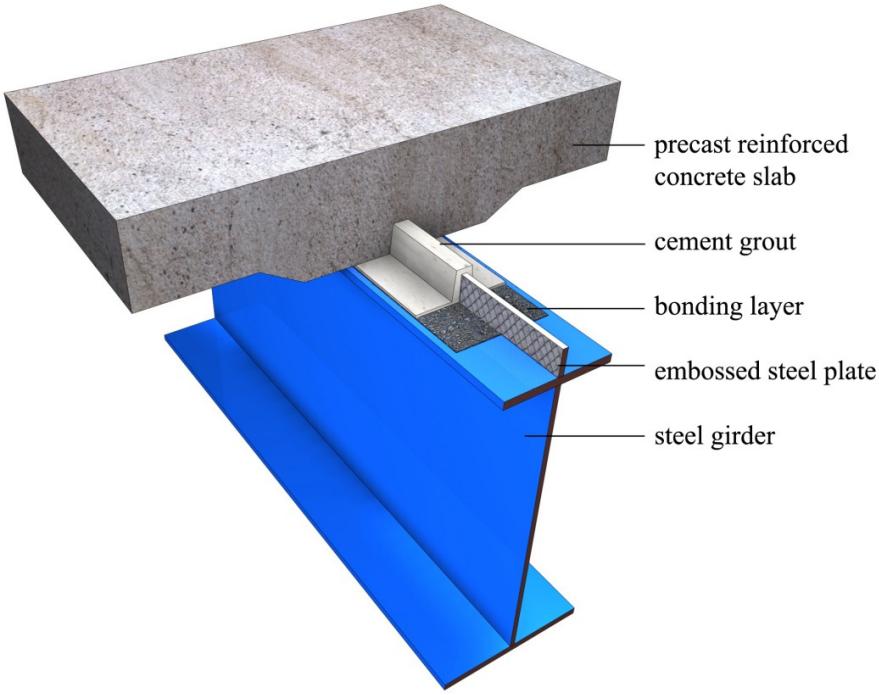

Fig.1.7: Connection with embossed steel connector and bonding layer [Thomann 2005]

The steel girder is provided with a connector over it. This connector is constituted by two embossed steel plates, welded together, and welded longitudinally to the upper flange of the steel girder perpendicular to it. The upper flange is covered by a bonding layer, created by an adhesive film in which sand aggregates are implemented. The deck consists of precast reinforced concrete segments which are fabricated with an inner rib at the lower part, the surface of which is roughened by using a retarding agent during casting followed by hydro-jetting and sandblasting (figure 1.8). The aggregates are exposed but firmly attached to the concrete mass. The slab segments are positioned over the steel connector and the void is filled with injecting a high strength cement grout. Once the cement grout is cured the connection is activated and the structural element becomes composite.

Fig. 1.8: Inner rib of slab with roughened surface [Dauner 2006]

The resistance of the connection is sourcing from the shear developed in three types of interfaces which are formed, the embossed steel-cement grout interface, the cement grout-rough concrete interface and finally the interface between cement grout and the bonding layer. A variation of this connection constitutes the same assembly with that of figure 1.7 with the absence of bonding layer on

the upper flange. Since the connections described are consisted of jointed interfaces, the terminology proposed by fib model code 2010 [fib Model Code 2010] can be used to nominate the connections. Consequently, in this thesis the innovative connections are called “Connections by adhesion, interlocking and friction”.

Following diagram presents, for the two versions of the innovative connection and for the classic connection with shear studs, their resistance in longitudinal shear force per unit length as a function of the slip between steel and concrete, obtained by performing push-out tests on specimens [Thomann 2005]. Embossed steel connector has a height of 110 mm, bonding layer is of type ICOSIT Haftmasse with a width 320 mm, whereas for the third connection nine shear studs, of 22 mm head diameter, per meter are used.

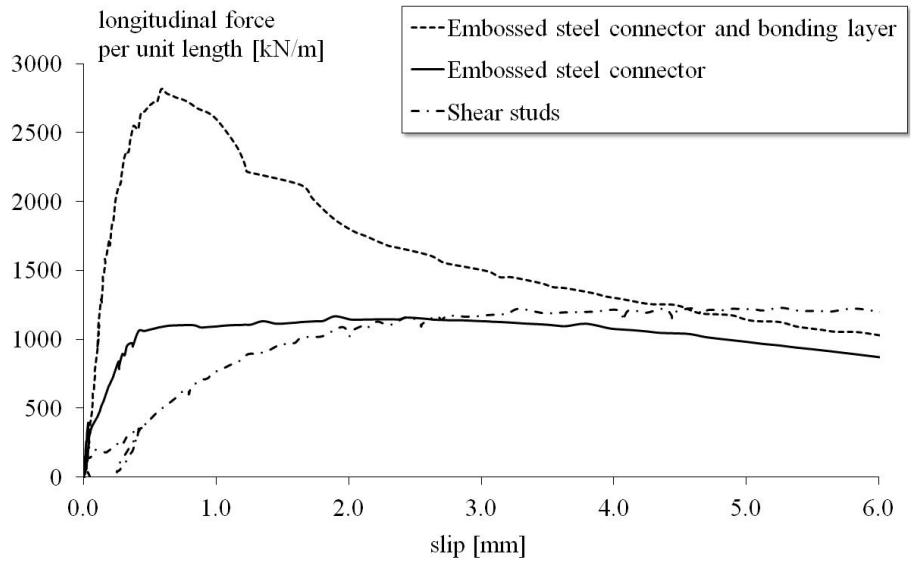

Fig. 1.9: Structural performance of innovative connections and shear studs [Thomann 2005]

As we observe in figure 1.9 the two versions of the innovative connection exhibit higher stiffness in comparison with the shear studs. The resistance is higher for the version with the bonding layer on the upper flange. Shear studs perform with high deformation capacity, the connection without the bonding layer exhibits less but significant deformation capacity whereas the version with the bonding layer presents a more brittle behaviour. The use of the bonding layer contributes significally to the resistance but presents several disadvantages:

- the connection exhibits less ductile behaviour,
- realization of the layer is costly and complicates the fabrication procedure,
- its long term performance and fatigue resistance are questionable.

For these reasons current project focuses on the study of the innovative connection without the bonding layer (figure 1.10). It’s a compromise of a little reduced deformation capacity, in comparison with the shear studs, and adequate resistance. It constitutes also a simple fabrication procedure with commonly used engineering materials.

The performance of the connection for static loading was studied by Thomann [Thomann 2005]. Thomann developed a model to predict the ultimate resistance of the connection for a certain reinforcement ratio of the slab section at the vicinity of the connection. The model incorporates the

structural behaviour of the interfaces, their interaction, and the confinement effect provided by the slab reinforcement when cracking occurs at ultimate limit state of connection.

So as to conclude the research and propose design tools for the connection for engineering practice, further research needs to be performed. The model which predicts the connections resistance should be enriched in order to simulate post-failure behaviour with more accuracy and provide thus the estimation of the deformation capacity of the connection, in terms of force-slip relationship. The confinement effect should also be incorporated to the model in such a way to apply both for SLS and ULS, in other words, prior and after cracking of the concrete at the vicinity of the connection. The option for using different reinforcement ratio should also be included. In addition, since this connection is proposed mainly for bridges, an important research should be performed in order to investigate the connection's resistance to fatigue.

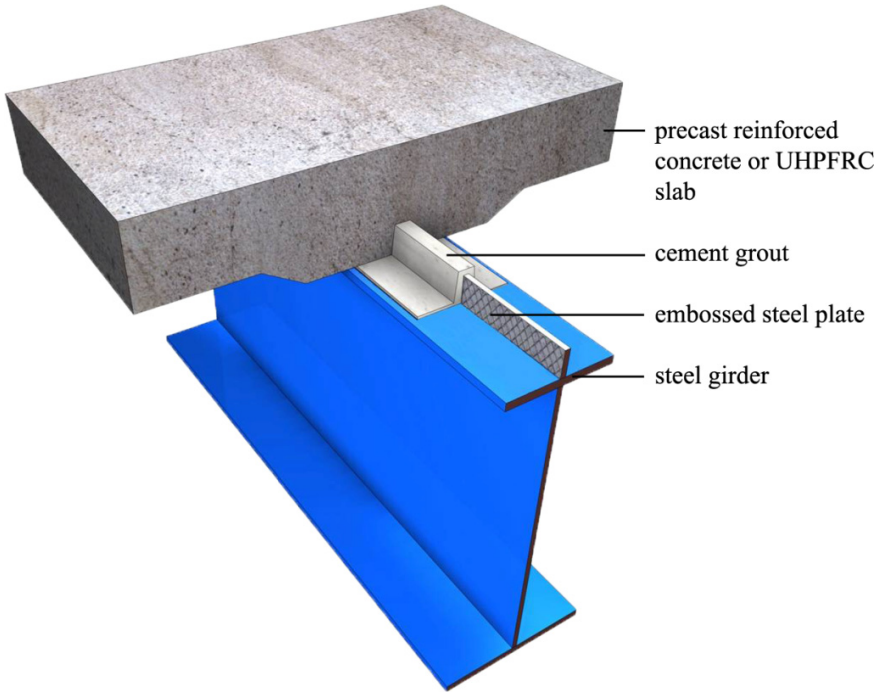

Fig. 1.10: Connection by adhesion, interlocking and friction [Thomann 2005]

Finally, due to the increased interest for using UHPFRC in bridges [Sorelli et al. 2006], the research should also be extended to include the applying of the connection also for the case that the deck slabs are fabricated from ultra high performance fibre reinforced concrete, UHPFRC.

1.2 Objectives and methodology

Epigrammatically the objectives have as following:

- Development of a numerical model to predict the resistance of connections by adhesion, interlocking and friction for static loading. The model should be valid also for high level of confinement of the interfaces, predict the post-failure behaviour and provide the deformation capacity of the connection.
- Develop a method, based on the connection's behaviour to cyclic loading, in order to predict the fatigue resistance of the new connection.
- Propose a design method for the connection of steel-concrete composite bridges, fabricated with the new connection and submitted to static and cyclic loading.

In order to accomplish the above objectives the following methodology will be applied:

- *Experimental investigation.* Firstly, a large series of direct shear tests will be performed to small specimens for three types of *interfaces* and for normal pressure to the interface up to 5 N/mm^2. Direct shear tests include both static and cyclic loading.
  Secondly, a series of push-out tests will be executed to study the *connection* and provide data to validate a model developed for the connection. Two types of specimens will be fabricated, one with reinforced concrete blocks and one with blocks of UHPFRC. Push-out tests include both static and cyclic loading.
  Finally a steel-concrete *composite beam* will be fabricated and will be submitted to a high cyclic loading test under constant amplitude, followed by a static test up to failure to investigate the remaining resistance.
- *Analytical study*. Based on the experimental data, *analytical laws* will be produced to describe the behaviour of interfaces under monotonic and cyclic loading. Analytical expressions for the residual slip in interfaces and connections, due to cyclic loading will also be proposed.
- *Finite Element Analysis*. The confinement effect in the interfaces imposed by the reinforce concrete slab will be studied by performing *finite element analysis* on variations of connections' section with different reinforcement ratio, geometry, and concrete quality, typically used in steel concrete composite bridges. This will help to develop analytical expressions for the needed relationship between the normal stress in the interface and the uplift, i.e. the opening in the interface, imposed by slip.
- *Numerical method.* The analytical laws for interfaces behaviour and the analytical expressions for the confinement effect will be used in a *model* to predict connection's resistance to longitudinal shear and its' deformation capacity at serviceability limit state, ultimate limit state and under cyclic loading. The model will allow through a parametric analysis, to investigate the influence of the parameters defining the resistance and the deformation capacity of the connection.
- *Design method.* The steps of the design method are presented together with the equations for the verification of the longitudinal shear force per unit length according to the limit state.

1.3 Contents of Thesis

Schematically the contents of the Thesis are presented at the following organization chart (figure 1.11).

Chapter 2 presents the *state of the art* in shear resistance and behaviour of interfaces between different materials, under static and cyclic loading. A short description of other types of innovative connections is also presented and a criticism is applied. Chapter ends with a reference to the type of loads that are acting on connections for existing composite bridges in order to define the forces which will be applied at the experimental program.

Chapter 3 presents in detail the *experimental investigation* executed during this project. It is divided in three parts. The first part describes the direct shear tests for three types of interfaces that are formed in the new connections. Static tests provide data for development of failure criterion, the constitutive law and the kinematic law of the interface. Cyclic loading permits to understand the damage mechanism of repeated loading and define limits for safe performance. The second part presents the push-out tests performed to investigate connection's behaviour under monotonic and cyclic loading and provide data for validation of connection's model developed later on. Finally the testing of a composite beam under cyclic loading and at ultimate limit state constitutes an experimental justification of the application of the proposed connection to bridge engineering.

Chapter 4 contains the *analytical study* of the behaviour of the interfaces at static loading. The influence of cyclic loading both for interfaces and connection is accounted by presenting analytical expressions of the evolution of the residual slip. A safe fatigue failure criterion is presented. Chapter includes analytical study of the composite beam tested both under cyclic loading and at ultimate limit state

Chapter 5 presents the finite element analysis, performed to investigate the confinement effect, the *numerical model* for the prediction of the connection's performance and the results of the parametric analysis.

Chapter 6 presents the *design method* for verification of the longitudinal shear force per unit length at FLS, SLS and ULS for composite bridges fabricated with the new connection. It provides also a design table for use in engineering practice.

Chapter 7 concludes this research with *conclusions*, propositions for further investigation, recommendations for engineering practice and other possible applications of the general conception.

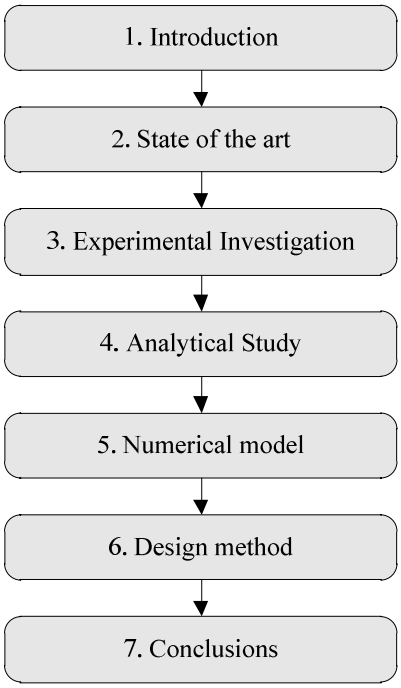

Fig. 1.11: Thesis organization chart

1.4 Limits of the research

The connection investigated constitutes an innovative conception for steel concrete composite bridges. This thesis proposes a model to calculate connection's performance under static and cyclic loading. It proposes also a design procedure for composite bridges fabricated with the new connection.
This research presents the following limitations:

- The results of this research are applied for connections with respect to the geometry as presented at figure 1.10. Even though the height of the embossed steel plate and the positioning of the reinforcement over the connection may vary, the main geometrical conception should be conserved.
- Concerning use of materials, a minimum quality of concrete C35/45 is needed for the slab for satisfactory performance of the connection. Cement grout to be used should have

characteristics similar to the product used in the research, i.e. compression strength about 90 N/mm^2, and limited shrinkage. Swelling behaviour is considered favorable.

- Constitutive, kinematic law and failure criteria have validity for confinement in the interfaces of the connection up to 5 N/mm^2. Thus prediction is accurate and safe if the confinement stresses applied, due to the geometry of the slab at the connection zone and the reinforcement positioning and ratio, do not exceed this value. Estimation of resistance for higher level of confinement should be accepted with cautiousness, for instance using as an upper limit of the shear stress in the failure criteria the limit proposed for indented surfaces by EC2 [EC2 2004] in paragraph 6.2.5, or by performing push-out tests, as indicated in EC4 [EC4 2005].
- Finally, as will be presented at chapter 2, the verification, for the longitudinal shear at serviceability limit state, ultimate limit state and fatigue limit state, is performed for actions calculated for a group of composite bridges [Jaunin 1996], mainly twin I-girder bridges with reinforced concrete prefabricated slabs, with spans from 30 to 120 m and with cross sections as defined in figure 1.12. The innovative connection can certainly be applied at other types of bridges, too, taking however into account supplementary considerations.

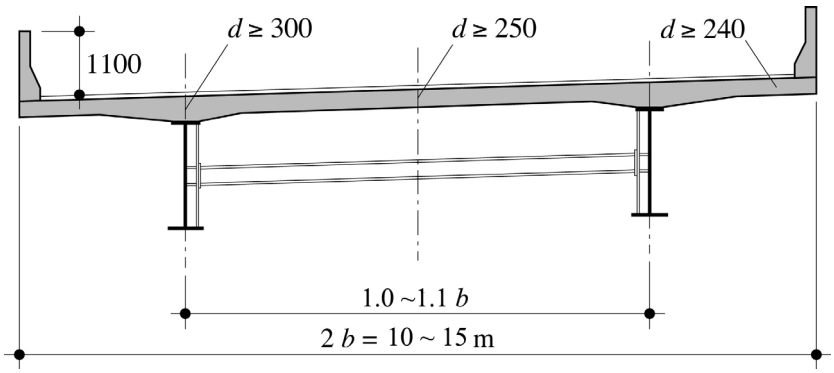

Fig. 1.12: Twin I-girder section of composite bridges [Lebet and Hirt 2009]

2. State of the art

This chapter presents the current state of the art regarding the behaviour of interfaces subjected to shear with application in connections for steel-concrete composite structures. It serves as a base for the research presented later, concerning the study of confined interfaces used in the new connection. In addition, state of the art in connections for steel-concrete composite bridges suitable for prefabrication is also presented.

2.1 Shear resistance of interfaces under monotonic loading

The transfer of shear at interfaces between materials takes place in many civil engineering applications such as prefabrication, seismic retrofit, structural upgrade, prestressing and assembly of composite bridges. Two main categories of interfaces are examined, firstly, joints of different concrete types (normal, lightweight, ultra high performance fibre reinforced concrete UHPFRC) including concrete-cement grout interfaces, and secondly steel-cement grout interfaces.

2.1.1 Interfaces between different concrete types, including cement grouts

Concrete-concrete interfaces

A fair amount of research has already been undertaken on concrete-concrete interfaces and several models have been proposed [Birkeland 1966, Walraven 1987, Tassios et al. 1987, Loov 1994, Climaco and Regan 2001]. Models accounting on shear resistance of concrete-concrete interfaces are also proposed in several codes [ACI 318-83 1983, EC2 2004, fib Model Code 2010].

With the above proposed models there is a need to characterize the roughness of the existing concrete. Several methods have been proposed to characterize this roughness, [ACI 318-83, BS 1134/1972, fib Model Code 2010, EC2 2004] and the corresponding instrumentation varies from optical observation to more sophisticated methods such as optical microscopy, mechanical profilometry, laser surfometry and advanced topometric sensors [Tateishi et al. 2003, Garbacz et al. 2005] The method described by Eurocode 2 suggests four categories of roughness, linking them with the production procedure or with visual inspection, without the need of complex calculations and instrumentations. The definitions are presented in table 2.1. Generally a concrete surface is considered rough when it is clean, free of laitance and has aggregate that are well protruding but firmly fixed in the matrix.

Table 2.1: Classification of joint faces according to Eurocode 2 [EC2 2004]

Category	Description
Very Smooth	A surface cast against steel, plastic or specially prepared wooden moulds
Smooth	A slip-formed or extruded surface, or a free surface left without further treatment after vibration
Rough	A surface with at least 3 mm roughness at about 40 mm spacing, achieved by raking or exposing of aggregate or other methods giving an equivalent result
Indented	Indented surface where the geometry complies with figure 2.2

In table 2.1 in the category characterized as “Rough”, the term “Roughness 3 mm” for a sampling length 40 mm, stands for the difference between the average height of the peaks and the average height of the valleys from an arbitrary baseline and for the certain sampling length of 40 mm as can be seen at figure 2.1. Figure 2.2 illustrates the definition of an “Indented” surface according to EC2.

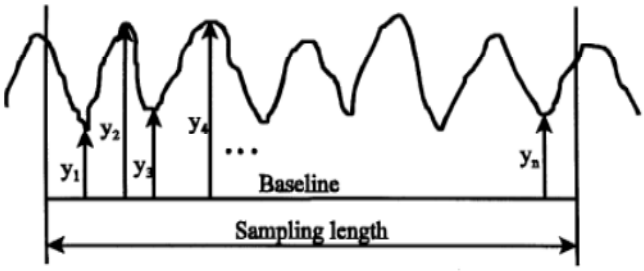

Fig. 2.1: Graphical representation of roughness measurements [EC2 2004]

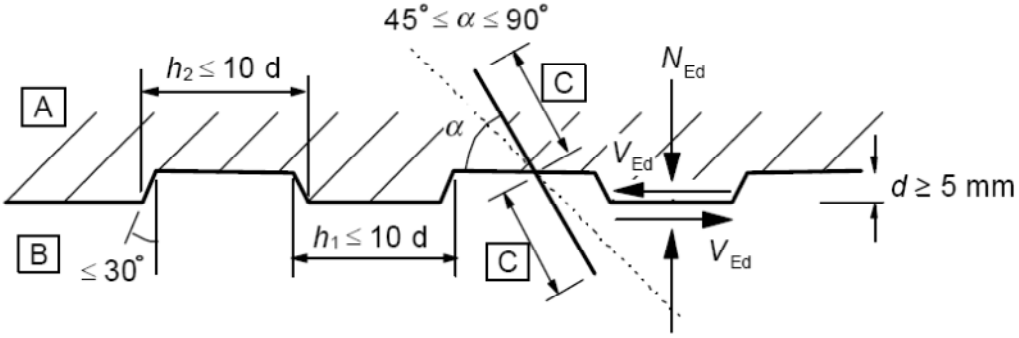

A: new concrete, B: old concrete, C: steel bar

Fig. 2.2: Geometrical requirements on indented joint face [EC2 2004]

Table 2.2 summarizes the equations proposed for the shear resistance of concrete-concrete joints where as table 2.3 explains the symbols of proposed equations together with other notations.

Table 2.2: Proposed equations for shear resistance of concrete-concrete joints

ACI 318-83	$V_n = \mu \cdot A_{vf} \cdot f_y$ (kN)
Birkeland	$V_n = 2.78 \cdot \sqrt{\rho_v \cdot f_y}$ (kN)
Walraven	$V_n = C_1 \cdot \left(\rho_v \cdot f_y\right)^{C_2}$ (kN)
Tassios et al.	$V_R = \beta_D \cdot F_D + \beta_F \cdot F_U$ (kN)
Loov	$v_n = \lambda \cdot k \cdot \sqrt{(0.1 + \rho_v \cdot f_y) \cdot f_c'} \le 0.25 \cdot f_c'$ (N/mm^2)
Climaco & Regan	$\tau = c + \mu \cdot \sigma$ (N/mm^2)
Eurocode 2	$\tau_{Rdj} = c \cdot f_{ctd} + \mu \cdot \sigma_n + \rho \cdot f_{yd} \cdot (\mu \cdot \sin\alpha + \cos\alpha) \le 0{,}5 \cdot \nu \cdot f_{cd}$ (N/mm^2)
fib Model Code 2010	$\tau_u = \tau_c + \left(\sigma + \kappa \cdot \rho \cdot f_y\right) + \alpha \cdot \rho \cdot \sqrt{f_y \cdot f_{cc}}$ (N/mm^2)

The failure criteria proposed by the models can be divided into two main categories; those who count only on the shear resistance of the rebar traversing the interface [ACI 318-83, Birkeland 1966, Walraven 1987], thus being more conservative and those who count also on the shear resistance of the concrete surfaces which constitute the joint. The latter consists of a constant term, accounting for the combined effect of adhesion and interlocking, plus the contribution of friction defined as a product of the friction coefficient and the normal stress on the interface.

Table 2.3: Abbreviations and values of coefficients of table 2.2

ACI 318-83, Birkeland,

A_{vf} = area of shear friction rebars

f_y = specified yield strength of rebars

ρ_v = steel ratio

μ = coefficient of friction

monolithic concrete 1.4

intenionally roughened surfaces ...1.0

untreated surfaces 0.6

Walraven,

$C_1 = 0.878 \cdot f_c^{0.406}$, $C_2 = 0.167 \cdot f_c^{0.303}$

f_c = concrete compressive strength

Tassios et al.,

$\beta_D = 0.6 \sim 0.7$, $\beta_F = 0.4 \sim 0.8$

$F_D = k_b \cdot 1.3 \cdot d_b^2 \cdot \left(f_c \cdot f_y \right)^{0.5}$

$F_U = 0.44 \cdot \left(f_c^2 \cdot \sigma_c \right)^{(1/3)} \cdot A_c \cdot f_c$

Loov,

$k = 0.6$, a lower bound for

roughened surfaces

λ = constant, used to account

for the density of concrete

normal concrete.....1.0

sand-lightweight concrete....0.85

all-lightweight concrete.....0.75

f_c' = concrete compressive strength

Climaco & Regan,

c = cohesion

$c = 0.25 \cdot f_{cc}^{2/3}$.....for rough interface

$c = 0.25 \cdot f_{cc}^{2/3}$.....for medium interface

$c = 0.5$ N/mm^2....for smooth interface

μ = coefficient of friction

rough interface 1.4

medium interface 0.9

smooth interface 0.6

Eurocode 2,

τ_{Rdj} = design shear resistance of joint

$c = 0.62$ .....for monolithic

$c = 0.5$ .....for indented surface

$c = 0.45$.....for rough surface

$c = 0.35$.....for smooth surface

$c = 0.25$.....for very smooth surface

f_{ctd} = design tensile strength for the

concrete grade of the insitu concrete

or the precast unit, whichever lower

$f_{ctd} = \frac{f_{ctk\,0.05}}{\gamma_c}$

μ = coefficient of friction

$\mu = 1,0$.....for monolithic

$\mu = 0,9$.....for indented surface

$\mu = 0,7$.....for rough surface

$\mu = 0,6$.....for smooth surface

$\mu = 0,5$.....for very smooth surface

σ_n = normal stress across the joint interface

$\sigma_n \le 0,6 \cdot f_{cd}$

$v = 0,6\left(1 - f_{ck} / 250\right)$ strength reduction factor

$\rho = A_s / A_j$

A_s = area of reinforcement crossing the joint at an agle a defined in fig. 2.2

A_j = area of joint intreface ($A_j = l_j \cdot b_j$)

fib Model Code 2010,

τ_u = ultimate shear stress

τ_c = adhesion/interlocking stress

$\kappa = \sigma_s / f_y$ interaction factor (bend.-tension)

α = factor for dowel action

values for τ_u and friction coefficient μ identical to Eurocode 2

Concrete-UHPFRC interfaces

The recent development of UHPFRC and its use in engineering practise has raised the question of the behaviour of concrete-UHPFRC interfaces.

Bending tests on composite reinforced concrete-UHPFRC beams and slabs performed by Habel and Wuest [Habel 2004, Wuest 2006] have shown no debonding of the interface neither under service load conditions nor due to internal deformations caused by autogenous shrinkage. Formation of interface cracks occur only far beyond service loads and they can lead to debonding cracks only on UHPFRC layers without any reinforcement. At the production of those composite beams the UHPFRC layer was applied to an already precast reinforced concrete with various roughness from 5 mm to an excessive, 10~15 mm, obtained by hydro-jetting. Monolithic behaviour was satisfied in all cases.

Lightweight concrete-UHPFRC interfaces

The behaviour of lightweight pumice aggregate concrete-UHPFRC interface has been investigated by Papanicolaou [Papanicolaou et al. 2002]. In that case absence of gravels at lightweight concrete leads to lack of aggregate interlocking because cracks propagate through the pumice aggregates, yet an interlocking action is provided by the general roughness of the interface undulations. Two Mohr-Coulomb type equations (table 2.4) are proposed for the shear resistance of the joint for smooth and rough interfaces.

Table 2.4: Shear resistance of pumice lightweight aggregate concrete-UHPFRC joints [Papanicolaou et al. 2002].

$\tau_{fu} = 1.7 \cdot \sqrt{f_{lct,d}} + 0.3 \cdot (\rho_{sw} \cdot f_{yd} + \sigma_{cd})$ (N/mm^2), smooth interfaces

$\tau_{fu} = 1.4 \cdot \sqrt{f_{lct,d}} + 0.45 \cdot (\rho_{sw} \cdot f_{yd} + \sigma_{cd})$ (N/mm^2), rough interfaces

$f_{lct,d} = 0.2 \cdot f_{lck}^{\,2/3} \cdot [0.4 + 0.6 \cdot (\rho / 2200)] / 1.5$ (N/mm^2)

$f_{lct,d}$ = design tensile strength of pumice lightweight concrete
f_{lck} = charactersistic compressive strength of lightweight concrete
ρ = oven-dry density of pumice lightweight concrete in kg/m^3
ρ_{sw} = steel ratio
f_{yd} = design yield stregth of steel reinforcement
σ_{cd} = design value of compressive stress at the interface by external force

Concrete-cement grout interfaces

Shear transfer along concrete-cement grout interface has been studied by Thomann [Thomann 2005]. For this type of interfaces several direct shear tests were executed with a normal stress at the interface that varied between 0.6 and 1.5 N/mm^2. The concrete surface was casted with a retarding agent and then roughened by hydro-jetting in that way that the aggregates were well protruding but firmly fixed in the matrix. The cement grout used was a product of VSL Company, a typical cement grout used for prestressing tendons with compressive strength about 90 N/mm^2. The failure criterion proposed for the ultimate shear resistance is a Coulomb type equation, described in table 2.5. The first term corresponds to the adhesion and interlocking of the interface, whereas the second term accounts for the contribution of friction. Further experimental work is needed in this field in order to investigate the failure criterion at higher levels of confinement such as 4 and 5 N/mm^2. Higher level of confinement is more likely to be developed at connections consisting of this type of interfaces, at ultimate limit state. This is shown later in the 5th chapter.

Table 2.5: Shear resistance criterion for concrete-cement grout interface [Thomann 2005]

$\tau_{max} = c + d \cdot \sigma$ (N/mm^2) $\quad \sigma \leq 1.5$ N/mm^2
τ_{max} = maximum shear stress in the interface σ = normal stress at the interface c = 0.94 N/mm^2 d = 2.28

2.1.2 Steel-cement grout interfaces

Even though steel-concrete interfaces are widely studied, only few studies exist about steel-cement grout interfaces. The majority of studies mainly concern grouted pile-to-sleeve connections, figure 2.3, used on typical offshore platforms. Lamport [Lamport 1988] investigated the different parameters that influence bond resistance. The study shows increased bonding stress with increased compressive resistance of grout and increased confinement stress. Increasing the shear key height or decreasing spacing of shear keys increases connection strength. There is however an optimal shear key height for given spacing, beyond which connection strength decreases due to a combination of high axial and shearing stresses in the grout.

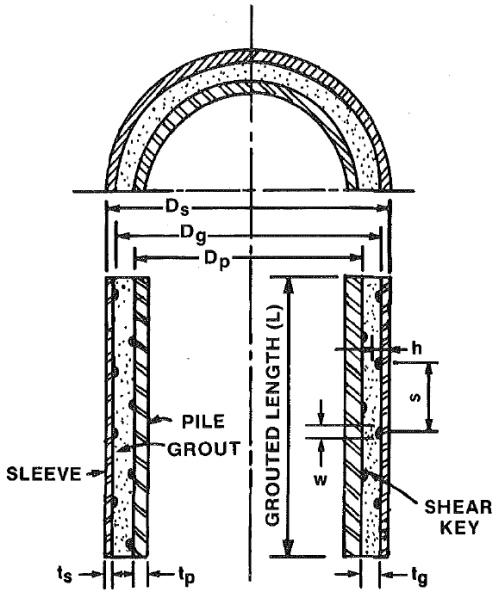

Fig. 2.3: Pile-to-sleeve connection [Lamport 1998]

Equations proposed from American Petroleum Institute [API 2000] and from the Offshore Technology Report 2001/016 of the Health and Security Executives [Health & Security Executives: Pile/Sleeve Connections 2002] are empirical and apply only to the certain geometry of the connection.

Thomann [Thomann 2005] studied also embossed steel-cement grout interfaces. Direct shear tests were executed with a normal stress at the interface that varied between 0.6 and 2 N/mm^2, for the case of high strength cement grout. The embossed steel plates were of steel S235 and their type was BRI 8/10 according to Construction Table C5/05 of the Swiss Centre of Steel Construction [C5/05 SZS 2005]. Figure 2.4 illustrates the geometry of the steel plate ribs. The cement grout, as for the tests in concrete-grout interface, was a product of VSL Company with compressive strength about 90 N/mm^2. Again a Coulomb type failure criterion is proposed, presented in table 2.6.

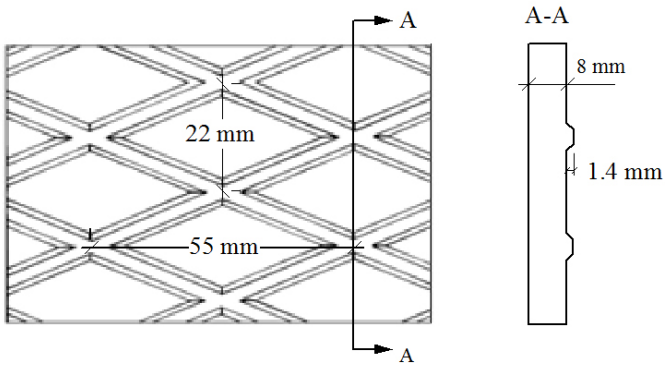

Fig. 2.4: Geometry of the steel plate ribs, type plate BRI 8/10 [C5/05 SZS 2005]

Table 2.6: Shear resistance criterion for embossed steel-cement grout interface [Thomann 2005]

$\tau_{max} = c + d \cdot \sigma$ (N/mm^2) $\quad \sigma \leq 2.0$ N/mm^2
τ_{max} = maximum shear stress in the interface σ = normal stress at the interface c = 0.94 N/mm^2 d = 1.96

2.1.3 Remarks

Several remarks can be done on the above mentioned studies on the different types of interfaces. The majority of the models presented describe the interface behaviour by proposing only a *failure criterion* for the shear resistance. Some models [Tassios 1987, fib Model Code 2010 and Thomann 2005] provide more information which is needed to better describe the behaviour of the interfaces. This supplementary information includes the shear-stress slip relationship, hereafter referred to as *constitutive law*, and the uplift-slip relationship, hereafter called the *kinematic law*. Especially for the case of concrete-cement grout and embossed steel-cement grout interfaces, which are found in connections by adhesion, interlocking and friction, the shear-stress slip relationship proposed by the existing model is limited to the failure slip; no models exist for the post-failure behaviour towards to the remaining pure frictional resistance of the interface.

Furthermore, it may be added that tests performed by Thomann, with high strength cement grout, were limited to a confinement of 1.5 N/mm^2 for the concrete-cement grout interface and to 2 N/mm^2 for the steel-cement grout interface. As will be presented later, the confinement effect to the interfaces of the connections by adhesion, interlocking and friction reach higher normal stresses.

Finally no research exists for UHPFRC-cement grout interface. All this information creates the frame, for the direct monotonic shear tests program, that needs to be executed during this project, for the interfaces that constitute the proposed connections. In the experimental part of this study, three types of interfaces will be tested, two of them for a confinement up to 5 N/mm^2 and the third for a confinement up to 4 N/mm^2.

2.2 Shear resistance of interfaces under cyclic loading

Cyclic or fatigue loading of interfaces occurs in many civil engineering constructions such as offshore platforms and bridges. Earthquake loading can also be approached as a combination of several high and low amplitude cycles fatigue loading. As for bridges, they are being submitted during their lifetime to numerous cyclic loading with different amplitudes. Consequently understanding the behaviour of interfaces under cyclic loading is necessary in order to develop safe design procedures.

2.2.1 Interfaces between different concrete types, including cement grouts

The work of Tassios [Tassios et al. 1987] concerning concrete-to-concrete friction, under cyclic loading, is pioneered in the field. Yet, the displacements imposed during testing resulted in shear stresses exceeding their elastic domain and created large permanent plastic deformations, thus concerning earthquake loading and not fatigue under service loads. fib Model Code 2010 [fib Model Code 2010] suggests no degradation of concrete-to-concrete friction for fatigue loading, in condition that the concrete surface is rough, good bonded and provided that no cracks appear in the interface. For poor bonding conditions and smooth surfaces a reduction up to 40 % of the shear resistance of a monolithic member is proposed by the model for cyclic loading.

Research on concrete-UHPFRC interfaces is currently being studied by Makita in the Civil Engineering Institute of EPFL. No referenced exist for cyclic loading of concrete-cement grout and UHPFRC-cement grout interfaces.

2.2.2 Steel-cement grout interfaces

As mentioned above, steel-cement grout interfaces are often found in the grouted pile-to-sleeve connections used to fix offshore structures to the seabed. Experimental investigation performed by Anders [Anders 2007] at interfaces with steel shear keys and high strength cement grout has shown that, as long as the stress range is kept below 0.5 times the limit of elastic behaviour, as defined in figure 2.5, grouted pile-to-sleeve connections exhibit no failure for more than one million cycles

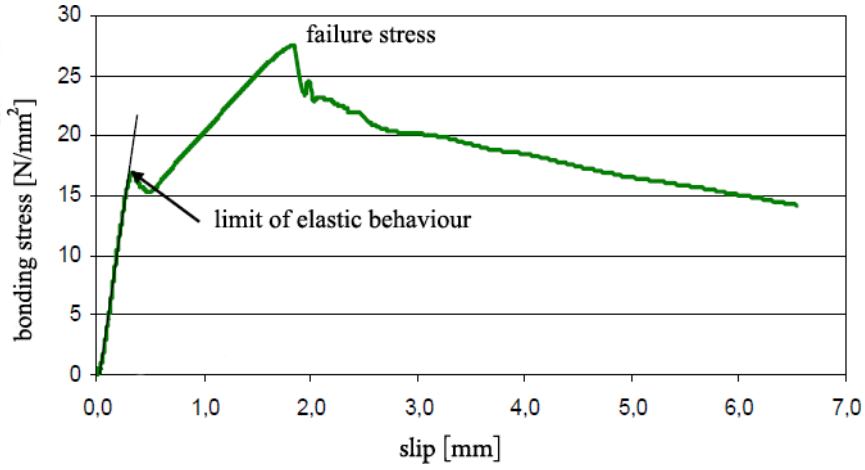

Fig. 2.5: Bonding stress versus slip for a grout pile-to-sleeve connection joint, type of cement grout C150, embossment height versus spacing h/s=0.056 [Anders 2007]

During cyclic loading a residual slip in the interface was observed and was accumulated with the number of cycles. Failure in the interface happened when the slip reached the value of the slip for failure at monotonic loading. In this type of connection, the value of slip which corresponds to the end of the elastic domain ranged between 0.3 and 0.5 mm whereas the slip at failure of the interface

exceeded the value of 1.5 mm. The ductility of the connection is due to the confinement effect imposed by the steel tubes.

2.2.3 Remarks

The existing reference concerning concrete-concrete interfaces subjected to cyclic loading concern generally the domain of large displacements. For cyclic loading under service loads no degradation of the shear resistance is considered provided that the surfaces are rough and no crack propagation occurs. No experimental evidence exists for rough concrete-cement grout interfaces and UHPFRC-cement gout interfaces. Consequently, the experimental investigation of this project should include the cyclic loading of these types of interfaces that are formed in the new connections.

Concerning steel-cement grout interfaces, cyclic loading tests on specimens with shear keys and high strength cement grout show that residual slip accumulates. Failure occurs when the slip accumulation reaches the value of the failure slip for monotonic loading. Similar behaviour is expected for the embossed steel-cement grout interface used in the proposed connection. Since no cyclic tests were performed so far for this interface, such tests will constitute an important part of the experimental study.

2.3 Development of composite steel-concrete bridges with innovative connections

Road bridges are the most important carrier for the transport of people and goods in Europe [Naumann 2006]. The traffic density is continuously growing. Existing bridges were not designed for high service loads and the current amount of traffic. Updating the traffic network requires the construction of new bridges and reconstruction or replacement of the deck in existing bridges. Fast erection is required to diminish the direct and indirect costs created by traffic interruption and diversion. Steel-concrete composite bridges are a promising solution since they allow prefabrication of the steel girder and the reinforced concrete deck; however, innovative steel-concrete connections should be developed to comply with the demand of fast erection and the necessity of increased bearing capacity. Innovative connections should also be able to work well with advanced materials such as UHPFRC that present increased interest for applications due to their long term durability [Project MIKTI 2008].

2.3.1 Innovative connections

Several types of innovative connections have been developed the last years. Bouazaoui et al. [Bouazaoui 2006, 2008] studied the connection between steel girders and concrete decks through bonding of an epoxy adhesive layer. It is a favorable method for prefabrication and relatively easy in execution. Bending tests on composite beams of this type, conducted at the *Université de Reims*, proved that the design rules, proposed in Eurocode 4 [EC4 2005] for total interaction, were applicable herein [Bouazaoui 2006]. Fatigue tests on adhesively bonded connections were executed at *Université Lyon 1* [Project MIKTI 2008]. A Wöhler curve was produced for the epoxy adhesive joint and is described by the following equation:

$$\tau_{adh} = 6 - 0.484 \cdot \log(N) \tag{2.1}$$

Where τ_{adh} is the shear stress applied to the bonded joint and N the number of cycles.

Several issues of great importance, such as the technological placement processes, need to be examined before applying the system in engineering practice.

An innovative connection was studied by Jurkiewiez [Jurkiewiez 2009] and concerns the use of steel beams with their web embedded in the slab. This process consists of removing the upper flange of the metal profile section and then cutting the upper part of the web in the form of slots to be embedded into the slab, on which horizontal thrust (rods) are supported, as indicated in figure 2.6.

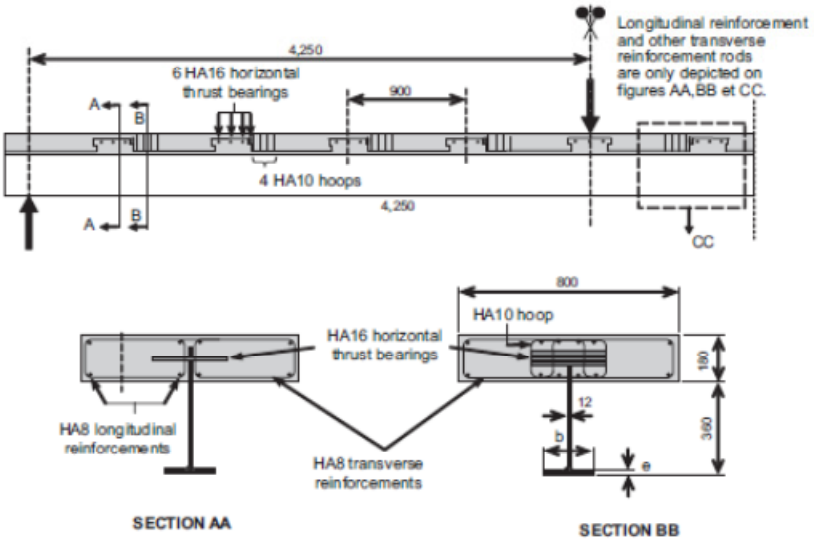

Fig. 2.6: Geometry of test beams with web openings [Jurkiewiez 2009]

Force transmission between the slab and profile section is achieved by the horizontal thrust bearings embedded in the reinforced concrete. Test results indicate that the beams exhibit behavior analogous to the case of composite beams fitted with studs, and in particular feature considerable ductility. In addition the assembly had satisfactory behaviour in fatigue, despite the development of cracks in the web. The use of the system in practice is compatible with a concrete operation over the entire slab thickness, where formwork is needed, or with partial prefabrication, followed by a second phase of concreting [Jurkiewiez 2009]. The system's application is limited to small span bridges [Project MIKTI 2008].

Another similar solution for both small and medium span bridges is the VFT and VFT-WIB® girder, illustrated in figures 2.7 and 2.8 respectively, which were developed by SSF engineering consultancy [Schmitt et al. 2004, Lorenc et al. 2008, Günter 2009].

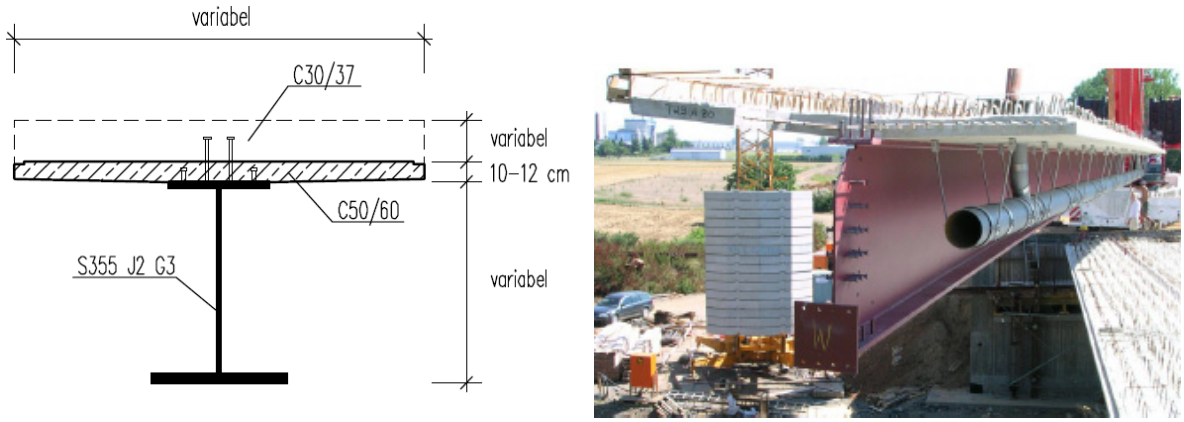

Fig. 2.7: VFT girder [Schmitt et al. 2004]

Fig. 2.8: VFT-WIB girder [Lorenc 2008]

The VFT girder consists of a steel beam equipped with shear studs to ensure composite action and a prefabricated concrete flange with a thickness 10-12 cm. The VFT-WIB girder is characterized by the absence of both shear studs and upper steel flange. The composite action is ensured by steel dowels created on the steel web by cutting a steel profile in two. In both types of girders, steel reinforcement exceeds the prefabricated concrete flange in order to connect with the cast-in place concrete. These types of girders are adapted to modular construction and allow fast erection. The second type with steel dowels performs sufficiently under fatigue loading [Feldmann et al. 2008] and in addition, can be used in construction with high strength materials-steel S460 and UHFPRC-when high performance and durability is needed by design [Rauscher and Hegger 2008]. However, it has not be noted, that bridge construction with these systems requires supplementary in-site concreting, concerning both the finalization of the concrete deck, the connection of modules and the continuity of the spans at intermediate supports.

2.3.2 Connections by adhesion, interlocking and friction

In comparison with the above mentioned innovative connection systems, connections by adhesion, interlocking and friction allow full prefabrication without additional concreting. The prefabricated slabs are connected together using an epoxy resin, figure 2.9, and applying longitudinal prestressing. Injection of high strength cement grout follows and once the grout is hardened, the composite action is present and the bridge can begin to service.

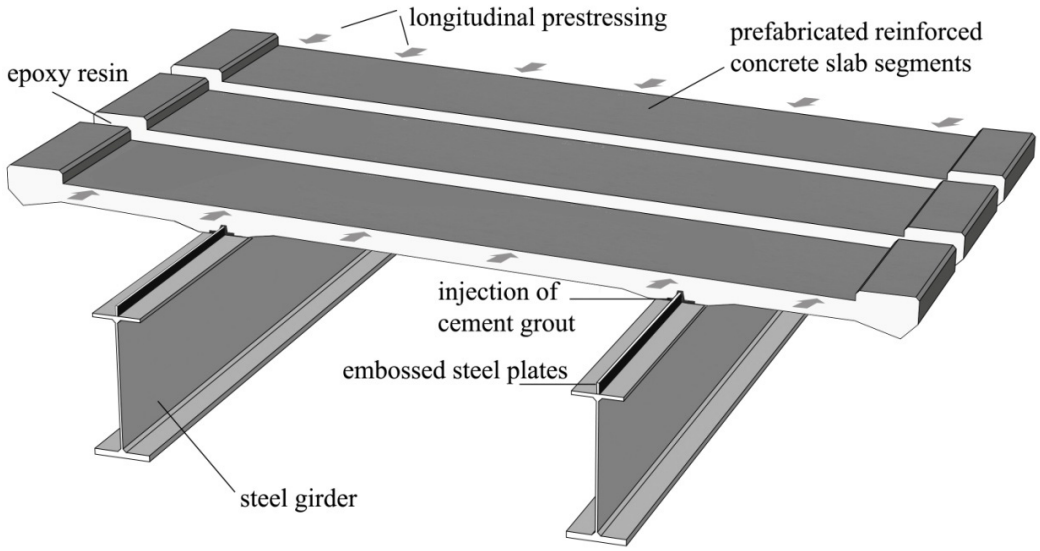

Fig. 2.9: Prefabricated deck segments positioned over steel girders

The resistance of the connection to longitudinal shear is based on the shear that is developed at two types of interfaces, as illustrated in figure 2.10. The two types include an interface between the embossed steel and the cement grout and an interface between cement grout and the material of the inner rib of the deck, either roughened concrete or UHPFRC. The contribution of the friction in the interface between the upper steel flange and the cement grout is neglected.

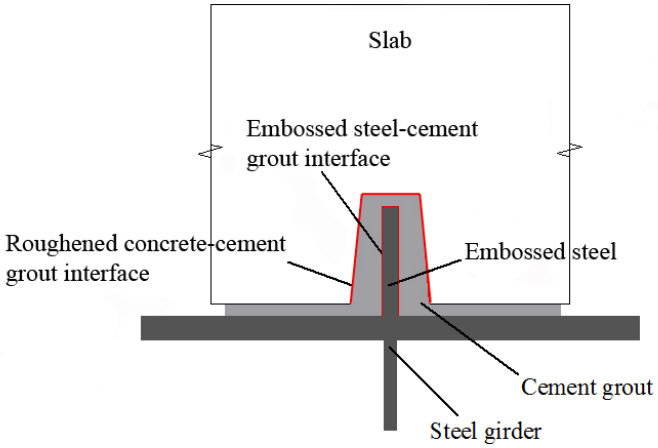

Fig. 2.10: Interfaces formed in the connection [Thomann 2005]

Due the development of the longitudinal shear in the connection, interfaces tend to slip. Because of the roughness of the interface, this slip, *s*, is accompanied by a separation of materials, uplift, *u*, at a direction normal to the slip, *s*. An equilibrium state is developed with tension in the concrete and the reinforcement over the connection and normal compression stresses, called hereafter confinement stresses, to the interfaces. Figure 2.11 illustrates the equilibrium state caused by the uplift in the embossed steel-cement grout interface. Equally, uplift between roughened concrete and cement grout is also developed but not presented at this figure.

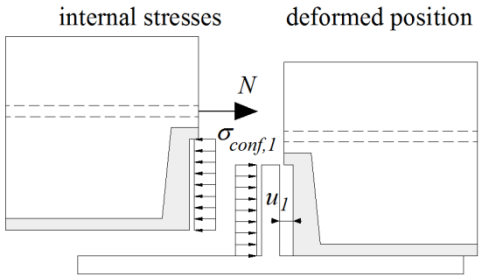

Fig. 2.11: Development of confinement stresses [Thomann 2005]

Thomann [Thomann 2005] takes into account this confinement effect by proposing a linear relationship between the confinement stress and the total uplift of the two interfaces, equation (2.2):

$$\sigma_{conf} = k_{slab} \cdot u \tag{2.2}$$

The concrete's resistance to tension is neglected. The slab is considered cracked. The term k_{slab}, which expresses the slabs translational stiffness, is in this case a constant, depending on the geometry of the slab and the positioning of the reinforcement (figure 2.12). The equation proposed (2.3) corresponds only to a specific reinforcement ratio equal to 1.31 mm^2/m.

$$k_{slab} = \frac{E_C \cdot h_3 \cdot}{33 \cdot h \cdot h_1} \left(\frac{h_2 + h_3}{h_2} \right)^{0.3} \tag{2.3}$$

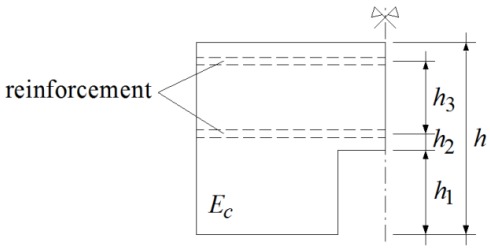

Fig. 2.12: Notations of the slab geometry [Thomann 2005]

In equation (2.2) the confinement stresses is increasing continuously with increasing uplift, which may be unsafe for the case in which the confinement stress calculated exceeds the provided normal stress which is limited due to yielding of the reinforcement. In order to predict the force-slip relationship for the new connections with higher accuracy and more safety, a new confinement relationship should be developed. This model, besides the geometry of the slab and the positioning of reinforcement, should take into account the concrete quality, concrete characteristics prior and after cracking (so as to apply both for SLS and ULS), the possibility to apply variable reinforcement ratio, and it should impose an upper limit for the value of the developed confinement stress. This limit should correspond to the yielding of the reinforcement.

It should be also noted that normal stresses in the interface, $\sigma_{ext,i}$, can be developed also due to transversal prestressing, in case of wide cantilever bridge decks, and due to the transversal bending of the bridge deck, caused from external loads, acting after the realization of the connection (figure 2.13). Such loads are the dead load from the asphalt covering of the bridge, from cornice and barrier and traffic load as well.

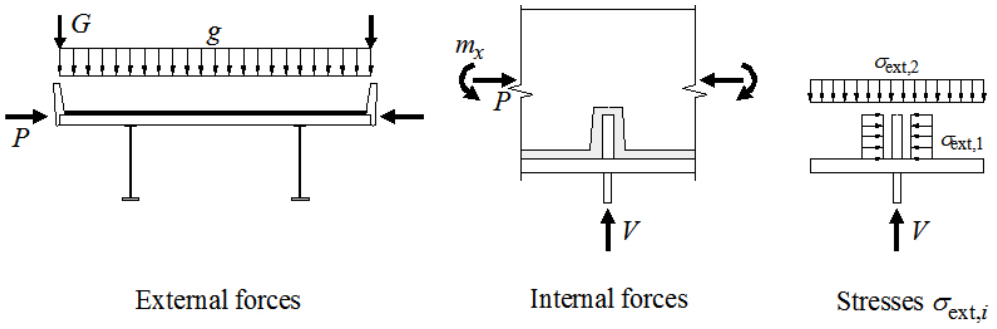

Fig. 2.13: Development of normal stresses on the interfaces due to the transversal bending of the bridge deck [Thomann 2005]

2.4 Longitudinal shear

Any type of connection between concrete decks and steel girders in composite bridges is submitted to longitudinal shear. Besides longitudinal shear, connections are submitted also to other types of actions as tension to prevent vertical uplift of the slab. In certain cases, connections can be locally submitted to concentrated longitudinal shear forces, at the extremity of the bridge due to shrinkage or temperature variation between slab and girder, prestressing acting only to the slab or only to the girder, or local actions introduced by local changes in geometry, as is the case at nodes of truss girders or nodes of frame composite bridges [Lebet and Hirt 2009].

Concerning composite bridges constructed with the proposed new connection, it is justified to neglect the effect of shrinkage in the connection since the slabs are prefabricated. The connection is submitted to longitudinal shear resulting from i) loads acting after the realization of the connection-such as dead loads from coating, cornice and safety barrier, thermal gradient and traffic loads- and ii) actions from removing provisory supports, that may be used during construction.
Longitudinal shear is controlled at the following limit states:

- Serviceability limit state, SLS
- Ultimate limit state, ULS
- Fatigue limit state, FLS

The following paragraphs present the values of the longitudinal shear acting in the connection for the different limit states. For the SLS and the ULS the values are obtained by Thomann [Thomann 2005]. For the FLS the values are obtained by the author's study. For the calculation of the longitudinal shear force, a database of 12 twin I-girder composite bridges [Jaunin 1996] is considered. From these bridges, 11 have main spans varying from 32 to 57 meters and one bridge has a main span of 128 meters. In order to calculate the longitudinal shear, the following considerations are made:

- Bridges are continuous twin I-girders with the several spans, of which the end spans have a length equal to 70 % of the internal spans.
- The bridge deck width varies from 10 to 15 m.
- Bridges are considered unsupported by provisory support during construction, resulting that connection is submitted to loads acting after the realization of the connection.
- For SLS and ULS, the Load Model 1 of Swiss code SIA 261 [SIA-261 2003] is taken into account.
- For FLS, the Load Model 1 of Swiss code SIA 261 [SIA-261 2003] and the load model of Meystre and Lebet [Meystre and Lebet 2011] are taken into account.
- The transverse influence line has the values 0.9 and 0.1 at the positions of the two steel girders.
- A coating of 100 mm is taken into account, whereas a load of 10 kN/m per side is considered for the dead load of the cornice and the safety barrier.
- Sections at internal support are considered cracked. However, so as to account for tension stiffening, the longitudinal shear calculated at these sections is multiplied with a factor n_v= 1.02 according to research performed by Gomez [Gomez 2000].
- A temperature difference between slab and steel girder is considered equal to + 12°C, for SLS and ULS.
- For the connections at the internal supports, the thermal gradient does not create longitudinal shear force [Ducret 1997]

Serviceability limit state [Thomann 2005]

The following figure presents the required resistance to longitudinal shear force per unit length due to quasi-permanent (long term) loads, $v_{long} = v_{Ed} \cdot \gamma_v$, acting after the realization of the connection.

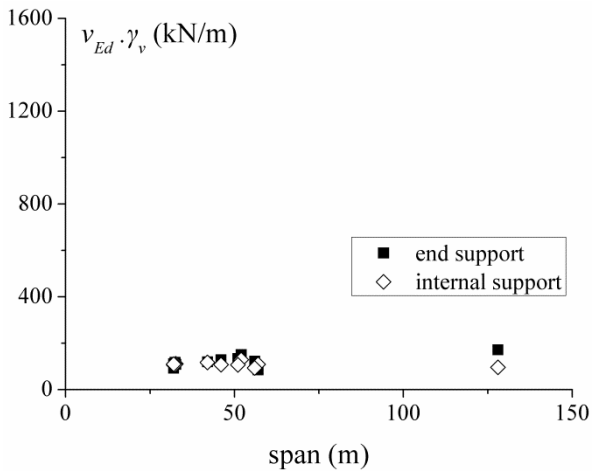

Fig. 2.14: Required resistance to longitudinal shear force per unit length due to long term actions at SLS [Thomann 2005]

Longitudinal shear varies between 85 to 170 kN/m for connections close to the end supports of the bridges, and between 93 to 130 kN/m for the connections at internal supports. A mean value of 150 kN/m was used by Thomann [Thomann 2005] for creep tests on the innovative connections. The values presented in figure 2.14 correspond also to an inferior value of the longitudinal shear force per unit length for cyclic loading of connection.

Figure 2.15 illustrates the required resistance to the longitudinal shear force per unit length, for the occasional load case, for loads acting after the realization of the connection. For this loading case, according to annex B of Swiss Code 260 [SIA-260 2003], the reduction factor for the occasional value ψ_0 is equal to 0.75 for traffic load and 0.60 for the thermal gradient. For dead loads the partial factor γ_g applied is equal to unity.

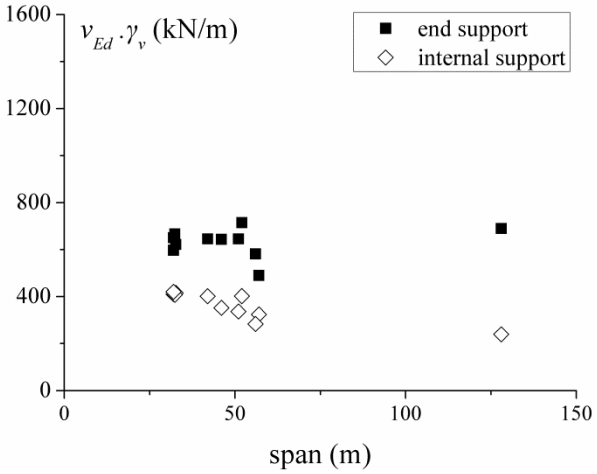

Fig. 2.15: Required resistance to longitudinal shear force per unit length for the occasional load case at SLS [Thomann 2005]

Figure 2.15 shows that in order to satisfy the verification at SLS the connection's behaviour should remain elastic for longitudinal shear of a maximum value of 750 kN/m. As expected the longitudinal shear reaches higher values to end supports in comparison with the internal supports.

Ultimate limit state [Thomann 2005]

Elastic Method

For the case where the composite structure does not enter the plastic domain, longitudinal shear at ULS is calculated with the elastic method. Verification at ultimate limit state is performed then according to equation (2.4).

$$v_{Rk} \geq v_{Ed} \cdot \gamma_v \tag{2.4}$$

$$v_{Ed} = \sum \frac{V_{Ed,i} \cdot S_{c,i}}{I_{b,i} \cdot n_{el,i}} + v_{\Delta T} \tag{2.5}$$

v_{Rk} : characteristic value of resistance to longitudinal shear force per unit length
v_{Ed} : design value of longitudinal shear force per unit length calculated with equation (2.5)
γ_v : partial factor for resistance of connection, γ_v = 1.25 [SIA-264 2003]
$V_{Ed,i}$: shear force due to load i acting after the realization of connection
$S_{c,i}$: first moment of inertia of the slab calculated from the neutral axis of the composite section
$I_{b,i}$: second moment of inertia of the composite section calculated with the corresponding modular ratio $n_{el,i}$
$n_{el,i}$: modular ratio for load i
$v_{\Delta T}$: longitudinal shear force per unit length due to thermal gradient ΔT

The value of $v_{\Delta T}$ is calculated with equations (2.6) and (2.7), [Lebet and Hirt 2009]

$$v_{\Delta T} = \frac{A_a}{b_{eff}} \cdot \left(\frac{N_{\Delta T}}{A_b} + \frac{M_{\Delta T}}{I_b} \left(z_b - z_a \right) \right) \tag{2.6}$$

$$N_{\Delta T} = a_{th} \cdot \Delta T \cdot E_{C0} \cdot A_C \quad \text{and} \quad M_{\Delta T} = N_{\Delta T} \left(z_c - z_b \right) \tag{2.7}$$

A_a : area of steel section
A_c : area of concrete section for width equal to b_{eff}
A_b : equivalent area of the composite action, $A_b = A_a + A_c/n_0$
n_0 : modular ratio for short term
$N_{\Delta T}$: normal force to the composite section due to thermal gradient ΔT
$M_{\Delta T}$: bending moment to composite section due to thermal gradient ΔT
z_a : position of centre of gravity of steel section
z_c : position of centre of gravity of concrete section
z_b : position of centre of gravity of composite section

The characteristic value of resistance to longitudinal shear force per unit length, for the bridges examined and for the zones close to support, is presented in figure 2.16. The zones at mid-span have lower shear force and hence lower longitudinal shear than zones closes to supports, thus they are not examined.

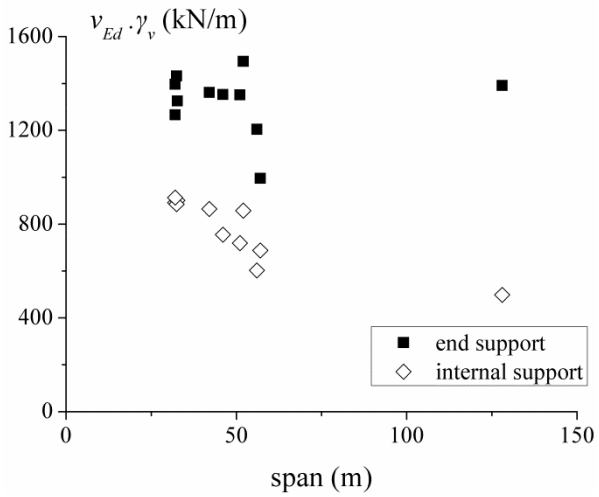

Fig. 2.16: Characteristic value of resistance to longitudinal shear force per unit length, $v_{Rk} = v_{Ed} \cdot \gamma_v$ [Thomann 2005]

The figure shows that v_{Rk} should reach higher values for the connection at end supports. It is also noted that, for end supports, the span length does not influence the value of v_{Rk}. The maximum value of resistance to longitudinal shear force per unit length is 1500 kN/m.

Plastic Method

For composite beams which develop plastic moment at ULS, the longitudinal shear force per unit length, for the length of the beam span with positive moment where the plastification occurs, is not proportional to the shear force acting on the composite section. For this zone the characteristic value of resistance to longitudinal shear force per unit length has a mean value which is given by equation (2.8) [Lebet and Hirt 2009]. For the zones close to support the plastic method does not apply.

$$v_{Rk} = \frac{N_{c,d} - N_{c,el}}{x_{pl}} \cdot \gamma_v \tag{2.8}$$

$N_{c,d}$: normal force acting to the slab on the position of maximum moment
$N_{c,el}$: normal force acting to the slab on the position where the plastification initiates
γ_v : partial factor for resistance of the connection, γ_v = 1.25 [SIA-264 2003]
x_{pl} : length of the beam from the position where plastification initiates till the position of the maximum moment.

Appling this method to the bridges examined results in a maximum value for v_{Rk} equal to 1600 kN/m. It is noted that application of equation (2.8) corresponds to ductile connections according to Eurocode 4, part-1 [EC4 2005].

Fatigue limit state [New development by the author]

Fatigue verification can be performed, according to code SIA 261, with respect to the fatigue limit, equation (2.9) or with respect to equivalent load range at 2 million cycles, equation (2.10).

$$\Delta v_D \geq \Delta v\left(Q_{fat}\right) \cdot \gamma_{fat} \tag{2.9}$$

$$\Delta v_C \geq \Delta v_{E2} \cdot \gamma_{fat} = \lambda \cdot \Delta v\left(Q_{fat}\right) \cdot \gamma_{fat} \tag{2.10}$$

Δv_D : constant amplitude fatigue limit for longitudinal shear force per unit length
Δv_C : fatigue resistance to longitudinal shear force per unit length for 2 million cycles
Δv_{E2} : equivalent longitudinal shear force range per unit length for 2 million cycles
$\Delta v(Q_{fat})$: variation of longitudinal shear force per unit length due to traffic load Q_{fat}
γ_{fat} : partial factor for fatigue strength
λ : correction load factor

Equation (2.9), implies that if variation of longitudinal shear force per unit length applied remains below the fatigue limit for the entire service life, failure will not occur.

Equation (2.10), implies that the equivalent longitudinal shear force range per unit length for 2 million cycles should not exceed the design fatigue resistance for 2 million cycles.

The calculation of internal forces needed to define the variation of longitudinal shear for fatigue is done with the elastic method using fatigue load model 1, Q_{fat} , of Swiss code SIA 261 [SIA-261 2003]. The volume of traffic considered is that of a highway with 70 years of service life. For sections to the end supports, within 3 meters from the carriageway joint, traffic loads are multiplied by a dynamic amplification factor Φ. Swiss code SIA 261 proposes Φ equal to 1.3. Recent research performed by Brühwiler and Lebet [Brühwiler and Lebet 2010] concerning existing bridges and by Gonzalez et al. [Gonzalez et al. 2011] concerning dynamic amplification for shear force, prove that this value is conservative for fatigue limit state. Based on these studies the value of 1.2 is used for the dynamic amplification factor Φ at FLS. The partial factor for fatigue strength, γ_{fat} , is considered as 1.15, according to Swiss code SIA 261. The correction load factor λ is valid for composite bridges with shear stud connection. Consequently the proof with respect to equivalent longitudinal shear range at two million cycles, using the correction load factor λ according to the code SIA 261, cannot be applied to the new connection, the S-N curve of which is unknown. For this reason verification in fatigue will be performed with respect to the fatigue limit.

Applying the fatigue load model 1 (code SIA 261) to sections of twin I-girder composite bridges, from a database of Swiss highway bridges with spans from 30 to 120 meters and considering γ_{fat} equal to 1.15, we obtain a maximum variation of longitudinal shear force per unit length equal to 400 kN/m at the fatigue limit (figure 2.18 a). Adding the value v_{min} (figure 2.14) to account for longitudinal shear in the connection due the permanent loading, we obtain the maximum longitudinal shear force per unit length v_{max} for cyclic loading at fatigue limit, which is equal to 530 kN/m.

However, it is found that the application of the fatigue load model 1 (code SIA 261) does not exclude certain cases of real traffic where the longitudinal shear force may exceed the value of 530 kN/m. In order to be consistent with the definition of fatigue limit, a higher variation of longitudinal shear and a higher v_{max} should also be taken into account.

Meystre and Lebet [Meystre and Lebet 2011] based on recordings concerning real traffic on eight bridges around Switzerland, for the period 2003 to 2009, calculated the 99% fractile values of trucks over 40 tones and propose hereafter a deterministic model of two typical heavy trucks. According to that model the two typical trucks are located the one next to the other in two fictitious lanes, figure 2.17, with a total load 780 kN and 540 kN correspondingly, including a dynamic amplification factor of 1.3 and 1.2 respectively.

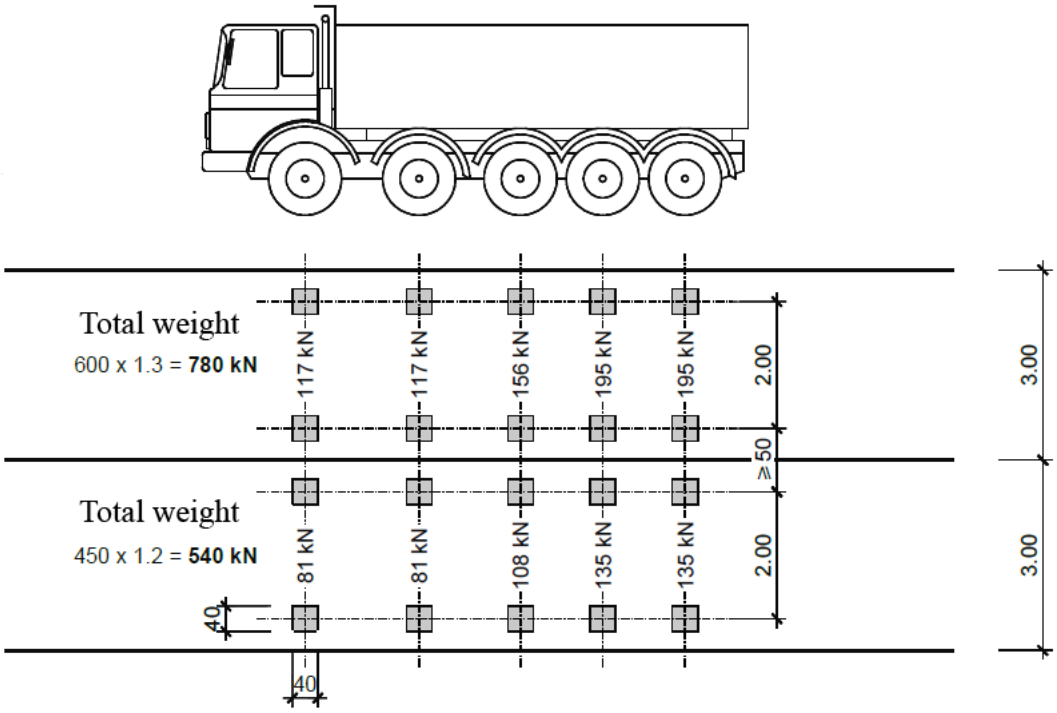

Fig. 2.17: Deterministic load model [Meystre and Lebet 2011]

Appling that model to sections of twin I-girder composite bridges, from a database of Swiss highway bridges with spans from 30 to 120 meters, and considering γ_{fat} equal to 1.15 results in a maximum variation of longitudinal shear equal to 670 kN/m (figure 2.18 b). This value is higher than the value proposed by the code SIA 261, fatigue load model 1. Finally the maximum value of the longitudinal shear force per unit length v_{max} for cyclic loading at fatigue limit is obtained by adding the value of 670 kN/m with the value 130 kN/m which is the longitudinal shear due to permanent loads acting in the connection after its realization. Hence v_{max} becomes equal to 800 kN/m.

Figure 2.18 presents the required resistance to the variation of the longitudinal shear at the fatigue limit according to a) fatigue load model 1, Q_{fat}, of code SIA 261 and b) considering heavy traffic [Meystre and Lebet 2011], for the connection at end supports as a function of the main bridge span.

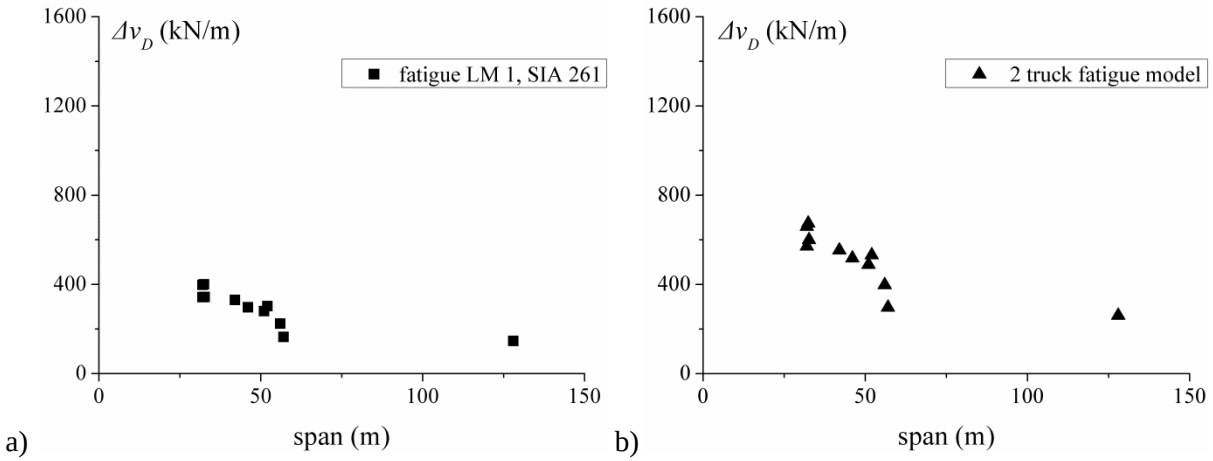

Fig. 2.18: Required resistance to longitudinal shear at the fatigue limit for end support connections using a) the fatigue load model 1 of code SIA 261 and b) a deterministic model with 2 trucks

The values presented in figure 2.18 will be chosen as the variation of the longitudinal shear force per unit length for the cyclic loading push-out tests performed in this project. The number of cycles to reach the fatigue limit is not known in advance for the new connection. Consequently and since the duration of tests is limited for practical reasons, if no failure occurs, tests will be stopped when no further damage in the connection by means of accumulated residual slip is possible. A static test will then follow the cyclic loading test in order to investigate the resistance at ULS after cyclic loading and define a ratio of the applied maximum cyclic load versus the ultimate resistance as a limit for safe design.

2.5 Conclusions

The state of the art shows that for innovative connections, the solutions proposed so far present several advantages for fast construction in comparison with older methods; however they either do not exclude supplementary concreting phases, as is the case for the VFT type girders, or they demand technological process issues to be solved, as is the case for bonding girders. Thus, the connection by adhesion, interlocking and friction, which reassures durability and is suitable for prefabrication, constitutes a very interesting alternative. The connection's resistance to longitudinal shear is based on the shear resistance of interacting confined interfaces that develop between different materials of the connection. However, before applying the new connection in engineering practice further investigation is needed.

State of the art in confined interfaces subjected to shear has shown that more experimental investigations are needed in order to define the behaviour of interfaces, especially concerning post-failure performance and the beneficial effect of confinement on the ultimate shear resistance. The importance of roughness in order to achieve high shear resistance values is also noted. So far investigation was limited for a confinement of up to 1.5 N/mm^2 for rough concrete cement grout interfaces and 2 N/mm^2 for embossed steel cement grout interfaces. No data exist for the UHPFRC-cement grout interface. Since the failure criterion, alone is inadequate to describe the connection's structural performance, constitutive and kinematic relationships in the interface should be recorded and should include the post-failure behaviour towards the remaining frictional resistance of the interface.

The following chapter presents in detail the experimental investigation performed in this project for various interfaces. Three types of interfaces, that constitute the innovative connections, will be examined in this project by means of direct shear tests: embossed steel-cement grout interface, roughened concrete-cement grout interface and finally UHPFRC-cement grout interface. Failure criterion for each interface under monotonic loading will be verified for a wide range of confinement stress, up to 5 N/mm^2 which is more likely to be developed, due to the confinement effect, at ultimate limit state.

Investigations are also necessary in the field of cyclic loading of interfaces in order to examine the development of the fatigue damage mechanism which is expressed, as found in literature for similar cases, with the development of an accumulated residual slip. Thus experimental investigation will include cyclic loading of interfaces by means of direct shear tests under confinement expected at the fatigue limit state. Data obtained will be used to propose analytical expressions for the residual slip as a function of the number of cycles.

The connection's longitudinal shear resistance to fatigue will be investigated by performing cyclic push-out tests. The loading range for proof with respect to the fatigue limit, according to fatigue load model 1 of code SIA 261 for the representative group of Swiss bridges, will vary between 130 kN/m to 530 kN/m. In addition to this verification since this value is likely to be exceeded in real traffic

situations a higher variation between 130 kN/m to 800 kN/m will also be applied. This variation is based on outgoing research for bridges in Switzerland, considering a deterministic model of two heavy trucks. Data from tests will be used to propose analytical expressions for the connection's residual slip, between the steel plate and the reinforced concrete blocks, with the number of cycles and define a ratio of the maximum applied cyclic load versus the ultimate resistance to be proposed for safe fatigue design.

The following table summarizes the required resistance to longitudinal shear force per unit length acting on the steel-concrete connection on the end support (abutment) of twin I-girder composite bridges. For the other sections along the composite beam, the longitudinal shear force is lower than the longitudinal shear force on the connection on the end support, with only exemption the areas of maximum positive moment where for the ULS and plastic calculation of the bending moment resistance the longitudinal shear force per unit length may reach up to 1600 kN/m considering ductile connection behaviour.

Table 2.7: Required resistance in longitudinal shear force per unit length, for different limit states, for connection on end support of twin I-girder of composite bridges.

Limit state	Required resistance in longitudinal shear force per unit length	Value
SLS	Permanent load	130 kN/m
	Occasional (rare) load	750 kN/m
ULS	Ultimate load-elastic method	1500 kN/m
FLS	Loading range for proof with respect to fatigue limit, according to fatigue load model 1 of SIA 261	400 kN/m
	v_{max} for proof with respect to fatigue limit, according to fatigue load model 1 of SIA 261	530 kN/m
	Loading range for proof with respect to fatigue limit, based on a deterministic model for 2 heavy trucks	670 kN/m
	v_{max} for proof with respect to fatigue limit, based on a deterministic model for 2 heavy trucks	800 kN/m

3. Experimental investigation

3.1 Introduction

This chapter presents the experimental investigation made in this research. Three types of specimens are tested: a) specimens of small blocks for direct shear tests in interfaces (section 3.2), b) large scale specimens for push-out tests of the connection (section 3.3) and c) a steel-concrete composite beam to be tested in bending (section 3.4). The goals of these tests are:

- Investigate, for three types of interfaces that are formed in the new connection, the laws that describe their resistance to shear and describe the kinematics. These laws are: a) the relationship between the ultimate shear resistance, τ_u, and the corresponding confinement stress, σ, called hereafter *failure criterion*, b) the relationship between shear stress in the interface, τ, and slip, s, called hereafter *constitutive law* and c) the relationship between the transversal separation, *uplift*, u, and the slip in the interface, hereafter refer to as *kinematic law*. Special attention is given in the post-failure.
- Study the influence of the cyclic loading on the interfaces in order to investigate the damage mechanism due to cyclic loading, such as the development of a residual slip in the interface.
- Study the influence of the cycle loading on the behaviour of connection.
- Provide data from push-out tests, on blocks fabricated with the new connection, in order to validate a model for predicting connections performance.
- Provide experimental justification of connection's performance in fatigue and investigate its remaining resistance at ULS, by means of a bending test of a steel-concrete composite beam.

3.2 Direct shear tests

3.2.1 Principles

Interfaces behaviour -i.e. the relationships between slip, s, uplift, u, shear stress, τ, and normal stress, σ- in an interface (figure 3.1) are investigated through a large number of direct shear tests.

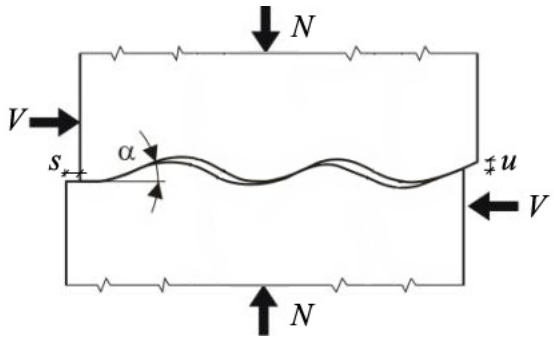

Fig. 3.1: Definition of physical quantities slip, s, and uplift, u, in an interface subjected to shear and normal force.

The two types of interfaces, the interface between embossed steel-cement grout and the interface between roughened concrete-cement grout, which are present in the new connection, are initially studied. Additionally, a third type of interface, the interface between, artificial roughened UHPFRC and cement grout is developed and studied, for the cases, as mentioned in 1.1, that the slab deck is made of UHPFRC.

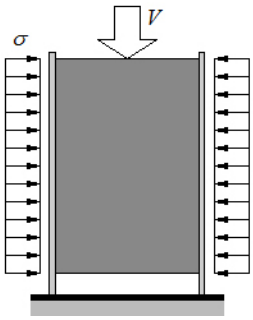

Fig. 3.2: Principal of the direct shear test used in this research [Thomann 2005].

The principal of the direct shear tests used is described in the figure 3.2. The force *V*, is applied to the specimen simultaneously with a normal force. The specimens are constituted of a block of cement grout which is casted between two embossed steel plates or two concrete or two UHPFRC plates. The vertical force *V* passes through the developed interfaces to the support of the specimen.

3.2.2 Specimens and materials

Three types of specimens are tested; their characteristics are presented in the figures 3.3 and 3.4.

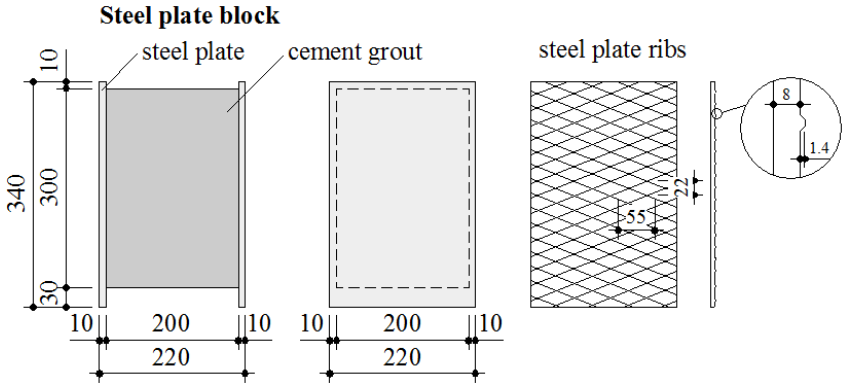

Fig. 3.3: Geometry of specimens with steel plates.

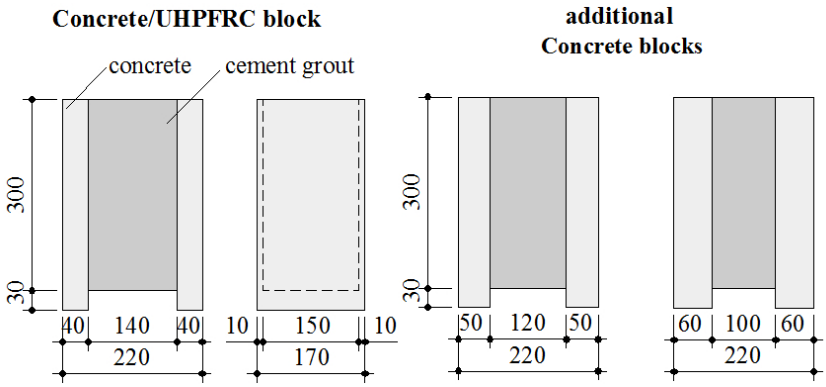

Fig. 3.4: Geometry of specimens with concrete or UHPFRC plates.

For tests with concrete blocks, plates with width that varies 40, 50 and 60 mm are used, to avoid cracking of concrete plates at high confinement stress and during cyclic loading.

The materials used at the direct shear tests specimens are as following:

- Steel plates are of type S235, sand-blasted. The embossed steel-plate conforms to type BRI 8/10 according to the construction table of the *Centre Suisse de la Construction Métallique* [C5/05 SZS 2005]. The ribs form rhombus, as illustrated at the figure 3.3 and the figure 3.5a, with 22 mm and 55 mm long diagonals. The ribs have a width of 5 mm and height of 1.4 mm.
- Cement grout is a commercial product provided by VSL-company, used to prestressing tendons, with a water to cement ratio varying from 0.28 to 0.33. Its compression resistance in cylinders (diameter 65 mm, height equal to 2xdiameter) varied from 80 to 132 N/mm^2. According to VSL-company the fluidity of the grout measured by performing the Marsh cone flow test is less than 25 sec [VSL 2002]. For cylinders, with resistance in compression 107 N/mm^2, the modulus of elasticity obtained is equal to 25800 N/mm^2.
- Concrete grade is C40/50 for the plates up to 50 mm width and C50/60 for plates with 60 mm width. Granularity is of maximum diameter 16 mm. The surface of the concrete plates is roughened by sand-blasting from a distance of 60 cm, with pressure 4.5 bars and for 40 seconds. The formwork used for the surfaces that are sand-blasted was covered with the retarding agent Pieri DRC 6/130. A typical roughened concrete plate is illustrated at figure 3.5b.
- UHPFRC. The DUCTAL© ready mixture is used, a product of Lafarge company, which contains 2% of volume fibers [Orange 1999]. The steel fibers have a length of 13 mm and a diameter of 0.2 mm. Since the finishing surface of this material is smooth an artificially roughened surface is created with regularly protruding cones of 8 mm height (figure 3.5c). This geometry can be achieved by using, as casting form, material like the plastic sheet DELTA-MS (figure 3.6), or by fabricating formwork, made of Teflon, with the opposite geometry. The geometry obtained, complies with the category 4, very rough, of the classification proposed by EC2 at paragraph 2.1.1. The choice of the product DUCTAL© is done since it is a typical UHPFRC already used in bridge engineering [Ghoneim et al. 2010] and can be used for decks for steel-UHPFRC composite bridges [Project MIKTI 2008].

(a) 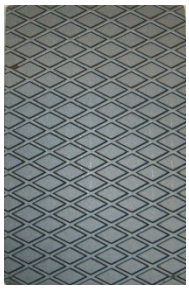 (b)  (c) 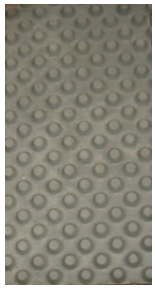

Fig. 3.5: Surfaces of plates for the direct shear block specimens a) embossed steel, b) roughened concrete, c) UHPFRC with conical studs

Fig. 3.6 : Form used to produce artificialy rough surfaces on UHPFRC with conical studs

3.2.3 Loading setup

The experimental setup, figure 3.7, is almost the same used also by Thomann [Thomann 2005]. The improvement consists of using, as shown in the figure 3.8, two load cells, situated underneath of each of the interfaces. Those load cells serve for the acquisition of the force that passes through each one of the interfaces.

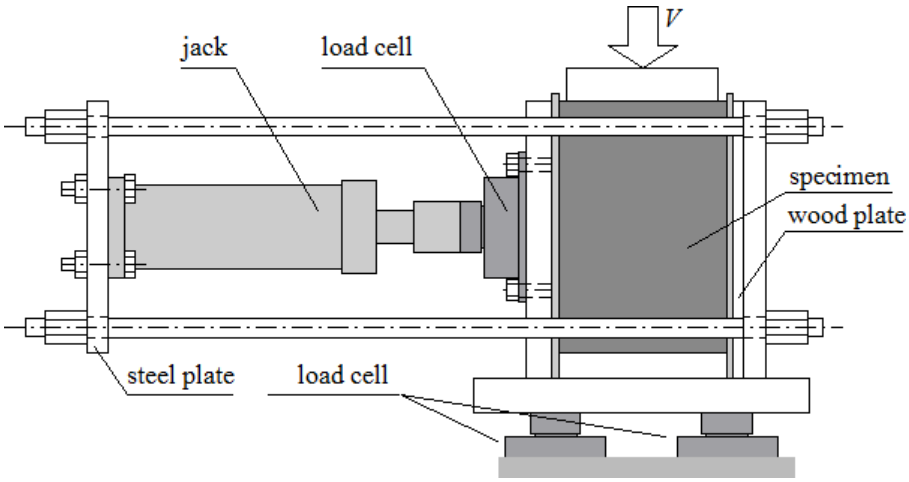

Fig. 3.7: Experimental setup for the direct shear test of a specimen with steel plates.

During the test, the interfaces are subjected to a constant normal stress, σ, applied by the horizontal hydraulic jack. A load cell, attached to this jack, allows the continuous measurement of the confinement force (figure 3.8). Shear force is applied under displacement control, while slip, in the interface, is increased until a failure and then until remaining shear frictional resistance is achieved.

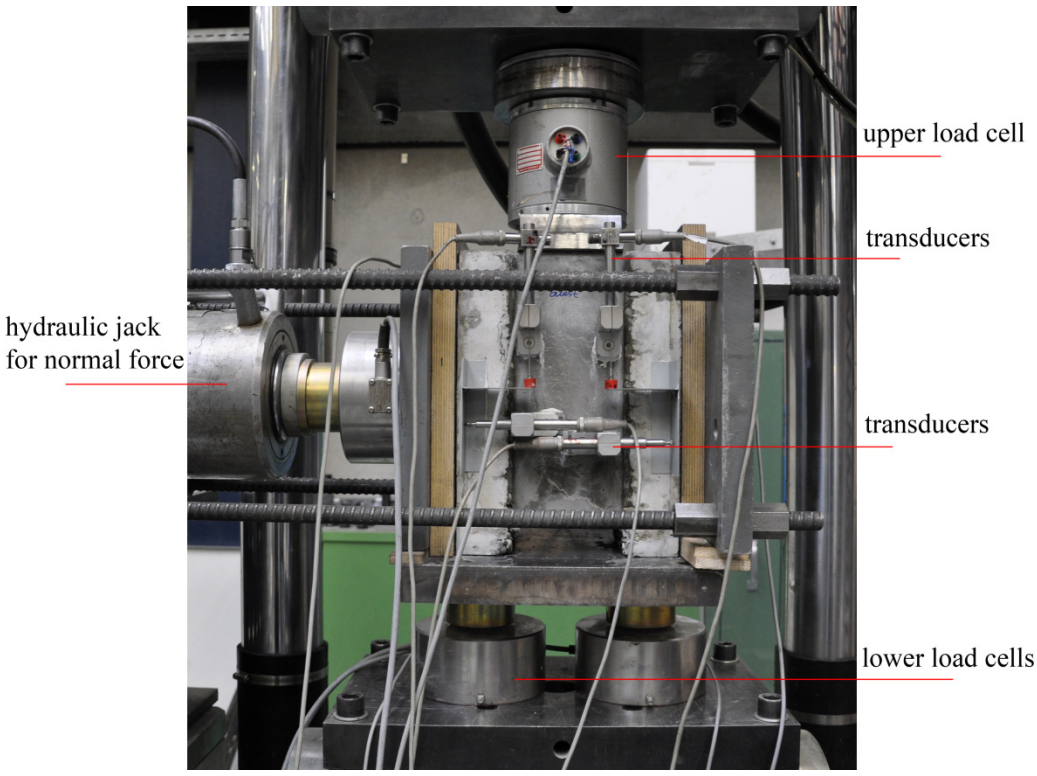

Fig. 3.8: Setup for the direct shear test of a specimen with concrete plates.

In addition to slip and shear force, the transversal separation (uplift, *u*,) of each plate from the cement grout block is measured. Figures 3.8 and 3.9 illustrate the instrumentation for measuring the slip and the transversal separation at each plate on a typical block, by means of inductive displacement transducers, type HBM [HBM 2000]. For each plate, two transducers, one at each side, are used to measure the slip, and two also to measure the uplift, located at mid height of the interface, for the slip, and located slightly lower for the uplift due to space limitation.

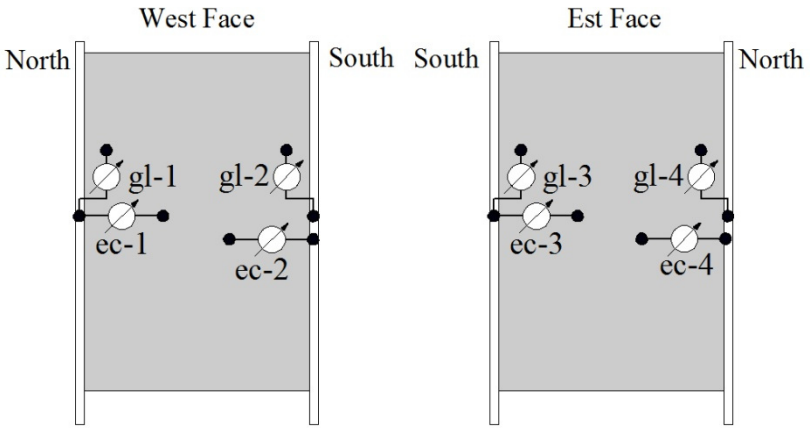

Fig. 3.9: Positioning of transducers for slip (gl-x) and uplift (ec-x) measurement on a typical block.

For the static direct shear tests of the interfaces, the load is applied with a velocity of 0.1 mm/min till failure, and 0.5 mm/min after failure and towards the development of the remaining friction.

The same experimental setup, figures 3.7 and 3.8, which is used for monotonic shear loading is used also for cyclic loading of the confined interfaces. Tests are performed under force control with limits in displacement for the case that failure occurs. A sinusoidal shear load is applied with a frequency of 2 Hz, while confinement stress, σ, is kept constant and equal to 1 N/mm^2. This value is chosen bearing in mind that in reality, on the connection, during fatigue loading, stresses remain on the elastic domain and consequently uplift, which is responsible for the development of the confinement, is limited. On the other hand, large values of confinement stress, 4 to 5 N/mm^2, are expected to be developed at ultimate limit state. The above two mentioned assumptions are verified by detailed finite element analysis of the cross section of the pushout specimens, using the Abaqus software. This finite element analysis is presented in chapter 5.

Transducers for measuring slip and uplift are used also for cyclic loading tests. Since at the frequency of 2 Hz it is impossible to register data, except for the force applied, in order to measure slip and uplift, certain cycles (loading up to V_{max} and unloading) were executed with a loading rate of 0.1 mm/min, equal to the loading rate, prior to failure, of the monotonic test. The unloading permits to register any residual-permanent- slip in the interface.

A total number of 51 specimens were fabricated for the three types of interfaces, from which 46 specimens are tested and 5 specimens are excluded due to damage or testing device malfunction.

3.2.4 Static loading

The following table presents the program of the direct shear tests with monotonic loading. The first column concerns specimen's name. Specimens with steel plate start with term TS-C, specimens with concrete plates start with term BR-C and specimens with UHPFRC plates with the term BFUP-C. The second column presents the confinement stress applied. The third column presents the specimens', or specimen group, mean compression resistance of the cement grout, as obtained by performing tests on cylinders at 28 days. Finally, the last column describes the type of failure: *Bearing failure* is produced when cement grout is debonding from the substrate. *Shear failure* is produced when failure surface is developed inside the cement grout, close to the interface, observed by a residual mass of cement grout remaining inside the undulations [Kitoh 1996].

Table 3.1: Program of direct shear tests

Specimen	confinement stress, σ (N/mm^2)	f_{cm} (N/mm^2)	Failure type
TS-C_1 & TS-C_2	0.5 & 1	107	*bearing*
TS-C_4	1		
TS-C_5 ~ TS-C_8	0.5 ~ 2	90	
TS-C_9	3		*bearing/shear*
TS-C_10	1		
TS-C_11 & TS-C_12	4	93	*shear*
TS-C_15 & TS-C_16	5	99.4	
TS-C_17	1	108	*bearing/shear*
BR-C_1 ~ BR-C_10	0.5 ~ 4	90 ~ 101	*shear*
BR-C_14 ~ BR-C_17	0.5 ~ 5	102	
BR-C_18 & BR-C_19	1	132	
BR-C_21	1		
BFUP-C_1 ~ BFUP-C_5	0.5 ~ 4	80	*shear*
BFUP-C_6	1		
BFUP-C_7 & BFUP-C_8	1	108	
BFUP-C_9 ~ BFUP-C_12	1 ~ 4	102 ~ 107	

Results

The use of load cell just beneath each plate (figure 3.8), allows registering of the force which passes from each interface. Consequently a mean shear stress in the interface can be calculated by dividing this quantity with the nominal area of the interface.

$$\tau = V/A \tag{3.1}$$

In reality, the contact area and the contact stresses are different but of no interest in the specific engineering application. The shear stress presented in the following diagrams refers to the quantity defined by equation (3.1). Another remark concerns registration of slip and uplift by transducers. Generally, since each specimen has two plates equipped with transducers, two shear-slip and two uplift-slip curves can be registered for each specimen.

During loading of the specimens, inclined cracks initiate in the interface and propagate few mm inside the cement grout; other cracks may also be present due to shrinkage of the cement grout. In certain

case, when cracking is initially excessive and for certain specimens at high confinement stress, cracking is resulting in debonding of the epoxy support, of the transducer, from the cement grout, and no further data is possible to be recorded. In that case only the ultimate shear and the remaining friction at the end of loading are recorded.

Failure criteria

The following diagrams present the *failure criteria*, i.e. the ultimate shear stress, τ_u , versus normal stress, σ, for each type of interface.

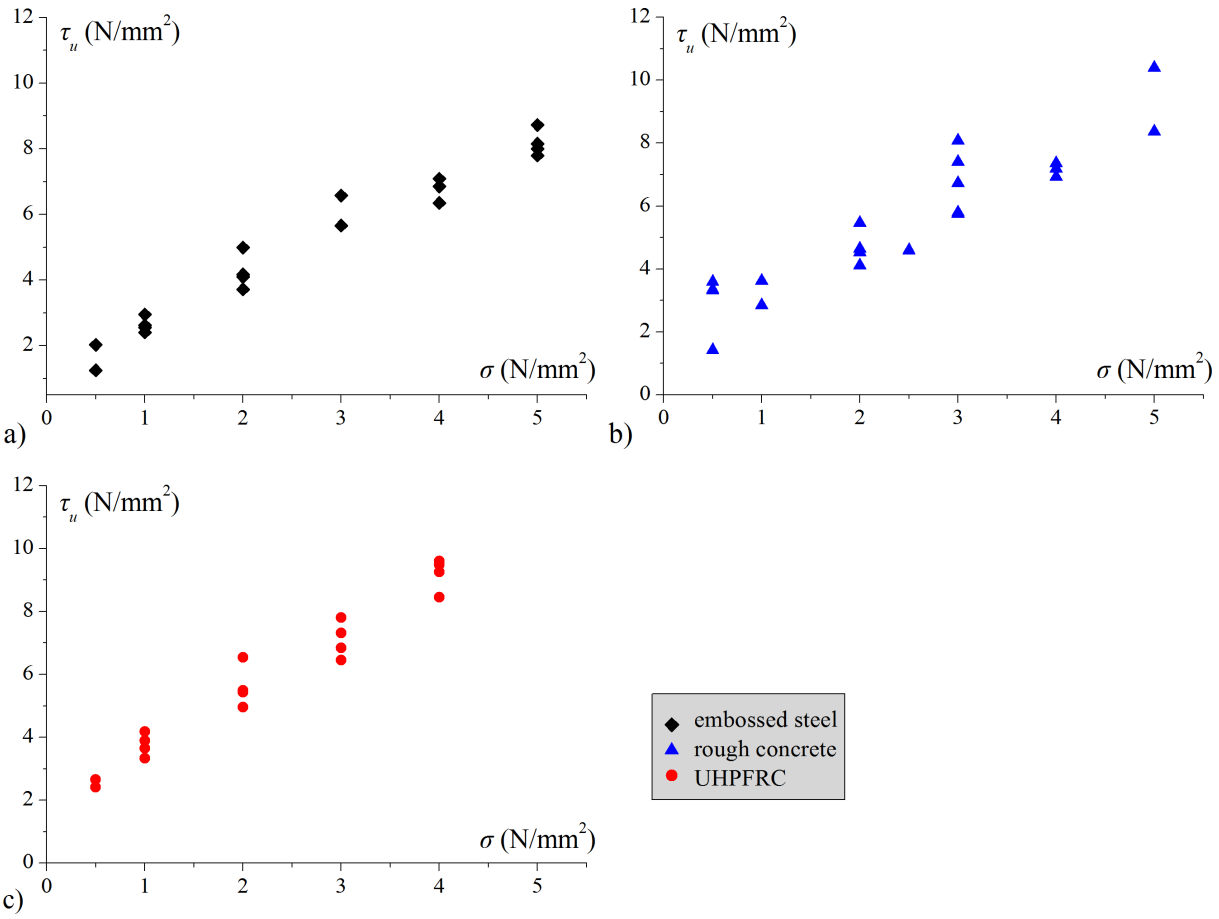

Fig. 3.10: Ultimate shear stress versus normal stress for the three types of interfaces: a) embossed steel-cement grout b) roughened concrete-cement grout and c) UHPFRC-cement grout

The results have less scatter for the embossed steel-cement grout interface due to the regularity of the surface. Scatter is higher for the roughened concrete due to different exposure of the aggregates of the plates. The beneficial effect of the presence of the normal stress is apparent in all types of interfaces. Skipping the scatter, the failure criteria follow a linear, Mohr-Coulomb type, criterion. In general, for the same normal stress, shear resistance is increasing with increased roughness which is in accordance to all existing models.

Besides ultimate shear resistance τ_u the remaining frictional resistance τ_{fr} is also obtained and is presented on diagrams in figure 3.11, as a function of the confinement stress, σ.

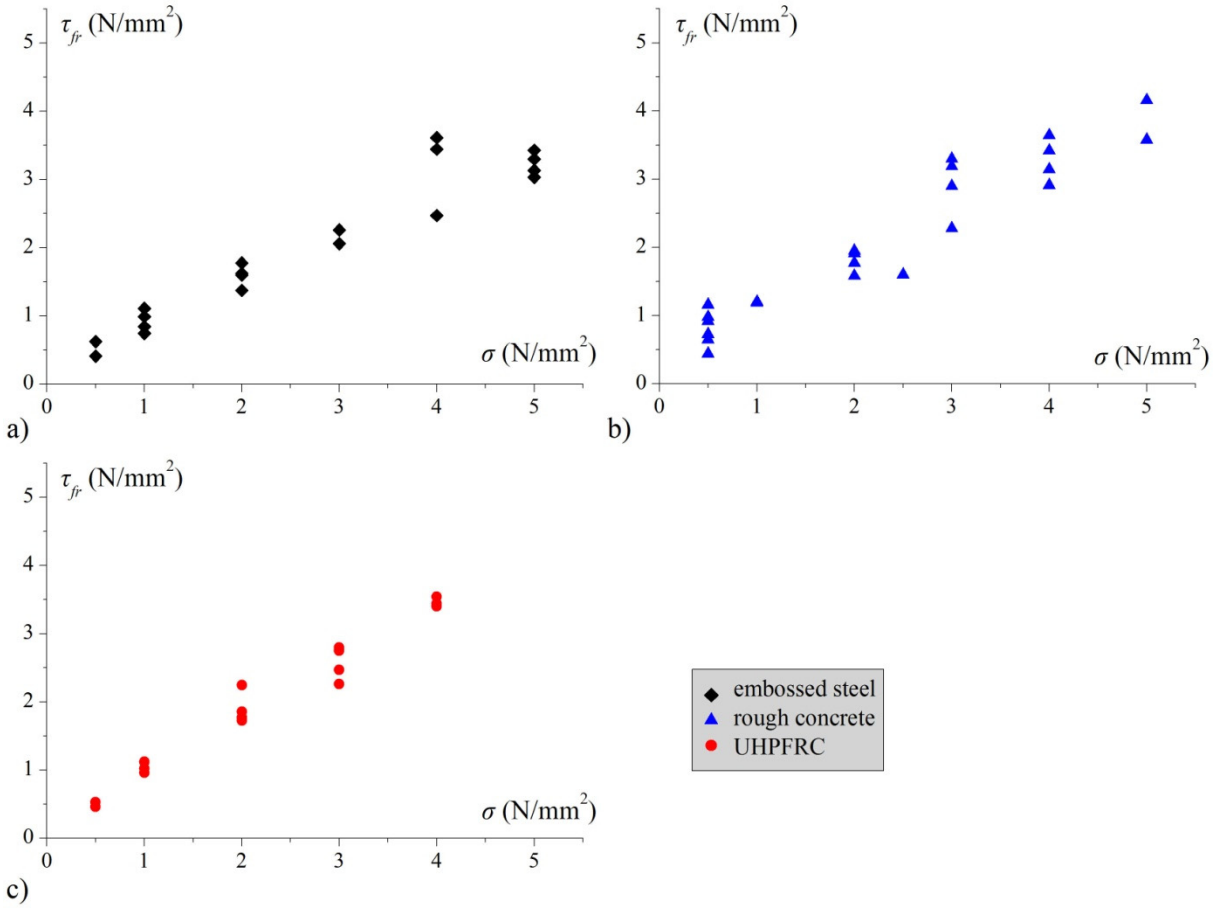

Fig. 3.11: Frictional resistance versus normal stress for the three types of interfaces:
a) embossed steel-cement grout b) roughened concrete-cement grout and c) UHPFRC-cement grout.

The frictional resistance is proportional to the normal stress, thus in accordance to the definition of friction. We notice also that it is not much different for the three interfaces.

Mean cement grout compression resistance, f_{cm}, is not considered as a parameter in this study. For embossed steel-cement grout interfaces, f_{cm} varies mainly from 90 to 99.4; three specimens with f_{cm} equal 107 N/mm^2, tested with a confinement stress of 0.5 and 1 N/mm^2, show similar resistance. Diagrams for rough concrete, present results for the specimens whose mean cement grout compression resistance f_{cm} varies from 90 to 102 N/mm^2. The three specimens with f_{cm} equal to 132 N/mm^2 concern specimens submitted initially to cycle loading and consequently to static loading in order to investigate the remaining resistance. Due to the exceptionally high f_{cm} of these three specimens, their performance is not including in the diagrams of this sub-chapter.

For UHPFRC specimens two groups with different cement grout resistance are tested, the first with f_{cm} equal to 80 N/mm^2, and the second with f_{cm} from 102 to 107 N/mm^2. Yet both groups present the same shear resistance for the same level of confinement. Fabrication of second group for UPHFRC is imposed by the excessive initial cracking of the first group (figure 3.12). The cement grout, produced for the first group of specimens, presented a thixotropic behaviour. The wanted liquidity for the cement grout is not achieved despite the adding of water. Water cement-ratio reached limit of 0.32, which justifies the cement grout lower compression resistance. This initial, shrinkage type cracking does not alter the ultimate shear resistance, but influences a lot the stiffness, so results concerning constitutive and kinematic relationship is excluded and a second group is fabricated and tested to obtain values for stiffness for non-cracked specimens.

Fig. 3.12: UHPFRC-cement grout specimen, with excessive initial cracking.

Constitutive law

Figure 3.13 presents a typical result for the embossed steel-cement grout interface, of the specimen TS-C_9. The diagram represents the *constitutive law*, i.e. the shear stress-slip relationship with some necessary definitions of physical quantities which are used afterwards at the comments made on the results.

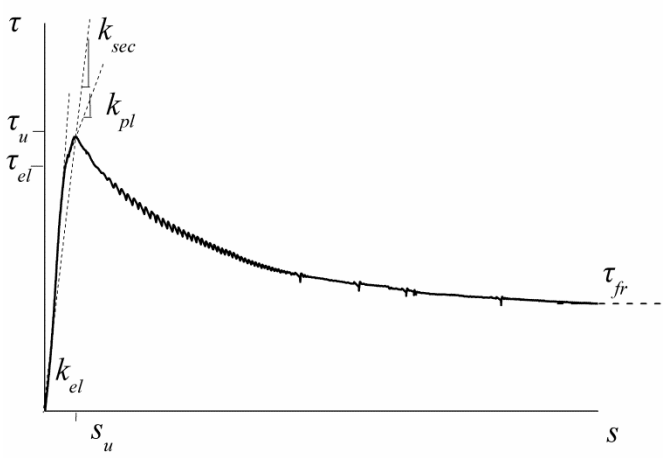

Fig. 3.13: Constitutive law for an embossed steel-cement grout interface, specimen TS-C_9

The following definitions are made in the above diagram:

- *Failure slip* s_u refers to the value of slip where the shear stress, τ, becomes ultimate τ_u and failure initiates.
- *Frictional shear resistance*, τ_{fr} refers to the asymptotic value of the shear stress, i.e. the remaining frictional resistance, generally after 10 to 12 mm.
- *Elastic shear stress* τ_{el} refers to the value of shear stress at the point where initial stiffness changes.
- *Elastic stiffness* k_{el} refers to the initial stiffness. It is the tangential angle of the curve of the constitutive law at the beginning point of the curve.
- *Plastic stiffness* k_{pl} refers to slope of the constitutive law for the branch following the initial quasi-elastic branch and till the point of failure initiation (τ_u , s_u).
- *Secant stiffness* k_{sec} refers to the tangential angle of the line (chord) defined by the cross point of the axes and the point (τ_u , s_u) of the constitutive law.
- *Failure uplift* u_{Su} refers to the value of uplift when failure initiates at s_u.
- *Maximum uplift* u_{max} refers to the ultimate uplift in the interface when shear stress is diminished to friction, τ_{fr}.

The following figures 3.14 to 3.16 present, for the three interfaces, the *constitutive law*. (Normal stress unit is in N/mm^2). The left figures present the entire diagram and the right figures a detailed representation up to 1.5 mm slip.

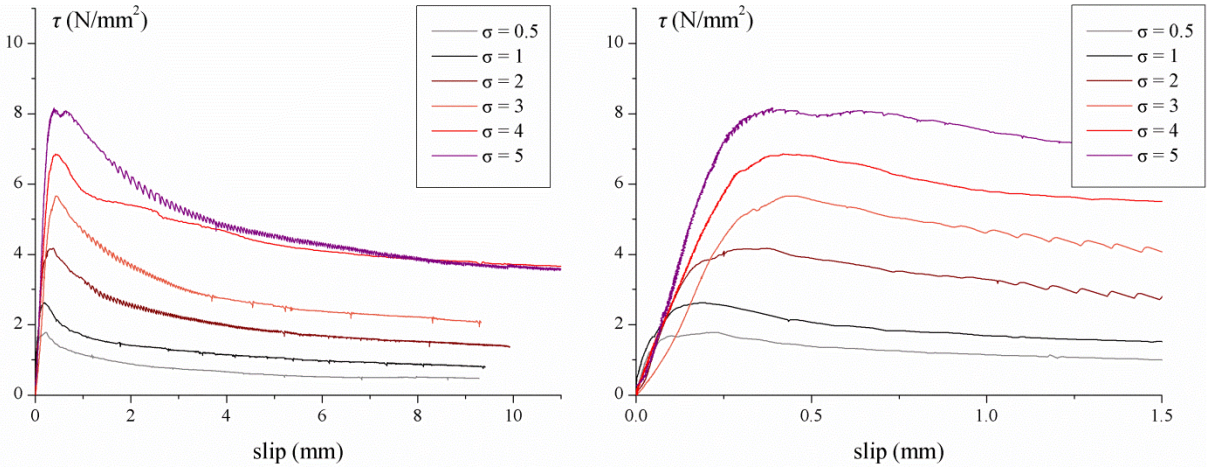

Fig. 3.14: Shear stress-slip relationship for embossed steel-cement grout interface

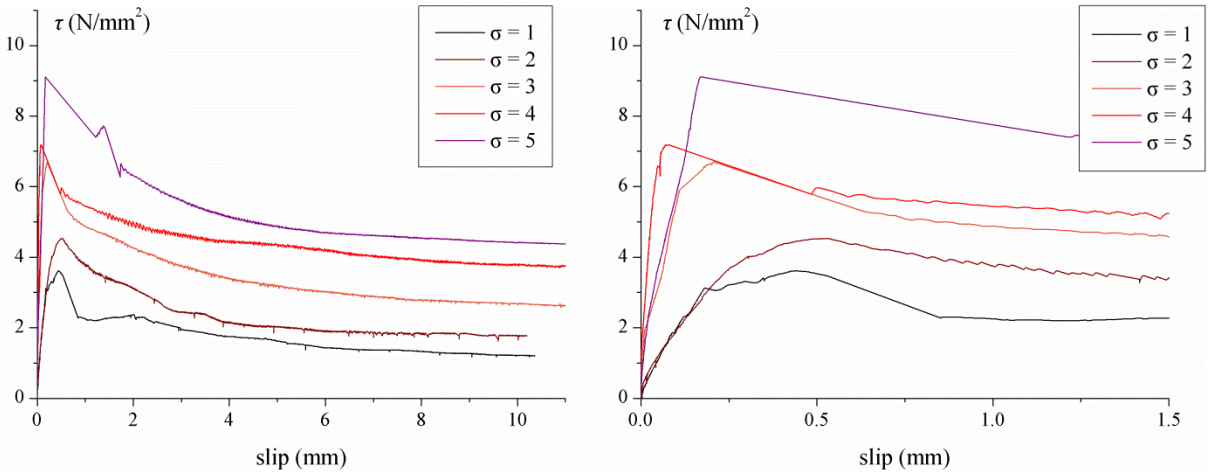

Fig. 3.15: Shear stress-slip relationship for roughened concrete-cement grout interface

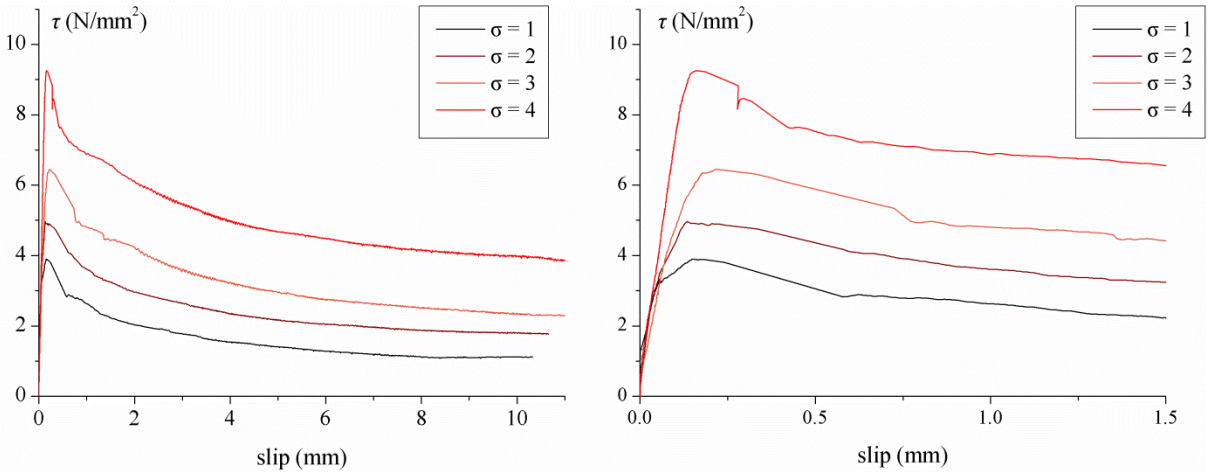

Fig. 3.16: Shear stress-slip relationship for UHPFRC-cement grout interface

Curves are presented for different level of the confinement stress, σ, which is applied on the interface. As we may observe in the figures above, shear stress for all interfaces exhibits initially an almost linear elastic behaviour. The end of this domain, generally close to τ_u, which defines also the value of the elastic shear stress τ_{el} is followed, in most cases, very soon by a yielding branch with increasing shear towards failure. For few cases the end of the elastic domain is not easily distinguished and goes almost up to τ_u. When the ultimate shear τ_u is mobilized, failure initiates which is characterized by an exponential decay of the resistance and rapid increase of slip in the interface. The shear resistance is diminishing asymptotically towards the remaining frictional resistance τ_{fr}. The value of slip at which the shear resistance is diminished to the remaining friction is located at 10 to 12 mm for all type of interfaces.

For the level of confinement in which this investigation was limited, i.e. up to 5 N/mm^2, the ultimate shear resistance increases with the increase of the normal stress in the interface. This influence of the normal stress applies to the whole constitutive relationship (figures 3.14~3.16), including the remaining frictional resistance as well.

The ratio between the elastic shear stress, τ_{el} and the ultimate shear resistance τ_u is independent of the confinement stress and varies around a mean value, dotted lines, which is a characteristic of the interface (figure 3.17).

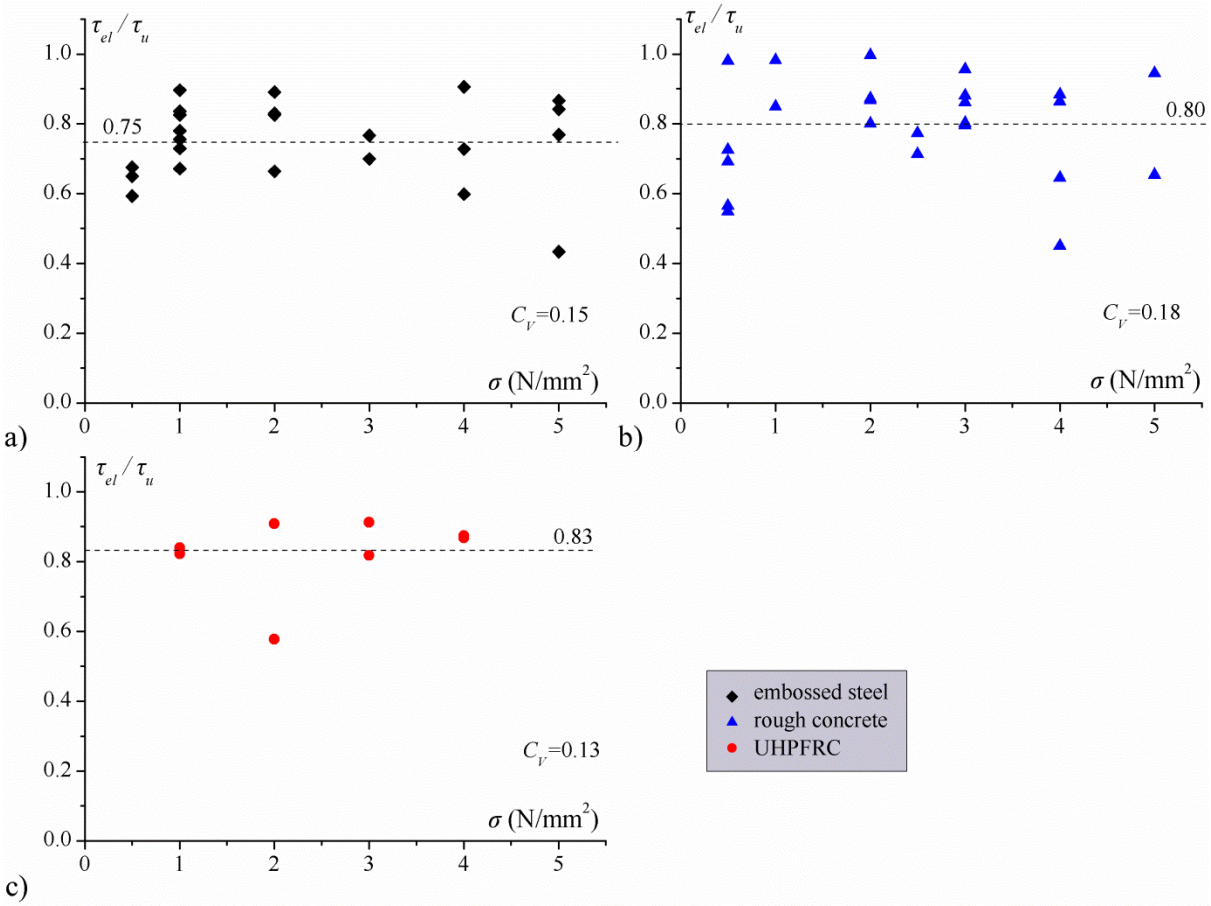

Fig. 3.17: Ratio between τ_{el} and τ_u as a function of the confinement stress a) embossed steel-cement grout interface b) rough concrete-cement grout interface and c) UHPFRC-cement grout interface

The initial elastic stiffness k_{el} , the plastic stiffness k_{pl} and the secant stiffness k_{sec} vary, having the majority of their values in a limited zone and they seem to be independent of the normal stress, meaning that there is not evident particular correlation. They constitute characteristics of the type of the interface. For the concrete plates which are not identical, due to the randomness of the exposed aggregates, the stiffness varies more than the other two types of interfaces (figure 3.18).

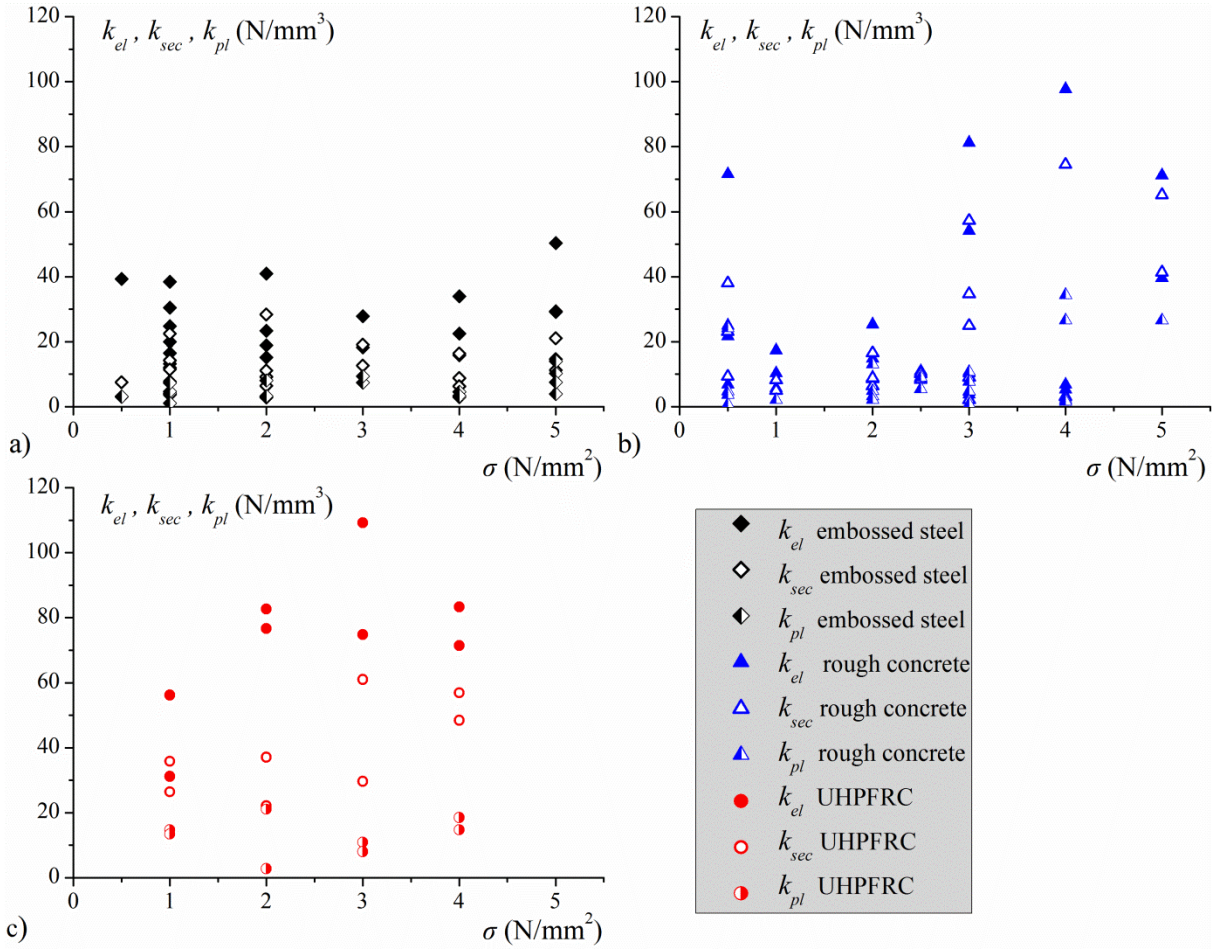

Fig. 3.18: Elastic, plastic and secant stiffness versus confinement stress a) embossed steel-cement grout interface b) rough concrete-cement grout interface and c) UHPFRC-cement grout interface

The stiffness, elastic, plastic and secant, of each type of interfaces will be taken into account with their mean values for the part of the constitutive law prior to failure.

Kinematic law

Figure 3.19 presents a typical result for the embossed steel-cement grout interface, of the specimen TS-C_9. The diagram represents the *kinematic law*, i.e. the uplift-slip relationship with some necessary definitions of physical quantities which are used afterwards at the comments made on the results.

- *Failure uplift* u_{Su} refers to the value of the uplift when failure initiates.
- *Maximum uplift* u_{max} refers to the ultimate uplift in the interface when shear stress is diminished to friction.

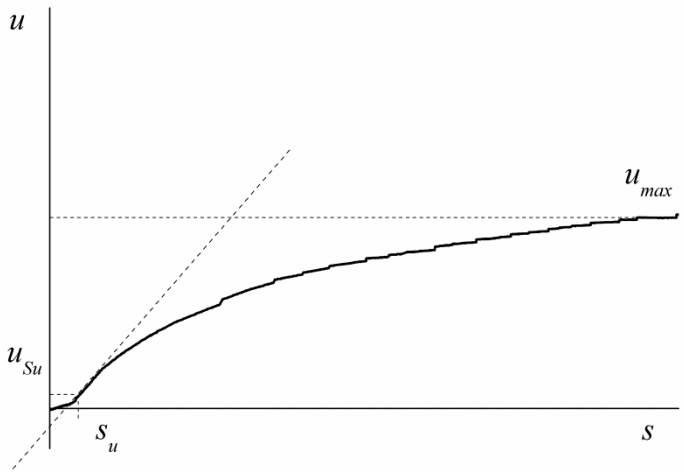

Fig. 3.19: Kinematic law for an embossed steel-cement grout interface, specimen TS-C_9

The following figures 3.20, 3.21 and 3.22 illustrate the *kinematic law*, i.e. the relationship between the uplift, *u* and slip, *s*, as recorded, for each type of interfaces, for different levels of the normal stress acting in the interface. (Unit of normal stress is in N/mm^2).

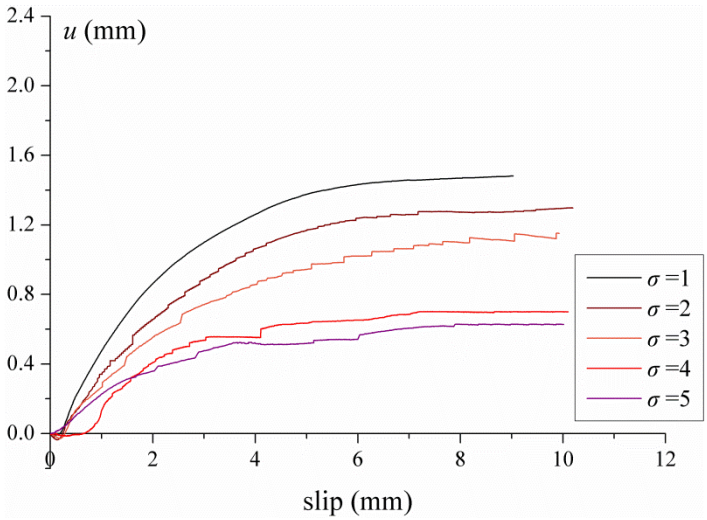

Fig. 3.20: Uplift-slip relationship for embossed steel-cement grout interface

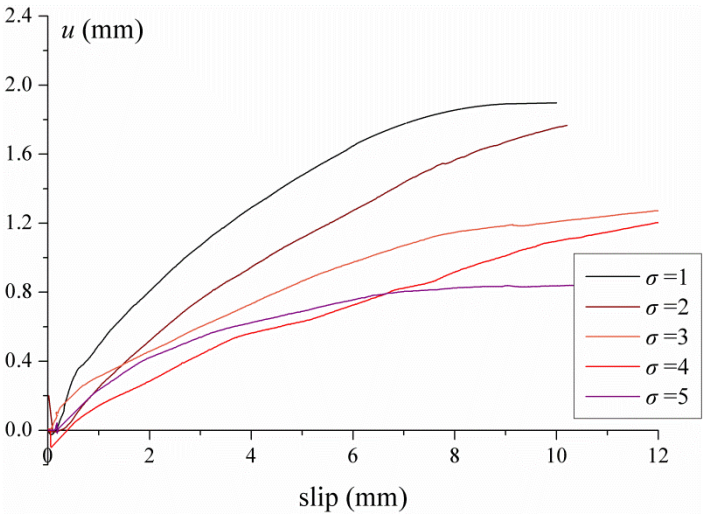

Fig. 3.21: Uplift-slip relationship for roughened concrete-cement grout interface

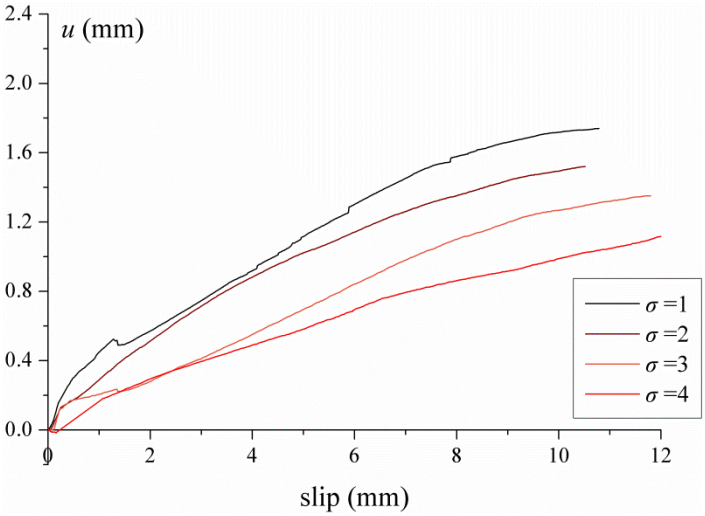

Fig. 3.22: Uplift-slip relationship for UHPFRC-cement grout interface

For all interfaces, uplift in the interface is hardly noticed before failure slip. Once failure occurs uplift increases with exponential rise asymptotically towards a maximum value (figures 3.20~3.22) which is achieved simultaneously with the remaining friction.

Figure 3.23 presents for the three interfaces the values of the uplift at initiation of failure u_{Su} and the maximum value of the uplift u_{max}, achieved when resistance reduces to the remaining friction.

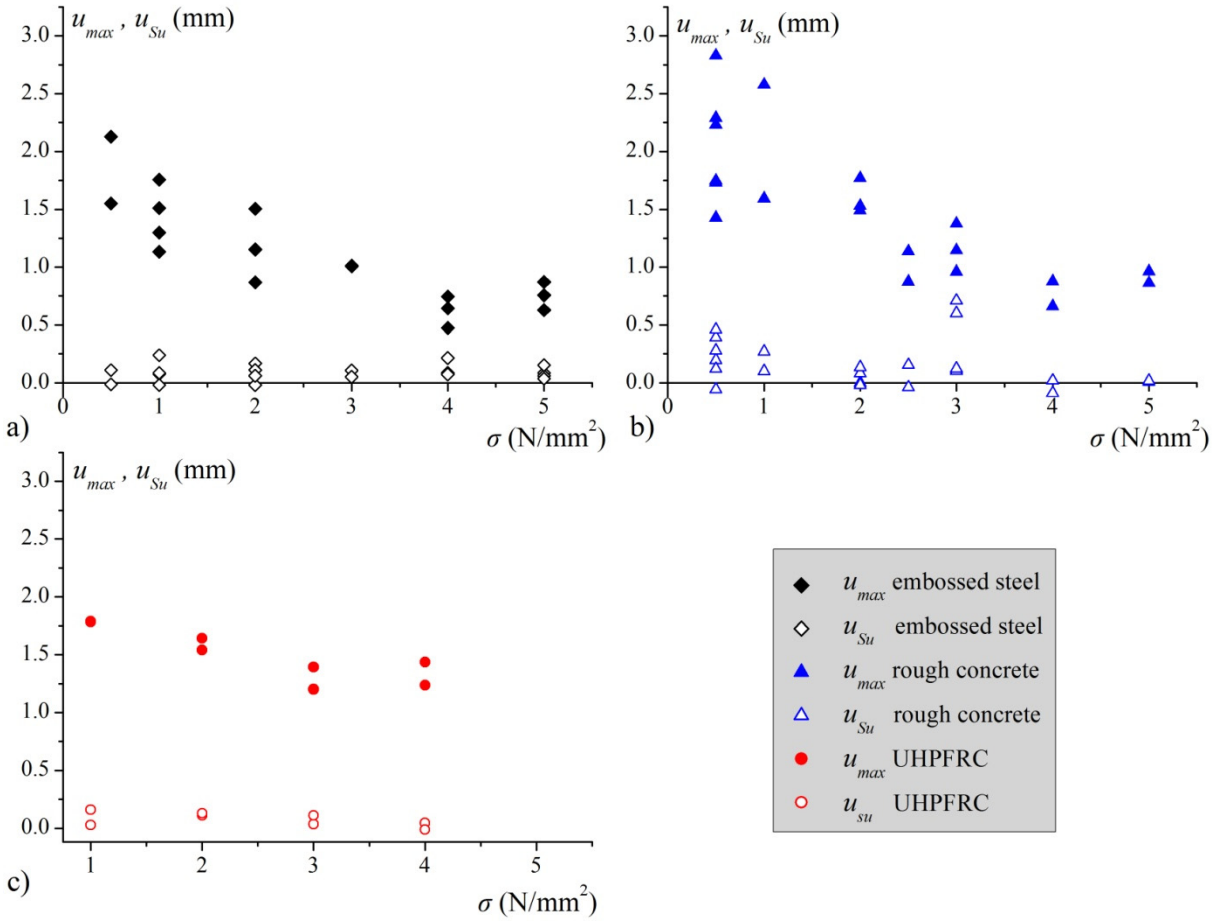

Fig. 3.23: Uplift at initiation of failure u_{Su} and maximum uplift at friction u_{max} as a function of confinement stress a) embossed steel-cement grout interface, b) rough concrete-cement grout interface and c) UHPFRC-cement grout interface

The uplift at initiation of failure u_{Su} is independent of the confinement stress. It varies around a mean value and can be considered a characteristic of the interface. This mean value is 0.09 mm for the embossed steel-cement grout interface, 0.16 mm for the rough concrete-cement grout interface and 0.09 mm for the UHPFRC-cement grout interface.

The maximum uplift u_{max} shows that it is inversely proportional to the confinement stress σ (fig. 3.23)

Observations

Two types of failures are observed for the embossed steel-cement grout interfaces, as already observed by Kitoh [Kitoh 1996], and one type for the other two interfaces. For the embossed steel-cement grout interface these types are the *bearing failure* and the *shear failure*, figure 3.24.

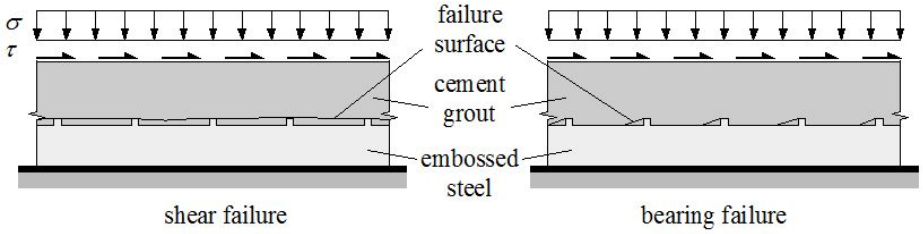

Fig. 3.24: Shear and bearing failure in an embossed steel-cement grout interface [Kitoh 1996]

Figure 3.25 illustrates the two types of failure for the embossed steel-cement grout interface. *Bearing failure*, i.e. debonding from the substrate, is observed for low levels of confinement up to 3 N/mm^2, and the *shear failure* for higher levels of confinement.

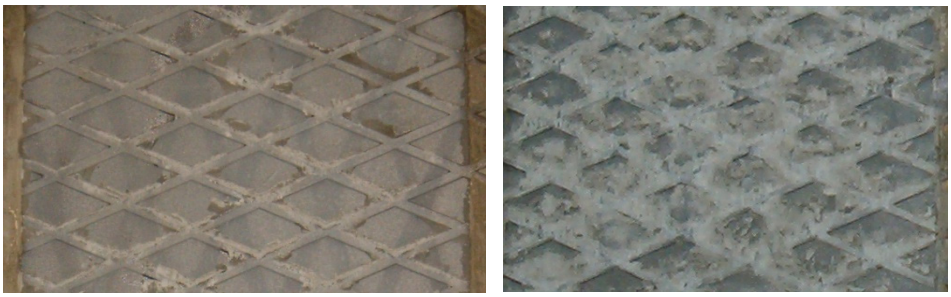

(a) *Bearing failure* (b) *Shear failure*

Fig. 3.25: Bearing and shear failure in an embossed steel-cement grout interface.

The development of the remaining friction, for slip grater than 10mm, is verified by the shiny surfaces on the cement grout block, figures 3.26 and 3.27.

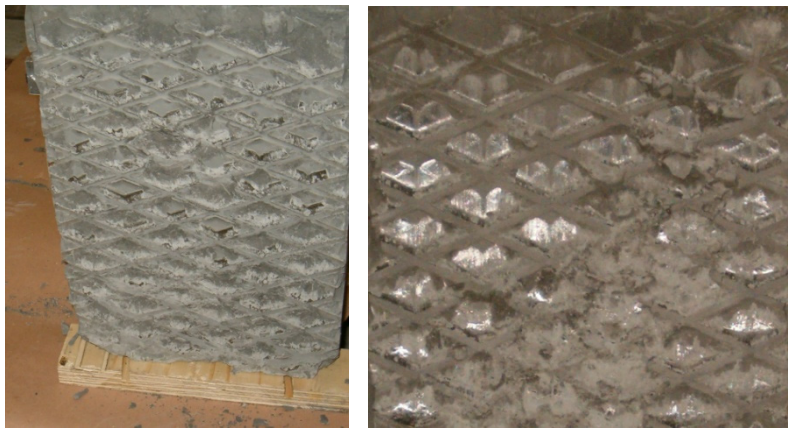

Fig. 3.26: View of cement block after test, surface submitted to friction Specimen TS-C_9.

For the other interfaces the failure type is *shear*, which takes place inside the cement grout which is interlocking with the asperities of the rough interface, for the rough concrete, and the 8 mm cones, for the UHPFRC plates (fig. 3.27).

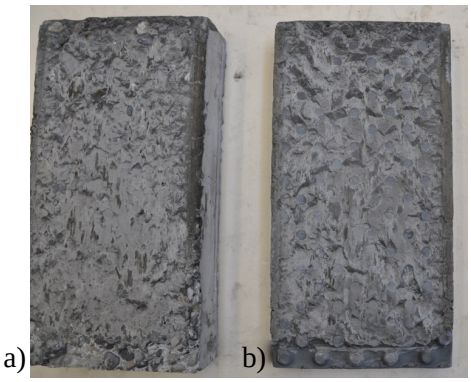

a) b)

Fig. 3.27: *Shear failure* a) in roughened concrete-cement grout interface (specimen BR-C_15) and b) in UHPFRC-cement grout interface (specimen BFUP-C_9)

For the cases where the cement grout has high resistance and the aggregates are not very resistant, it is possible that failure develops inside the concrete, as illustrated at figure 3.28 for specimen BR-C_4.

Fig. 3.28: *Shear failure* inside the concrete block of specimen BR-C_4

Remarks for static loading of interfaces

A main conclusion for static loading of interfaces is that the shear resistance prior to failure exhibits an elastic behaviour followed by a yielding plastic branch. The stiffness of these domains is independent of the normal stress. Another conclusion is that once failure occurs, slip and uplift in the interface increase rapidly where as shear exhibits an exponential decay towards to the frictional shear resistance. The normal stress in the interface has a beneficial effect increasing the overall shear resistance.

As observed at figure 3.13, the point of the initiation of failure, point of ultimate shear resistance τ_u, and failure slip s_u, corresponds to the inflection point of the curve of the kinematic law, i.e. the point where the curvature of the kinematic law changes sign. This leads to the conclusion that the post failure constitutive law can be obtained by the kinematic law with differentiation of its expression, as we may see in the following chapter.
The uplift at initiation of failure, u_{Su} is independent of the confinement stress. It varies around a mean value and can be considered as a characteristic of the interface. Once failure initiates, uplift increases. The maximum value that uplift reaches at remaining friction, u_{max} is inversely proportional to confinement stress.

It was mentioned in this chapter that, for the embossed steel interface, failure is of *bearing* type at low confinement and gradually passes to *shear* for higher values of the normal stress. For the other interfaces failure is of shear type.

Recent development of cement grout has resulted to the development of mixture with enhanced characteristics. The current cement grout proposed by VSL Company, due to its expansive agent during curing, counterbalances shrinkage, resulting to better bonding interfaces. The specimens, of the above tests, are fabricated with the previous type of VSL cement grout, thus the results are more conservative. Three direct shear tests performed lately with the new cement grout VSL-HPI for the embossed steel and rough concrete and for a confinement stress of 1 N/mm^2 show that shear resistance is increased of more than 25 %. Furthermore due to better bonding conditions, failure is also of shear type for the embossed steel plates, even with normal stress of only 1 N/mm^2, (figure 3.29).

Fig. 3.29: *Shear failure* in embossed steel-cement grout interface for confinement stress1 N/mm^2. Cement grout VSL-HPI.

Bearing in my mind, that a similar failure surface is developed for the cement grout, without expansive agent, for higher normal stresses -more than 3 N/mm^2- it is reasonable to assume that the expansive agent creates due to its action an initial additional confinement effect. (The steel plates were prevented from moving due to the casting set up, for about four days).The same effect explains the higher resistance obtained in comparison with tests, where cement grout with no expansive agent was used. Since this new type of cement grout is used now in engineering practice, it is used also for the last two push-out specimens and the fabrication of the composite beam, as we see in section 3.3.3.

3.2.5 Cyclic loading

The following tables summarize the charactersistics of the cyclic tests executed for the three interfaces. For several specimens no failure occurs for a certain number of cycles. Concequently another loading sequence is applied, which is either a higher amplitude cyclic loading or a static test up to failure.

Table 3.2: Cyclic shear loading for embossed steel-cement grout interface

Test name	V_{min} (kN)	V_{max} (kN)	$\Delta V/V_{u,stat}$	$V_{max}/V_{u,stat}$	Cycles	f_{cm} (N/mm^2)	$V_u/V_{u,stat}$	failure type
TS-C_10	95	190	0.30	0.59	5E+6*	90	0.97	*bearing/shear*
TS-C_13	95	280	0.57	0.87	4208	93	-	*bearing/shear*
TS-C_17	95	190	0.30	0.59	5E+6*	108	0.98	-
	95	235	0.44	0.74	2E+6*			*shear*
TS-C_18	95	190	0.30	0.59	5E+6*	102	-	-
	15	205	0.59	0.64	2E+6*			-
	15	285	0.84	0.89	1184			*shear*
Index * means that no failure occurs and another loading sequence follows								

Table 3.3: Cyclic shear loading for a rough concrete-cement grout interface

Test name	V_{min} (kN)	V_{max} (kN)	$\Delta V/V_{u,stat}$	$V_{max}/V_{u,stat}$	Cycles	f_{cm} (N/mm^2)	$V_u/V_{u,stat}$	failure type
BR-C_18	30	120	0.31	0.41	5E+6*	132	1.04	*shear*
BR-C_19	30	170	0.47	0.58	2E+6*	132	1.10	*shear*
BR-C_20	30	260	0.78	0.88	2E+6*	132	-	-
	10	290	0.90	0.98	10860			*shear*
Index * means that no failure occurs and another loading sequence follows								

Table 3.4: Cyclic shear loading for UHPFRC-cement grout interface

Test name	V_{min} (kN)	V_{max} (kN)	$\Delta V/V_{u,stat}$	$V_{max}/V_{u,stat}$	Cycles	f_{cm} (N/mm^2)	$V_u/V_{u,stat}$	failure type
BFUP-C_6	34	204	0.52	0.62	2E+6*	80	1.02	*shear*
BFUP-C_7	34	204	0.52	0.62	5E+6*	108	0.80	*shear*
BFUP-C_8	34	204	0.52	0.62	2E+6*	108	1.07	*shear*
Index * means that no failure occurs and a static test up to failure follows								

- V_{min} refers to the minimum load applied in the cyclic loading sequence
- V_{max} refers to the maximum load applied in the cyclic loading sequence
- $V_{u,stat}$ is the ultimate load that an interface can resist for monotonic loading, for normal stress, σ =1 N/mm^2. This mean value is 322 kN for the embossed steel-cement grout interface, 295 kN for the roughened concrete-cement grout interface and finally 329 kN for the UHPFRC-cement grout interface. The values are obtained from the results of the static tests presented previously at 3.2.4
- $V_u/V_{u,\mathrm{stat}}$ refers to the ratio between the ultimate value which the load reaches at the monotonic test that follows a cyclic loading, versus the ultimate load that the specimen would stand if it was directly submitted to static loading.

Results

Initially, a ratio of the loading range versus ultimate static resistance, $\Delta V/V_{u,stat}$ equal to 0.30 was chosen for verification at fatigue limit for three specimens with embossed steel-cement grout and one specimen with roughened concrete-cement grout interface. This limit is slightly higher than the one obtained considering fatigue limit according to fatigue load model 1 of the code SIA 261. (For the UHPFRC-cement grout interface a higher ratio of $\Delta V/V_{u,stat}$ equal to 0.52 was chosen since interface exhibits enhanced resistance to fatigue). When no failure occurred for five million cycles, it was decided to continue with another loading sequence. Specimens TS-C_10, BR-C_18 and BFUP-C_7 were submitted to a static test up-to failure and specimens TS-C_17 and TS-C_18 were subjected to another cyclic loading with higher amplitude.

For verification at fatigue limit according to the load model proposed by Meystre and Lebet [Meystre and Lebet 2011] a ratio of $\Delta V/V_{u,stat}$ equal to 0.44 is obtained and was used. As it is presented in the tables above, six specimens, two for each type of interfaces were subjected to 2 million cycle loading with a ratio $\Delta V/V_{u,stat}$ 0.44 or higher. No failure occurred and other loading sequences followed.

For all specimens that resist fatigue without failure, the maximum applied load V_{max} provokes shear stress, in the interface, lower than the elastic stress τ_{el}, figure 3.13, of the monotonic test. Failure occurs for three loading cases when the maximum applied load is resulting to shear stress that exceeds the elastic domain.

The following figures 3.30 to 3.32, present the constitutive relationship, as registered during certain cycles for three specimens, TS-C_18, BR-C_19 and BFUP-C_8 respectively. Besides, the constitutive law of the final static test up to failure is also presented. Normal stress in the interface is always constant and equal to 1 N/mm^2. For specimen TS-C_18 three loading sequences are applied, as mentioned at table 3.2. For comparison reasons, together with the curves of specimen TS-C_18, the constitutive law of the monotonic test for specimen TS-C_2 is also presented to demonstrate the estimated yielding stress τ_{el} and the ultimate stress τ_u for the embossed steel-cement grout interface for normal stress 1 N/mm^2.

In the diagrams, the two horizontal doted lines, parallel to the axes of the slip, present the variation of the shear stress developed during the cyclic loading. As mentioned, for the cycles in which data are registered, an unloading takes place to record also the residual slip in the interface. In order to compare the stress amplitude during cyclic loading with the elastic stress τ_{el} and the ultimate shear stress τ_u both these limits are also marked in the diagram for the curve of the monotonic loading.

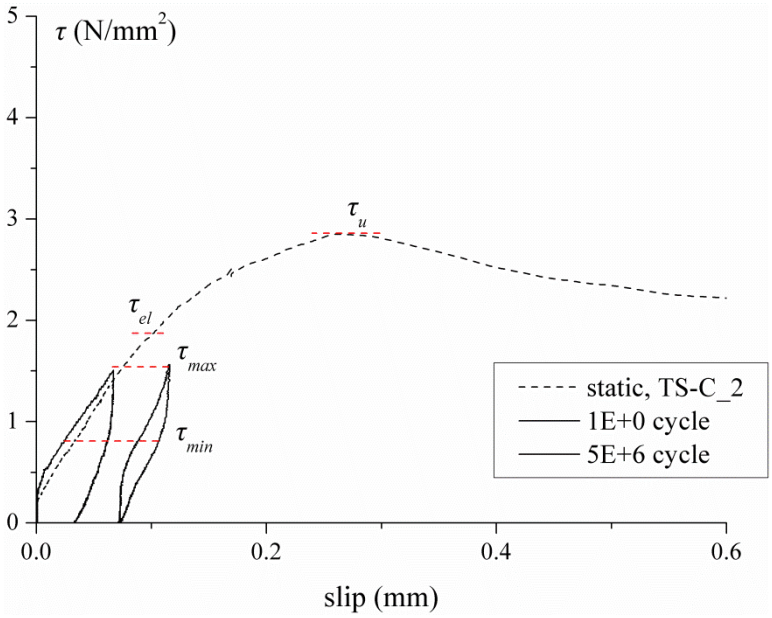

a) TS_C18, 1st loading sequence (95-190 kN)

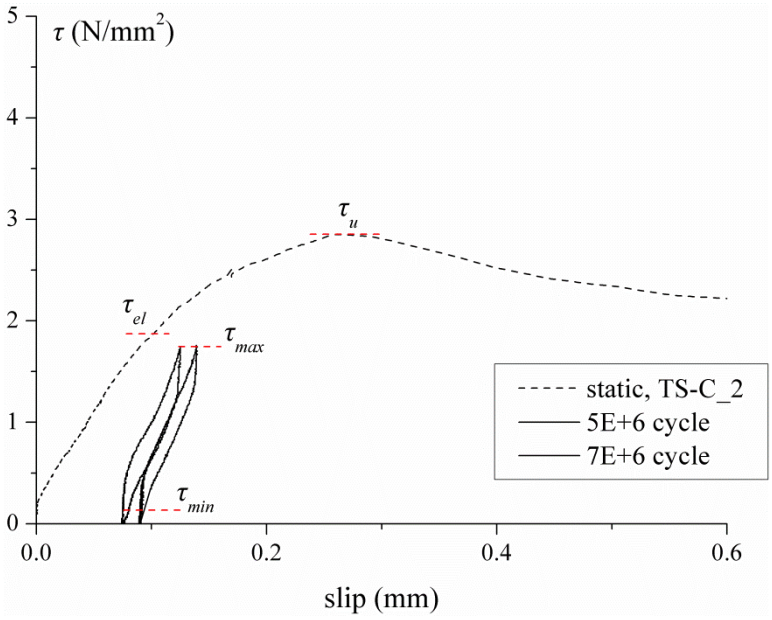

b) TS_C18, 2nd loading sequence (15-205 kN)

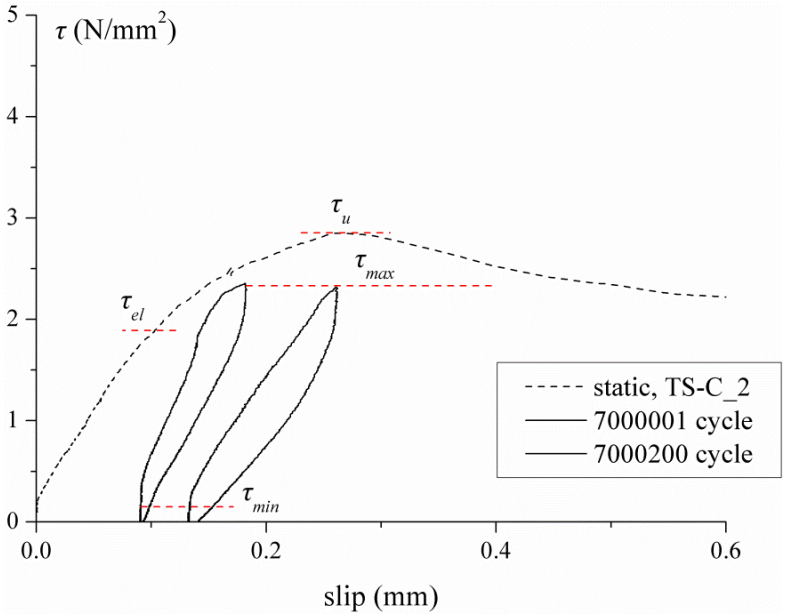

c) TS_C18, 3rd loading sequence (15-285 kN)

Fig. 3.30: Shear stress-slip relationship for embossed steel-cement grout interface, specimen TS-C_ 18 (cyclic loading, 3 sequences) and specimen TS-C_2 (monotonic loading)

At the first and the second sequence, fig 3.30 a) & b), in which the maximum imposed shear stress is less that than the elastic yielding limit τ_{el}, the residual slip which develops in the interface stabilizes and no failure occurs. For the third sequence, in which the applied stress exceeds the elastic yielding limit, residual slip starts to increase; the constitutive law enters the failure branch and the specimen fails.

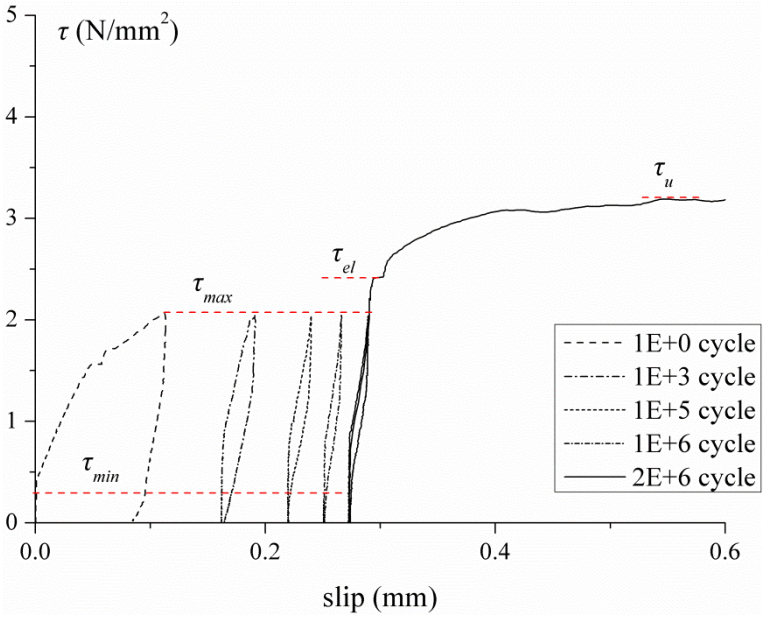

Fig. 3.31: Shear stress-slip relationship for rough concrete-cement grout interface, specimen BR-C_19 (30-170 kN)

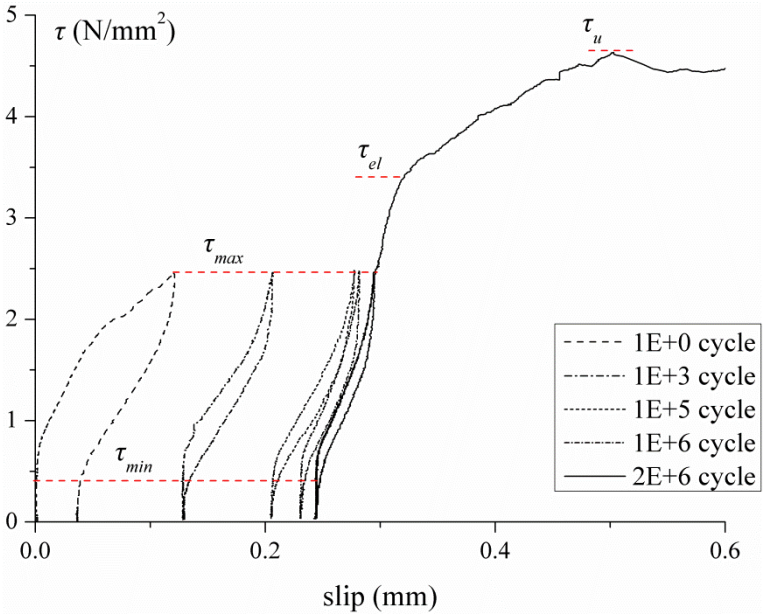

Fig. 3.32: Shear stress-slip relationship for UHPFRC-cement grout interface, specimen BFUP-C_8 (34-204 kN)

From figures 3.31 and 3.32 it is noticed, likewise to the interface with the embossed steel, that as long as shear stress variation is not exceeding the elastic limit, no failure occurs. The influence of cyclic loading is expressed by a residual slip in the interface which is accumulated with the number of cycles and which practically stabilizes after one to two million cycles.

The evolution of the residual slip as a function of the number of cycles for the embossed steel-cement grout interface, the rough concrete-cement grout interface and the UHPFRC-cement grout interface is demonstrated in figures 3.33 to 3.35. The residual slip s_{res} practically stabilizes after one to two million cycles. The vertical scale is different for the first two interfaces for better visualization of results.

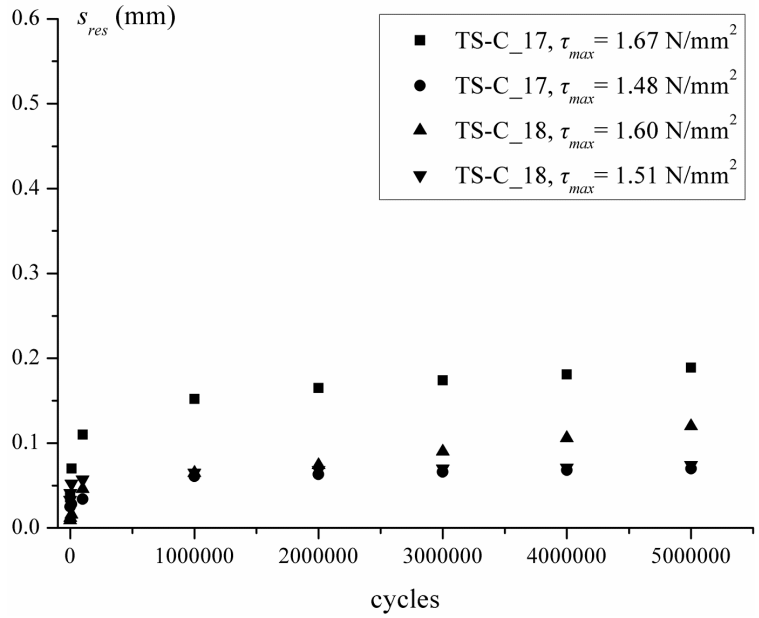

Fig. 3.33: Residual slip, s_{res} as a function of the number of cycles, for cyclic loading for an embossed steel-cement grout interface

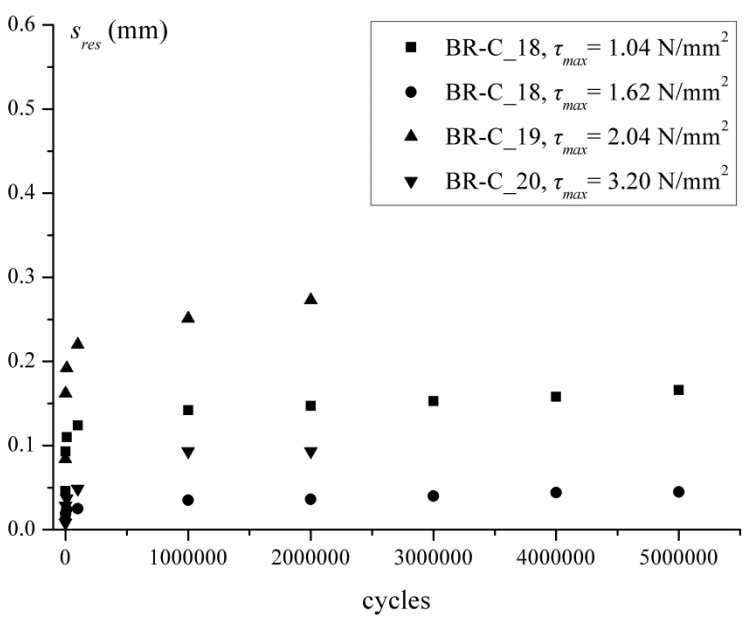

Fig. 3.34: Residual slip, s_{res} as a function of the number of cycles, for cyclic loading for a rough concrete-cement grout interface

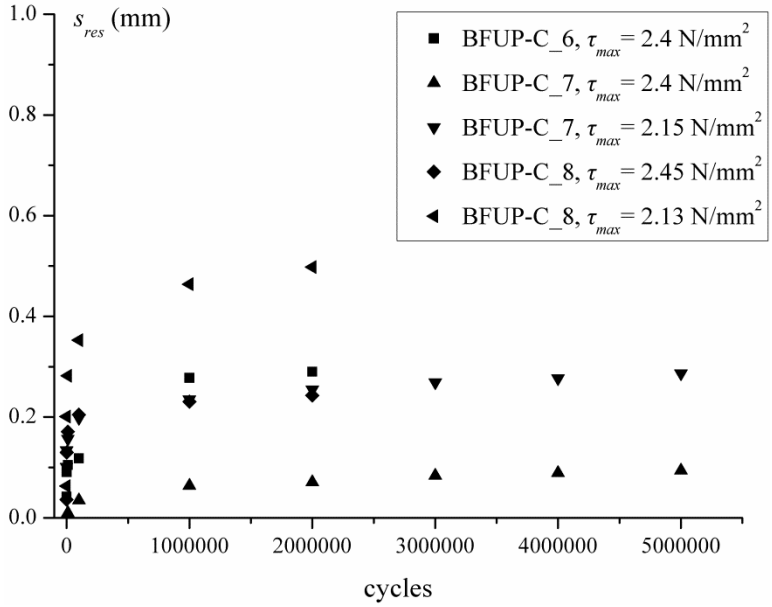

Fig. 3.35: Residual slip, s_{res} as a function of the number of cycles, for cyclic loading for an UHPFRC-cement grout interface

Figures 3.36 to 3.38 illustrate, for the three types of interfaces, the evolution of slip under maximum cyclic load, s_{Vmax} , as a function of the number of cycles. The vertical scale is different for the first two interfaces for better visualization of results.

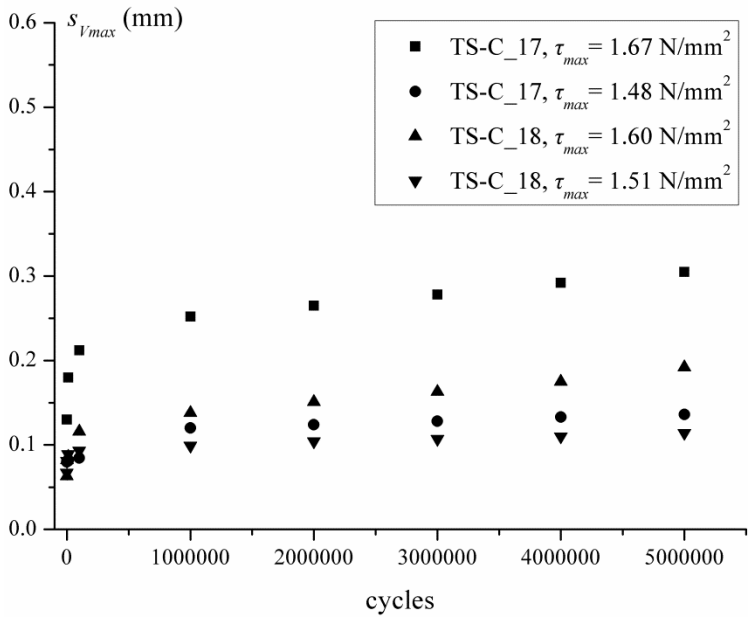

Fig. 3.36: Slip under maximum cyclic load, s_{Vmax} , as a function of the number of cycles, for cyclic loading for an embossed steel-cement grout interface

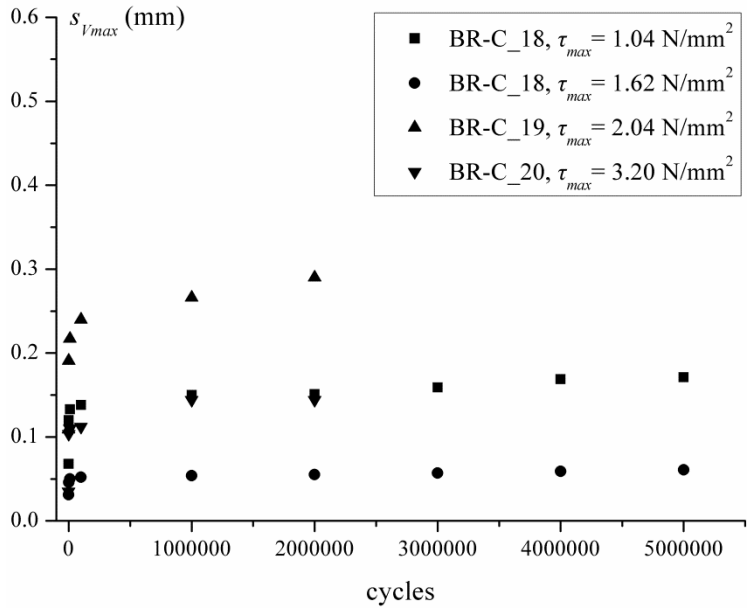

Fig. 3.37: Slip under maximum cyclic load, s_{Vmax} , as a function of the number of cycles, for cyclic loading for a rough concrete-cement grout interface

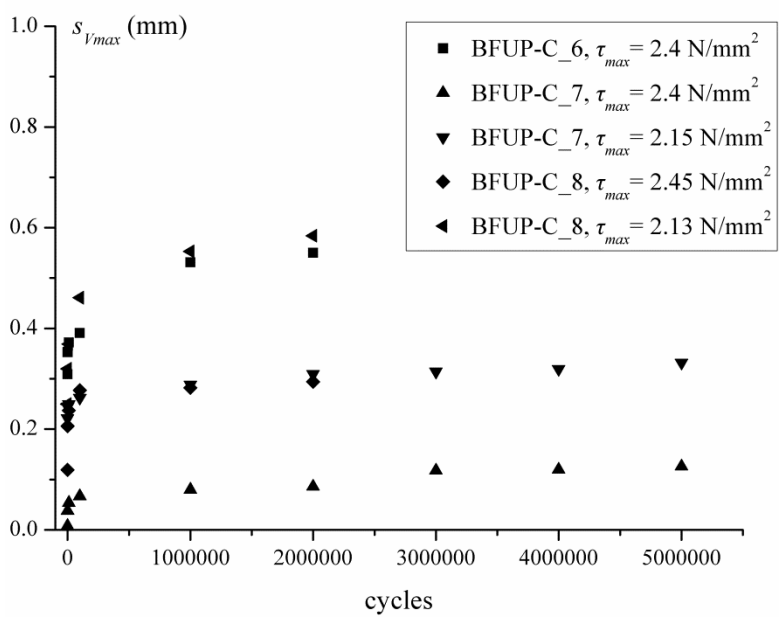

Fig. 3.38: Slip under maximum cyclic load, s_{Vmax} , as a function of the number of cycles, for cyclic loading for an UHPFRC-cement grout interface

Similarly to the residual slip, the slip, s_{Vmax} under the maximum cyclic load, as observed in figures 3.36 to 3.38 and in figures 3.30 to 3.32 from the peaks of the cycles, it is increasing with the number of cycles. However it starts to stabilize practically after one to two million cycles.

The data from cyclic loading of interfaces concerning the residual slip, s_{res} and the slip s_{Vmax}, under load V_{max}, are used in the following chapter to form analytical expressions. These expressions should make it possible to describe the evolution of the constitutive law with the number of cycles.

Figure 3.39 illustrates the evolution of the uplift during cyclic loading, typically of the same manner for all three interfaces, for the rough concrete-cement grout interface and for specimen BR-C_19 as an example.

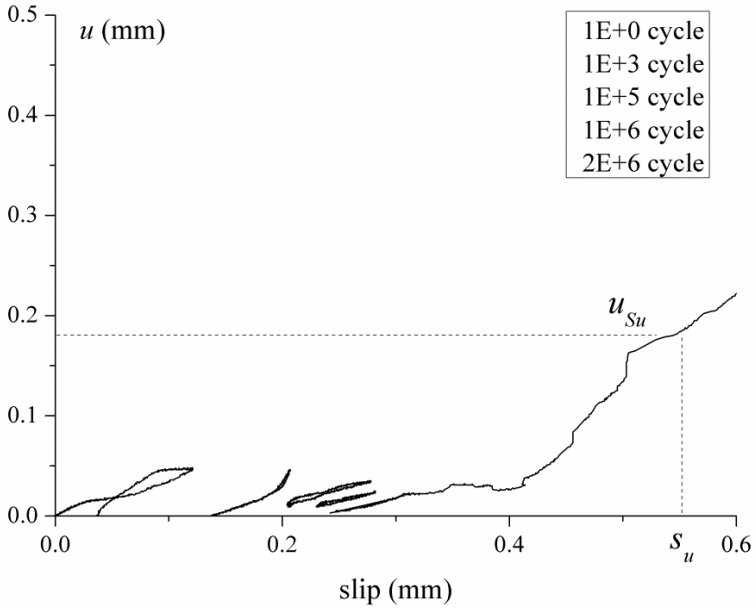

Fig. 3.39: Uplift-slip relationship for rough concrete-cement grout interface, specimen BR-C_19

It is noticed in figure 3.39 that, during cyclic loading and for a loading range inside the quasi-elastic behaviour, uplift in the interface is hardly noticeable and remains lower than the value of the uplift, u_{Su} which corresponds to the initiation of failure for static loading. The value of the uplift u_{Su} for the specimen BR-C_19 is equal to 0.18 mm (figure 3.39) and almost coincides with the average value u_{Su} for the rough concrete-cement grout interface which is 0.16 mm, as seen in paragraph 3.2.4 (fig. 3.23).

The other interfaces, embossed steel-cement grout and UHPFRC-cement grout, exhibit similar behaviour concerning the evolution of the uplift during cyclic loading.

We may conclude that the value of slip, s_u and the uplift, u_{Su} at failure, as recorded from the constitutive law of the monotonic loading, for all three types of interfaces, present limits of failure also for cyclic loading of interfaces. Hence, it can be implied that a safe fatigue failure criterion for interfaces should take into account this limits into consideration.

Observations

Failure for specimens with embossed steel-cement grout interface subjected to cyclic loading is either a mixed type of *bearing* and *shear failure*, as it is the case for specimens TS-C_10 and TS-C_13 or *shear* type, specimens TS-C17 and TS-C_18 (figure 3.40).

a)  b) 

Fig. 3.40: a) mixed type of *bearing- shear failure* in embossed steel-cement grout interface for cyclic loading of specimen TS-C_ 10 and b) *shear failure* type for specimen TS-C_18

Repeated loading for an embossed steel cement-grout interface results to the accumulation of residual slip and consequently to better bonding and interlocking conditions, thus the failure for a static test following a cyclic loading is either of mixed type, *bearing* and *shear*, or just of *shear* type. For the other two types of interfaces failure is of *shear* type as for static loading.

Remarks for cyclic loading of interfaces

Several remarks can be made which set the frame for the analytical modeling of interfaces under cyclic loading which will be presented at chapter 4.

- All interfaces exhibit similar behaviour. The shear stress-slip relationship is developed, during cyclic loading, inside an envelope defined by the constitutive law of the monotonic loading.
- Cyclic loading results to a kind of damage expressed by the development of a residual slip in the interface. For a variation of shear stress inside the quasi-elastic domain, the residual slip stabilizes with the number of cycles and as long as slip and uplift in the interface are lower than the slip s_u and the uplift u_{Su} at failure for monotonic loading, the fatigue failure is

avoided. On the other hand, when the applied stress exceeds the elastic limit of the monotonic law, the residual slip increases towards the failure of the specimen.

- The stabilization of residual slip for loading range inside the elastic domain justifies the verification of fatigue with respect to fatigue limit.
- Due to the fact that the interface behaviour to cyclic loading seems to be controlled by an envelope, the constitutive law of monotonic loading, the development of the residual slip has a direct impact on the stiffness of the interface. Interface subjected to shear cyclic loading develops a kind of "memory effect". Once a certain number of cycles are executed they result to the development of the residual slip. From that point and after, any further static loading applied result to a shear-slip curve that starts with a slip (residual slip) and has the tendency to follow the constitutive law for the monotonic loading. This "memory effect" takes place also in the domain of the post failure behaviour.

3.3 Push-out tests

3.3.1 Principles

The push-out tests are performed to obtain experimental values of the behaviour of the innovative connection to be used for the validation of the numerical model developed for the connection. Both static and cyclic loading tests are performed. A push-out specimen consists of two blocks of reinforced concrete (or UHPFRC) assembled together with a steel connector by filling the void between them with cement grout. Figure 3.41 presents the principle of the push-out test. The force is applied to the steel element of the specimen and then is transmitted by shear, through the interfaces, to the blocks of reinforce concrete (or UHPFRC) and from them to the base of the testing setup.

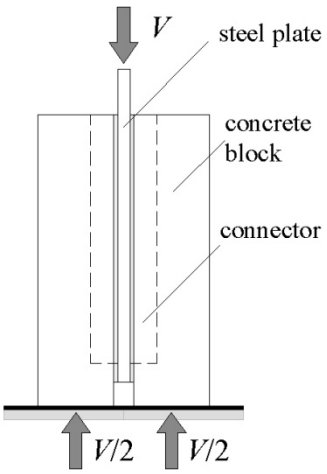

Fig. 3.41: Principal of the push-out test [Thomann 2005]

3.3.2 Specimens and materials

Fifteen symmetrical specimens for push-out tests have been fabricated. The blocks for twelve specimens are made of reinforced concrete-concrete quality C50/60 and for three specimens of UHPFRC, the DUCTAL© product. The steel connector consists of a steel plate in which the embossed steel plates are welded. The latter are of the same type as those at the direct shear tests. The common VSL cement grout is used for ten specimens with concrete blocks. For the last two push-out specimens with concrete blocks and for the specimens with blocks of UHPFRC, the new cement grout VSL-HPI,

with enhanced characteristics is used. The following figures illustrate the geometry of the parts which constitute the specimens and the assembly as well.

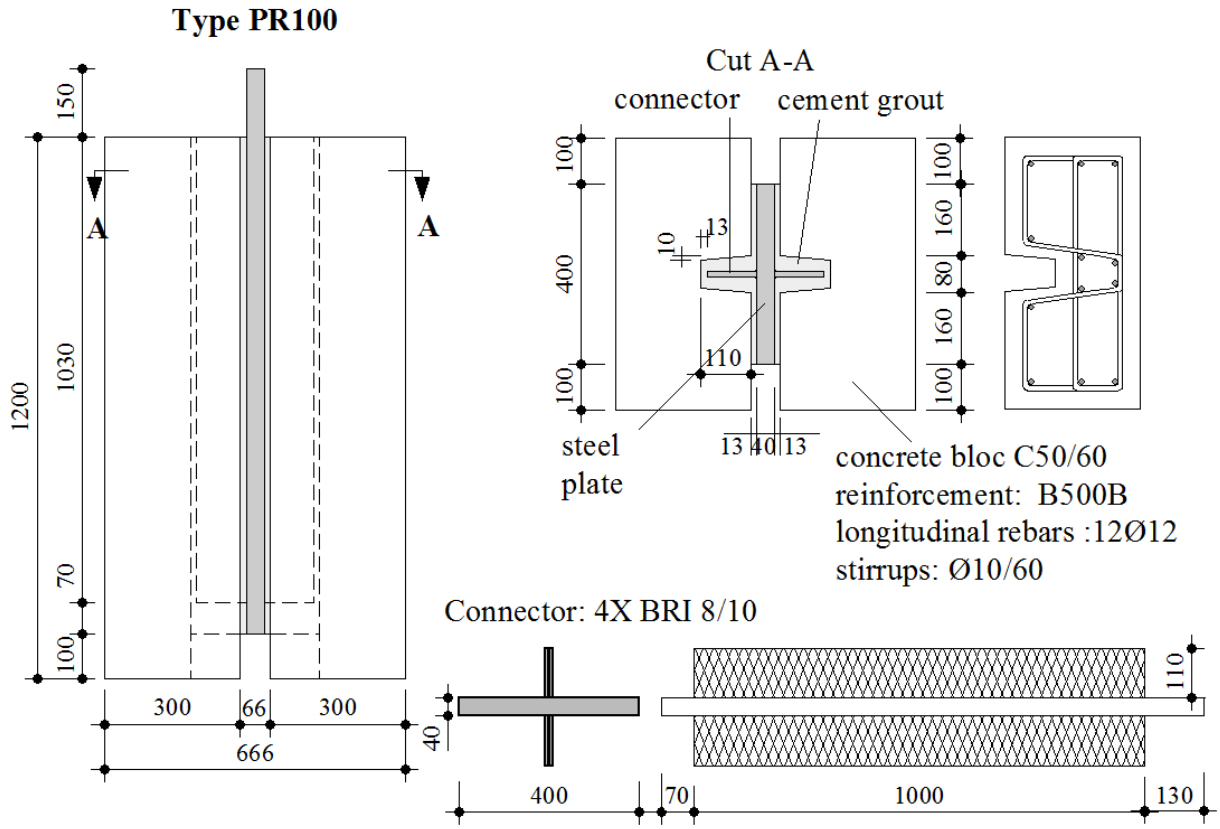

Fig. 3.42: Geometrical characteristics of push-out specimens consisted of blocks of reinforced concrete, steel connector and cement grout

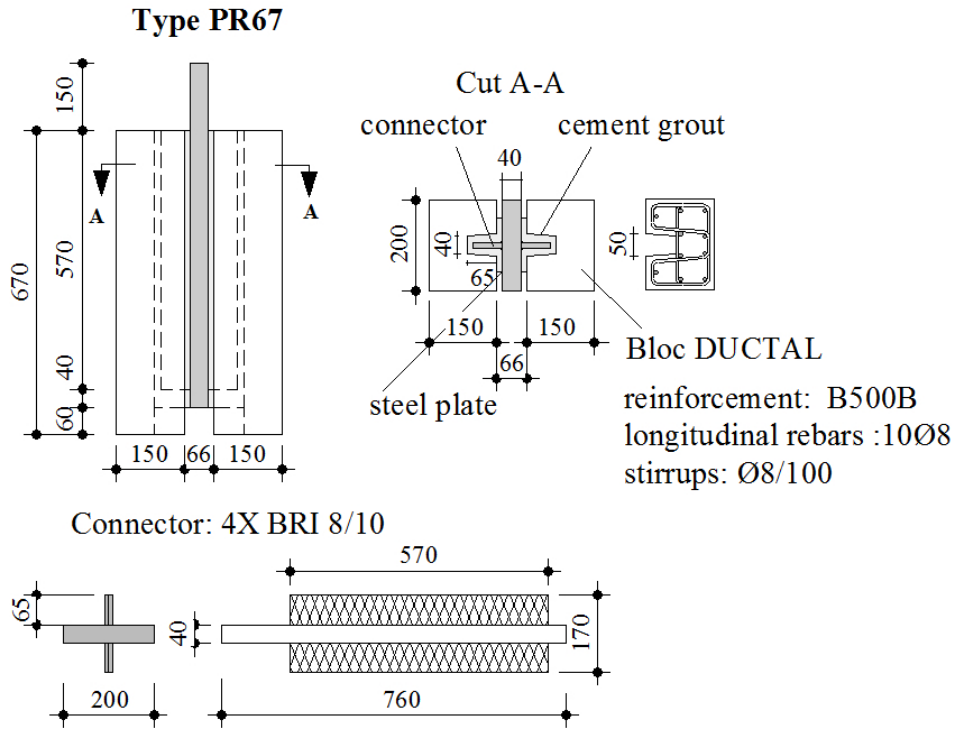

Fig. 3.43: Geometrical characteristics of push-out specimens consisted of blocks of DUCTAL© with steel reinforcement, steel connector and cement grout

For the blocks made of reinforced concrete the surface of the inner rib is roughened by the same procedure used for the concrete plates of the direct shear tests, as described above at 3.2.2. Figure 3.44 shows the inner rib of such a block with the exposed aggregates.

Fig. 3.44: Reinforced concrete block for push-out tests, with rough inner rib

As it concerns the blocks made of UHPFRC (DUCTAL©), an artificial rough surface is created in the inner rib, with 8 m conical studs, using a proper formwork. Figure 3.45 illustrates a block of UHPFRC used for the push-out specimens and the geometry detail of the formed artificial rough surface.

a) 

b) 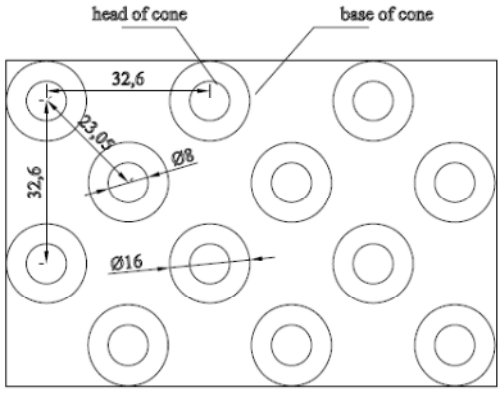

Fig. 3.45: a) UHPFRC block with conical studs in its inner rib, b) geometry detail

3.3.3 Testing procedure

Tests are performed with the machine Trebel Schenk of the laboratory of the Civil Engineering Institute. The load is applied under displacement control, for static tests, with a loading rate of 0.25 mm/min till failure and 1 mm/min for post-failure.

Cyclic tests are performed under force control with security limits in the displacement of the hydraulic jack, and with a frequency of 1.5 Hz. During cyclic loading only the shear force is recorded, hence in order to record the evolution of the force-slip relationship, with the number of cycles, the cyclic loading stops at certain moments, and a complete loading-unloading cycle is performed at 0.25 mm/min to register data. In addition, the unloading allows registering of the residual slip that develops in the connection, with the number of cycles.

Figures 3.46 and 3.47 illustrate the major instrumentation used for the push-out tests. Eight transducers, attached at the steel plate at the first and at the second third of the height of the connector, are used to measure the relative slip between the steel plate and the blocks (figure 3.46).

a) 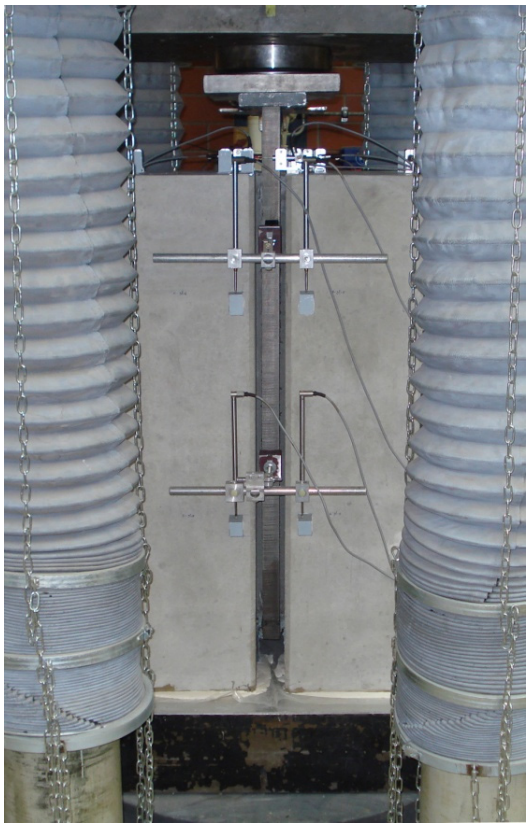 b) 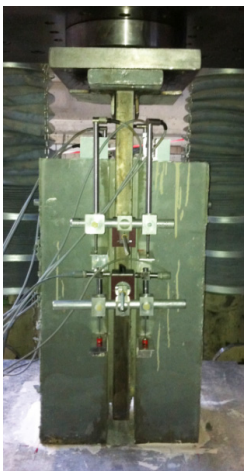

Fig 3.46: Instrumentation for measurement of slip between steel plate and the blocks a) Reinforced concrete blocks b) UHPFRC blocks

At the upper part of the specimen four transducers, two at each connector, serve to measure the uplift between connector and the concrete blocks. Other transducers are used to measure several displacements between parts of the specimen assembly (figure 3.47).

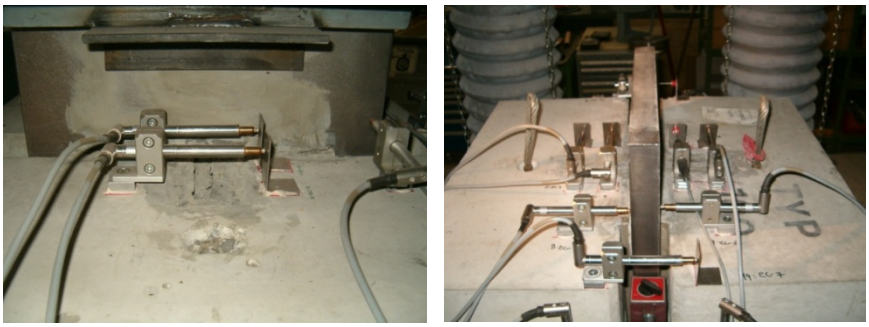

a) Transducers at upper part of reinforced concrete blocks

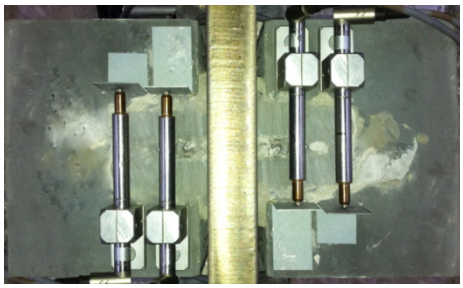

b) Transducers at upper part of UHPFRC blocks

Fig 3.47: Instrumentation at the upper part of push-out specimens

It has to be noted that fabrication of specimens is limited in a certain period of months to avoid aging of cement of sacs offered by VSL Company. This fact and the availability of the testing machine, have as a result that for several specimens the application of the load is done more than a month from the fabrication of the specimen. However, information obtained by compression tests on cylinders, form VSL Company, have shown very limited increase of compression resistance due to aging, for the period after the curing of 28 days.

For specimens PR100_8 and PR100_9 the produced cement grout lacked fluidity and the removing of formwork has shown voids on the connection. These voids are verified by diamond cutting of specimens. Hence these two specimens are excluded from the study. (These kinds of problems are not however to be encountered in real practice with the new type of cement grout, as mentioned in the next paragraph).

The last two specimens with reinforced concrete blocks, PR100_11 and PR100_12 and the specimens with blocks of UHPFRC are filled with the cement grout VSL-HPI, the currently used grout for prestressing tendons from VSL Company. As already mentioned, despite its lower compression resistance in comparison with the common cement grout VSL, this new grout leads to a better performance of the connection due to its expansive agent that compensates shrinkage volume loss during curing. This type of cement grout has also the appropriate characteristics of fluidity.

The following tables summarize the main characteristics of the push-out tests. Table 3.5 provides information on tests for specimens with blocks of reinforced concrete whereas table 3.6 for specimens with blocks of UHPFRC. Notation f_{cm} stands for the mean cement grout resistance at 28 days after the fabrication. V_{max} and V_{min} correspond to the lower and higher values of the applied load for cyclic loading, where V_u corresponds to the ultimate load. Notation t_o stands for the time from the specimens' fabrication till the application of the load, whereas t for the time from the specimens' fabrication till the application of the load at the final test that follows the runnout.

Table 3.5: Push-out tests, specimens with reinforced concrete blocks

Specimen name	Cement grout	f_{cm} (MPa)	t_o (days)	t (days)	V_u (kN)	V_{min} (kN)	V_{max} (kN)	V_{max}/ V_u	Cycles executed
PR100_1	VSL	86.4	50	-	2538	-	-	-	1
PR100_2	VSL	86.4	78	127	2565	260	1060	0.41	5E+6
PR100_3	VSL	76.4	32	-	1836	-	-	-	1
PR100_4	VSL	76.4	33	-	-	260	1060	-	4E+6*
PR100_5	VSL	94.3	109	152	2407	260	1060	0.44	5E+6
PR100_6	VSL	94.3	107	-	1963	-	-	-	1
PR100_7	VSL	99.4	185	230	3081	260	1600	0.52	5E+6
PR100_8	VSL	99.4	145	171	2900	260	1600	0.55	2E+6
PR100_9	VSL	123.8	32	-	1801	-	-	-	1
PR100_10	VSL	123.8	33	-	1795	-	-	-	1
PR100_11	VSL-HPI	66.8	28	91	4130	260	1860	0.45	2.5E+6
PR100_12	VSL-HPI	66.8	94	-	3230	-	-	-	235**
* test stopped due to jack malfunction which damaged the specimen									
**5 cycles of variable high amplitude and 230 cycles post failure									

Table 3.6: Push-out tests, specimens with blocks of UHPFRC

Specimen name	Cement grout	f_{cm} (MPa)	t_o (days)	V_u (kN)
PR67_1	VSL-HPI	56	28	1040
PR67_2	VSL-HPI	56	29	1010
PR67_3	VSL-HPI	56	30	930

The loading range mentioned in table 3.5 and applied in cyclic loading is chosen according to assumptions made in paragraph 2.3.3. More precisely the minimum applied load 260 kN in the specimen corresponds to longitudinal shear per unit length equal to 130 kN/m. This value is a mean value of longitudinal shear acting in the connection of a twin-girder steel-concrete composite beam for long term loads such as dead loads from coating, cornice and safety barrier.

Verification of connection with respect to limit of fatigue according to fatigue load model 1 of code SIA 261 implies for the region of end support an added longitudinal shear of 400 kN/m (maximum value, corresponding to short span about 30 m), thus the total value of longitudinal rises to 530 kN/m. Consequently, verification with respect to the limit of fatigue for the type of bridges consider and according to code SIA 261, imposes a maximum load, V_{max} equal to 1060 kN.

Verification of connection with respect to fatigue limit according to load model proposed by Meystre and Lebet [Meystre and Lebet 2011], implies for the region of end support an added longitudinal shear of 670 kN/m (maximum value, corresponding to short span about 30 m), resulting to a total value for the longitudinal shear of 800 kN/m. Consequently the maximum load V_{max} for this check rises to 1600 kN/m.

The value of V_{max} equal to 1860 kN chosen for specimen PR100_11 aims to provoke failure to specimen so as to have a failure point on an a S-N resistance curve for the connection. However the specimen resisted more than 2 million cycles, the test continued and finally it was decided to stop at 2.5 million cycles to perform a static test to investigate the remaining resistance.

3.3.4 Static loading

Results and observations

The following figures 3.48 and 3.49 illustrate the force-slip relationship (slip is the average of the values measured with the transducers) obtained from static testing, including static tests which follow runnout cyclic tests. Hence, for the latter, the initial slip is different from zero and corresponds to the residual slip which develops during the cyclic loading.

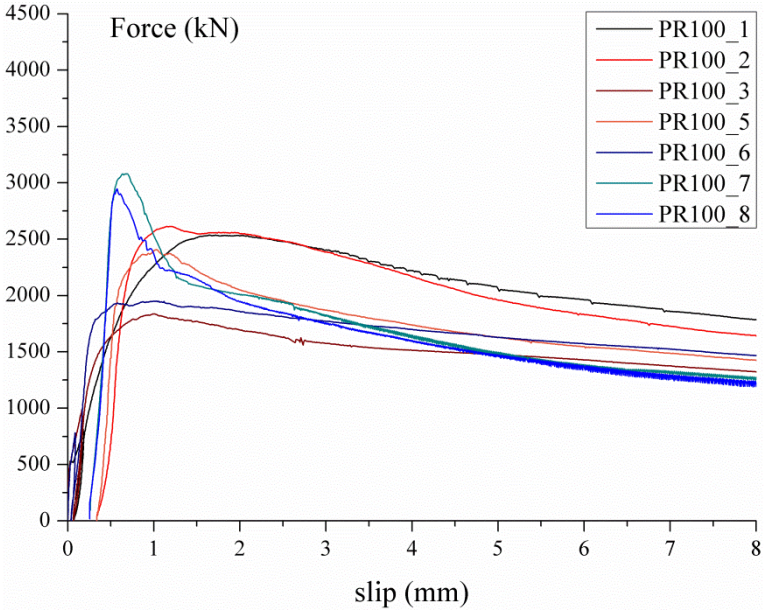

Fig. 3.48: Force-slip relationship for push-out specimens with concrete blocks and cement grout VSL

According to fig. 3.48 the resistance of the specimens varies. Generally specimens filed with cement grout of the same fabricated mixture develop similar resistance. Diamond cutting of failed specimens permits to do several observations which justify the reduced resistance of specimens PR100_3 and PR100_6, as described later on.

Generally the connection exhibits a primary stiff ascending branch prior to failure, meaning that the longitudinal shear force per unit length increases followed by a moderate slip, between concrete blocks and the steel plate, which at failure point varies from 0.7 to 1.8 mm. Once the ultimate resistance is reached, failure initiates expressed by an increase of slip. The post failure branch is characterised also by a decrease of the resistance, which can be abrupt (specimens PR100_7 and PR100_8) or ductile.

The force slip relationship for specimen PR100_11 is presented in figure 3.49. This specimen is filled with another type of cement grout, the VSL-HPI grout, which despite its reduced compression resistance in comparison with the cement grout of the specimens of figure 3.48 (table 3.5, column f_{cm}), contains an expansive agent that promises better bonding conditions between the materials that form the interfaces and consequently better structural performance.

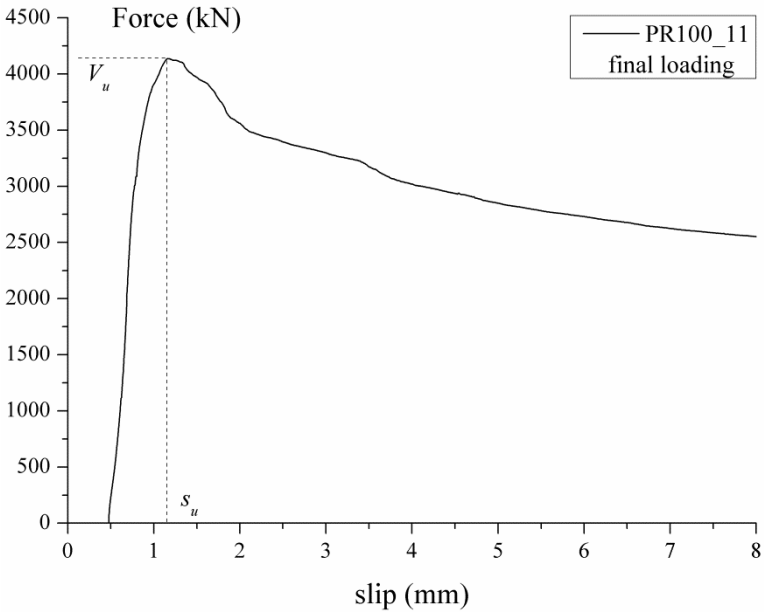

Fig. 3.49: Force-slip relationship for push-out specimen PR100_11, with concrete blocks and cement grout VSL-HPI

Figures 3.50 and 3.51 illustrate for the specimens of figures 3.48 and 3.49 the uplift-slip relationship. The uplift in this case is the transversal separation between the steel connector and the block, at the upper part of the specimen (figure 3.47). This value is the half of the value measured by transducers, figure 3.47a, since the transducers measure the uplift of both sides from the connector. The presented uplift corresponds to the addition of the uplift between rough concrete-cement grout and the uplift of embossed steel plate - cement grout, with the second part being the most significant.

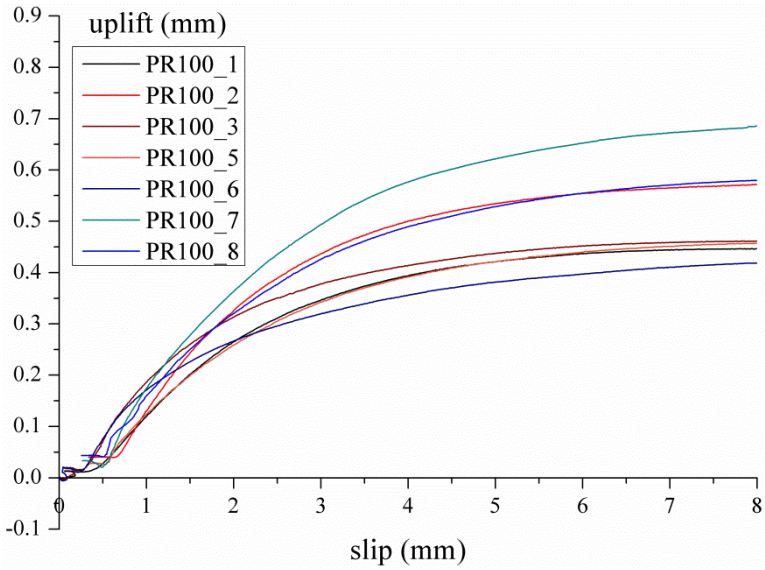

Fig. 3.50: Uplift-slip relationship for push-out specimens with concrete blocks and cement grout VSL

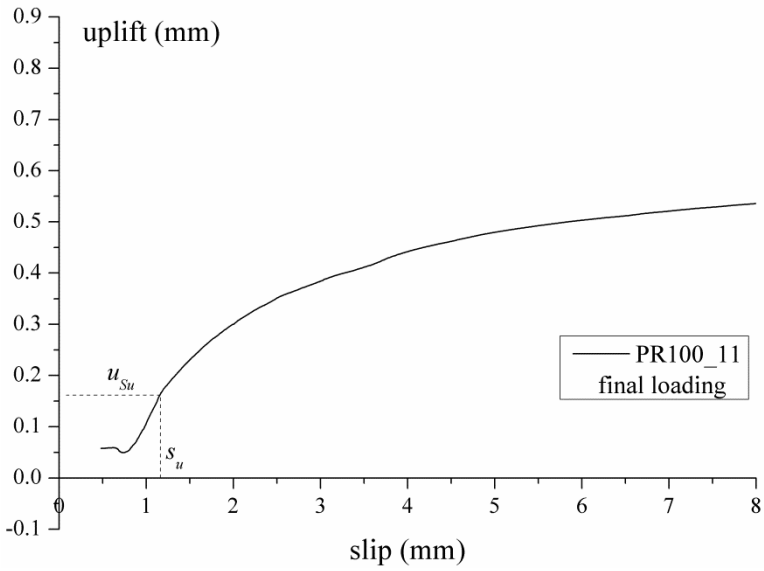

Fig. 3.51: Uplift-slip relationship for final test of push-out specimen PR100_11, with concrete blocks and cement grout VSL-HPI

Uplift in the interface presents prior to failure relatively low values, less than 0.2 mm. After failure, $s>s_u$, uplift increases to an asymptotic value which is achieved at about 8 mm of average slip in the interface.

The figure 3.52 illustrates the force-slip relationship for specimens with UHPFRC blocks and VSL-HPI cement grout. Prior to failure, an unloading takes place to investigate its influence in the structural performance.

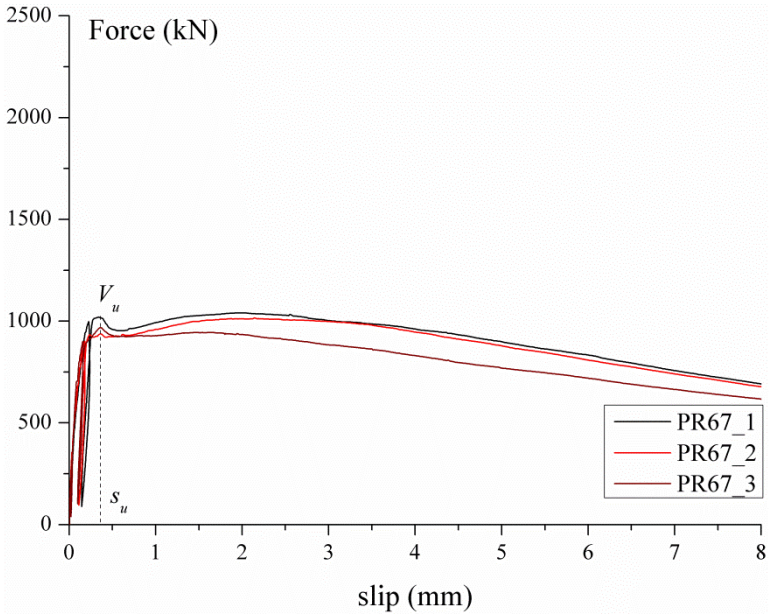

Fig. 3.52: Force-slip relationship for push-out specimens with blocks of UHPFRC

Specimens with blocks of UHPFRC with 8 mm conical undulations and embossed steel plates exhibit a primary stiff and elastic ascending branch prior to failure. Contrary to the specimens with concrete

blocks failure branch is more ductile. This can be attributed to a normal stress in the interface which results both of the used reinforcement but also of the tension resistance of UHPFRC. It should be also added that the confinement imposed by reinforcement is not thoroughly uniform at the longitudinal sense, its efficiency is related to distance of the rebars that provide confinement, whereas the confinement due to fibres of UHPFRC is more likely to be uniform.

Concerning uplift in the connection, as illustrated in figure 3.53 the behaviour is similar to that of specimens with blocks of reinforced concrete. It is the result of the addition of the uplift between cement grout-UHPFRC and the uplift of cement grout-embossed steel plate, with the second term being the most significant. Uplift is hardly noticeable before initiation of failure (slip s_u), whereas after that it follows an exponential rise towards an asymptotic value.

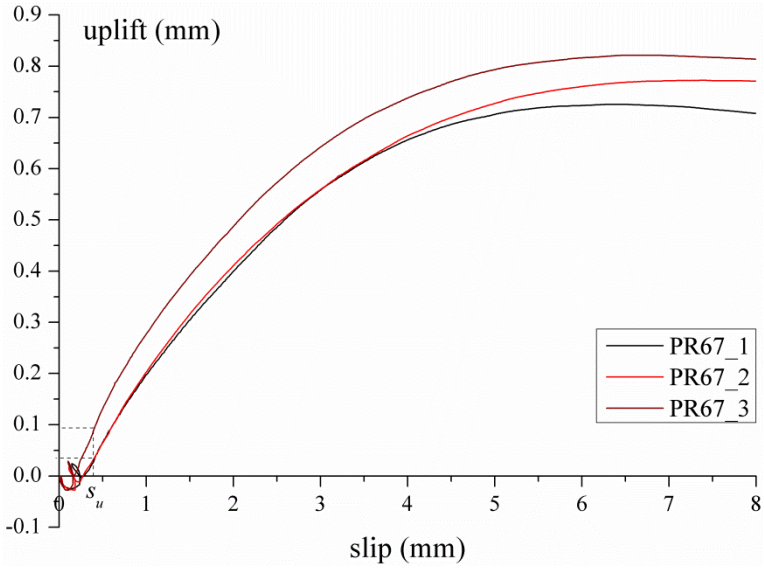

Fig. 3.53: Uplift-slip relationship for push-out specimens with blocks of UHPFRC

Remarks for static loading

The figure 3.54 illustrates two typical examples of the development of cracks at the upper part of the concrete blocks of the push-out specimens.

Fig. 3.54: Cracking of concrete blocks at the upper part after failure
(specimens PR100_1 & PR100_6).

Cracks initiate in the cement grout at the end of the connector and propagate inside the reinforced concrete block. Initially cracks are inclined and they are redirected vertically at the level of the

position of the lower transverse reinforcement. Cracks close at the level of the upper reinforcement. As noticed in the figures above, the slip between the concrete block and the connectors corresponds mostly to the relative slip between the embossed plates of the connector and the cement grout. The relative slip between rough concrete and cement grout is hardly noticed. The same conclusion is reached when examining the failure surface as obtained after diamond cutting of failed specimens.

The figures 3.55 and 3.56 present the view obtained after cutting the failed specimen PR100_5. The main mass of cement grout is separated from the embossed steel plates. Shear type of failure of cement grout inside the rhombus, is noticed. As illustrated, the failure surface develops between the embossed steel-plate and the cement grout. Any slip between rough concrete and cement grout is relative small since, after the diamond cutting procedure, the cement grout remains attached to the rough concrete (figure 3.56).

Fig. 3.55: Steel connector after diamond cutting of block, specimen PR100_5.

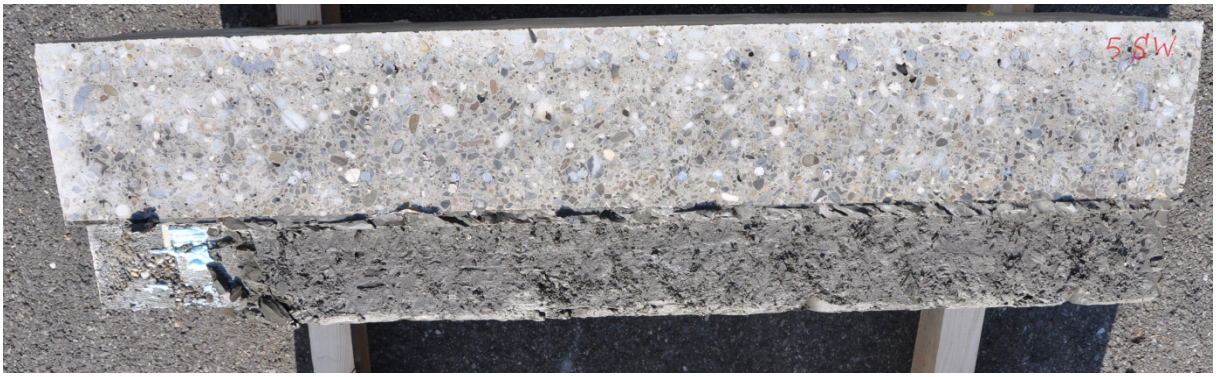

Fig. 3.56: Concrete block after diamond cutting. Cement grout remains attached to rough concrete. Specimen PR100_5

Cutting of specimens allows also making several hypotheses for the scatter of the ultimate resistance, noticed at figure 3.48. Besides influence of the scatter of the failure criteria of the shear resistance of the interfaces mentioned at 3.2.4, the following suggestions are proposed. Concerning specimen PR100_3, the lower resistance can be attributed to local weakness at the base of the concrete block which cracked close to the interface, figure 3.57. It could also be attributed to some voids created at filling of the assembly with the cement grout figure 3.58.

Fig. 3.57: Cracking of concrete block of specimen PR100_3 close to the interface

Fig. 3.58: Block of specimen PR100_3, missing part of cement grout

Concerning the specimen PR100_6, one of the two blocks was partly cracked, before testing, as seen at figure 3.59. Furthermore, as may be seen at figure 3.60 several rhombus of the embossed steel plate are without cement grout, the latter remained attached to concrete block. From the above, a combined bearing-shear failure type may be assumed, caused by a weaker confinement effect, in comparison with the other specimens and thus resulting to lower longitudinal shear resistance.

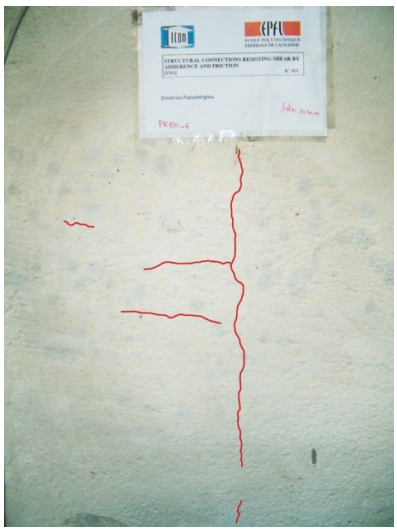

Fig. 3.59: Pre-cracking of concrete block of specimen PR100_6.

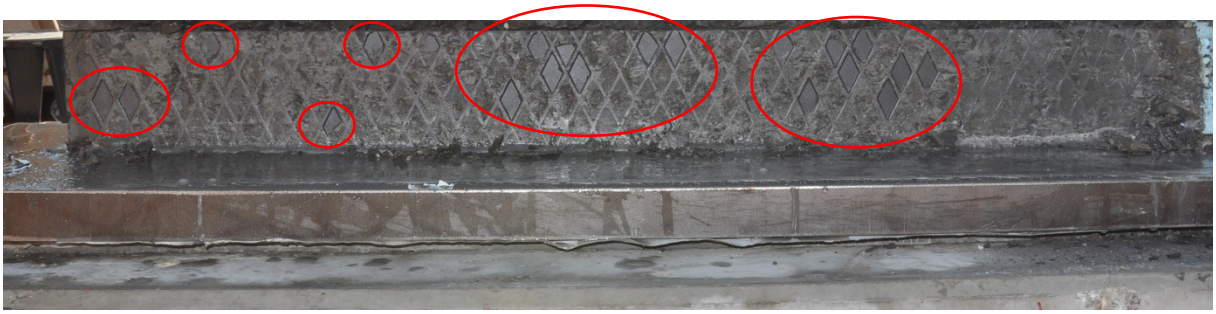

Fig. 3.60: Combined bearing-shear failure of interface. Specimen PR100_6

Cutting of specimens has also revealed that the positioning of the middle reinforcement that crosses over the inner rib of the concrete block was not located on the same exactly distance from the edge of the rib for all specimens. The distance varies between 35 to 45 mm and is generally inferior for the specimens that show higher resistance revealing a more effective confinement as will be proven in the 5th chapter.

Figure 3.61 illustrates the cracking of the upper part for the push-out specimens, whose blocks are of UHPFRC and steel reinforcement.

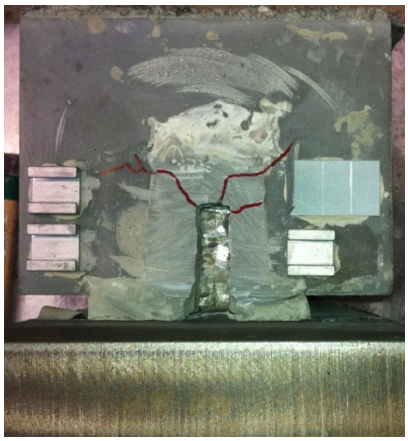

Fig. 3.61 Cracking of UHPFRC block after failure

As for the concrete blocks, the cracks initiate in the cement grout, at the edge of the embossed steel plate and enter inside the block. Their propagation is limited both by the lower reinforcement and by the tension capacity of the fibre reinforced concrete as well. Again, the slip between the block and the connector is almost totally defined by the weaker of the two interfaces, which is the one between the embossed-steel plate and the cement grout.

Concerning the connection behaviour to monotonic shear, the following general remarks are made:

- Connection exhibits high initial stiffness prior to failure.
- Initiation of failure in the interface is happening when the ultimate value of longitudinal shear force is reached and it is a non-reversible situation, followed by continuous increase of slip for further loading of the connection.
- When confinement in the interface is sufficient, the failure type is shear and develops in the embossed-steel cement grout interface which is the less resistant interface.

- Uplift in the developed interfaces is limited prior to failure, after failure, it increases to an asymptotic value at about 8-10 mm of slip.
- The characteristic slip capacity, as defined by Eurocode 4 [EC4 2004] in paragraph 6.6, is not always 6 mm so as to characterise connection as ductile. Yet, the ductility of the connection is not negligible. The ductility of the connection is significant for the case of UHPFRC blocks, and varies for the case of reinforced concrete blocks.
- For the geometry connection and reinforcement of the specimens tested, the value 1500 KN/m, of the longitudinal shear force per unit length, calculated with the elastic method, defined in 2.4 for ULS, was satisfied for both specimens fabricated with new cement grout VSL-HPI, and for one specimen fabricated with the common VSL cement grout (table 3.5). This remarks arises the need for a model to predict the connection's resistance and investigate the parameters that are favourable in order to provide design tools, for engineering practice, which will permit a design of the connection for the needed level of resistance at ULS.

3.3.5 Cyclic loading

Results and observations

The verification of connection's resistance to fatigue is performed, according to paragraph 2.3.3, with respect to fatigue limit, a) according to fatigue load model 1 of SIA 261, for loading range Δv = 400 kN/m and maximum cycle load v_{max} = 530 kN/m, and b) according to fatigue load model proposed by Meystre and Lebet [Meystre and Lebet 2011] for loading range Δv = 670 kN/m and maximum cyclic load equal to v_{max} = 800 kN/m.

Following graphs 3.62 and 3.63 illustrate the force-slip relationship, for several characteristic cycles and the final static test, for specimens PR100_2 and PR100_5.

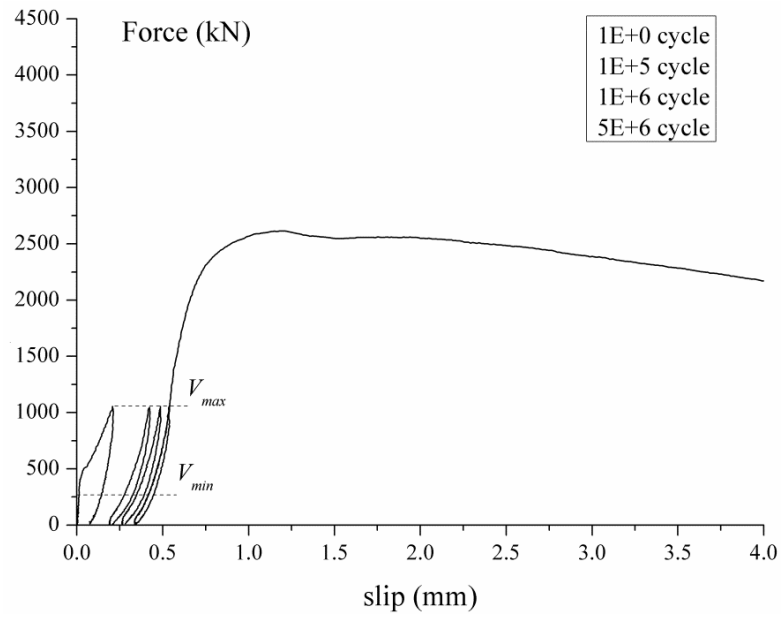

Fig. 3.62: Force-slip relationship for push-out specimens PR100_2

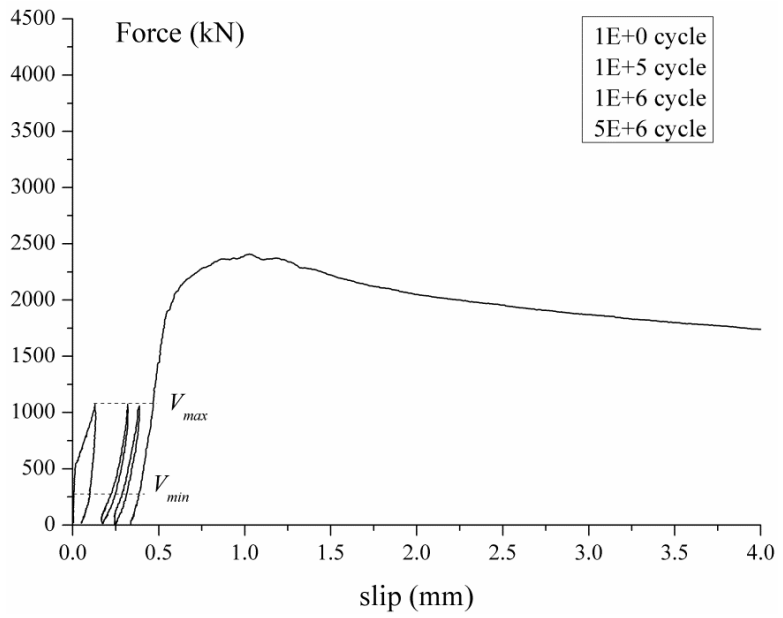

Fig 3.63: Force-slip relationship for push-out specimens PR100_5

Specimens PR100_2 and PR100_5 are tested for loading range Δv = 400 kN/m and maximum longitudinal shear force per unit length, v_{max} = 530 kN/m for 5 million cycles (correspondingly ultimate load, V_{max} is 1060 kN). Both specimens exhibit similar behaviour. Cyclic loading results to the development of a residual slip between steel and concrete block, which stabilizes as the number of cycles increases.

Fig. 3.64 presents the comparison between specimen PR100_1, which was subjected to monotonic loading, and specimen PR100_2 which was subjected initially to cyclic loading and finally to a static test. Both specimens were fabricated with the same cement grout.

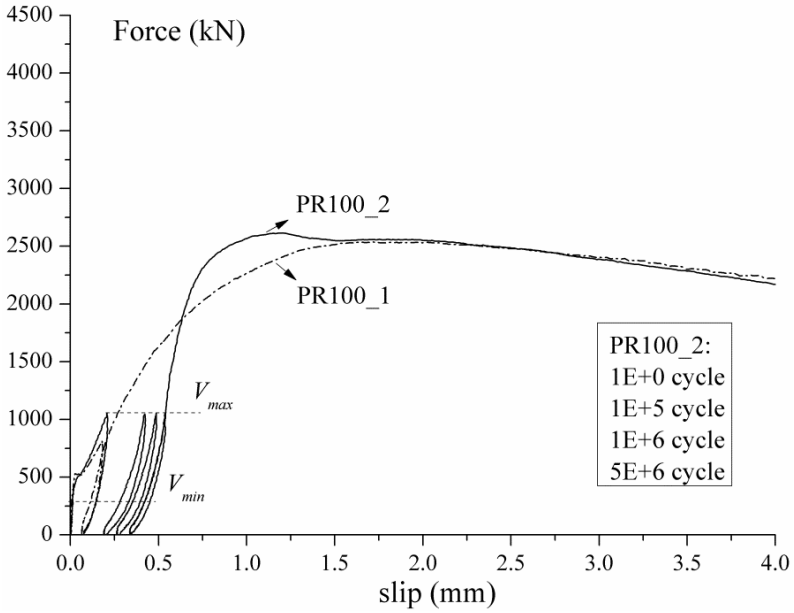

Fig 3.64: Comparison of the force-slip relationship, for specimens PR100_1 and PR100_2

Graph in figure 3.64 shows that for repeated loading for 5 million cycles, and for a variation of longitudinal shear force per unit length equal to 400 kN/m (correspondingly V_{max}-V_{min} = 800 kN), no degradation of the bearing capacity occurs for specimen PR100_2 in comparison with specimen PR100_1.

In addition, the "memory effect" defined in 3.2.5 for cyclic loading of interfaces is also present for cyclic loading of connection. As we observe in figure 3.64 the increase of the force as a function of the slip becomes more abrupt as the number of cycles increases and at the final static test following, the constitutive law tends to meet the curve defined by the monotonic loading.

Once experimental verification of connection's resistance to fatigue limit, applying fatigue load model 1 of SIA 262, was successful, a higher loading range was selected and was applied at specimens PR100_7 and PR100_8. The loading range becomes equal to 670 kN/m resulting to a maximum applied longitudinal shear force per unit length, v_{max} = 800 kN/m. This loading range and maximum load correspond to verification at fatigue limit using fatigue load model of Meystre and Lebet [Meystre and Lebet 2011].

Figures 3.65 and 3.66 illustrate the force-slip relationship, for several characteristic cycles and the final static test, for specimens PR100_7 and PR100_8.

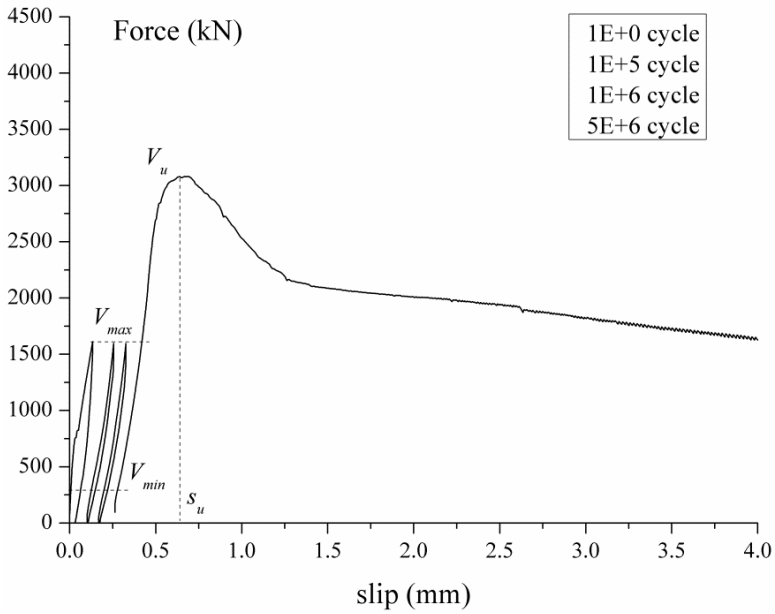

Fig 3.65: Force-slip relationship for push-out specimens PR100_7

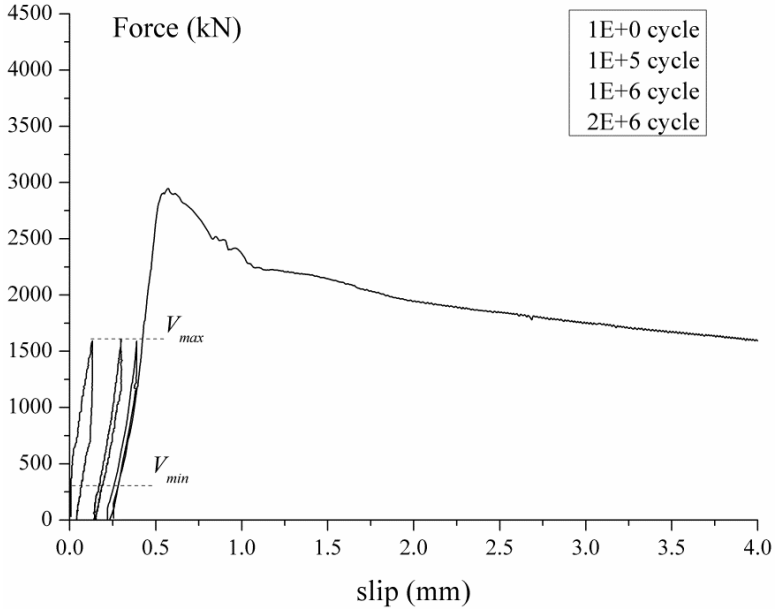

Fig 3.66: Force-slip relationship for push-out specimens PR100_8

It is observed in the above figures 3.65 and 3.66 that for both specimens, the connection resists the imposed loading range and the remaining resistance, at the final static test, is even higher than the resistance of specimen PR100_1, which was submitted directly to a static test. This can be attributed to aging of the cement grout. For the specimen PR100_7 the test was continued even after the needed two million cycles and since no failure occurred the cyclic test was stopped at five million cycles to perform a static test. Cyclic loading results to the development of a residual slip between steel and concrete block, which stabilizes with the number of cycles.

Since experimental verification of connection's resistance to fatigue limit (for both fatigue load model used) was accomplished, it was decided, concerning remaining specimens PR100_11 and PR100_12, to fabricate them using the cement grout VSL-HPI. This type of cement grout, as mentioned in 3.3.3,

despite its reduced compression resistance in comparison with cement grout of the previous specimens (table 3.5, column f_{cm}), contains an expansive agent that promises better bonding conditions between the materials that form the interfaces and consequently better structural performance.

Since better structural performance is expected, it is decided for specimen PR100_11 to increase even further the loading range during cyclic loading from 670 kN/m, which was applied to previous series, to 800 kN/m (correspondingly V_{max}-V_{min} = 1600 kN). Fig. 3.67 presents the force-slip relationship for specimen PR100_11.

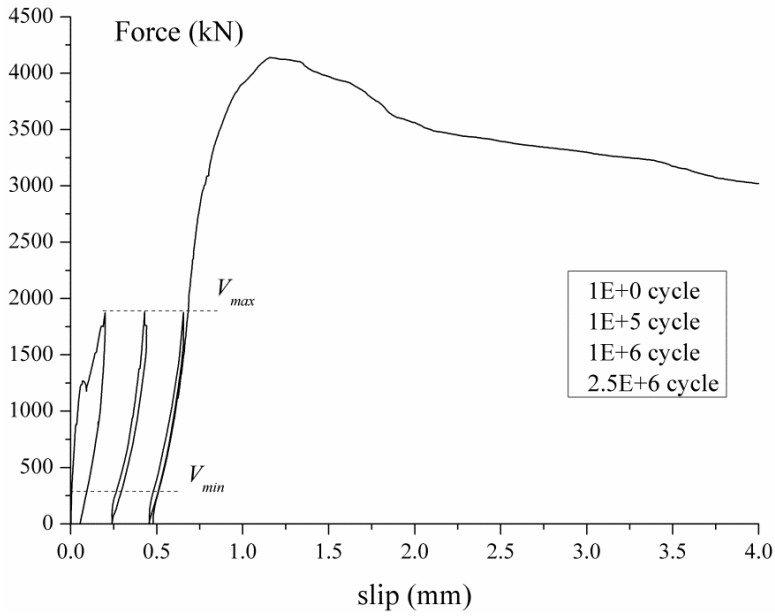

Fig 3.67: Force-slip relationship for push-out specimen PR100_11

The specimen resisted the applied cyclic load without failure for two and a half million cycles. As we observe in figure 3.67 the residual slip in the connection practically stops to increase after one million cycles. Hence, the cyclic loading is stopped and a final static test is performed to examine the remaining resistance which is found to be superior to the resistance of all the previous specimens which are fabricated with the old type of cement grout.

To all above specimens submitted to cyclic loading, the damage due to this type of loading is expressed with the accumulation of the residual slip as we observe in figures 3.62 to 3.67. The importance of this phenomenon is already described in the paragraph concerning the cyclic loading of interfaces, where it is mentioned that failure due to fatigue occurs when the accumulated slip reaches the value of slip, s_u, related to failure for monotonic loading. It is reasonable to suppose the same behaviour for the connection, since its resistance sources from the developed interfaces. The evolution of the residual slip in the connection should be studied and analytical expressions should be developed to relate this phenomenon with the duration of the cyclic loading. The following figures 3.68 and 3.69 present, correspondingly, the evolution of the residual slip, s_{res}, and the evolution of the slip under maximum cyclic load, s_{Vmax}, as a function of the number of cycles for the specimens whose constitutive relationship is presented at figures 3.62 to 3.67.

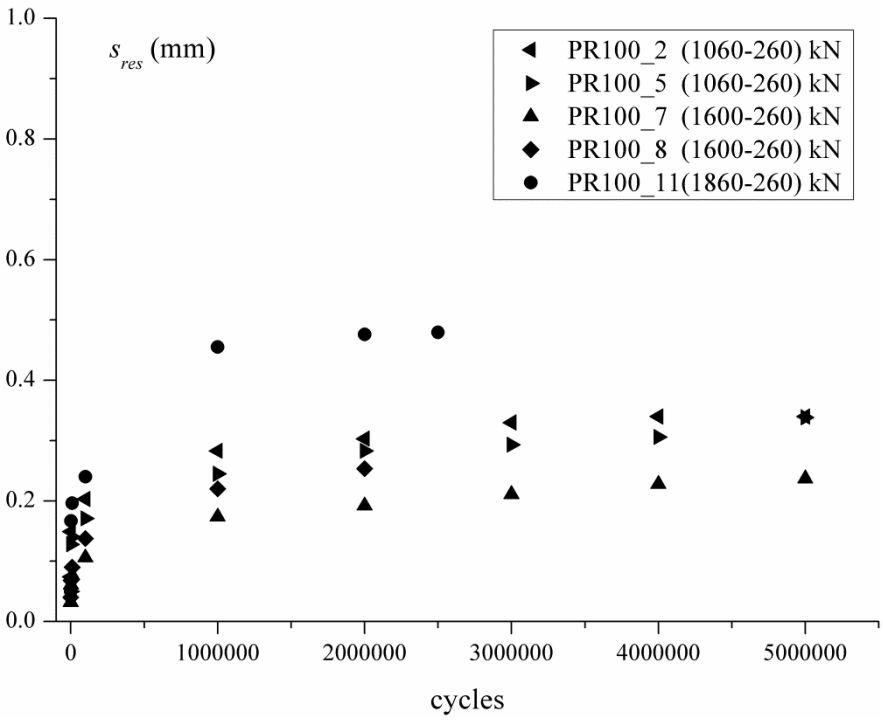

Fig. 3.68: Residual slip, s_{res}, as a function of the number of cycles

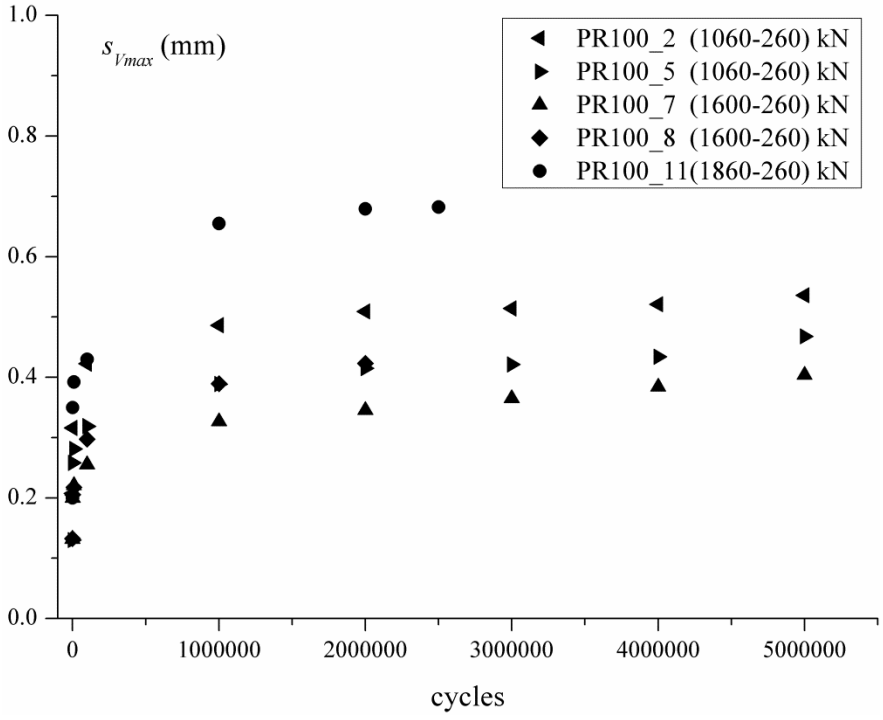

Fig. 3.69: Slip under maximum cyclic load, s_{Vmax}, as a function of the number of cycles

It is observed in figures 3.68 and 3.69 that both the residual slip, s_{res}, and the slip under maximum cyclic, s_{Vmax}, load are increasing with the number of cycles. However they tend to stabilize practically after two million cycles, and furthermore, they present close values. Based on figures 3.68 and 3.69 analytical expressions will be developed. These expressions together with the constitutive law of the first cycle, the latter obtained by a numerical model for connections behaviour-chapter 5-, will be used to predict the connection's force slip relationship with the number of cycles. The numerical model will also enable to verify, for a given connection, the value of V_{max} for which the stresses in the interfaces remain elastic (elastic domain of the connection behaviour). For the specimens of figures 3.68 and 3.69 the stabilisation of s_{res} and s_{Vmax} indicates, according to the observed behaviour for cyclic loading of interfaces, that the shear stresses developed in the interfaces remain elastic, for the corresponding, of course, normal stress acting on the interfaces.

For the final specimen, PR100_12, fabricated also with the cement grout VSL-HPI, it was decided to perform a high amplitude low cycle loading to initiate failure in the connection. Once this occurs, a low amplitude cycle loading is applied, in order to examine the resistance to cyclic loading in the post failure part. The following figure 3.70 presents the force-slip relationship of specimen PR100_12.

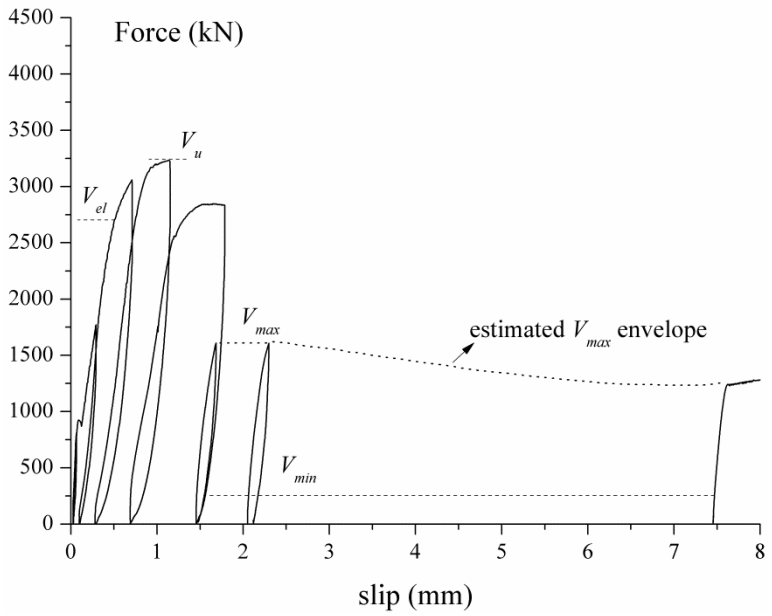

Fig 3.70: Force-slip relationship for push-out specimens PR100_12

It is observed in figure 3.70 that once the applied force reaches values close to the ultimate resistance, the residual slip obtains higher values than the ones for cyclic loading within the elastic domain (as it was the case for the specimens of figures 3.68 and 3.69). Furthermore at failure, when the ultimate value V_u is achieved, the resistance to fatigue becomes very limited. For a variation of longitudinal shear force per unit length equal to 670 kN/m, after failure, a number of only 230 cycles is executed till the slip of the connection reaches about 7.5 mm which corresponds almost at the point where only remaining friction contributes to the resistance.

Figure 3.71 illustrates the evolution of the relationship of uplift versus slip with the number of cycles for the connection of specimen PR100_7. Similar behaviour is observed by the other specimens that are submitted to cyclic loading.

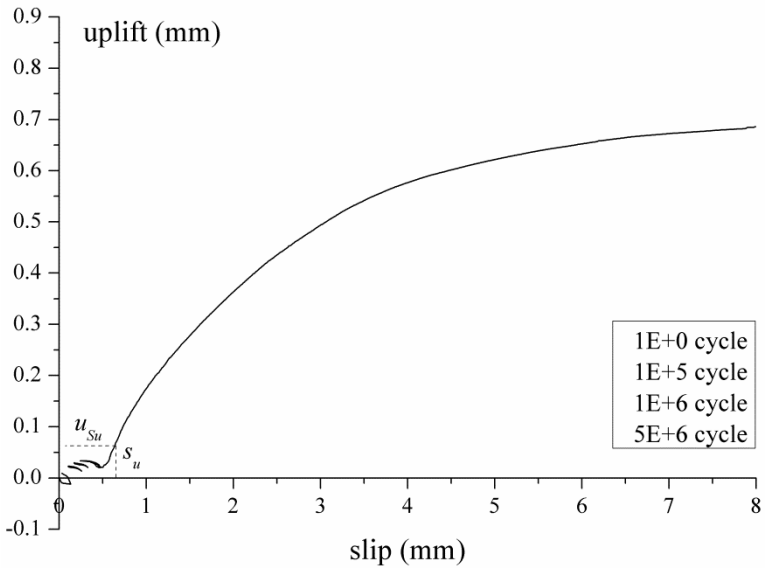

Fig. 3.71: Uplift-slip relationship for connection of specimen PR100_7

During the cyclic loading, the uplift remains low and as long as no failure occurs, it does not exceed the value which corresponds to failure. This behaviour is similar to that observed at the experimental study of interfaces and it is expected since this measured slip in the connection is the addition of the uplifts of the two interfaces, the uplift between rough concrete-cement grout, which is almost zero, and the uplift between embossed steel-cement grout, which is the major part of this addition.

The connections resistance to longitudinal shear under cyclic loading can be expressed in the figure 3.72 where the ratio of the maximum applied cyclic longitudinal shear versus the ultimate longitudinal shear resistance for static loading, v_{max}/v_u, is presented as a function of the number of cycles in logarithmic scale.

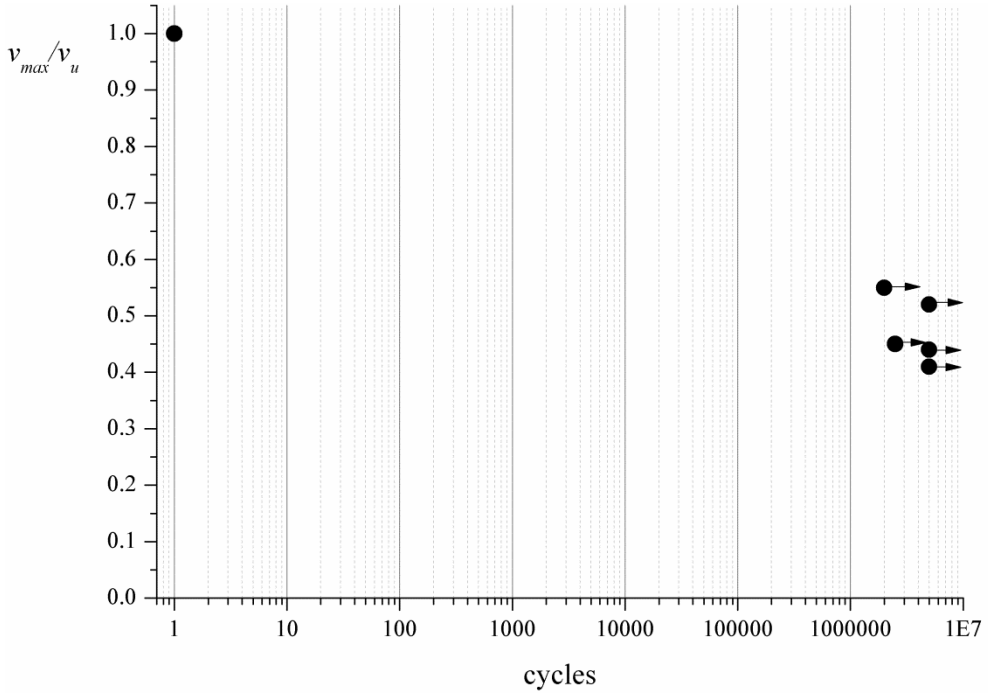

Fig. 3.72: v_{max}/v_u as a function of the number of cycles.

Additionally, for the connection geometry of the specimens tested, the connection's resistance achieved can be expressed in a graph which presents, for each specimen submitted to cyclic loading, the ultimate longitudinal shear resistance -as obtained at the final static test- and the value of the maximum applied cyclic load related to the number of cycles in logarithmic scale.

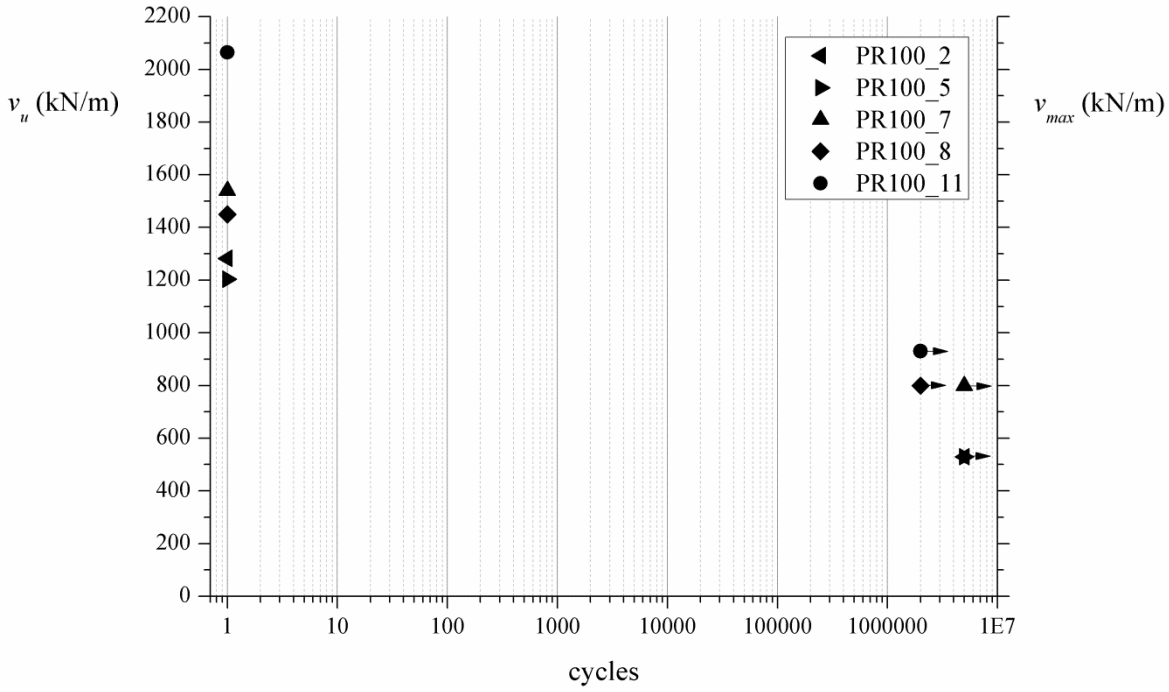

Fig. 3.73: Push-out specimens' resistance to longitudinal shear force per unit length under cyclic loading.

The values presented in figure 3.72 and 3.73 taking into the account the tendency of the stabilization of the residual slip in the connection, consist a possible domain for the defining the fatigue limit for the specific connection geometry. For different connection geometry, concrete type and steel reinforcement quantity and geometry a scientific tool is needed to define the corresponding fatigue limit. This is shown in the 5th chapter using the numerical model which is developed to predict the connection's behaviour to longitudinal shear.

Remarks for cyclic loading

Concerning the connection behaviour in cyclic loading, the following general remarks can be made:

- For the geometry of the specimens tested the connection's required resistance at FLS, as defined at table 2.7 in the state of the art, with respect to fatigue limit for both fatigue load models used, is experimentally verified.
- The connection exhibits sufficient resistance to cyclic loading, respected that the maximum applied load does not exceed the value that defines the limit of the elastic domain (domain in which the shear stresses in the interfaces remain elastic, for the corresponding normal stress on the interfaces). The influence of cyclic loading in this case is limited to the development of a residual slip in the connection which stabilizes with the number of cycles, practically after two million cycles. More precisely, analytical expressions for the residual slip will permit to verify its value for the 70 years life time. Whereas this value is inferior to the value if slip s_u

which corresponds to initiation of failure for monotonic loading, the connection is considered secure.

- The overall behaviour during cyclic loading seems to be governed by the constitutive law, i.e. the force-slip relationship, for monotonic loading. The latter acts as a failure envelop. As observed at the experimental investigation of interfaces, after a certain number of cycles and the development of the residual slip, any loading results to a force-slip curve that has the tendency to follow the continuation of the loading path for monotonic loading from virgin state, a kind of "memory effect". This applies also for the post failure behaviour.
- Another significant result is that once slip reaches the value of slip at failure for monotonic loading, the connection continues to resist loads, but with increasing slip, and any further cyclic loading is limited to only few hundred cycles.
- Uplift in the connection is limited for amplitude cycles within the quasi-elastic domain. The uplift-slip relationship for cycle loading is developed within the envelope defined by the uplift-slip relationship (kinematic law) for monotonic loading. In fact the uplift during cyclic loading, while no failure occurs, remains lower than the uplift which corresponds to the failure for static loading.

3.4 Composite beam

3.4.1 Introduction

Experimental investigation is concluded with the study of a composite beam, fabricated with the innovative connection. The choice of the section of the steel beam and the reinforced concrete slab are done in such a way to reproduce in the connection a longitudinal shear force per unit length equal to the one expected in twin composite girders in bridges in real practice. The objective of the beam testing is to verify experimentally the resistance and the structural performance at FLS and consequently at ULS of a composite beam fabricated with the new connection. The difference of this type of testing in comparison to push-out tests is that the development of the longitudinal shear in the connection is imposed indirectly, due to bending, as in reality. In addition, the overall structural performance of the composite beam is examined and the study is not limited to the connection. According to state of the art in loading of composite bridges, for proof with respect to fatigue limit the variation of longitudinal shear per unit length, $\Delta v = v_{max} - v_{min} = 530-130 = 400$ kN/m is taken into account which is obtained applying the fatigue load model 1 of the code SIA 261. For the composite section chosen, this is achieved by applying a vertical cyclic load to the third of the span which varies from 140 to 550 kN. The composite beam is submitted to a five million cycle three point bending test. Since no failure occurs and the damage, expressed by the accumulation of the residual slip is stabilized, the cyclic test ends. Consequently a final four point bending static test is executed to investigate the structural performance of the composite beam at ultimate limit state.

3.4.2 Materials and fabrication

The composite beam is assembled by the following parts:

a) Steel: Steel beam profile is HEA 500, in the upper flange of which, the connector is welded longitudinally. The connector consists of two embossed steel plates of type BRI 8/10 welded together. Steel of connector is of quality S235. Steel of the section profile is of quality S355 J0-M [EN 10025-2]. The total length of steel profile used is 9.50 m. Coupons are cut from a part of the same steel initial profile; two from each flange and three from the web, in order to define the precise stress-strain curves for the analysis. Figure 3.74 illustrates the steel profile HEA 500 with the welded connector on it, where Figure 3.75 illustrates the geometrical characteristics of the steel cross sections, for the span and at the supports with the stiffeners.

Fig. 3.74: Steel profile HEA 500 and connector of embossed steel plates

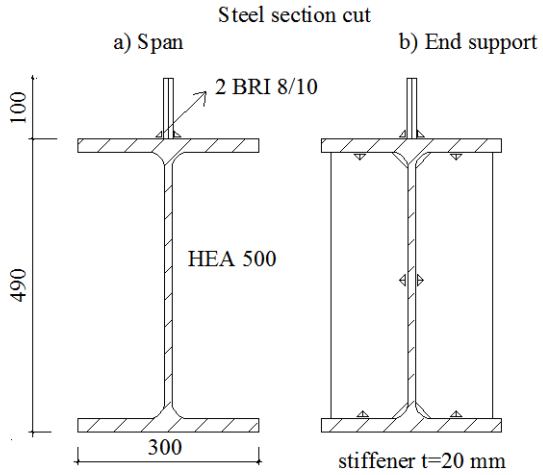

Fig. 3.75: Cross section of steel part at span and supports

b) Reinforced concrete: A reinforced concrete block with a length of 9.5 meters is fabricated. Concrete is designed to be of quality C40/50 according to code SIA 262 [SIA-262 2003]. The maximum aggregate diameter, d_{max}, is 16 mm. Figure 3.76 illustrates the geometrical characteristics of concrete section and reinforcement detail.

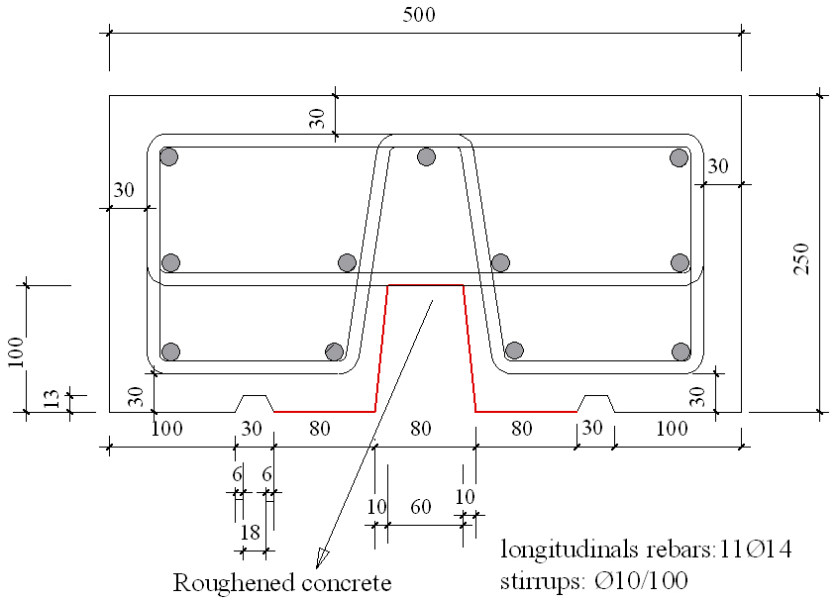

Fig. 3.76: Reinforced concrete cross section

The inner rib of the concrete part is roughened with the same procedure used for the push-out blocks. Figure 3.77 illustrates the roughened inner rib; the part of the lower reinforcement that crosses over the rib is exposed. The placement of the rebar, over the slab's rib, in this actual position is chosen in purpose so that the confinement of the rebar becomes mostly efficient. This is explained more in detail in the 5th chapter where the confinement effect is studied extensively by performing finite element analysis on the slab's section.

Fig. 3.77: Roughened inner rib of concrete part

Six cylindrical simples, of the same concrete used for the beam, were formed during casting and tested in compression at 28 days, in order to obtain the actual compression resistance and the modulus of elasticity. Mean compression resistance, f_{cm}, is found equal to 56.7 N/mm^2 and modulus of elasticity 36950 N/mm^2. Steel reinforcement longitudinal rebars and stirrups are of type B500B.

c) Cement grout: The cement grout injected to realize the connection is the product VSL-HPI. Its compression resistance is defined by tests on typical prisms and is equal to 75.5 N/mm^2. The cement grout used has swelling of 2.7 % which compensates for volume loss due to shrinkage. The complete information for the cement grout is provided in the annex I.

The assembly of the beam and the injection of the cement grout are performed in the laboratory of the Civil Engineering Institute (figure 3.78). During curing of the cement grout the beam is fully supported to avoid loading in the connection.

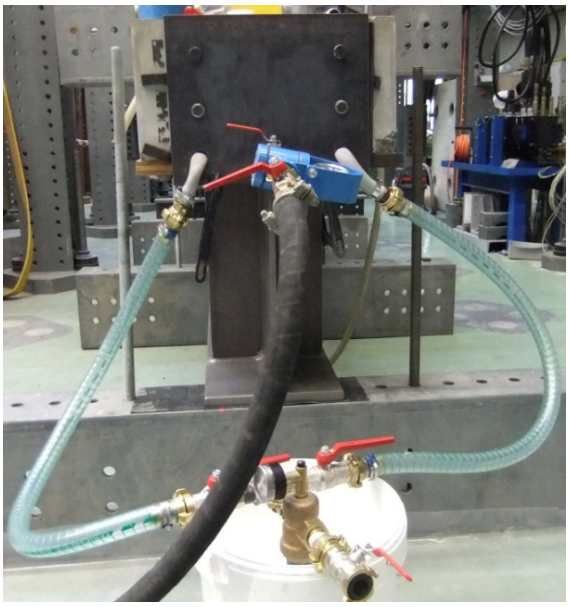

Fig. 3.78: Injection of cement grout

3.4.3 Testing arrangement and instrumentation

After the curing period of 28 days, the composite beam is placed over the two supports. The beam is simply supported with a static span of 9 m. The support to the south is roller and the support to the north is hinge.

Figure 3.79 illustrates the instrumentation arrangement. The instrumentation is the same for both the cyclic and the final static loading. Load cells are placed at the two supports and at the loading jacks. The deformation of the concrete is measured by means of omega-gauges, indicated by the letters o-, and the deformation of the steel by means of strain gauges. Transducers, indicated by the letters gl-, are fixed at the upper flange of the steel profile, symmetrically at both sides of the beam in order to measure the relative slip between the reinforced concrete “slab” and the steel beam. Other transducers indicated by the letters ec-, are placed in order to measure any possible vertical uplift between steel beam and concrete and finally four transducers, indicated by letter w-, are placed underneath the beam at mid span and the thirds from the edges of the beam in order to measure the vertical displacement.

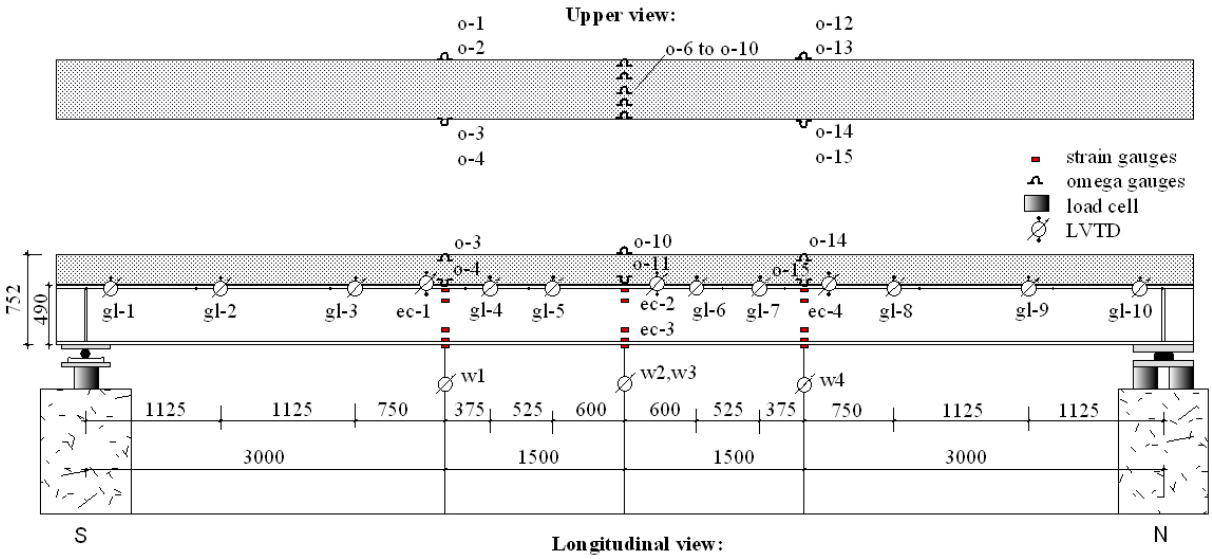

Fig. 3.79: Instrumentation for data recording

3.4.4 Cyclic loading

Testing arrangement

A vertical cyclic load with constant amplitude and at a frequency of 1 Hz is applied at the first third of the composite beam. The vertical load varies from 140 to 550 kN, resulting to a calculated longitudinal shear per unit length which varies from 137 to 537 kN/m for the first 3 meters of the span, and from 68.5 to 268.5 kN/m for the rest 6 meters of the span, (figure 3.80).

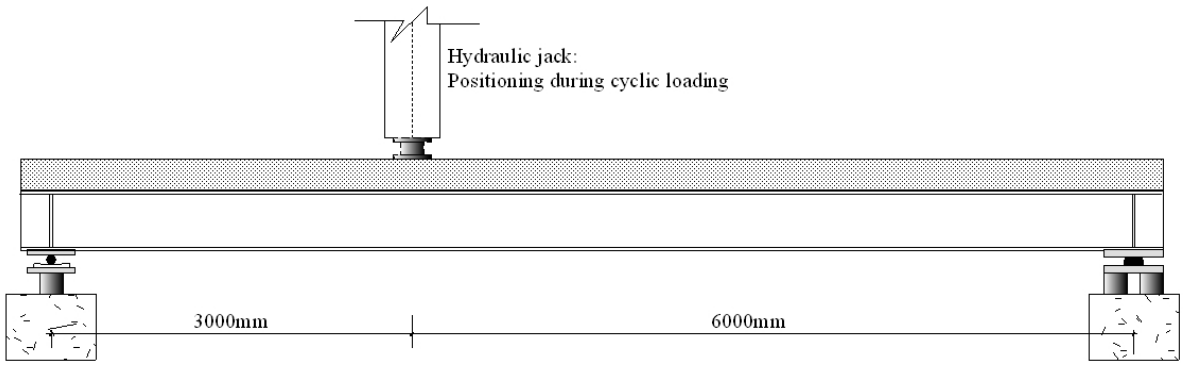

Fig. 3.80: Positioning of jack during cyclic loading

The transducers measuring vertical deflection are withdrawn during the cyclic loading so as not to be damaged. Furthermore during cyclic loading due to the frequency applied no measurement but the force is possible. Thus in order to measure values from strain gauges and the transducers, test is stopped after certain number of cycles achieved and intermediate cycles are performed with a loading rate that allows measuring of data. The transducers for the vertical deflection are placed during these intermediate cycles. Any developed permanent vertical deflection is recorded by the positioning of the hydraulic jack.

Results and observations

The figure 3.81 presents the evolution, at several positions along the beam, of the slip between the upper steel flange and the concrete slab, under the load V_{max} = 550 kN, with the number of cycles.

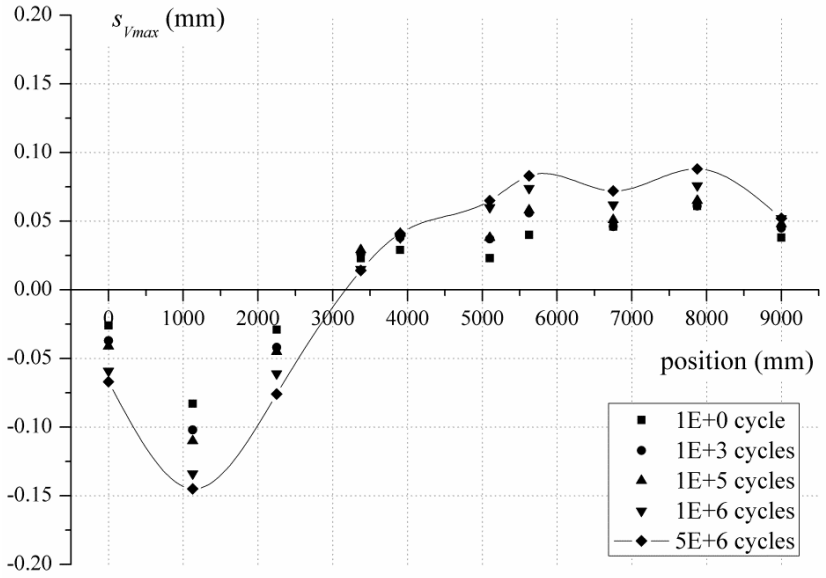

Fig. 3.81: Slip between the steel flange and the slab, under V_{max} along the composite beam

The slip under maximum load follows the sign of the longitudinal shear. However it is not uniform along the two parts of the span. An increase of the slip takes place with repeated loading but stabilizes with the number of cycles. This is more evident at the illustration of the slip under V_{max}, with the number of cycles, for two sections at a distance 1125 mm and at a distance 5100 mm from the left support of the beam, (figure 3.83).

Unloading of the beam takes place in several characteristic time intervals in order to record the residual slip, s_{res} . Figure 3.82 presents the evolution of the s_{res} as a function of the number of cycles.

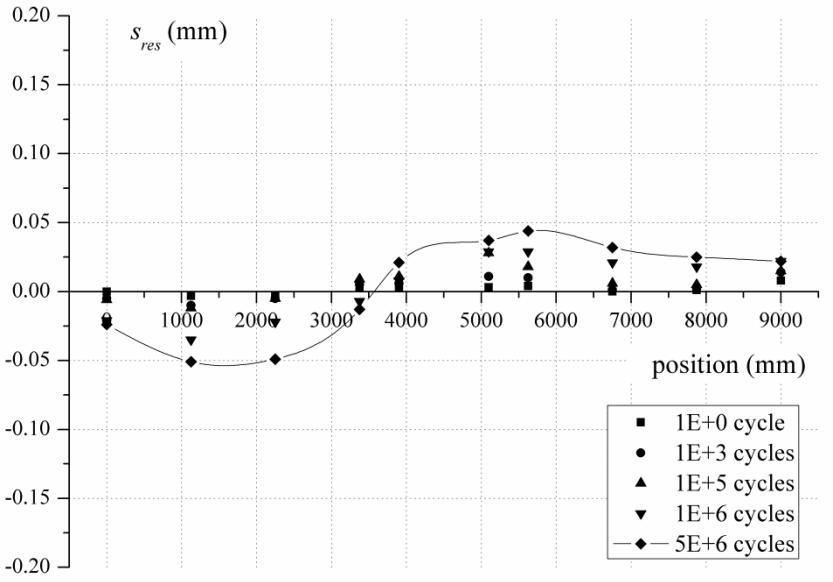

Fig. 3.82: Residual slip, s_{res}, between steel flange and the slab, along the composite beam

The residual slip, s_{res} follows the sign of the longitudinal shear. It increases with repeated loading but it stabilizes with the number of cycles, as seen also in figure 3.83 for sections at a distance 1125 mm and 5100 mm from the left support.

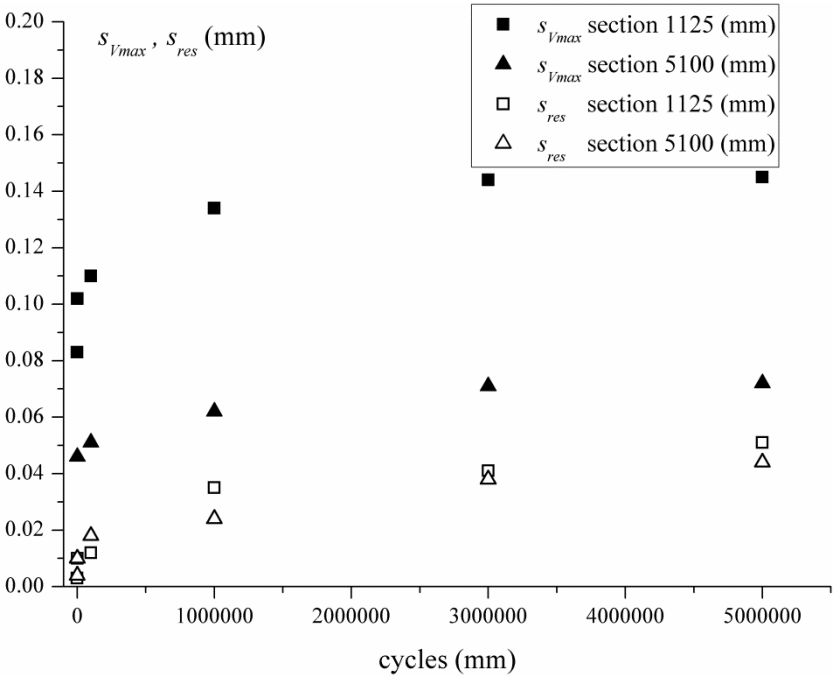

Fig. 3.83: Slip under $V_{max,}$ and residual slip for two sections, as a function of the number of cycles

During the cyclic loading no cracking and no failure occurs for five millions cycles. The damage in the connection, expressed by the residual slip which stabilizes with the number of cycles, is insignificant since it does not exceed at any point the value of 0.05 mm. This value is of not great importance for the resistance in longitudinal shear, if we recall the force-slip relationships of the push-out specimens.

A minor influence, due to cyclic loading, for the overall bending performance of the beam is the change of the position of the elastic neutral axis of the beam, as recorded by the strain gages (figure 3.84) in the section located at 3000 mm of the left support where the cyclic load is applied.

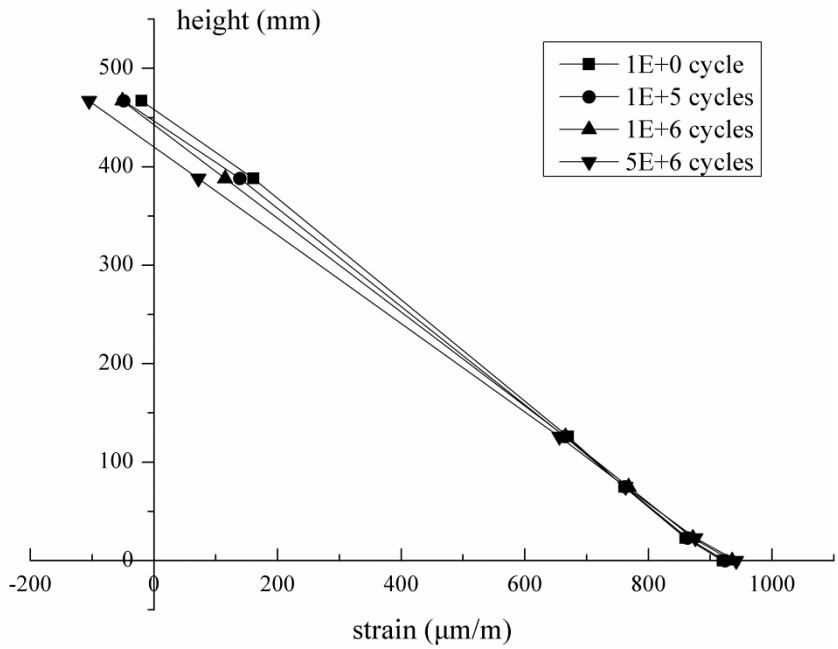

Fig. 3.84: Strains at steel section and neutral axis at maximum cyclic load, as a function of the number of cycles, for the section located at 3000 mm of the left support.

For the section at the third of the span, where the vertical load is applied, the neutral axis under maximum cyclic load is gradually moving downwards with a value equal to about 40 mm. Since in this section the slip under maximum load is almost zero, this phenomenon should be attributed mostly to the influence due to cyclic loading on the concrete of the slab (viscosity, invisible micro-cracking).

Since no damage is noticed after five million cycles, the cyclic tests ends and a static test is performed to investigate the structural performance of the composite beam at ULS.

3.4.5 Static test up-to-failure

For the final static test, two hydraulic jacks are used and they are placed in the middle of the span in a distance of 960 mm between them (figure 3.85). The final test is performed under displacement control with a loading velocity equal to 0.1 mm/sec.

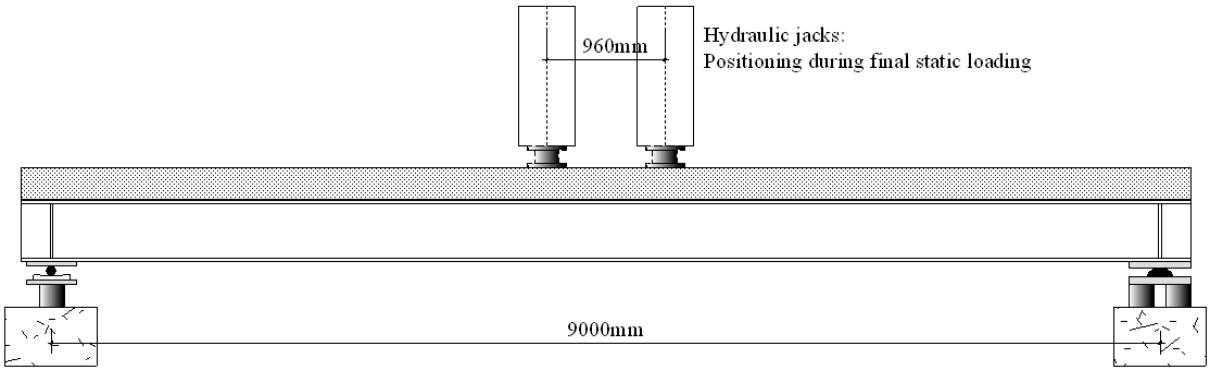

Fig. 3.85: Positioning of jack during final static loading

At the final test several cycles are executed within the elastic domain, and two cycles after yielding before loading up to failure. The figure 3.86 presents the relationship between the reaction force at the support and the vertical deflection in the middle of the beam. The value of the reaction force due to dead load 22.4 kN is added on that of the measurement to obtain the total value of it.

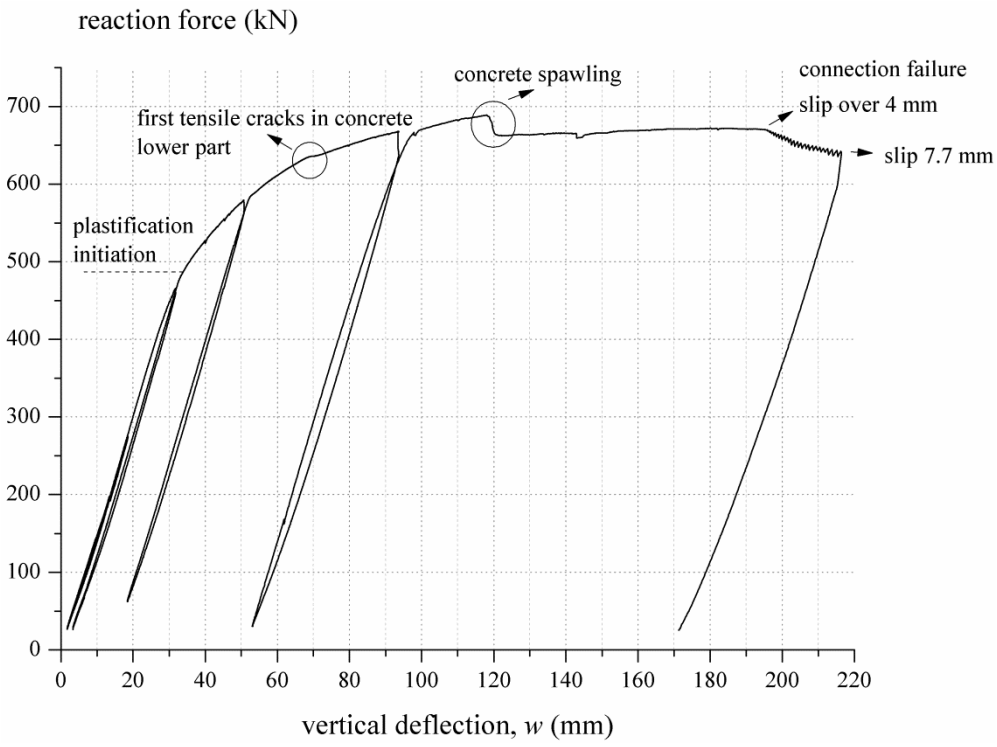

Fig. 3.86: Reaction force at support versus vertical deflection in the middle of the beam

The structural performance of the composite beam is significally ductile. The composite beam starts to fail by plastification of the steel beam at a load of at about 470 kN, with increasing bearing capacity as more steel fibers are plastified. For a vertical deflection about 70 mm the first tensile cracks appear in the lower part of the concrete slab, in the middle of the beam (figure 3.87), revealing the development

of two neutral axes, as it is presented in detail in the end of the 4th chapter. This is due to the fact that slip, which is kept below 0.2 mm on the elastic domain, at this point starts to increase. The bearing capacity continues to increase.

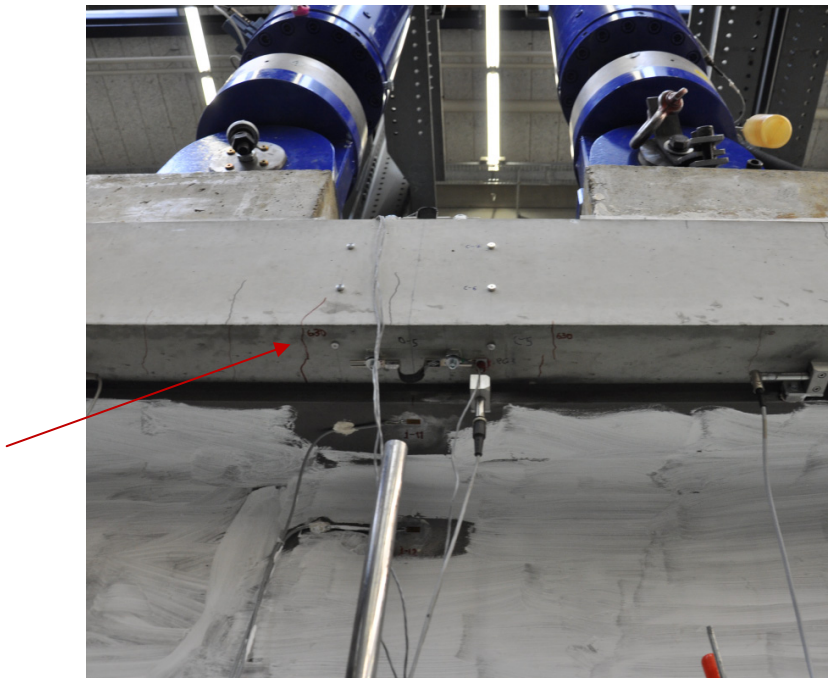

Fig. 3.87: Tensile cracks at the lower part of the reinforced concrete slab, in the middle of the span revealing the development of two neutral axes

The first point where a small drop of the resistance is noted, for vertical deflection at about 117 mm (figure 3.86), corresponds to the initiation of the spawling of the concrete, outside of the stirrups, in the middle of the span (figure 3.88). Plastification of concrete follows.

a) 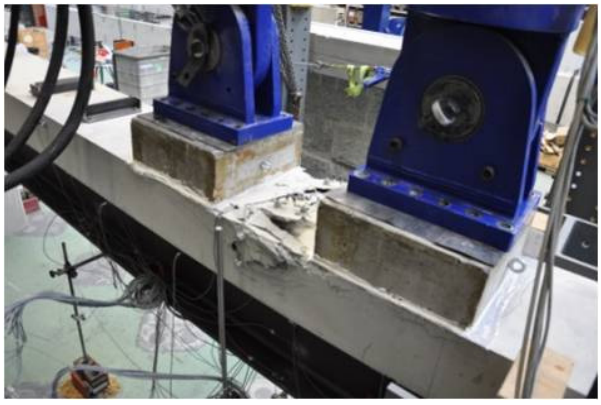 b) 

Fig. 3.88: Spawling of concrete outside the stirrups at middle of span a) general view b) detail view after unloading and removing of failed material

Finally the beam starts to lose bearing capacity when the slip in the north part of the composite beam, increases more than 4 mm (figures 3.86 & 3.89) for a vertical deflection in the middle of the beam about 193 mm. Further loading results to increase of slip up to the value of 7.7 mm, visible also on the north edge of the beam (figures 3.89 & 3.90). At that point, with vertical deflection 214 mm (figures

3.86 & 3.91), the loading jacks reach their displacement capacity and it was decided to unload the composite beam which develops a permanent deflection of 165 mm.

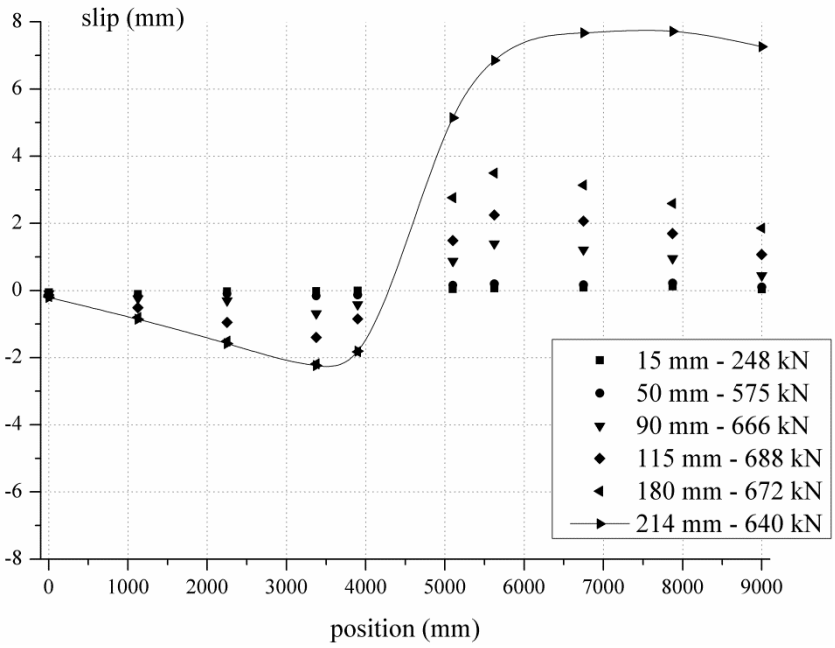

Fig. 3.89: Slip between the steel profile and the concrete block for different values of the vertical deflection in the middle of the beam, and correspondingly support force reaction.

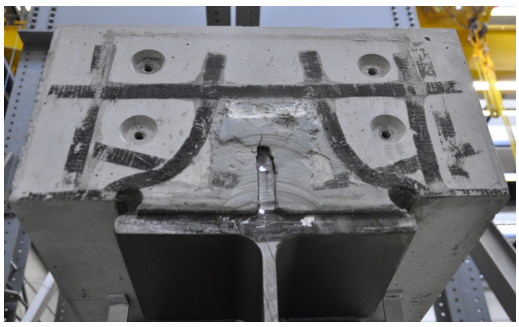

Fig. 3.90: Slip at the north edge of the beam

Fig. 3.91: Deformation capacity at the end of test before unloading.

Concluding remarks for beam testing

The following concluding remarks are made concerning testing of the composite beam fabricated with the innovative connection.

- The composite beam exhibits significant resistance to cyclic loading. Proof with respect to fatigue limit with variation of longitudinal shear per unit length, Δv=400 kN/m for five millions cycles, is experimentally verified.
- The residual slip between the concrete slab and the upper flange of the steel beam, measured at several points along the composite beam, is stabilized with the number of cycles. For the load applied, after five million cycles, it does not exceed the value of 0.05 mm. The beam exhibits full composite action under cyclic loading.
- For static loading, the beam exhibits full composite action for the whole elastic domain.
- At ultimate limit state, slip in the connection starts to increase as beam starts to plastify resulting to the development of two neutral axes in the beam. For values of slip in the connection up to 4 mm, the composite beam develops its plastic moment and rotation capacity. Once slip exceeds 4mm the bearing capacity of the beam starts to decrease. It is hence possible, under certain conditions, to apply plastic design for beams fabricated with the innovative connection as it will be shown in the 4th chapter.

3.5 Conclusions

This chapter presents conclusions from an experimental investigation on the behaviour of interfaces, connection and a composite beam under static and cyclic loading. Conclusions are based on i) direct shear testing of different types of confined interfaces ii) push-out testing of composite connections and iii) bending testing on a composite beam. The major outcomes for each test are described below.

Direct shear tests

Static loading

- The ultimate shear stress, τ_u developed in a confined interface is in a linear relationship with the applied normal stress in the interface. The failure criterion, i.e. the ultimate shear-normal stress relationship, is valid for a normal stress up to 5 N/mm^2 (the maximum applied normal stress during testing). The remaining frictional resistance in an interface, τ_{fr} is found as the product of a coefficient (friction coefficient of the interface) and the normal stress.
- The constitutive law, i.e. the shear stress-slip relationship includes three characteristic domains. An initial almost linear elastic part up to a certain value, τ_{el}, a second yielding domain up to the ultimate resistance and a softening branch towards the remaining frictional resistance. The initial stiffness of the elastic domain, the secant stiffness to the ultimate resistance, and the ratio, τ_{el}/τ_{max}, of the elastic shear stress versus the ultimate shear stress are independent of the normal stress and characterize the type of interface.
- Concerning the kinematic law, i.e. the uplift-slip relationship, for values of slip lower than the slip, s_u, which corresponds to the development of the ultimate shear stress, the uplift in the interface remains below a certain value, u_{Su}, which is independent of the normal stress and constitutes a characteristic of the interface. The uplift exhibits an exponential rise, after u_{Su}, with increasing slip, towards an asymptotic value, u_{max}, which is achieved when the frictional shear resistance is reached. The value u_{max} is inversely proportional to the normal stress.
- Analytical expressions will be developed in the 4th chapter for the constitutive and the kinematic law, based on the experimental data. It should be taken into account that the point of the initiation of failure in the constitutive law, point to the ultimate shear resistance τ_u, and failure slip s_u, corresponds to the inflection point of the curve of the kinematic law, i.e. the point where the curvature of the uplift-slip relationship changes sign. This leads to the conclusion that the post failure constitutive law can be obtained by the kinematic law with differentiation of its expression.

Cyclic loading

- The shear stress-slip relationship is developed, during cyclic loading, inside an envelope defined by the constitutive law of the monotonic loading.
- Cyclic loading results in a kind of damage expressed by the development of a residual slip at the interface. For a variation of shear stress inside the elastic domain, the residual slip stabilizes with the number of cycles and as long as the slip and the uplift in the interface are inferior to slip s_u and uplift u_{Su} at failure for monotonic loading, the failure is avoided. On the other hand, when the applied stress exceeds the elastic limit of the monotonic law, the residual slip, s_{res}, increases towards the failure of the specimen, occurring when the slip reaches the slip s_u, practically, in that case in few thousand cycles.
- In an interface subjected to cyclic loading, both the slip under maximum cyclic load and the residual slip-the latter obtained when unloading- increase with the number of cycles but they tend to stabilize within one or two million cycles. Analytical expressions will be developed for the residual slip, s_{res}, and the slip under the maximum cyclic load, s_{Vmax}, as functions of the

number of cycles. These expressions can be used to describe the shear-slip relationship after a certain number of cycles applied as it will be presented in the 4th chapter.

Push-out tests

Static loading

- Connections by adhesion, interlocking and friction, exhibit, as it concerns the force-slip relationship, high, in comparison with shear studs, initial stiffness prior to failure.
- Initiation of failure in the interface happens when the ultimate value of longitudinal shear force is reached; it is non-reversible and followed by continuous increase in slip for further loading.
- Prior to failure, uplift in the developed interfaces is limited. After failure uplift in the developed interfaces increases to an asymptotic value.
- Connection ductility varies for the case of reinforced concrete blocks. The characteristic slip capacity, as defined by Eurocode 4 [EC4 2004], paragraph 6.6, is not always 6 mm so as to characterize the connection as ductile. Yet, the ductility of the connection is not negligible. The ductility of the connection is significant for the case of UHPFRC blocks.
- For the specific connection geometry and reinforcement of the specimens tested, the value 1500 KN/m for the longitudinal shear force per unit length, calculated with the elastic method, defined in 2.4 for ULS, was satisfied for both specimens fabricated with new cement grout VSL-HPI, and for one specimen fabricated with the common VSL cement grout (table 3.5). This raises the need for a model to predict the connection's resistance and investigate the parameters that are favorable in order to provide design tools, for engineering practice, which will permit a design of the connection for the needed level of resistance at ULS.

Cyclic loading

- For the geometry of the specimens tested, the connection's verification with respect to the fatigue limit, as defined in the table 2.7 in the state of the art, is experimentally verified.
- The connection exhibits sufficient resistance to cycle shear loading, as long as the maximum cyclic applied load remains lower than a certain percentage of the ultimate resistance, which for the particular geometry of the push-out specimens is located between 0.41 to 0.55. The influence of cyclic loading is limited to the development of a residual slip in the connection which stabilizes after nearly two million cycles. The overall behaviour during cyclic loading seems to be governed by the constitutive law, i.e. the force-slip relationship, for monotonic loading. The latter acts as a failure envelop. After a certain number of cycles and the development of the residual slip, any loading results in a force-slip curve that has the tendency to follow the continuation of the monotonic loading path from initial state, a kind of "memory effect". This applies also for the post failure behaviour.
- Uplift in the connection, for the specific geometry, is limited for cycling loading with load limited to a range 0.41 to 0.55 of the ultimate resistance. The uplift-slip relationship for cyclic loading is developed within the envelope defined by the uplift-slip relationship (kinematic law) for monotonic loading. In fact the uplift during cyclic loading, while no failure occurs, remains lower than the uplift which corresponds to failure for static loading.
- Analytical expressions for the residual slip will permit the development of a safe fatigue failure criterion based on the remark that when the accumulated residual slip is lower than the value slip s_u, which corresponds to failure for monotonic loading, the connection is safe. This criterion will be presented in the 4th chapter.
- The stabilization of the residual slip, for maximum applied cyclic load varying between 0.41 to 0.55 of the ultimate resistance, indicates that the shear stresses in the interfaces remain

elastic for the corresponding normal (confinement) stress. The development of the numerical model which predicts the connections structural performance will enable to define the limit of the elastic behaviour for tested specimens and any given connection geometry.

Bending of composite beam

Cyclic loading

- The composite beam exhibits significant resistance to cyclic loading. Proof with respect to the fatigue limit with variation of longitudinal shear per unit length, Δv=400 KN/m for five millions cycles, is experimentally verified.
- Residual slip between the concrete slab and steel beam stabilizes with the number of cycles and remains low enough, equal to 0.05 mm, so that it can be supported that the composite beam exhibits full composite action during cyclic loading.

Static loading (which follows after the cyclic loading)

- For static loading, the beam exhibits full composite action for the whole elastic domain.
- The deformation capacity of the connection, despite the fact that it does not comply with the ductility criterion proposed by Eurocode 4 [EC4 2004] paragraph 6.6, makes it possible, under certain conditions, to develop plastic moment.
- Hence a design method for the connection should allow the plastic behaviour of the composite beam to fully develop.

4. Analytical study

4.1 Introduction

The structural behaviour of confined interfaces subjected to shear constitutes an important part of this research since the resistance of the new connection to longitudinal shear sources on the development and the resistance to shear of such interfaces both for static and cyclic loading.

Similarly to the work done by Thomann [Thomann 2005] the results from the direct shear tests are used to calibrate the three laws that describe the behaviour of confined interfaces under monotonic loading. These laws are:

- The *failure criterion*, i.e. the relationship between the ultimate shear stress τ_u and the normal stress σ acting in the interface.
- The *kinematic law*, i.e. the relationship between the uplift u developing in the interface and the corresponding slip s.
- The *constitutive law*, i.e. the relationship between the shear stress τ developing in the interface and the corresponding slip s.

The above laws will be used in the 5th chapter to a developed model to predict the structural performance of the connection.

The experimental results from cyclic loading in interfaces are used to develop *analytical expressions* for i) the residual slip s_{res}, developed in the interface during the cyclic loading ii) the slip under maximum cyclic load s_{Vmax}. Based on these expressions a model is proposed to describe the force-slip relationship as a function of the number of cycles.

Analytical expressions, based on results from push-out tests, are also developed in this chapter to describe the residual slip in the connection due to cyclic loading and the evolution of the force-slip relationship, for the connection, with the number of cycles. These expressions result to a model describing the behaviour of the connection at ULS which follows a cyclic loading. A safe failure criterion for cyclic loading is also proposed for the connection.

This chapter ends with the analytical study of the tested beam where the exact plastic moment of the composite beam is calculated considering two neutral axes due to the slip between the concrete slab and the steel girder.

4.2 Interfaces

4.2.1 Static loading

Failure criterion

The failure criterion proposed, for the three interfaces which are investigated, is a linear Mohr Coulomb type relationship expressed by equation (4.1).

$$\tau_u = c + \mu \cdot \sigma \ \ (\mathrm{N/mm^2}) \tag{4.1}$$

The first term which corresponds to the shear resistance in the interface when normal stress is absent expresses the combined effect of adhesion and interlocking. The second term accounts for the contribution of the frictional resistance due to the normal stress acting in the interface. The coefficients c and μ of equation (4.1) are calibrated using the results from direct shear tests and are presented in table 4.1 for the three interfaces examined in this study:

- embossed steel-cement grout interface,

- rough concrete-cement grout interface and
- UHPFRC-cement grout interface

Figure 4.1 presents the failure criteria obtained for the three interfaces examined.

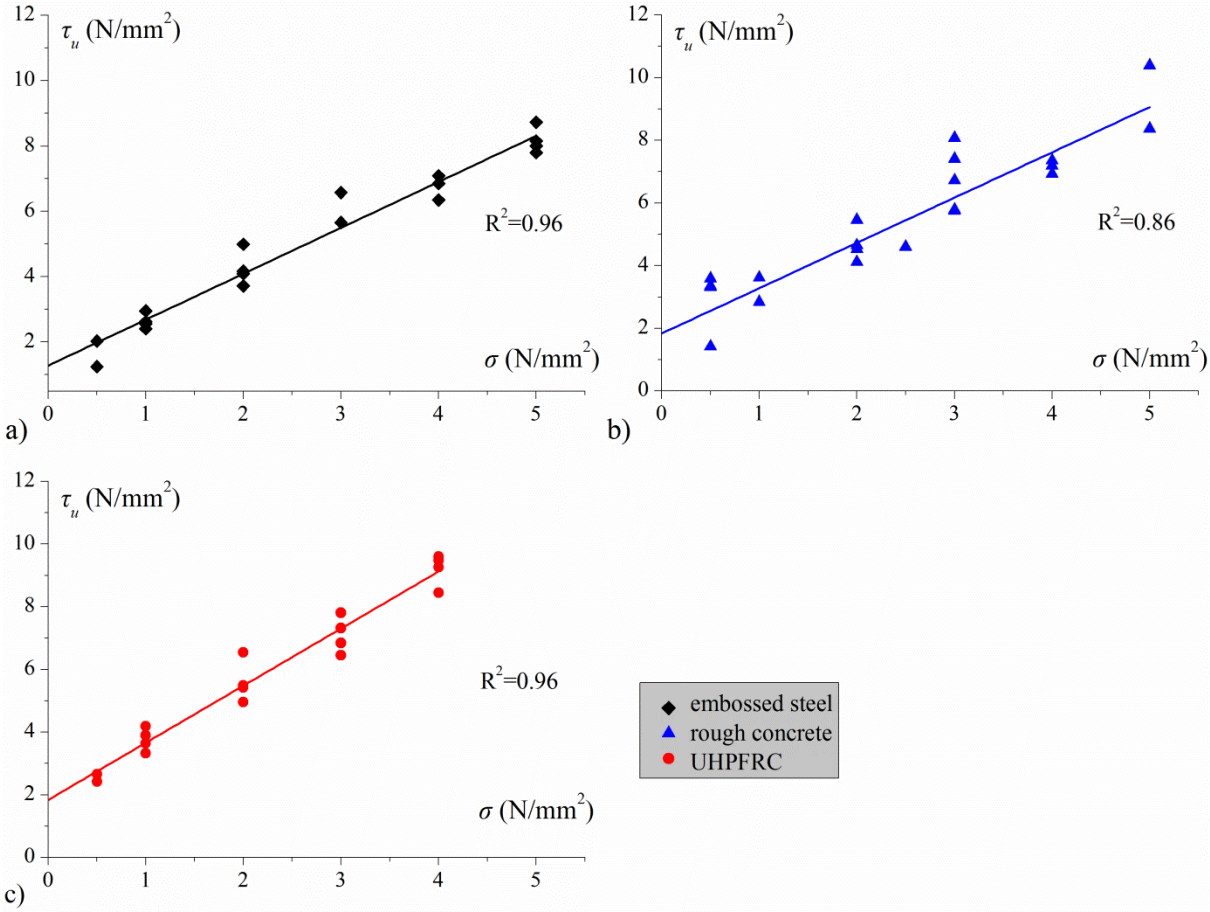

Fig. 4.1: Failure criteria; a) embossed steel-cement grout interface, b) rough concrete-cement grout interface, c) UHPFRC-cement grout interface

Table 4.1: Coefficients of failure criteria of interfaces, c (adhesion/interlocking) and μ (friction)

Interface: Cement grout-	c (N/mm^2)	μ	R^2	Stand. Deviation (N/mm^2)	Cement grout f_{cm} (N/mm^2)
Embossed steel	1.28	1.40	0.96	0.47	90 ÷ 99.4
Rough concrete	1.84	1.45	0.86	0.87	90 ÷ 102
UHPFRC	1.84	1.82	0.96	0.49	102 ÷ 107

According to table 4.1 the coefficient of determination R^2 is lower and the standard deviation (root mean square of the error) is higher, for the less regular interface which is the rough concrete-cement grout interface; due to the random exposure of aggregates of the surface of concrete. Another remark is that for the same normal stress σ on the interface, the resistance is higher for the interface, the contact surface of which presents the higher peak to valley height, i.e. R_{max}. This descriptive magnitude of roughness, R_{max}, defined in the different codes [BS 1134/1972], is higher for the plates of UHPFRC, equal to 8 mm-the height of the conical studs- and it is lower for the embossed steel plate with height of ribs equal to 1.4 mm.

Besides the failure criteria, the equation of the remaining frictional resistance, τ_{fr}, for the three interfaces can be calibrated using the results from direct shear tests (figure 4.2) and equation (4.2).

$$\tau_{fr} = \mu_r \cdot \sigma \ \ (\text{N/mm}^2) \tag{4.2}$$

The remaining frictional resistance is the product of the normal stress σ acting in the interface and the remaining friction coefficient μ_r. This coefficient is generally known also as *kinetic* friction coefficient and is given in table 4.2, together with the coefficient of determination R^2 and the standard deviation (root mean square of the error), for each type of interface.

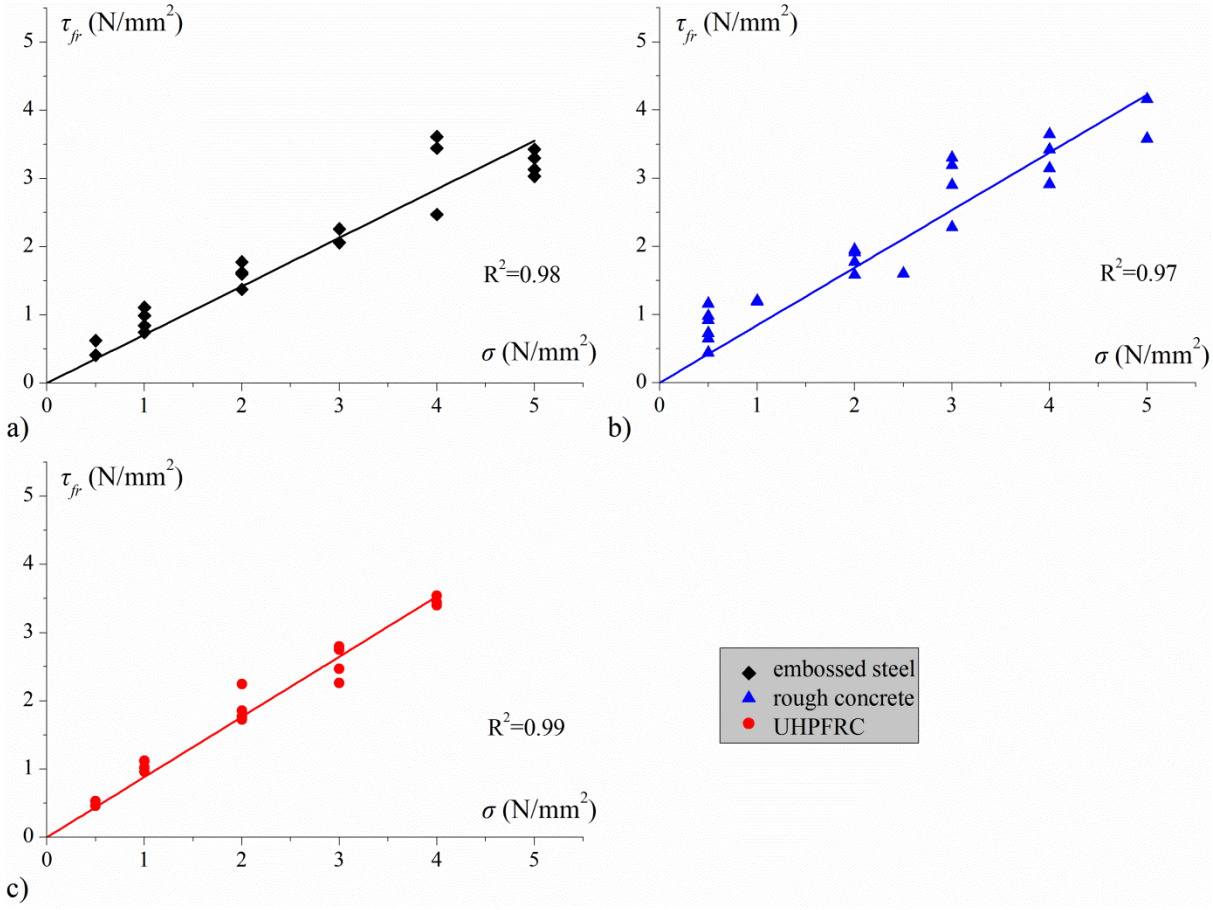

Fig. 4.2: Remaining frictional resistance; a) embossed steel-cement grout interface, b) rough concrete-cement grout interface, c) UHPFRC-cement grout interface

Table 4.2: Coefficient of remaining frictional resistance of interfaces, μ_r

Interface: Cement grout-	μ_r	R^2	Stand. Deviation (N/mm^2)	Cement grout f_{cm} (N/mm^2)
Embossed steel	0.71	0.98	0.35	90 ÷ 99.4
Rough concrete	0.85	0.97	0.43	90 ÷102
UHPFRC	0.88	0.99	0.20	102 ÷107

It is noticed that the kinetic friction coefficient μ_r presents lower values than the friction coefficient μ, which accounts for the contribution of friction to the ultimate shear stress τ_u. This can be explained by the fact that the slip surface, created at the moment that the shear resistance obtains its ultimate value, is rougher than the contact surface which corresponds to the remaining frictional resistance. During

the transition from initiation of failure (where the friction coefficient μ applies) to the development of the remaining friction (the coefficient μ_r applies), takes place a gradual smoothing of the slip surface, as already seen in chapter 3 (figure 3.26). This phenomenon is also related to the kinematic law as it will be described in the following paragraphs.

Kinematic law

The kinematic law proposed for the interfaces is based on the experimental results of this research and the "shear friction theory" for shear joints as described in the literature [fib Model Code 2010]. According to that theory interfaces are described by a simple saw-tooth model. Due to the roughness, the shear force causes not only parallel displacements, but also forces the joint to open (fig. 4.3a). The normal stresses acting on the interface permit the development of frictional forces which decrease with increasing slip due to the interface deterioration:

Thomann [Thomann 2005] studied the kinematic law and proposes an exponential increase for the joint opening, uplift u, as illustrated in figure 4.3:

$$u = u_{max} \cdot (1 - e^{-s/s_a})$$

whereas $u_{max} = u_{max,0} - r\frac{\sigma}{f_c}$ *with* $s_a = \frac{u_{max}(\sigma)}{tan(\alpha)}$ [Thomann 2005]

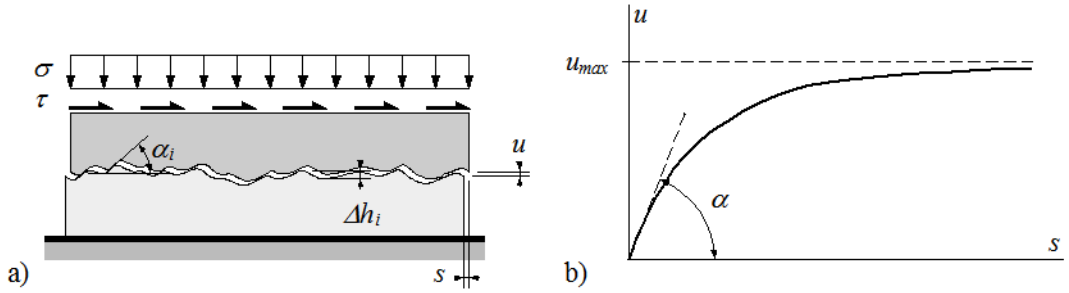

Fig. 4.3: Kinematics of failure, a) failure in the interface b) kinematic law [Thomann 2005]

The term u_{max} is a function of the normal stress σ, and the compressive strength of the cement grout, it corresponds to the asymptotic value of the uplift, when the shear stress is diminished to the remaining frictional resistance. The term $u_{max,0}$ corresponds to the asymptotic value of the uplift for absence of the normal stress. The parameter s_a (units in mm) is defined graphically and the parameters $u_{max,0}$ and r (units in mm) are obtained from regression analysis and are characteristics of the interface.

This study proposes and alteration on the above law. The uplift-slip relationship, as recorded in the experimental investigation and presented in chapter 3, presents two branches. The first branch describes the values of uplift for slip in the interface prior to failure. As it is already mentioned, in chapter 3, the value of uplift u_{Su} at the moment of failure, when the shear stress reaches its ultimate value τ_u , is independent of the normal stress and has a characteristic value for each type of interface. The first part of the kinematic law can be presented with a parabola which reaches the value u_{Su} at the moment of failure. The second branch describes the uplift-slip relationship after the failure, the post-failure behaviour. This part begins where the uplift-slip curve presents an inflection point which is the threshold of the exponential rise of the uplift which describes the post failure behaviour (figure 4.4).

The following equations (4.3) and (4.4) describe the proposed kinematic law. The coefficient s_a is obtained graphically as shown in the figure 4.4. It corresponds to the slip for which uplift would reach the asymptotic value u_{max} if after the failure the kinematic law would be linear following the tangent of the inflection point. Physically, this would correspond to the case where the undulations of the

developed failure surface would not be smoothed and deteriorated from contact. As will be shown in the next paragraphs the parameter s_a is related also to the constitutive law and the slip fracture energy release rate. The parameters s_a, $u_{max,0}$ and r are calibrated by results from direct shear tests and are presented in the table 4.3 with their mean statistical values for the three interfaces. Due to its importance in the form of the post-failure behaviour, as it will be shown in the 5th chapter, the sample standard deviation (Gauss distribution) of the parameter s_a is also included in the table 4.3

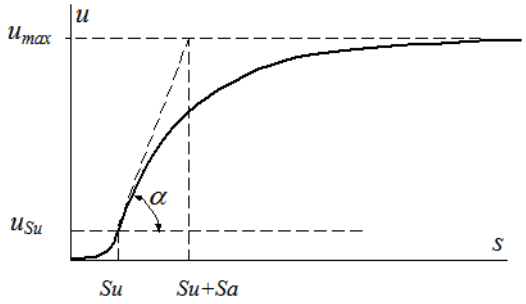

Fig.4.4: Graphical representation of the kinematic law

$$u = \begin{cases} u_{Su} \cdot (s/s_u)^2 & s \le s_u \\ u_{Su} + (u_{max} - u_{Su}) \cdot (1 - e^{-(s-s_u)/s_a}) & s \ge s_u \end{cases} \quad (4.3)$$

$$u_{max} = u_{max,0} - r\frac{\sigma}{f_c} \quad (4.4)$$

Table 4.3: Parameters for the kinematic law

Interface: Cement grout-	u_{Su} (mm)	$u_{max,0}$ (mm)	r (mm)	s_a (mm)	St. Dev. of s_a (mm)	Cement grout f_{cm} (N/mm^2)
Embossed steel	0.09	1.69	16.9	2.07	0.28	90 ÷ 99.4
Rough concrete	0.16	2.18	29.2	2.75	0.39	90 ÷ 102
UHPFRC	0.08	1.91	16.9	2.29	0.41	102 ÷ 107

The following diagrams present, for the embossed steel-cement grout interface and the rough concrete-cement grout interface, the kinematic law as predicted by equations (4.3) and (4.4) and as recorded from some direct shear tests for different level of normal stress on the interface.

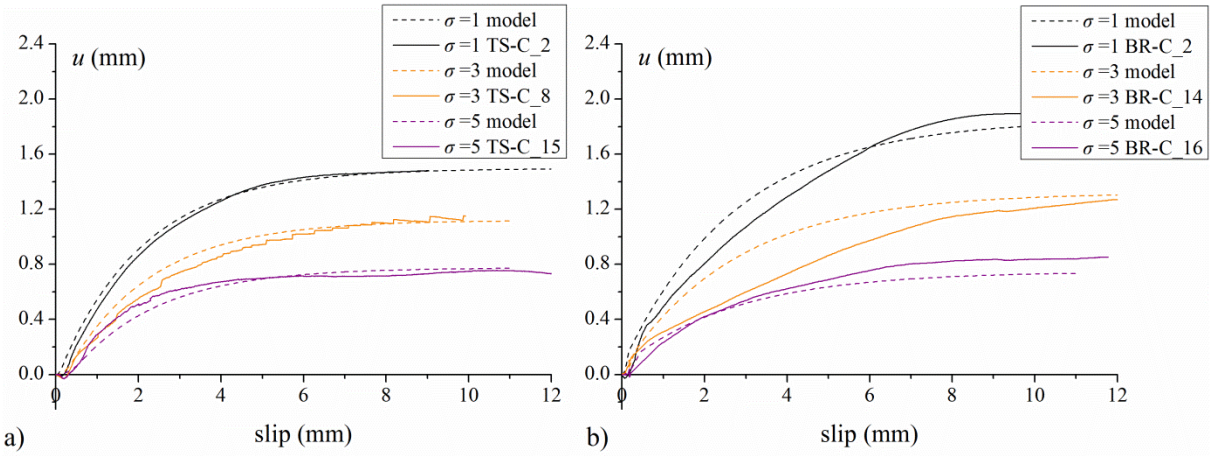

Fig.4.5: Comparison of kinematic law as recorded from direct shear tests and as predicted by the model; a) embossed steel-cement grout interface, b) rough concrete-cement grout interface

The values of parameters $u_{max,0}$ and r for embossed steel-cement grout interface and rough concrete-cement grout interface are close to those proposed by Thomann [Thomann 2005] for a similar type of cement grout and lower level of confinement stress.

Constitutive law

The observations from direct shear tests have shown that the constitutive law, i.e. the shear stress-slip relationship, consists of two discrete branches with different behaviour (figure 4.6). The first branch presents the increasing shear till the ultimate value τ_u (damage initiation). The second branch represents the softening behaviour towards an asymptotic value which corresponds to the remaining frictional resistance τ_{fr}.

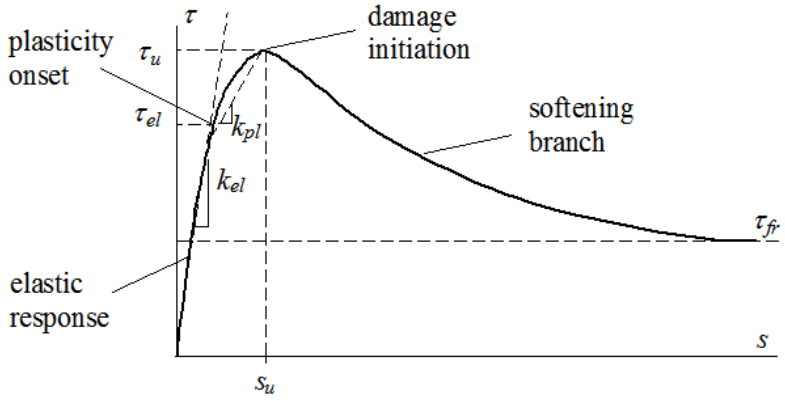

Fig. 4.6: Typical shear stress-slip relationship

The first branch can be simulated with a bilinear law. Firstly the response is elastic with an initial stiffness k_{el} till the plasticity onset. The shear stress at the end of the elastic response τ_{el} is a fraction of the ultimate shear stress. This fraction α is evaluated, in paragraph 3.2.4, to be independent of the normal stress σ and is a characteristic of the interface. The plastic behaviour can be simulated by a linear relationship with slope a k_{pl} up to the point of damage initiation. It is found also in chapter 3 that the elastic stiffness k_{el} and the secant stiffness k_{sec}, are independent of the normal stress σ and are characteristics of the type of the interface (figure 4.7) with values around a mean with important coefficient of variation. For interface behaviour, the mean values will be used (table 4.4). In another words, the initial stiffness k_{el} , the slope k_{pl} for the plastic response and the secant stiffness k_{sec} up to point of damage initiation, have constant values for a specific interface, independently from the normal stress. This conclusion concerning the behaviour prior to failure is the same with that proposed by Thomann [Thomann 2005] for a lower level of normal stress on the inteface.

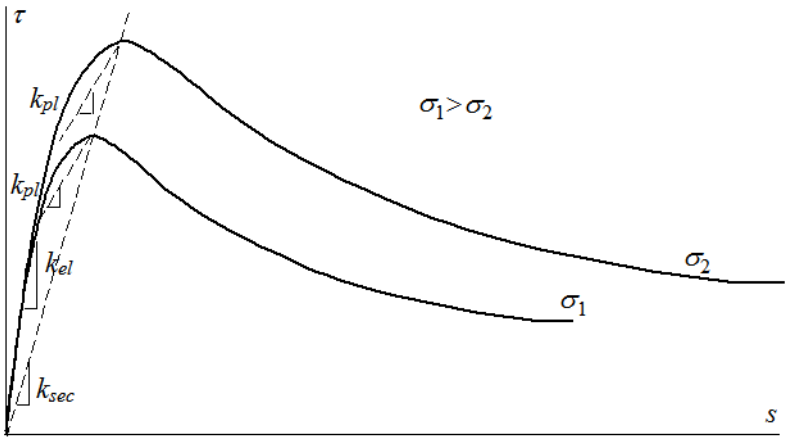

Fig. 4.7: Evolution of the constitutive law with increasing normal stress on the interface

The softening branch follows an exponential decay, with limit values τ_u for failure point and τ_{fr} the asymptotic value (figure 4.6). The transition of the ultimate shear resistance τ_u to the remaining frictional resistance is related to the degradation of the contact slip surface and consequently to the kinematic law. Furthermore, as it is already mentioned in chapter 3, the shear stress reaches the ultimate value τ_u for the slip s_u at which the kinematic law presents an inflection point (figure 4.8). From the above we deduce that the constitutive law, for the softening behaviour, can be obtained from the kinematic law by differentiation, equation (4.5) and applying as boundary values the shear stresses τ_u for slip equal to s_u and τ_{fr} for infinite slip.

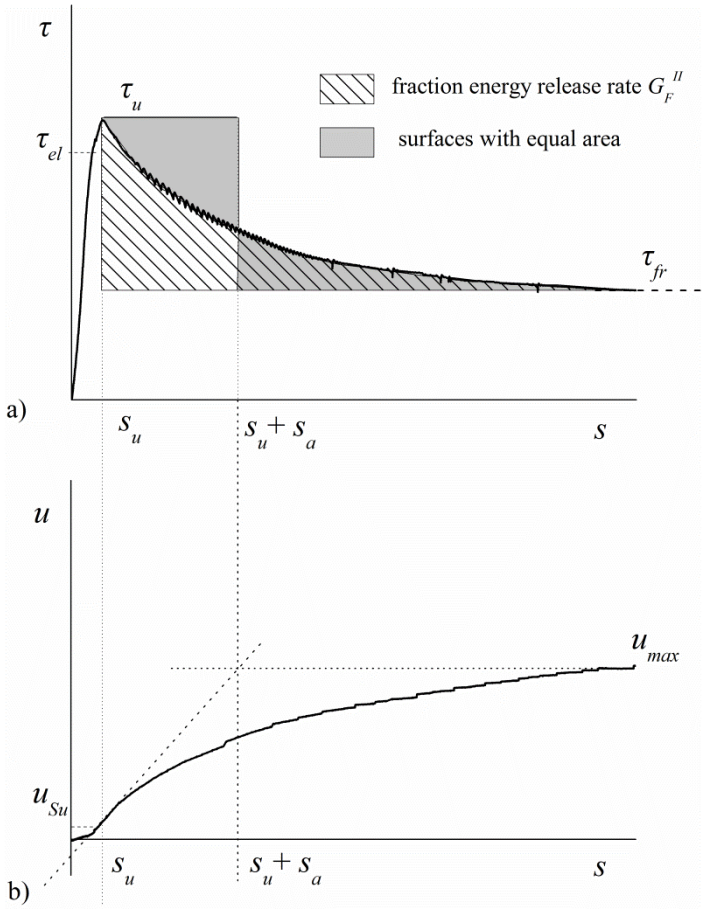

Fig. 4.8: Results for an embossed steel-cement grout interface, specimen TS-C_9;
a) constitutive, b) kinematic law

$$\tau(s) = C_1 + C_2 \frac{du(s)}{ds} \tag{4.5}$$

Applying the boundary values in equation (4.5), we obtain the expression for the softening branch. The constitutive law for each type of interfaces is expressed by equation (4.6). Several parameters such as the term α, the slip at the end of elastic response s_{el} and the slip at initiation of failure s_u are defined in equation (4.7).

$$\tau(s) = \begin{cases} k_{el} \cdot s & s \le s_{el} \\ \alpha \cdot \tau_u + k_{pl} \cdot (s - s_{el}) & s_{el} < s < s_u \\ \tau_{fr} + (\tau_u - \tau_{fr}) \cdot \left(e^{-(s - s_u)/s_a} \right) & s \ge s_u \end{cases} \tag{4.6}$$

$$\left\{\begin{array}{l}\alpha = \tau_{el}/\tau_u \\ s_{el} = \alpha \cdot \tau_u / k_{el} \\ s_u = \tau_u / k_{sec} = \tau_u \cdot \left(\alpha / k_{el} + (1-\alpha)/k_{pl}\right)\end{array}\right\} \quad (4.7)$$

The mean statistical values of the parameters defining the constitutive law are presented in table 4.4, for the three interfaces.

Table 4.4: Parameters for the constitutive law

Interface: Cement grout-	k_{el} (N/mm^3)	k_{pl} (N/mm^3)	k_{sec} (N/mm^3)	s_a (mm)	α	St. Dev. of α	f_{cm} (N/mm^2)
Embossed steel	29.4	5.5	14.3	2.07	0.75	0.11	90 ÷ 99.4
Rough concrete	29.7	10.19	20.9	2.75	0.80	0.15	90 ÷102
UHPFRC	73.2	13.0	39.7	2.29	0.83	0.11	102 ÷ 107

A comparison for the constitutive law as recorded from same tests and as predicted from the equations (4.6) and (4.7) is presented in figure 4.9 for the three interfaces. The mean values, presented in table 4.4, are used for this simulation.

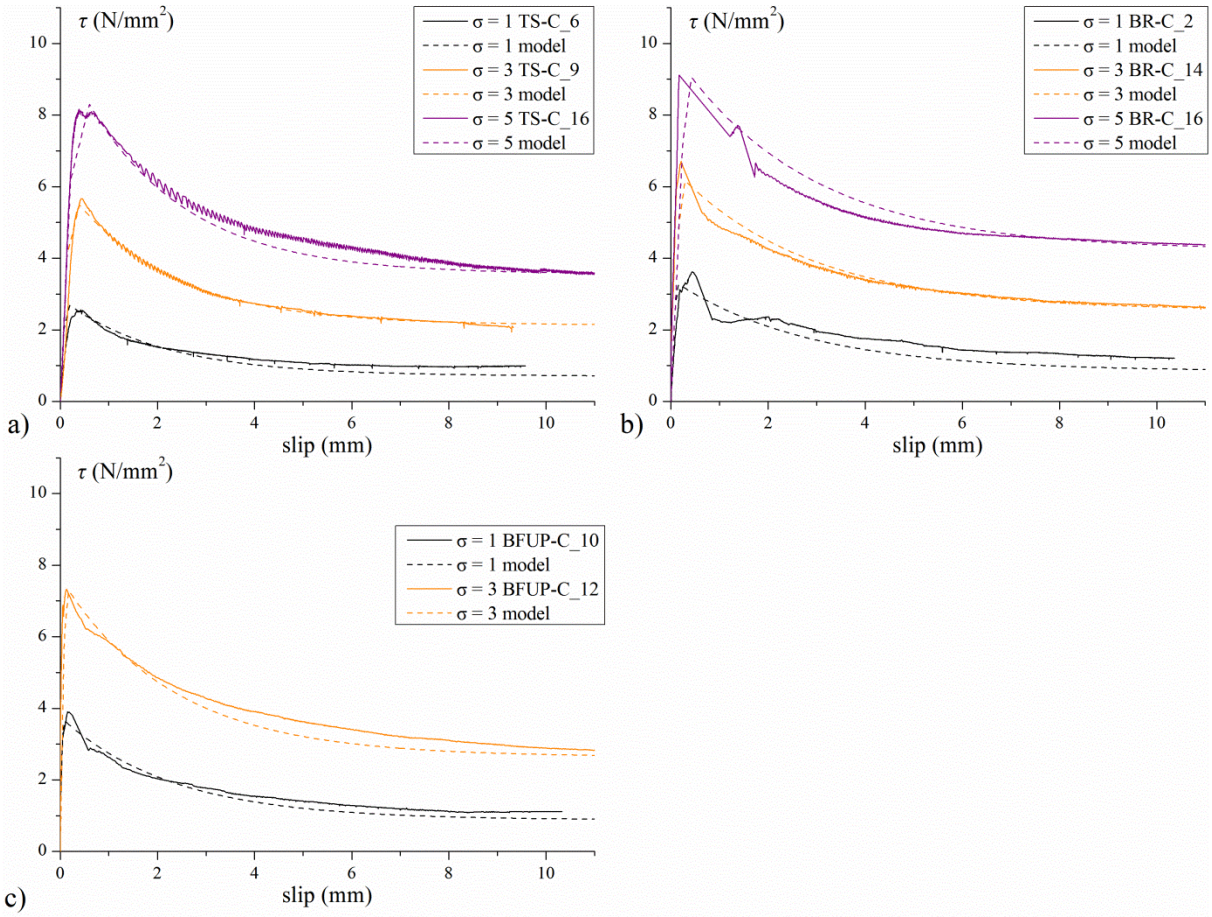

Fig. 4.9: Constitutive law from direct shear tests and as predicted by the model; a) embossed steel-cement grout interface, b) rough concrete-cement grout interface, c) UHPFRC-cement grout interface

The third expression of the equation (4.6) describing the softening branch can also be written alternatively by replacing the ultimate shear stress τ_u and the remaining frictional resistance τ_{fr} by equations (4.1) and (4.2).

$$\tau(s) = c \cdot \left(e^{-(s - s_u)/s_a} \right) + \left[(\mu - \mu_r) \cdot \left(e^{-(s - s_u)/s_a} \right) + \mu_r \right] \cdot \sigma \qquad s_u \le s \qquad (4.8)$$

Equation (4.8) helps to understand the physical phenomenon of the degradation of the shear resistance after failure. The shear resistance consists of two parts; the first part corresponds to the contribution of adhesion and interlocking which present an exponential decay with increasing slip due to the opening of the interface. The second part corresponds to the contribution of the friction which is decreasing with increasing slip towards to the remaining friction, due to the damage of the contact surface (degradation-smoothing of the undulations, as it was verified by visual observations presented in figure 3.25 and figure 3.26). From equation (4.8) it is easily proven that the friction coefficient can be expressed as a function of the slip, equation (4.9). For slip equal to s_u it presents its higher value and for an infinite slip it decreases to the known kinetic friction coefficient.

$$\mu(s) = (\mu - \mu_r) \cdot \left(e^{-(s - s_u)/s_a} \right) + \mu_r \qquad (4.9)$$

This result concerning the expression, for the transition zone, of the friction coefficient is the same to that of other researchers [Oden and Martins 1985].

Some interesting remarks are arising from figure 4.8 concerning the coefficient s_a which governs the exponential rise of the uplift and the exponential decay of the shear stress, too. Figure 4.8 depicts the fracture energy release rate G_F^{II} which is the area, inside the limits for the softening branch, beneath the curve of the shear stress an over the horizontal line for the value of the remaining frictional resistance τ_{fr}. Integration of the equation of shear stress versus slip, for the softening branch leads to the following equation (4.10):

$$G_F^{II} = (\tau_u - \tau_{fr}) \cdot s_a \qquad (4.10)$$

Equation (4.10) presents another definition of coefficient s_a besides the one proposed in the kinematic law. It expresses that the coefficient s_a corresponds to the slip that would be needed to produce the same amount of fracture energy release rate G_F^{II} to that of the softening branch, for a constant shear equal to the difference of the ultimate value τ_u and the remaining frictional resistance τ_{fr}. Replacing τ_u and τ_{fr} according to (4.1) and (4.2) we obtain an expression of the fracture energy release rate G_F^{II} of the interface as a function of the coefficients of the failure criterion, the kinetic friction coefficient, the coefficient s_a and the normal stress acting in the interface (4.11). The normal fracture energy release rate G_F^{I} which is related to the opening of the interface after failure is easily expressed by equation (4.12), since the normal stress is constant during each direct shear test.

$$G_F^{II} = (\mu - \mu_r) \cdot s_a \cdot \sigma + c \cdot s_a \qquad (4.11)$$

$$G_F^{I} = \left(u_{max,0} - r\frac{\sigma}{f_c} - u_{Su} \right) \cdot \sigma \qquad (4.12)$$

Expressions (4.11) and (4.12) are useful for simulation of interfaces (joints) in structural engineering, performing finite element analysis using contact interface layers with the appropriate mechanical characteristics [Lee et al. 2011].

Interaction of laws and the confinement effect

The failure criterion, the constitutive law and the kinematic law proposed make it possible to describe the behaviour of interfaces under static loading. In the direct shear tests that were performed the normal stress in the interface is kept constant. In reality, the normal stress in an interface of a connection of a steel-concrete composite bridge beam, results from the equilibrium of forces in the slab section that encloses the connection, created from the applied loads and the kinematic law of the interfaces. Since the normal stress is not constant but an evolution of normal stress takes place, the force-slip relationship cannot be calculated directly and analytically using the constitutive law for constant normal stress. It is needed to develop a relationship which describes the *confinement effect* relating the developed normal stress σ and the uplift u of the kinematic law of the interface. Once this relationship is known it can be combined with the failure criterion, the constitutive and the kinematic laws for constant normal stress, in order to predict the constitutive law (force path) for the actual evolution of the developed normal stress.

This type of approach for the behaviour of interfaces submitted to shear was initially proposed by Tassios [Tassios 1987]. The same approach, adapted for the case of interfaces for connections by adhesion, interlocking and friction, was used by Thomann [Thomann 2005] and can be described in figure 4.10.

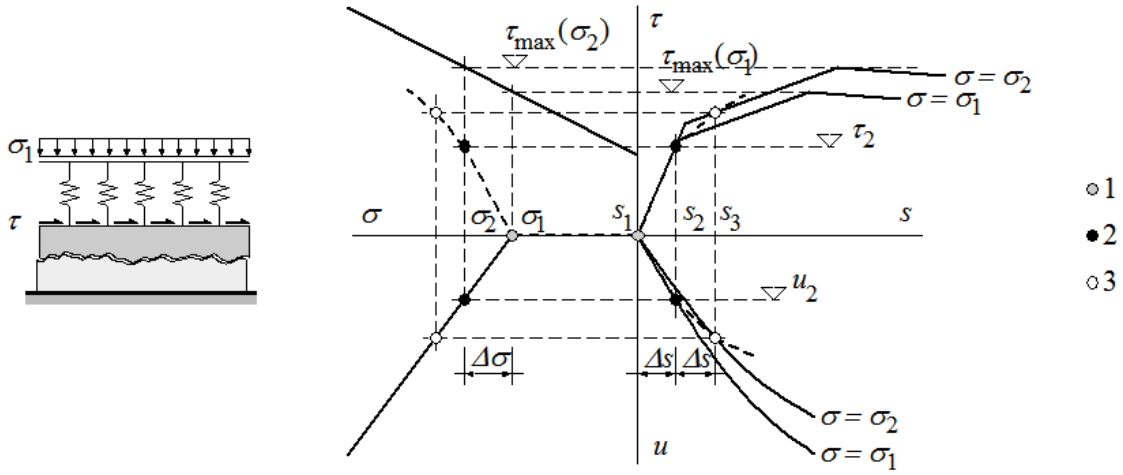

Fig. 4.10: Interface and real stress path [Thomann 2005]

In figure 4.10, the initial state of the interface is described by point 1. A pre-existed normal stress σ_1 is acting in the interface prior to loading. The uplift u and the slip s are initially zero. For incremental slip Δs the stress path follows the constitutive law for a normal stress σ_1 and the shear stress reaches the value τ_2. For the same incremental slip the uplift, based on the kinematic law for normal stress σ_1, reaches the value u_2. Due to the relationship between the normal stress and the uplift which is presented in the third (clockwise) quadrant and which describes the confinement effect, the normal stress reaches the value σ_2 (point 2). For further incremental slip Δs, the constitutive and kinematic laws corresponding to normal stress σ_2 are taken into account to define the point 3. The stress path and the actual kinematics of the interface are presented by the dotted lines in the forth quadrant, where when the dotted line intercepts the failure criterion the interface fails. It has to be noted that the incremental slip must be limited so that the increase of the normal stress σ is gradual. This is required because the coordinates of the point at a specific step are corresponding to a certain normal stress whereas for the same uplift the normal stress at the confinement relationship is higher (it is the normal stress that defines the next step). In the opposite case iteration should be applied to overcome the mismatch.

In the next chapter a numerical model will be proposed to predict the resistance of connections by adhesion, interlocking and friction. Due to its importance, the relationship between the normal stress in an interface and the uplift will be studied extensively to include all parameters which have an influence. A new relationship will be proposed which in addition to the various parameters that have an influence, takes into account the evolution of the stress state in concrete (initially non-cracked at SLS, FLS and cracked at ULS) and imposes a necessary upper limit for the confinement stress, related to the yielding of the reinforcement which is responsible for the confinement effect.

4.2.2 Cyclic loading

The results from the experimental investigation presented at chapter 3 are used to model the constitutive law of interfaces under cyclic loading. A necessary first step is the calibration of analytical expressions for the residual slip and the slip under shear stress as a function of the number of cycles. The proposed equations concern the cycling loading of interfaces, with constant amplitude and a maximum applied shear that does not exceed the elastic stress τ_{el}. Each fitting curve corresponds to the mean maximum shear stress τ_{max} applied in the specific interface. For the same direct shear stress specimen the value of the applied τ_{max} in one interface may differ from the value of it in the interface of the other side, due to different resistance and response of each interface. In few cases, the recording was only possible to one of the interface due to debonding of the supports of the transducers caused by repeated loading.

Figures 4.11, 4.12 and 4.13 depict the fitting curves for the residual slip and figures 4.14, 4.15 and 4.16 depict the fitting curves for the slip under maximum shear stress τ_{max}, for the three interfaces submitted to constant amplitude cyclic loading. The vertical scale for the specimens with the UHPFRC-cement grout interfaces is different due to higher obtained values.

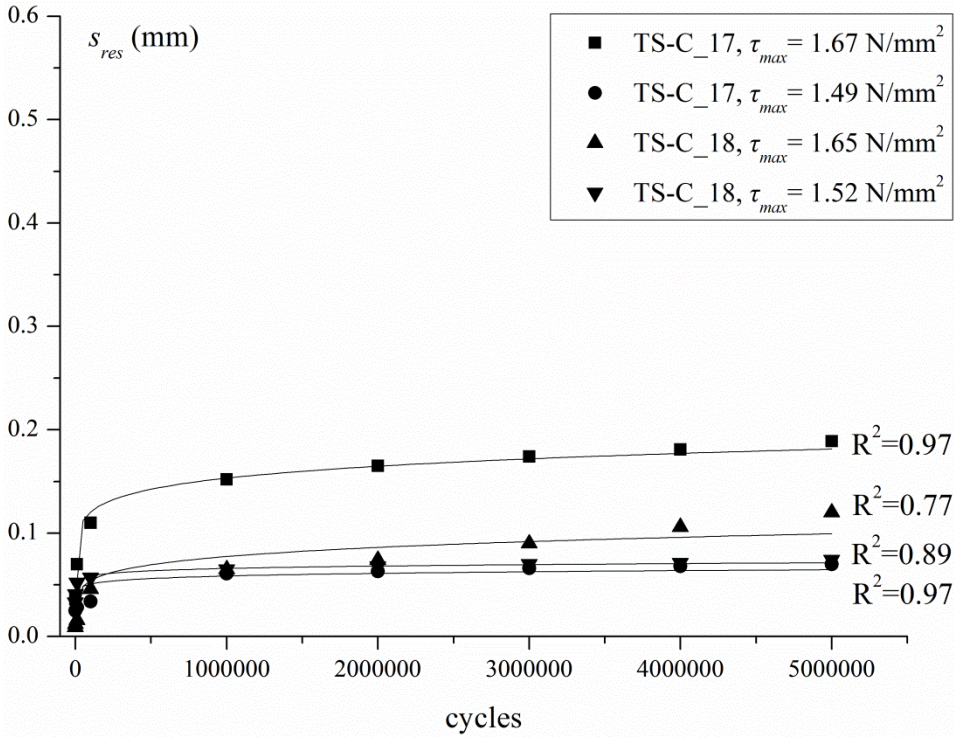

Fig. 4.11: Residual slip and fitting curves for an embossed steel-cement grout interface. Constant amplitude loading, V_{max}-V_{min}=190-95 (kN).

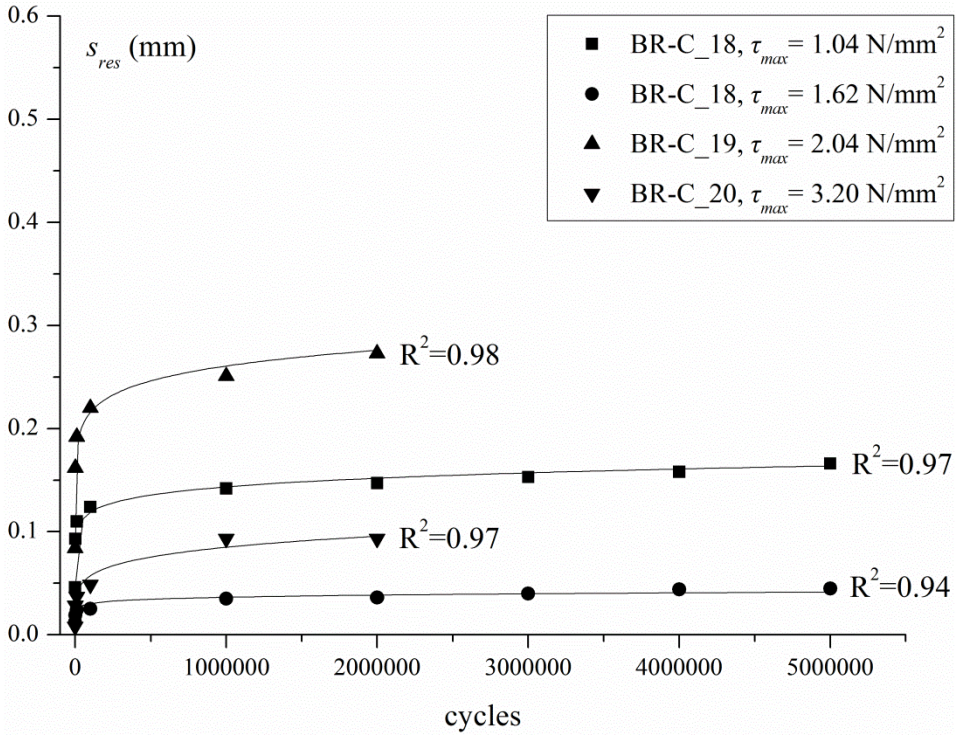

Fig. 4.12: Residual slip and fitting curves for a rough concrete-cement grout interface. Constant amplitude loading, V_{max}-V_{min}=120-30, 170-30 and 260-30 (kN) respectively for the three specimens BR-C_18, BR-C_19 and BR-C_20.

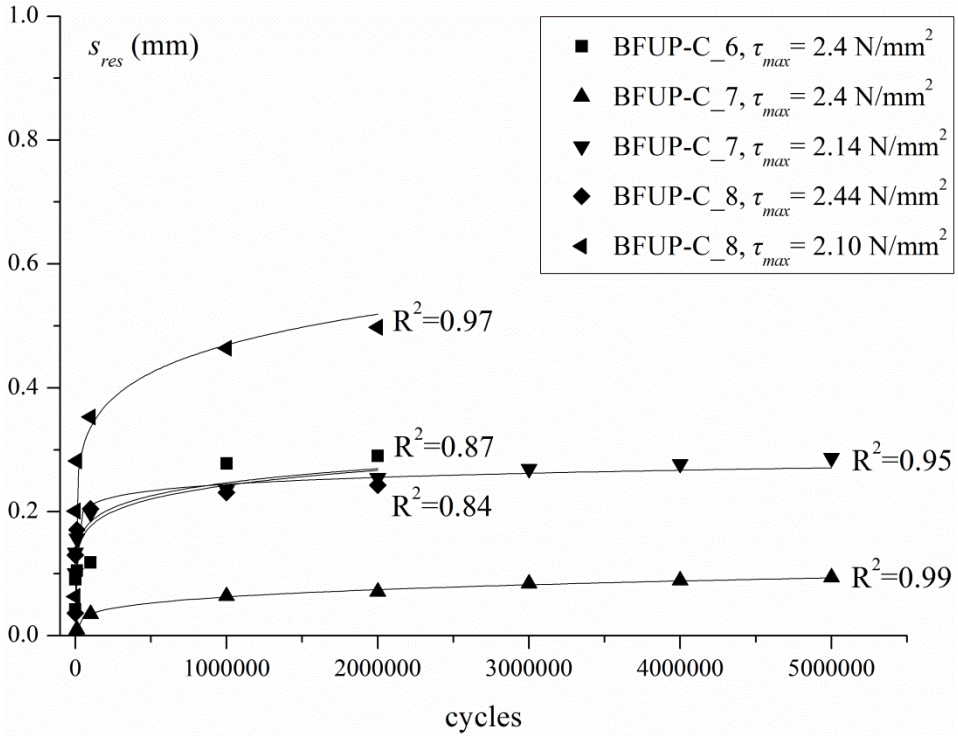

Fig. 4.13: Residual slip and fitting curves for an UHPFRC-cement grout interface. Constant amplitude loading, V_{max}-V_{min}=204-34 (kN).

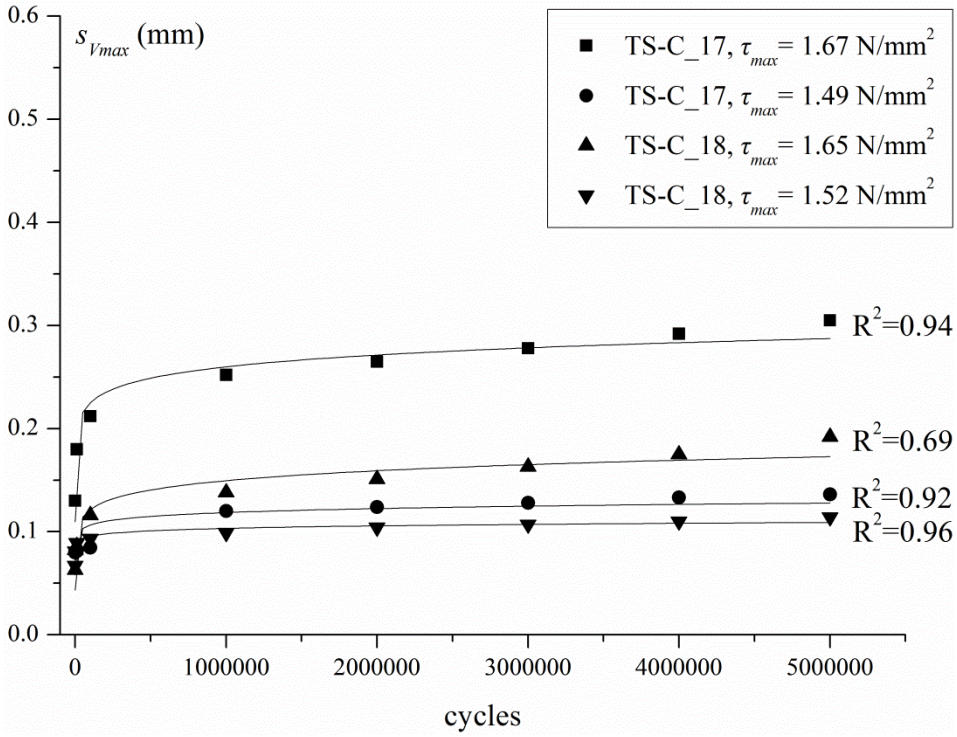

Fig. 4.14: Slip under τ_{max} and fitting curves for an embossed steel-cement grout interface. Constant amplitude loading, V_{max}-V_{min}=190-95 (kN)

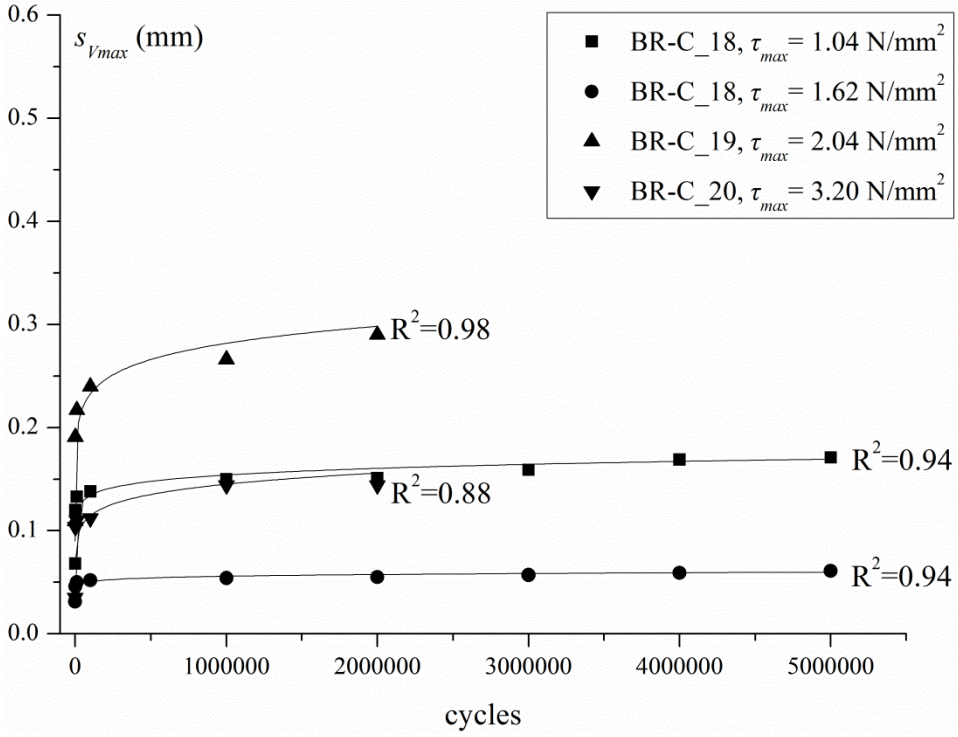

Fig. 4.15: Slip under τ_{max} and fitting curves for an embossed steel-cement grout interface. Constant amplitude loading, V_{max}-V_{min}=120-30, 170-30 and 260-30 (kN) respectively for the three specimens BR-C_18, BR-C_19 and BR-C_20.

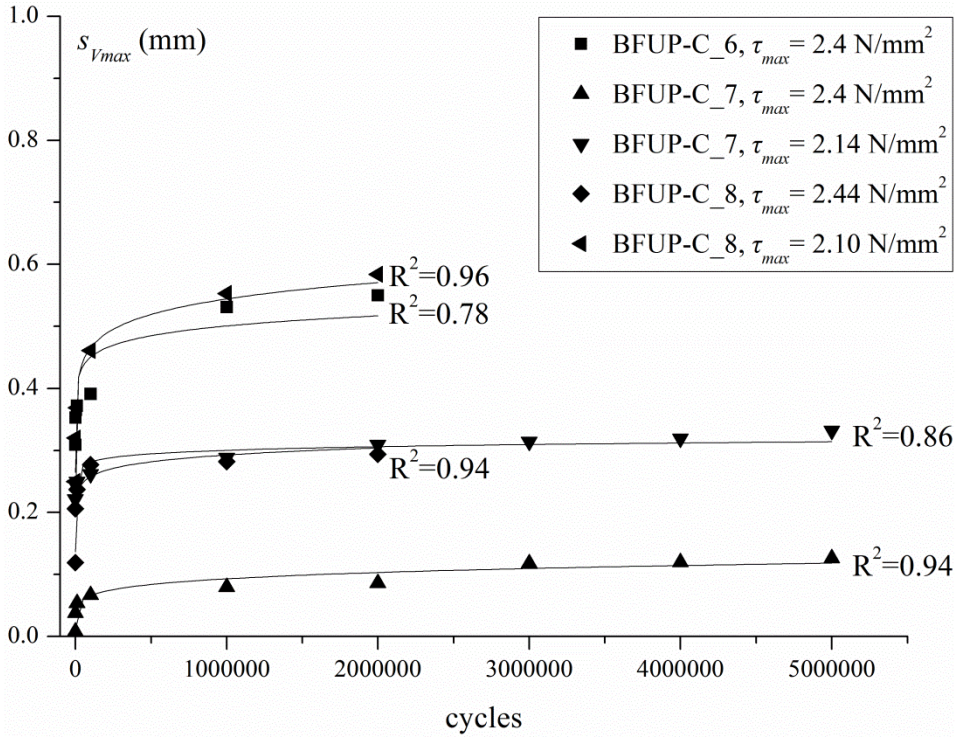

Fig. 4.16: Slip under τ_{max} and fitting curves for an embossed steel-cement grout interface. Constant amplitude loading, V_{max}-V_{min}=204-34 (kN)

The residual slip and the slip under maximum shear stress are governed by a power law and are practically stabilized after 2 million cycles or present a minor increase. This evolution with the number of cycles can be expressed by equation (4.13) and (4.14). The same type of power model was proposed in the study of Oh and Kim [Oh and Kim 2007] for concrete-steel reinforcement slip under repeated loading.

$$s_{res,N} = s_{res,1} \cdot N^{b_{res}} \tag{4.13}$$

$$s_{Vmax,N} = s_{Vmax,1} \cdot N^{b} \tag{4.14}$$

The term N in the equations (4.13) and (4.14) is the number of cycles applied. The coefficients b and b_{res} are the power index of the laws. Their values, for each of the three examined interfaces, and for the presented curves, are summarized in table 4.5. The values for test with specimen BR-C_20 are excluded from the statistical processing because the calculated shear is exceeding the elastic stress τ_{el} . The statistical mean values, of the coefficients b and b_{res} of table 4.5, are presented in table 4.6.

Table 4.5: Recorded power index for the slip under maximum cyclic shear stress and for residual slip, (τ_{max} inferior to the elastic stress τ_{el}, cyclic loading limited to the quasi-elastic behaviour)

Embossed steel				Rough concrete				UHPFRC (BFUP)			
Specim.	τ_{max}/τ_u	b	b_{res}	Specim.	τ_{max}/τ_u	b	b_{res}	Specim.	τ_{max}/τ_u	b	b_{res}
TS-C_17	0.63	0.062	0.105	BR-C_18	0.47	0.048	0.083	BFUP-6_C	0.60	0.046	0.128
TS-C_17	0.54	0.047	0.062	BR-C_18	0.34	0.036	0.080	BFUP-C_7	0.78	0.149	0.249
TS-C_18	0.61	0.090	0.156	BR-C_19	0.63	0.060	0.082	BFUP-C_7	0.75	0.028	0.064
TS-C_18	0.61	0.034	0.050					BFUP-C_8	0.53	0.055	0.138
								BFUP-C_8	0.62	0.068	0.145

Table 4.6: Statistical mean and sample standard deviation (for Gauss distribution) of power index b and b_{res} (for τ_{max} inferior to the elastic stress τ_{el}, cyclic loading in the quasi elastic domain)

Interface: Cement grout-	b	Sample St. Deviation	b_{res}	Sample St. Deviation
Embossed steel	0.058	0.024	0.093	0.048
Rough concrete	0.048	0.012	0.082	0.002
UHPFRC	0.069	0.047	0.145	0.066

In equations (4.13) and (4.14) the term $s_{Vmax,1}$ is the slip under τ_{max} and the term $s_{res,1}$ is the residual slip for the first cycle. They can be obtained by equations (4.15), (4.16), from the maximum applied shear stress τ_{max} and the stiffness k_{el} of the loading branch and the stiffness k_{des} of the unloading branch correspondingly.

$$s_{Vmax,1} = \tau_{max} / k_{el} \tag{4.15}$$

$$s_{res,1} = \tau_{max} / k_{des} \tag{4.16}$$

The stiffness k_{el} of the loading branch is that of the constitutive law for static loading, presented in table 4.4. The statistical data for defining the stiffness k_{des} of the unloading branch of the first cycle are limited. It can be measured though from its ratio with the stiffness k_{el}, which varies around a mean value, characteristic of each type of interface, described in table 4.7. However, it is reasonable to consider a correlation of the stiffness k_{des} not only with the stiffness k_{el} but also with the power index b and b_{res} and the ratio τ_{max}/τ_u, as it is shown later on, in equation (4.27).

Table 4.7: Ratio of the stiffness k_{des} of the unloading branch with the stiffness k_{el}

Interface: Cement grout-	k_{des}/k_{el}
Embossed steel	3.96
Rough concrete	1.79
UHPFRC	4.16

Substitution of equations (4.15) and (4.16) to equations (4.13) and (4.14), we obtain the expressions where the only variable is the number of cycles.

$$s_{res,N} = \frac{\tau_{max}}{k_{des}} \cdot N^{b_{res}} \tag{4.17}$$

$$s_{Vmax,N} = \frac{\tau_{max}}{k_{el}} \cdot N^{b} \tag{4.18}$$

The proposed constitutive law for the three interfaces, under constant amplitude cyclic loading is presented in figure 4.17. The proposed law concerns an applied maximum shear τ_{max} inferior to the elastic stress τ_{el} (quasi-elastic behaviour). The constitutive law for ULS following the cyclic loading history is also presented.

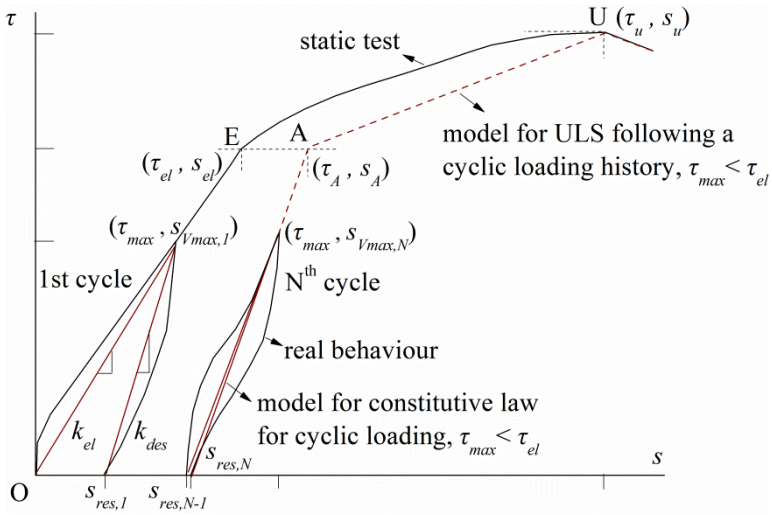

Fig. 4.17: Constitutive relationship for cyclic loading of an interface, real behaviour and modeling.

The model in figure 4.17 proposes for the behaviour for the first cycle and the ascending part a linear relationship with stiffness that of the monotonic test. The descending part of the first cycle is realized with a different stiffness k_{des}. The following cycles can also be described with linear relationships of shear stress versus slip and can be defined by the evolution, with the number of cycles, of the residual slip and the slip under maximum load. For example, after having performed N-1 cycles, the loading ascending branch of the N cycle is presented by equation (4.19) and is linking the points $(0,s_{res,N-1})$ and $(\tau_{max}, s_{Vmax,N})$.

$$\tau = \frac{k_{el} \cdot k_{des} \cdot s + \tau_{max} - k_{el} \cdot (N-1)^{b_{res}}}{k_{des} \cdot N^{b} - k_{el} \cdot (N-1)^{b_{res}}} \qquad s_{res,N-1} \le s \le s_{Vmax,N} \tag{4.19}$$

The unloading branch follows the line connecting the peak point $(\tau_{max}, s_{Vmax,N})$ and the point $(0,s_{res,N})$.

Based on the observations from tests, the model in figure 4.17 proposes also the behaviour at ULS after a sequence of cyclic shear loading, in which the applied τ_{max} is inferior to the elastic stress τ_{el} and the slip under maximum load is not higher than the slip s_u. According to the model, further loading after the peak of the N cycle is resulting to a stress-slip relationship which continues with the same stiffness as the actual loading branch, so equation (4.19) applies for this case, too. The stiffness changes, at point A (τ_A,s_A) when the value of the shear stress becomes equal to τ_{el} $(\tau_{el} = \alpha\ \tau_u)$. Substitution to the equation (4.19) of coordinates of point A results to the equation (4.20) for the slip at point A.

$$s_A = \frac{a \cdot \tau_u}{k_{el}} \cdot N^{b} - \left(\frac{a \cdot \tau_u - \tau_{max}}{k_{des}} \right) \cdot (N-1)^{b_{res}} \tag{4.20}$$

From point A and after a linear relationship applies towards the point of initiation of failure for static loading, equation (4.21). The post-failure behaviour is the same with the one of an interface subjected directly to static loading.

$$\tau = \tau_u \cdot \left[1 - \frac{(1-\alpha) \cdot (s_u - s)}{(s_u - s_A)} \right] \qquad s_A \le s \le s_u \tag{4.21}$$

It was mentioned in the 3rd chapter that, for constant amplitude shear loading of an interface, that initiation of failure occurs when the slip under cyclic loading reaches the value of the slip s_u which corresponds to initiation of failure for the static loading. This conclusion establishes a *safe fatigue failure criterion* expressed by equation (4.22):

$$s_{Vmax,N} \le s_u \tag{4.22}$$

The criterion enables together with the equations (4.7), and (4.18) to derive the number of cycles for fatigue failure N_f (4.23).

$$N_f = \left(s_u \cdot \frac{k_{el}}{\tau_{max}} \right)^{1/b} \Rightarrow N_f = \left(\frac{k_{el}}{k_{\sec}} \cdot \frac{\tau_u}{\tau_{max}} \right)^{1/b} \Rightarrow N_f = \left[\left(\alpha + (1-\alpha) \cdot \frac{k_{el}}{k_{pl}} \right) \cdot \frac{(c + \mu \cdot \sigma)}{\tau_{max}} \right]^{1/b} \tag{4.23}$$

This criterion ensures that the remaining structural performance at ULS, following the previous constant amplitude loading in which τ_{max} is kept inferior to τ_{el} , will reach the ultimate shear resistance τ_u of the static loading.

The equation (4.23) can also be expressed alternatively with the ratio between the maximum applied shear stress for cyclic loading versus the ultimate resistance of the interface for the same normal stress in the interface, equation (4.24).

$$N_f = \left[\left(\alpha + (1-\alpha) \cdot \frac{k_{el}}{k_{pl}} \right) \cdot \frac{1}{\tau_{max} / \tau_u} \right]^{1/b} \tag{4.24}$$

Using, for example, a ratio τ_{max} / τ_u equal to 0.50 in equation (4.24) results to N_f equal to several billion cycles for an embossed steel-cement grout interface or a rough concrete-cement grout interface. This practically means that if during service life of the connection the ratio τ_{max} / τ_u in the interfaces remains lower than 0.50 no fatigue failure is expected in the connection. However, equation (4.24) is largely sensitive to the power index *b*. Even a minor increase of the power index *b* reduces drastically the number of cycles to failure.

The definition of the safe fatigue failure criterion can lead to an expression for the stiffness of the descending branch k_{des} for the first cycle, needed for the evolution of the residual slip in the interface. It is reasonable to make the hypothesis that for cycles up to failure, i.e. up to N_f , the slip under maximum shear remains higher than the residual slip of the descending branch:

$$s_{Vmax,N} \ge s_{res,N} \Rightarrow \frac{\tau_{max}}{k_{el}} \cdot N^b \ge \frac{\tau_{max}}{k_{des}} \cdot N^{b_{res}} \Rightarrow k_{des} \ge k_{el} \cdot N^{b_{res} - b} \tag{4.25}$$

Hence a minimum value for the stiffness k_{des}, for the first cycle, can be deduced by the equality of equation (4.25) by substitution of the number of cycles with N_f. Thus equation (4.25) becomes:

$$_{min}k_{des} = k_{el} \cdot \left(\frac{1}{\tau_{max} / \tau_u} \cdot \frac{k_{el}}{k_{sec}} \right)^{\left(\frac{b_{res}}{b} - 1 \right)} = k_{el} \cdot \left[\frac{1}{\tau_{max} / \tau_u} \cdot \left(a + (1-a) \cdot \frac{k_{el}}{k_{pl}} \right) \right]^{\left(\frac{b_{res}}{b} - 1 \right)} \tag{4.26}$$

Equation (4.26) suggests a minimum value for the stiffness k_{des} , which can be used instead of values of table 4.7, when the evolution of the residual slip in the interface is searched. Apparently using equation (4.26) results to the equality of $s_{Vmax,N}$ and $s_{res,N}$ at fatigue failure, i..e. after N_f cycles.

4.3 Connection

In a similar way to that applied for the interfaces, the experimental investigations made it possible to register the evolution of the residual slip s_{res} and the slip under maximum load s_{Vmax} for push-out specimens fabricated with the new connection. The fitting curves for the s_{res} and the s_{Vmax} are presented in figures 4.18 and 4.19.

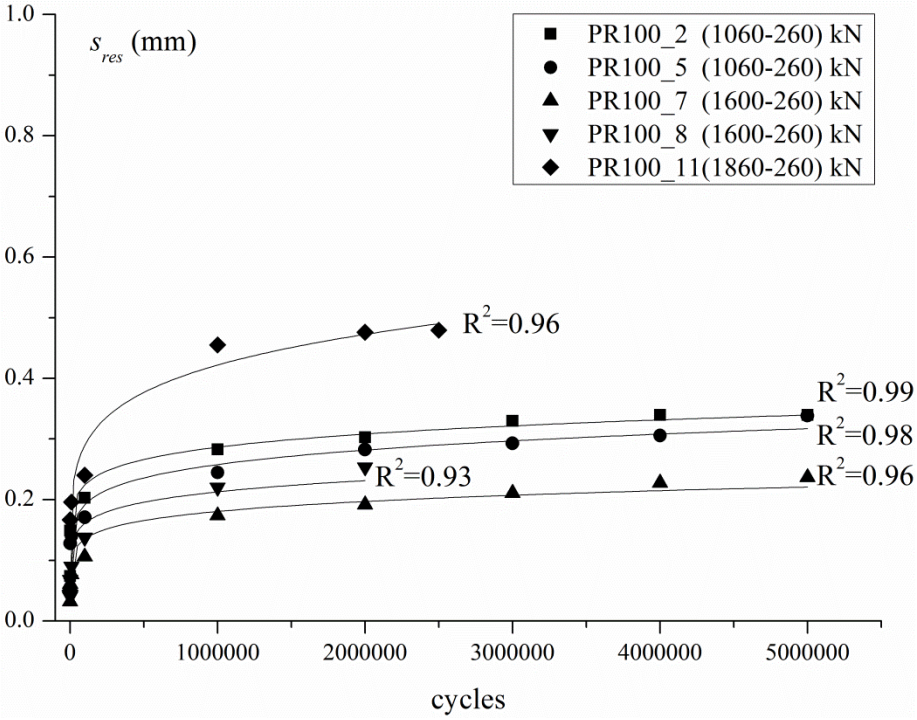

Fig. 4.18: Residual slip in the connection, s_{res} as a function of the number of cycles and fitting curves.

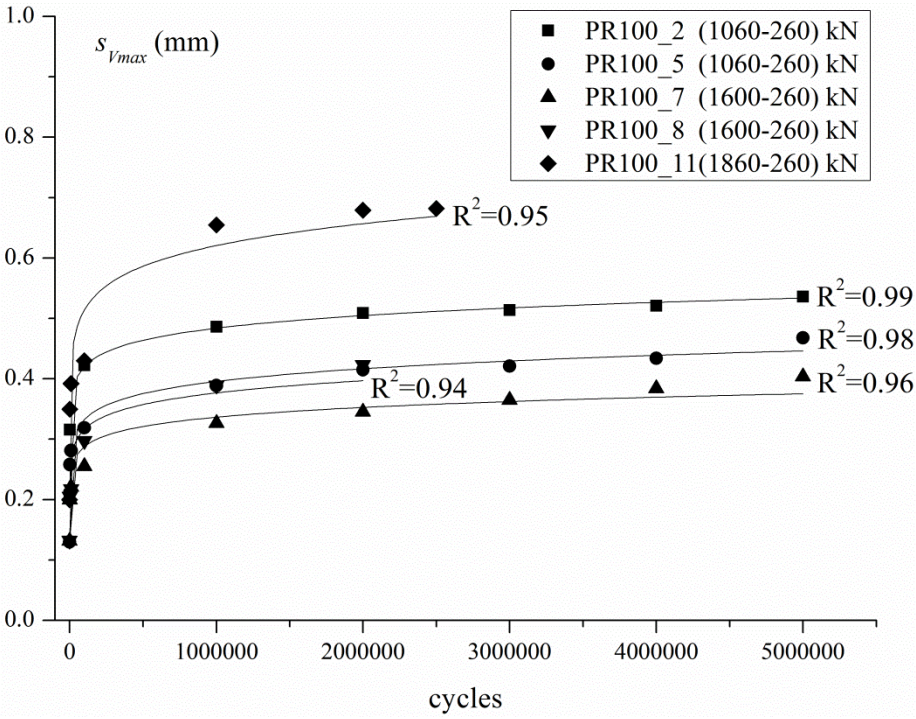

Fig. 4.19: Slip in the connection under maximum cyclic load, s_{Vmax}, as a function of the number of cycles and fitting curves

The residual slip and the slip under maximum longitudinal shear in the connection are governed by a power law and practically stabilize after 1 to 2 million cycles. Their evolution with the number of cycles can be expressed, similarly to the expression for interfaces, by equation (4.27) and (4.28). The power index b_{con} and $b_{con,res}$ for each test are presented in table 4.8 and the mean statistical values in table 4.9.

$$s_{res,N} = s_{res,1} \cdot N^{b_{con,res}} \tag{4.27}$$

$$s_{Vmax,N} = s_{Vmax,1} \cdot N^{b_{con}} \tag{4.28}$$

Table 4.8: Recorded power index for the residual slip and slip under maximum cyclic loading.

Specimen	V_{max}/V_u	b_{con}	$b_{con,res}$
PR100_2	0.41	0.062	0.106
PR100_5	0.44	0.075	0.128
PR100_7	0.52	0.068	0.125
PR100_8	0.55	0.076	0.121
PR100_11	0.45	0.082	0.163

Table 4.9: Statistical mean of power index for residual slip and slip under maximum longitudinal shear

b_{con}	Sample St. Deviation	$b_{con,res}$	Sample St. Deviation
0.072	0.008	0.129	0.021

The values presented in table 4.9 are close to the values for the embossed steel-cement grout interface which is the less resistant than the rough concrete-cement grout interface.

The connection's performance at ULS after the cyclic loading, in which the maximum applied longitudinal shear V_{max} is such that does not lead to primary failure, is presented schematically at figure 4.20. The maximum applied longitudinal shear V_{max} varies between 41 to 55% of the ultimate resistance, for the specific connection geometry and confinement reinforcement of the push-out specimens tested.

In figure 4.20 the longitudinal shear force-slip relationship, which follows the cyclic loading, is defined by the curve that has the residual slip, $s_{res,N-1}$, as a threshold. When crossing the point (V_{max}, $s_{Vmax,N}$) the curve continues with the same stiffness-as seen from experimental investigation- up to the point where it reaches the curve for static loading. From that point it follows the static loading curve.

It has to be noted that the total slip of the connection is the addition of the slip developed in the embossed steel-cement grout interface and the rough concrete-cement grout interface. As it will be presented in the next chapter, the normal stress on the interfaces is not constant but it increases, for the loading ascending branch with increasing slip. Consequently the residual slip in the connection, which is the addition of the residual slip from two interfaces, is developed under various normal stresses and cannot be expressed analytically from the expressions for interfaces. It was however observed, in the section 3.3.5, that the residual slip in the connection tends to be equal to the slip under maximum longitudinal shear, after a significant number of cycles-more than a million-. Thus, for simplification, the longitudinal force-slip relationship prior to failure, at ULS after cyclic loading, can be simulated by a line which starts from point (0, $s_{Vmax,N}$) and ends at the point (V_u, s_u) without crossing the point (V_{max}, $s_{Vmax,N}$) to avoid an infinite stiffness in that part. The needed value $s_{Vmax,N}$ can be calculated from equation (4.28) in which the term $s_{Vmax,1}$ is obtained from the curve for static loading. The latter can

be predicted by the numerical model which is developed for the connection and presented in the next chapter. The post failure behaviour is the same to that for static loading, as it was found at the experimental investigation.

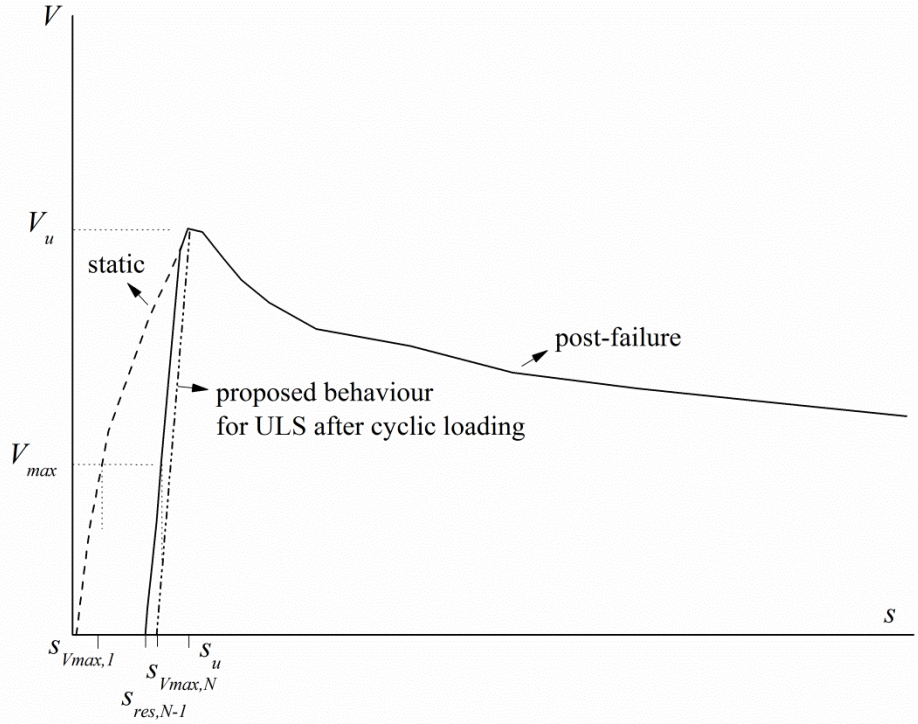

Fig. 4.20: Influence of cyclic loading to the longitudinal shear force-slip relationship of the connection at ULS that follows cyclic loading.

Similarly to what was proposed for the interfaces, a *safe fatigue failure criterion* can also be established for the connection, equation (4.29). The criterion can be expressed by the following statement:

No failure due to cyclic loading occurs in the connection as long as the accumulated slip under maximum applied longitudinal shear force is inferior to the slip which corresponds to failure for static loading.

$$s_{Vmax,N} \leq s_u \tag{4.29}$$

Equation (4.29) allows calculating the number of cycles which lead to failure of the connection for constant amplitude cyclic loading.

$$N_f = \left(\frac{s_u}{s_{Vmax,1}} \right)^{1/b_{conn}} \tag{4.30}$$

In equation (4.30) the slip $s_{Vmax,1}$ under the maximum load for the first cycle and the slip s_u (slip for initiation of failure) are deduced from the longitudinal force-slip relationship for static loading, obtained from experimental data when those are provided from push-out tests on specimens with the specific connection geometry. When this not possible, as it is the common case when designing the connection for a steel-concrete composite bridge, a scientific tool is necessary in order to predict the longitudinal force-slip relationship for static loading.

Another question which rises and which is related to a safe performance of the connection for cyclic loading is the choice of the maximum applied longitudinal shear V_{max}. It was found for the specific connection geometry of the push-out specimens that a safe maximum applied longitudinal shear V_{max} for cyclic loading varies between 41 to 55% of the ultimate resistance. However a scientific tool is needed so as to define a non-arbitrary limit for a safe V_{max} for cyclic loading which should correspond to the specific connection geometry and the confinement reinforcement proposed in the design.

These demands are answered in the next chapter where a numerical model is proposed for the connection. It will be shown also how this model proposes a non-arbitrary limit for a safe V_{max} for cyclic loading with general application.

4.4 Beam

This chapter ends with an analytical study of the developed plastic moment of the tested composite beam at ULS that followed a five million cycle loading. A refined approach is used to calculated the plastic moment taking into account the measured values of strains and the existence of two neutral plastic axes, one in the steel beam and one in the reinforced concrete, as it is verified experimentally from the cracking in the lower part of the reinforced concrete (see paragraph 3.4.5) due to slip between the reinforced concrete slab and the steel beam. The estimated ultimate load is compared to the experimental recorded value.

- Reinforcement, passive and active, are accounted for with estimated yield strength of 500N/mm^2.
- For the compressive part, the concrete is considered to develop an equivalent orthogonal stress distribution with value equal to 0.85 times the estimated compressive strength at the time of testing. This value $f_{cm}{}^t$ equal to 65.16 N/mm^2 is calculated from the mean compressive strength at 28 days, f_{cm} =56.66 N/mm^2 and the increase due to aging.
- Stress distribution within steel beam is deduced from strain measurements and the real stress-strain curves for the web and the flanges. The strain measurements are those of the time when the applied load reaches its ultimate value. Concerning the steel connector extrapolation of strains is made from the strain measurements of the steel beam and the yield strength is considered 235 N/mm^2.
- The surface of the cement grout is taken into account included in the surface of the concrete.

Distribution of stresses for the ultimate load is presented in the figure 4.21.

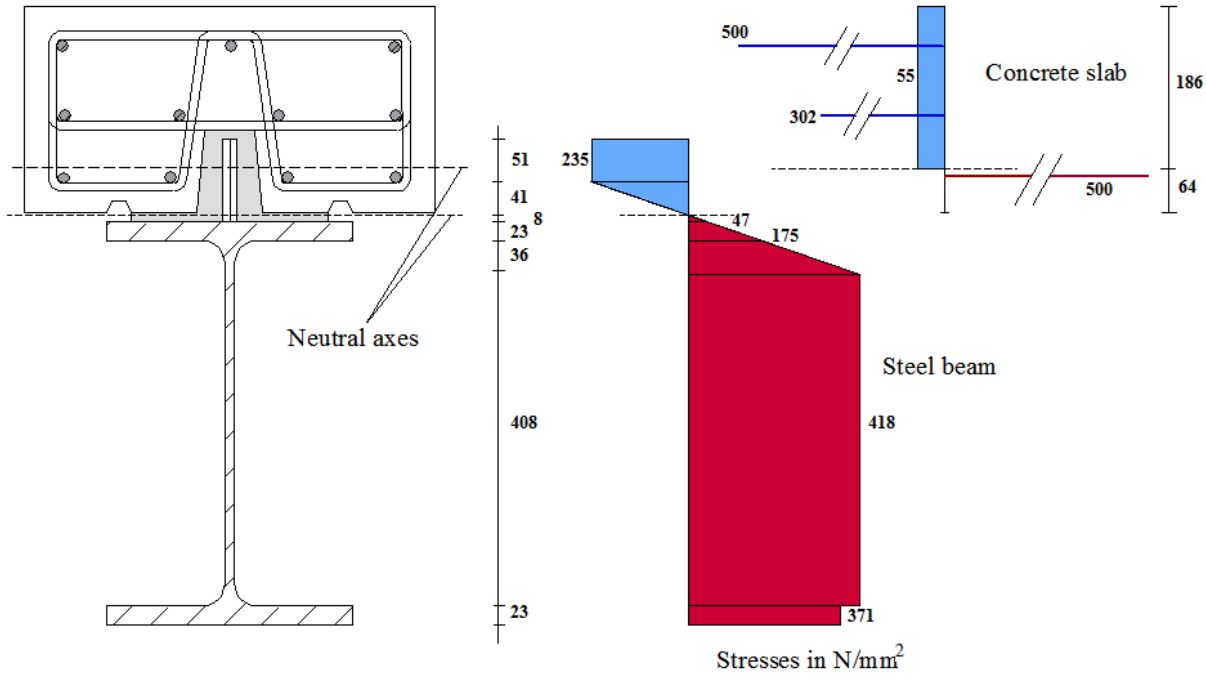

Fig. 4.21: Distribution of stress in the composite section at ultimate load with slip in the interface

Due to the slip in the interface, a partial connection is developed and two neutral axes are formed. The neutral axis for the steel girder is found to be formed, from extrapolation of the measured strains in the beam, in the bottom part of the embossed steel plates at 8 mm from the upper flange of the beam. The neutral axis for the reinforced concrete is found, from equilibrium of forces in the cross section, to be

located at 64 mm from its bottom which is in accordance to the visual observation of the tensile cracking of the concrete (figure 4.22).

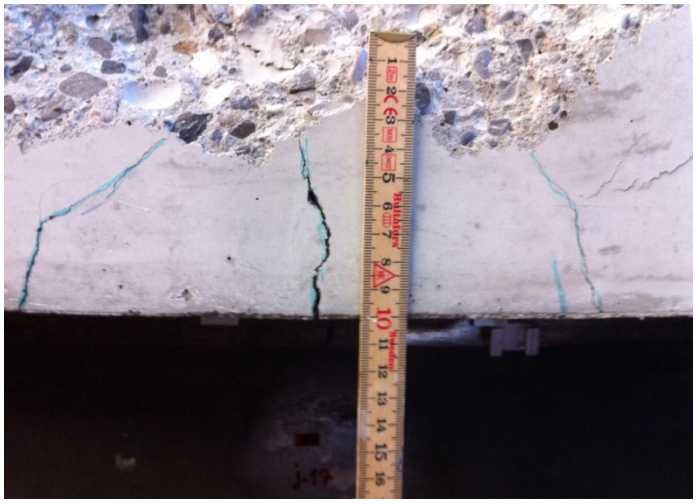

Fig. 4.22: Tensile cracking on the lower part of the reinforced concrete of the composite beam for the section with ultimate moment

The plastic moment calculated in that way, i.e. for a section with partial interaction (slip), is equal to 2721 kNm, slightly lower than the plastic moment, 2764 kNm, for full interaction (no slip) and real values of yielding strength of the steel and the compression resistance of the concrete. The estimated ultimate load is equal to 665 kN almost identical to the highest value of the recorded applied force which is equal to 664 kN. (Note that in the reaction force presented in figure 3.86 is been added the non-recorded part of the reaction force which corresponds to dead load and has the value of 22.4 kN. This is why in figure 3.86 the reaction force goes up to 686 kN). It should also be added that the calculated plastic moment (2721 kNm) exceeds by far the design plastic moment of such a composite section ($M_{pl,Rd}$ = 1870 kNm) with the specific mechanical characteristics of the materials used. This is due to the hardening of the steel and secondly due to the increased compression resistance of the concrete in comparison to the design value.

This analytical study shows that despite the slip developed in the new connection at ULS, which follows a cyclic loading, the composite beam is capable to develop its design plastic moment due to the connection's sufficient deformation capacity.

4.5 Conclusions

The analytical study performed in this chapter has made it possible to simulate the behaviour of the three examined interfaces under static and cyclic loading for constant normal stress in the interface. Analytical expressions have also been proposed to describe the behaviour of connections for cyclic loading for a maximum applied load that does not exceed, as found experimentally, 55% of the ultimate resistance of the connection.

Static loading:

- A *failure* Mohr-Coulomb linear *criterion* is proposed for the shear resistance in the interface.
- A *kinematic law* describes the opening of the interface under constant normal stress, consisting of two branches, a branch simulated by a parabola, up to the value of uplift for failure initiation u_{Su}, and a second branch, an exponential rise which describes the smoothing of the undulations of the failure surface.

- The *constitutive law* is also consisted of two branches. The first one, simulated by a bilinear law, refers to the developed shear stress prior to failure and indicates also the extent of the quasi-elastic domain. The second branch describes the transition phase towards the kinetic friction with an exponential decay of the shear resistance due to the smoothing of the failure surface. For this branch, analytical expressions were proposed also for physical quantities related to fracture mechanics such as the fracture energy release rate and the normal fracture energy release rate in the interface, which can be used in finite element analysis as mechanical characteristics of interlayer in order to describe, together with friction constrains the behaviour of joints.

Cyclic loading:

- The constitutive law for cyclic loading of interfaces is defined taking into account the analytical expressions which are developed for the residual accumulated slip in the interface and the slip under the maximum applied cyclic loading. Similar expressions have been proposed also for the new connection.
- The behaviour for ULS after submission to cyclic loading is also defined, both for interfaces and the connection.
- A safe fatigue failure criterion is proposed in such as way that the remaining resistance in the interface or in the connection is equal to that for a virgin monotonic loading.

The above laws and considerations will be used in the following chapter in a numerical model in order to predict the connections structural performance for static and cyclic loading. Since the normal stress in an interface is not constant during loading of a connection, a relationship relating the normal stress and the uplift in connection should be incorporated in such a model. This expression for the confinement effect should take into account the mechanical characteristics of the concrete such as the compressive strength and the modulus of elasticity, should be able to reproduce the uplift-normal stress relationship prior and after cracking of concrete and finally it should consider the geometry of the connection and the reinforcement ratio.

The prediction of the connection's structural behaviour by the numerical model should include, besides the ultimate resistance, the post-failure behaviour, providing thus the whole deformation capacity of the connection which is mobilized at the ULS of the composite beam.

The numerical model should also provide, for the specific connection geometry chosen by the designer, a non-arbitrary limit for the maximum applied longitudinal shear, V_{max}, for cyclic loading, which should avoid fatigue failure at service life and should guarantee the required resistance at a following ULS.

5. Numerical model to predict the connection resistance

5.1 Introduction

In this chapter a numerical model is proposed to predict the connection's resistance and its deformation capacity. This model is based on several hypotheses concerning the mechanical behaviour of the connection. The latter takes into account the constitutive and the kinematic law of the interfaces, their interaction and the confinement effect caused by the concrete slab. The needed laws which describe the constitutive and the kinematic law of the interfaces, under constant normal stress, were developed in the previous chapter. The confinement effect is described by a relationship which relates the normal separation, uplift u, in the interfaces and the normal (confinement) stress σ, which is developed due to the interaction of the kinematic in the interfaces and the response of the reinforced concrete section which encloses the connection. As seen in the 2nd chapter in the state of the art, Thomann [Thomann 2005] proposed a linear relationship between the normal stress and the uplift by introducing a constant translational stiffness of the slab at the cracked stage. Since this issue is crucial for the prediction of the connection's structural performance, this study goes further proposing a more general analytical expression for the confinement effect especially for loading level before cracking of the concrete, as it was observed during the cyclic loading push-out tests.

The confinement effect should take into account the mechanical characteristics of the concrete, the section geometry and the positioning of the reinforcement, the reinforcement quantity and the evolution of the stress field starting with a non-cracked section (suitable for SLS and FLS) and ending with the formation of the cracks (ULS). Furthermore it is necessary to impose an upper limit for the confinement stress, related to the yielding of the reinforcement which is responsible for the confinement effect.

Once the analytical expressions describing the confinement effect are developed, the numerical model for the connection is proposed and is validated with the results from push-out tests. The numerical model predicts the ultimate resistance and provides the complete longitudinal shear force per unit length-slip relationship including the post-failure behaviour.

A parametric analysis is performed to investigate the influence of the various parameters on the resistance and the deformation capacity of the connection in order to propose useful recommendations.

Finally, a method is proposed by applying the numerical model, in order to define a justified and non-arbitrary limit for the maximum applied longitudinal shear, V_{max}, for cyclic loading, which should guarantee a safe behaviour for the service life under cyclic loading and allow the development of the ultimate resistance at an ULS following the cyclic loading.

5.2 Mechanical behaviour of the connection

The resistance of the connection to longitudinal shear is based on the shear that it is developed in the two types of interfaces, as illustrated in figure 5.1, an interface between the embossed steel and the cement grout and an interface between cement grout and the material of the inner rib of the slab, either roughened concrete or UHPFRC.

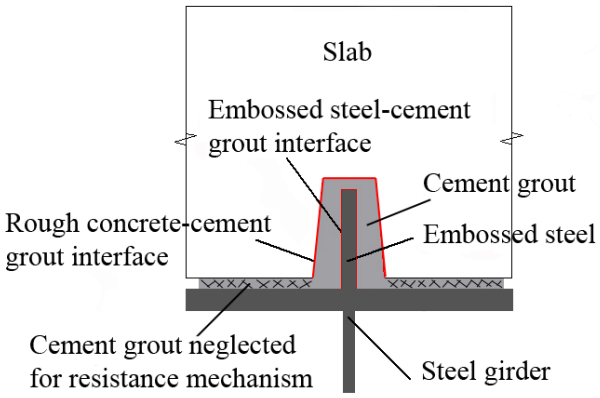

Fig. 5.1: Cross section of a composite beam and interfaces creating the connection

The mechanical behaviour of the connection is presented in figure 5.2. A longitudinal shear applied in the composite beam causes a slip in the interfaces which is accompanied by a transversal separation, uplift and a hardly noticed rotation (presented in figure 5.2 with a scale factor for the displacement).

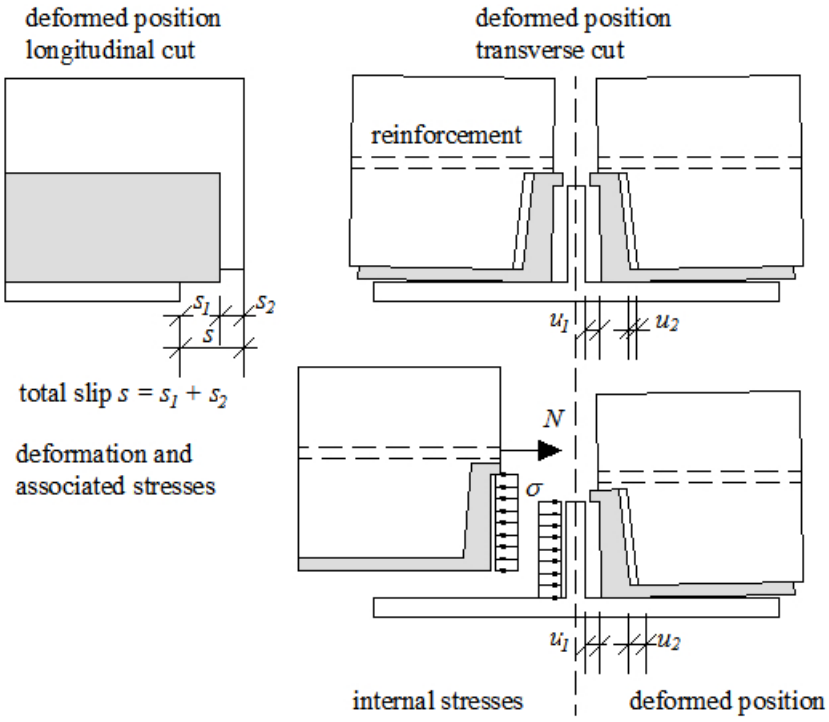

Fig. 5.2: Mechanical behaviour of the connection

The following hypotheses are made for the mechanical behaviour presented in figure 5.2, on which will be based the numerical method for the prediction of connection's resistance and deformation capacity. Hypotheses a) to g) are adopted by the model developed by Thomann [Thomann 2005]. Hypotheses h) to j) constitute additions of the author.

a) The total slip s between the slab and the steel girder is the addition of the slip s_1 developed in the embossed steel-cement grout interface and the slip s_2 developed between cement grout and the slab. The same applies to the transversal separation. At each side of the embossed steel plates, the uplift u between the slab and the embossed steel plate is the addition of the uplift u_1 between the embossed steel plate and the cement grout and the uplift u_2 between the cement grout and the slab.
b) The interfaces that are considered to contribute with their shear resistance are the vertical interfaces: a) the embossed steel-cement grout interface and b) the cement grout-rough concrete interface (or cement grout-UHPFRC for the cases that UHPFRC is used instead of concrete for the deck). No shear resistance is considered between the cement grout and the upper flange of the steel girder.
c) The developed normal (confinement) stresses in the interface resulting from the equilibrium of forces are considered uniformly distributed on the height of the interfaces.
d) The two types of interfaces contributing to the resistance are considered to be connected in series, thus the same longitudinal force passes through them.
e) The slip at each side of the connection is distributed in the two types of interfaces according to the shear stress-slip stiffness defined by the constitutive law of each interface.
f) The connection shows symmetrical behaviour, meaning that the slip and the uplift at the two sides of the embossed steel plates are identical.
g) The cement grout is considered not to be deformed.
h) No vertical uplift, due to rotation, is considered for the part of the cement grout which contributes to interfaces' resistance and is situated between the inner rib of the slab and the embossed steel plate.
i) The translational movement of the slab is also followed by a rotation resulting to non-uniform transversal uplift, which based on measurements from push-out tests is considered linearly distributed along the interface.
j) The translational stiffness of the slab is not constant during the development of slip and the uplift. Initially the slab is not cracked, as it was observed during cyclic loading push-out tests, and the translational stiffness has large values. Once the crack is formed and reinforcement is mobilized the stiffness will decrease. Because of its high importance on the connection behaviour and the need for generalization for applications, the confinement effect is studied and presented more in detail in the paragraph 5.3.

5.3 The confinement effect

The confinement effect between the normal (confinement) stress σ on the interface and the transversal separation uplift u is studied by performing finite element analysis. The finite element analysis software ABAQUS [Simulia 2011] has been used. A 2-D analysis has been performed using as a section the symmetric half of the cross section of the slab presented in figure 5.1.

Figure 5.3 presents the geometry of section studied, and the definition of several geometrical parameters which are taken into account.

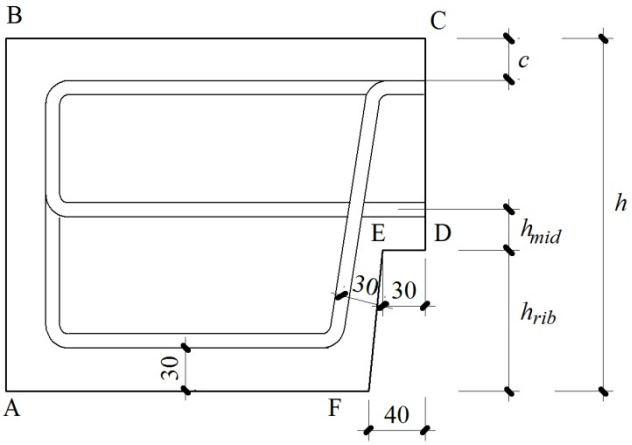

Fig. 5.3: Concrete section used for finite element analysis (FEA)

The boundary conditions originated from the symmetry were set along the line CD. The following parameters are taken into account:

- The total height h of the section.
- The height h_{rib} which corresponds to the height of the inner rib and the height of the embossed steel plate.
- The height h_{mid} which is the distance between the center of the steel reinforcement located over the rib and the upper edge ED of the rib.
- The covering c of the upper reinforcement.
- The modulus of elasticity E_{cm} and the characteristic strength of the concrete f_{ck}.
- The ratio of the area of the reinforcement at each height level versus the spacing S of the rebars at the longitudinal direction A_S/S. The area of reinforcement is the same for each level (upper, middle and lower reinforcement) for the studied detail.

In the finite element program the reinforcement is simulated by means of beam elements. A full bond between concrete and steel reinforcement is considered and applied by using the appropriate constrain of the software called embedded constrain [Simulia 2011]. Concerning the material model for the reinforcement, an idealized stress-strain diagram is been considered according to the code SIA 262 [SIA-262 2003] for rebars of type B500B, having a strain-hardening ratio k_s equal to 1.08 and ultimate strain ε_{ud} equal to 0.045.

The concrete is simulated by a 4-node plain strain element. The material property for the concrete is defined used a non-linear material model. For uniaxial compression of the concrete, the stress-strain diagram according to fib Model Code 2010 [fib Model Code 2010] is applied. For uniaxial tension of the concrete, since the tensile failure is a discrete phenomenon, a linear stress-strain diagram is used for the uncracked concrete and once the tensile strength is reached a stress-crack opening diagram

applies, figure 5.4. Concerning the fracture energy, G_f, the equation (5.1) from fib Model Code 2010 is used, in which f_{cm} is in N/mm^2.

$$G_f = 10 \cdot \left(1 - 0.77 \cdot \frac{10}{f_{cm}}\right) \cdot \text{N/mm} \tag{5.1}$$

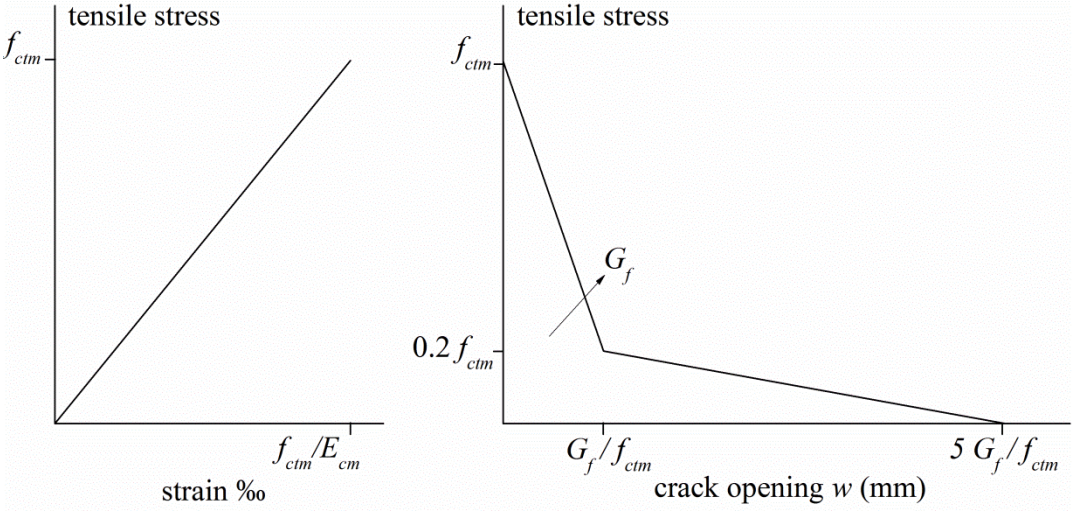

Figure 5.4: Stress-strain and stress-crack opening diagram for uniaxial tension of concrete [fib Model Code 2010]

The analysis is performed by applying an incrementally increasing, uniformly distributed, horizontal normal stress σ along the height of the inner rib of the slab, (line EF in figure 5.3). For each incremental level of the applied normal stress the translational displacement or uplift u, of the line EF is recorded. The distribution of uplift along the height of the inner rib is found to be linear and its mean value corresponds to the uplift in the middle of the line EF. The diagram of the normal stress σ versus the mean uplift u along the height of the inner rib is then created.

A typical example of such a confinement effect is the one presented in figure 5.5, which corresponds to the half section of the concrete block used for the push-out specimens. Initially, before cracking of the concrete the stiffness is high, as expected. Once the crack is formed, point A in the figure, the reinforcement steel is submitted to an increasing tension and the normal (confinement) stress continues to increase but with an inferior ratio. At the moment where the middle steel reinforcement yields another change occurs in the curve, point B, and the normal (confinement) stress exhibits a limited increase due to the hardening of the reinforcement and the contribution of the upper reinforcement. At about 2 mm of uplift, point C, the normal stress stops to increase. The slope of the third part BC of the curve, k_c, (figure 5.5) has practically a constant stiffness, equal to 0.5 N/mm^3, as it was found by performing FEA.

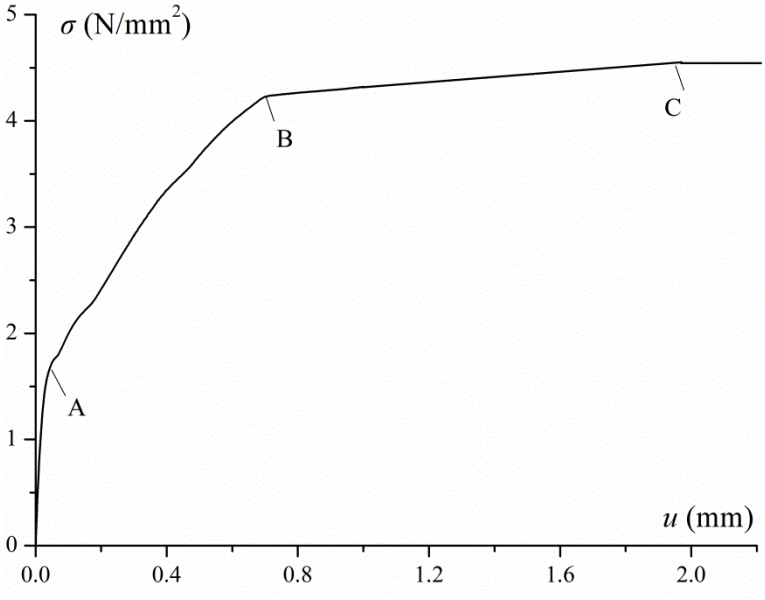

Fig. 5.5: Typical result of the confinement effect

The finite element analysis makes it also possible to visualize the formation of the discrete crack that is formed due to uplift. Figure 5.6_b presents the cracking strain for the half symmetric segment of the concrete block of the push-out specimens, once the reinforcement over the inner rib has reached yielding. Crack initiates from the corner of the rib and is directed vertically forming some secondary cracks. Cracks direction is in good accordance with the observed cracks from push-out specimens, figure 5.6_a. In addition to the cracking, figure 5.6_b shows also the uplift and the rotation of the block from the original position, by using a deformation scale factor equal to 5 for the need of visualization.

a) 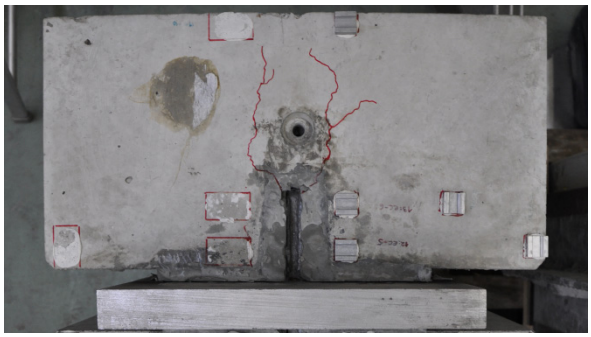 b) 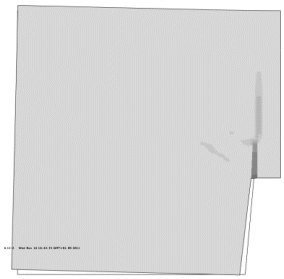

Fig. 5.6: Cracking at failure a) Specimen PR100_6 b) FEA

The same type of curve, as that presented in the figure 5.5, is produced for several different types of slab sections in which the mechanical characteristics of the concrete and the geometry, presented in figure 5.3, are varying. Table 5.1 presents the parameters studied and the domain of variation of these parameters, corresponding to slabs of composite bridges of the practice, as shown in figure 1.12.

Table 5.1: Parameters taking into account the study of the confinement effect.

Parameter	Description	Min. value	Max. value
E_{cm} (N/mm^2)	modulus of elasticity of concrete	22400	44000
f_{ck} (N/mm^2)	compression characteristic strength of concrete	30	50
h (mm)	total height of the slab locally at the connection	300	525
h_{rib} (mm)	height of the inner rib	60	200
h_{mid} (mm)	distance of the steel reinforcement, located over the inner rib, from the edge of the rib	5	45
A_S/S (mm^2/mm)	area of steel reinforcement versus spacing	0.75	3.93
c (mm)	covering of the upper reinforcement	40	65

The obtained normal stress-uplift relationship diagrams are analyzed in order to obtain the needed analytical parametric expressions for the confinement effect. The uplift parameters u_α , u_b (points A and B in figure 5.7) and the stiffness k_α and k_b are defined with a regression analysis of the finite element results. The confinement effect is presented graphically in figure 5.7 and is expressed by the following equations:

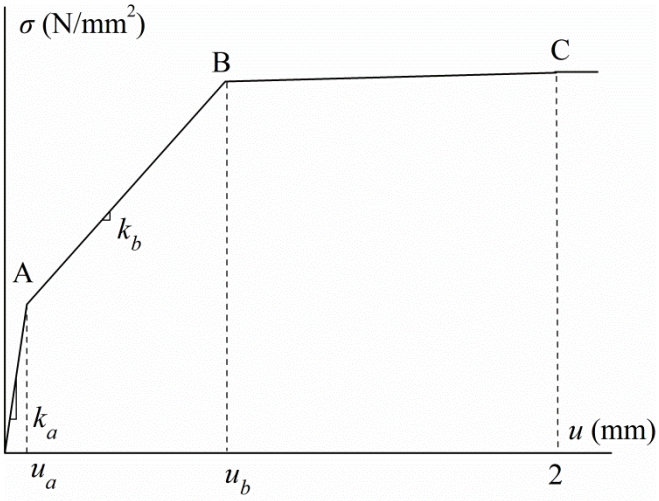

Fig. 5.7: Schematic representation of the confinement effect

$$\sigma = k_a \cdot u \qquad u \le u_a \tag{5.2}$$

$$\sigma = k_a \cdot u_a + k_b \cdot (u - u_a) \qquad u_a < u \le u_b \tag{5.3}$$

$$\sigma = k_a \cdot u_a + k_b \cdot (u_b - u_a) + k_c \cdot (u - u_b) \qquad u_b < u < 2 \text{ mm} \tag{5.4}$$

$$\sigma = k_a \cdot u_a + k_b \cdot (u_b - u_a) + k_c \cdot (2 - u_b) \qquad u > 2 \text{ mm} \tag{5.5}$$

$$u_a = 0.043 \cdot \left(\frac{33000}{E_{cm}}\right)^{0.8} \cdot \left(\frac{f_{ck}}{35}\right)^{0.2} \text{ mm} \tag{5.6}$$

$$u_b = 2.1 \cdot \left(\frac{30000}{E_{cm}}\right)^{0.1} \cdot \left(\frac{A_S}{S \cdot h_{rib}}\right)^{0.3} \cdot \left(\frac{35}{f_{ck}}\right)^{0.2} \cdot \left(\frac{h_{rib}}{h - h_{rib} - h_{mid}}\right)^{0.5} \cdot \left(\frac{h_{mid}}{10}\right)^{0.2} \text{ mm} \tag{5.7}$$

$$k_a = \left(\frac{E_{cm}}{30000}\right)^{0.7} \cdot \left(\frac{A_S}{S \cdot h_{rib}}\right)^{0.2} \cdot \left(\frac{f_{ck}}{35}\right)^{0.2} \cdot \left(\frac{h - h_{rib} - h_{mid}}{h_{rib}}\right)^{0.9} \cdot 60 \ \frac{\mathrm{N}}{\mathrm{mm}^3} \tag{5.8}$$

$$k_b = \left(\frac{E_{cm}}{30000}\right)^{0.2} \cdot \left(\frac{A_S}{S \cdot h_{rib}}\right) \cdot \left(\frac{h - h_{rib} - h_{mid}}{h}\right) \cdot \left(\frac{35}{f_{ck}}\right)^{0.1} \cdot \left(\frac{c}{6 \cdot h_{mid}}\right)^{0.2} \cdot 10^3 \ \frac{\mathrm{N}}{\mathrm{mm}^3} \tag{5.9}$$

$$k_c = 0.5 \ \frac{\mathrm{N}}{\mathrm{mm}^3} \tag{5.10}$$

The comparison between the analytical expressions and the ones calculated by performing FEA enables to define the coefficients k_a, k_b, u_a, u_b .This comparison, illustrated in figure 5.8, is satisfactory

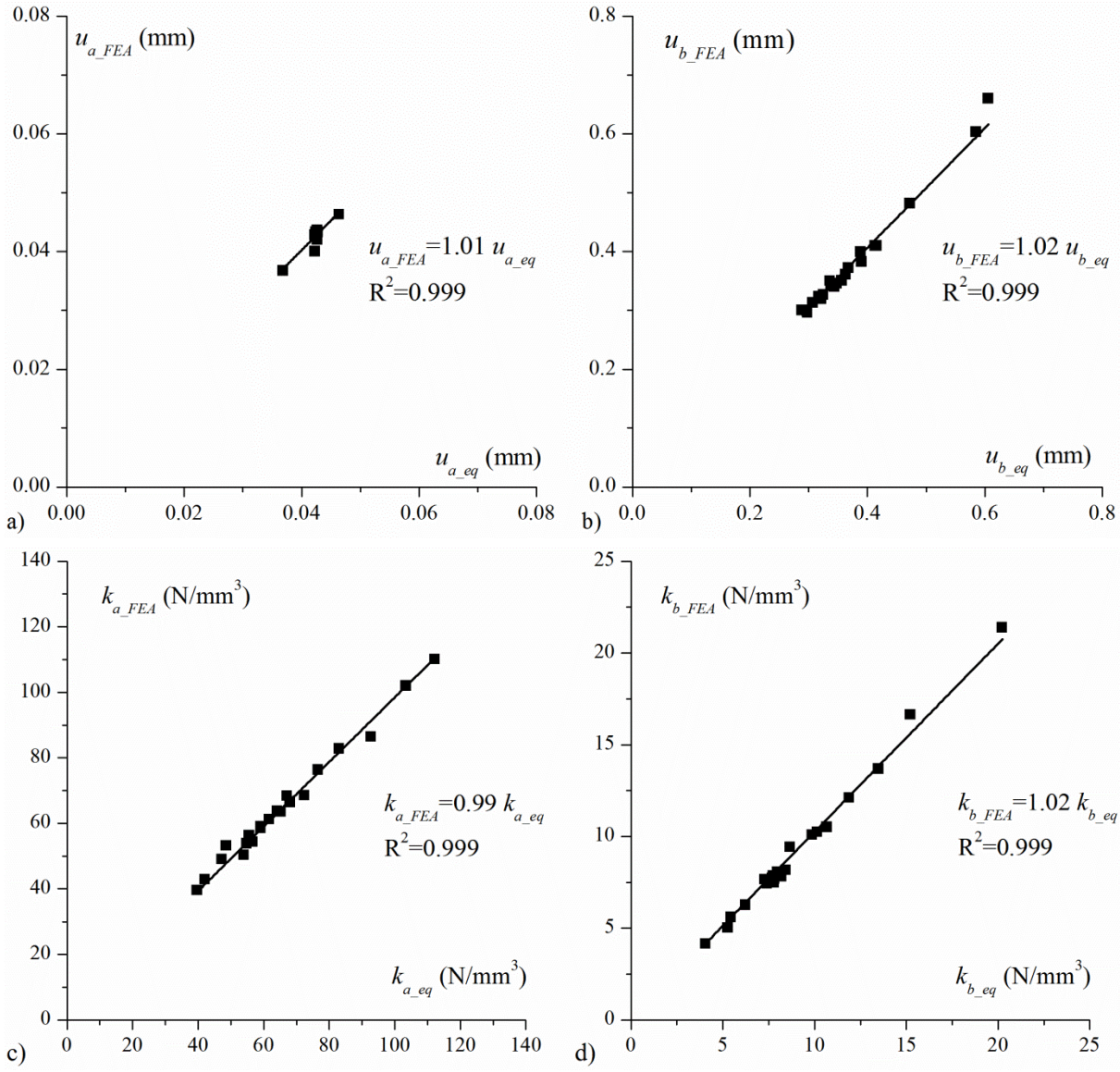

Fig. 5.8: Comparison between values calculated by FEA and analytical expressions, for coefficients describing the confinement effect a) k_a b) k_b c) u_a and d) u_b

The above equations (5.2) to (5.10) reveal, as expected, that higher values of translational stiffness and normal stress are obtained for increased values of the modulus of elasticity and the quantity of the

steel reinforcement. Concerning the positioning of the middle reinforcement (distance h_{mid}), it is favorable for confinement to minimize the distance of the steel reinforcement which is located over the rib, as possible closer to it. This particular conclusion was the reason to apply the middle reinforcement, of the slab of the composite beam, just over the rib without any covering (figures 3.76 and 3.77). As it concerns the height of the slab and the height of the inner rib (height also of the connector), it comes out that the higher the slab and the lower the height of the inner rib are, the higher is the stiffness and the normal stress. However the influence of the height of the inner rib to the overall resistance of the connection is a more complex parameter since, for instance, a lower inner rib may result to higher confinement but diminishes the area which contributes to the resistance. An optimum ratio of the height of the inner rib versus the height of the slab will be proposed by a performing parametric analysis with the model that predicts the connection's resistance and structural performance. This model is presented in the following paragraph.

5.4 Development of the numerical model of the connection

The model hypotheses presented in paragraph 5.2, the failure criteria for the shear resistance, the constitutive and the kinematic law of the interfaces and finally the confinement effect can be combined in a model to predict the connection's resistance and deformation capacity. Such a model is proposed by Thomann [Thomann 2005] in figure 4.10. Based on this model a new model is proposed (figure 5.9) with updated and complementary interface laws and a new law for the confinement effect, more detailed and general (e.g. the ratio of the steel reinforcement may vary).

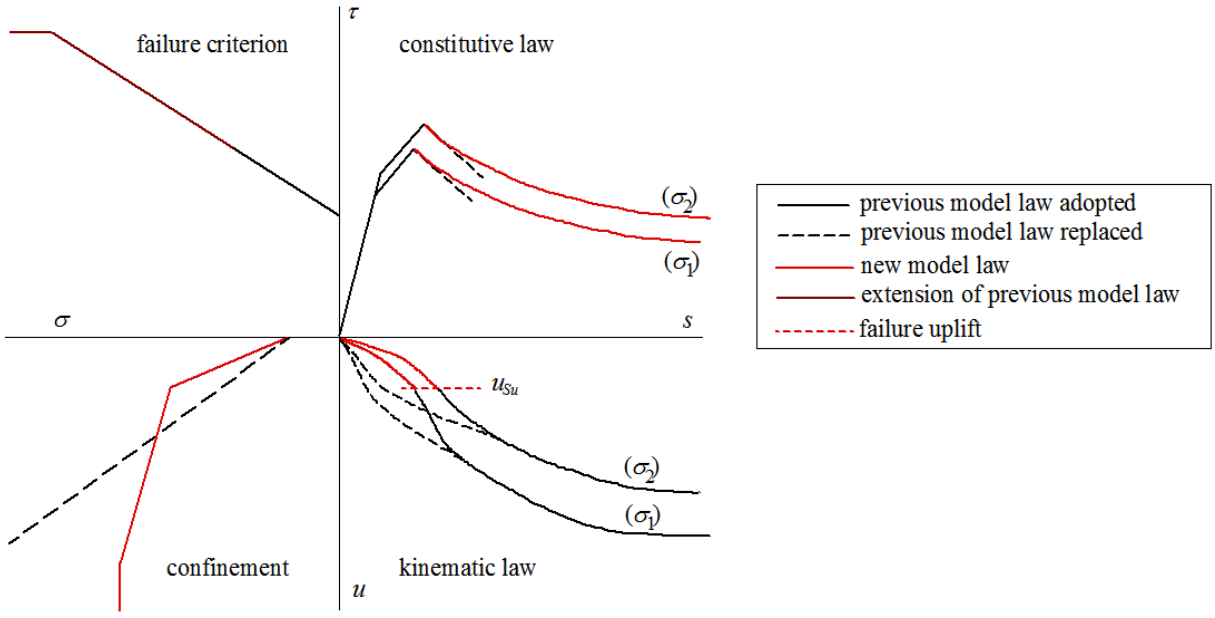

Fig. 5.9: Schematic presentation of the interaction of the failure criteria, the interface laws and the confinement effect according to the numerical model by Thomann [Thomann 2005] and as proposed by the author.

The combined action of the two interfaces according to the hypotheses is presented schematically in figure 5.10. In this mechanical model the two interfaces are connected in series. The configuration of each of the interfaces presents the constitutive law and is consisted of a linear spring parallel to another linear spring, the later in series with a skate and a softening element. The mechanical model proposed by Thomann [Thomann 2005] is adopted for the interfaces with updated values of the failure criteria and updated interface laws, obtained by the analytical study performed on the experimental results which are extended to a higher level of confinement. More precisely for the constitutive law, a

new expression is added for the softening element in the configuration which exhibits behaviour of an exponential decay both for the adhesion and for the friction (figure 5.9), as described by equation (4.8). Concerning the kinematic law a new curve is proposed by the author for the part prior to failure (figure 5.9), which occurs at a specific for each type of interface value of the uplift, u_{Su}.

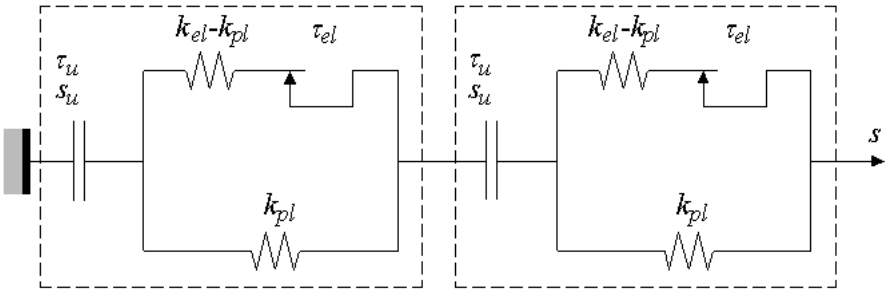

Figure 5.10: Mechanical model of the two interfaces connected in series; 1) embossed steel-cement grout interface, 2) rough concrete-cement grout interface [Thomann 2005]; model updated with new values and analytical expressions by the author.

This mechanical behaviour is in accordance with the hypothesis of paragraph 5.2 concerning the total slip, its repartition and the total force. From the mechanical model, using the index 1 for the embossed steel-cement grout interface and the index 2 for the rough-concrete cement grout interface, we obtain the following equations.

$$s = s_1 + s_2 \text{ (conformity of slip)} \tag{5.11}$$

Calling v the total longitudinal shear force per unit length of the connection, v_i (i=1,2) the longitudinal shear force for each of the interfaces and due to the fact that the interfaces are connected in series we obtain equation (5.12), where k_i (i=1,2) is the secant stiffness for an interface for a given slip s_i, figure 5.12.

$$v/2 = v_1 = v_2 \tag{5.12}$$

$$v_1 = \tau_1 \cdot h_1 = k_1 \cdot s_1 \cdot h_1 \tag{5.13}$$

$$v_2 = \tau_2 \cdot h_2 = k_2 \cdot s_2 \cdot h_2 \tag{5.14}$$

The heights of the two interfaces are equal as seen in figure 5.11

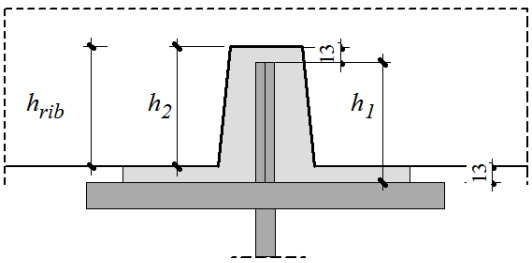

Fig. 5.11: Geometrical proof of equality of heights, h_1 and h_2

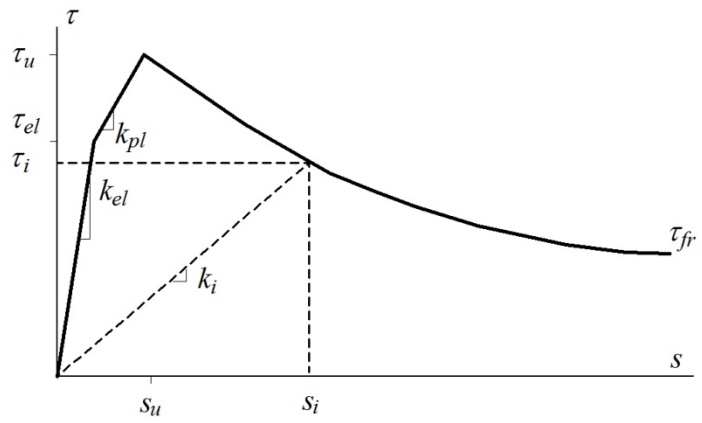

Fig. 5.12: Constitutive law and definition of secant stiffness k_i for a given slip s_i of an interface

From equations (5.11) to (5.14) and equality of heights h_1 and h_2 we obtain the repartition of the total slip in the connection to slip in each interface, equations (5.15) and (5.16).

$$s_1 = \frac{h_2 \cdot k_2}{h_1 \cdot k_1 + h_2 \cdot k_2} \Rightarrow s_1 = \frac{k_2}{k_1 + k_2} \cdot s \tag{5.15}$$

$$s_2 = \frac{h_1 \cdot k_1}{h_1 \cdot k_1 + h_2 \cdot k_2} \Rightarrow s_2 = \frac{k_1}{k_1 + k_2} \cdot s \tag{5.16}$$

The shear stress τ_i at each interface and the longitudinal force per unit length v of the connection are given from equations (5.17) and (5.18).

$$\left.\begin{matrix}\tau_1 = k_1 \cdot s_1 \\ \tau_2 = k_2 \cdot s_2\end{matrix}\right\} \Rightarrow \tau_1 = \tau_2 = \frac{k_1 \cdot k_2}{k_1 + k_2} \cdot s \tag{5.17}$$

$$v = 2 \cdot v_1 = 2 \cdot v_2 = 2 \cdot h_1 \cdot \frac{k_1 \cdot k_2}{k_1 + k_2} \cdot s = 2 \cdot h_2 \cdot \frac{k_1 \cdot k_2}{k_1 + k_2} \cdot s = 2 \cdot h_{rib} \cdot \frac{k_1 \cdot k_2}{k_1 + k_2} \cdot s \tag{5.18}$$

It is noted that in equation (5.18) the term $2 \cdot h_{rib} \cdot k_1 \cdot k_2 / (k_1 + k_2)$ expresses, for a given slip s, the secant stiffness k_{con} of the connection by adhesion, interlocking and friction.

Numerical model

The numerical model which can predict the resistance of the connection and its deformation capacity consists as following.

Part 1: Input of data and initialization of variable.

- Input of the parameters that define the constitutive law and the kinematic law of each type of the two interfaces. Those parameters are provided from table 4.3 and table 4.4. The initial stiffness of each interface is set equal to the quasi- elastic domain of the constitutive law, i.e. k_{el}.
- Calculation of initial values of s_{el} and s_u for each interface for zero initial normal stress on the interface by equation (4.7).
- Input of the compression resistance of the cement grout, needed for the calculation of the maximum uplift u_{max}.

- Input of modulus of elasticity and characteristic compressive strength of the concrete slab, geometry of the slab section (figure 5.3), reinforcement area and spacing. Calculation by equations (5.6) to (5.10) of the parameters for the confinement effect.
- Input of any, other than confinement, normal stresses, $\sigma_{ext,i}$, acting on the interfaces (figure 2.13). Those normal stresses on the interface, $\sigma_{ext,i}$, can be developed due to transversal prestressing, in case of wide cantilever bridge decks, and due to the transversal bending of the bridge deck, caused from external loads, acting after the realization of the connection. Such loads are the dead load from the asphalt covering of the bridge, from cornice and barrier and traffic loads. Due to their favorable effect for the resistance, when $\sigma_{ext,i}$ are taken into account, a load factor γ_{Ginf} equal to 0.8 should be considered for the dead loads that create them [SIA-261 2003].
- Input of increment of slip. An increment slip equal to 0.005 mm is applied so that increase of the normal stress is gradual (see comment at the end of the section 4.2.1).

Part 2: Loop with calculation of longitudinal shear force per unit length for each increment.

The second part consists of a repetitive procedure, loop, in which the following steps takes place.

- *Step 1*. Repartition of the slip s to a slip s_1 for the embossed steel cement grout interface and a slip s_2 for the rough concrete cement grout interface using equations (5.15) and (5.16). In those equations the stiffness of the interfaces are initially equal to the elastic stiffness and for next increments are calculated at step 6.
- *Step 2*. Calculation by equations (4.3) and (4.4) of the uplift at each interface and the total uplift as the addition of them.
- *Step 3*. Depending on the value of the total uplift u, the normal stress σ which is developed in the interfaces due to the confinement effect is calculated using equations (5.2) to (5.5).
- *Step 4*. Calculation according to the failure criteria and the definition of the residual friction, using equations (4.1) and (4.2), of the ultimate shear stress τ_u and the residual friction τ_{fr} which correspond to the current normal stress and slip increment.
- *Step 5*. The updated values of s_{el} and s_u are calculated for each type of interface. These values correspond to the normal stress calculated at step 3.
- *Step 6*. The updated secant stiffness for each type of interfaces is calculated from the updated constitutive law as the ratio of the shear stress versus the slip for the current increment.
- *Step 7*. The shear stress at each interface, the connection's stiffness, and the longitudinal shear force per unit length v in the connection are calculated, equations (5.17) and (5.18).

Once the step 7 is concluded another increment is added to the total slip and the loop starts again from step 1 and goes on till the remaining resistance reduces to a small amount, such as for instance 0.25 times the ultimate resistance.

The second part of the model actually applies the mentioned interaction of the constitutive law, the kinematic law, the analytical expression for the confinement effect and the failure criteria. This interaction was mentioned in 4th chapter and is presented in this chapter in the figure 5.9.

It should be noted on this point that failure criteria and constitutive and kinematic laws have been investigated for a normal stress on the interface up to 5 N/mm^2. The validity for higher values of the normal stress is unknown. However, experimental investigation of an embossed steel-mortar interface for use on inclined struts for the widening of bridge deck slabs [Brühwiler and Menétrey 2008] has shown that the upper limit for the developed shear stress was in accordance with the limit proposed by Eurocode 2 [EC2 2004], table 2.2, and in addition, the linearity of the failure criterion for the type of

mortar used was valid for a normal stress up to 10 N/mm^2. The upper value limit for the shear resistance of the interface proposed by Eurocode 2 [EC2 2004] is also adopted in this study.

A code in visual basic is developed according to the numerical model and is presented in the annex II so that can be used by engineers in practice. The program provides for a given section geometry, reinforcement ratio and quantity, and specific concrete mechanical characteristics the connection's ultimate resistance to longitudinal shear and the deformation capacity.

5.5 Validation

The numerical model developed is validated by comparing its prediction with the experimental results of the push-out tests. For the push-out specimens the concrete is of type C50/60 and a modulus of elasticity E_{cm} equal to 38600 N/mm^2 is considered according to fib Model Code 2010 [fib Model Code 2010]. The transversal steel reinforcement has an area of has a diameter of 10 mm spacing 60 mm. The section of typical block of the push-out specimens is illustrated in figure 5.13. The height of the block is 300 mm and the height of the inner rib equal to 110 mm.

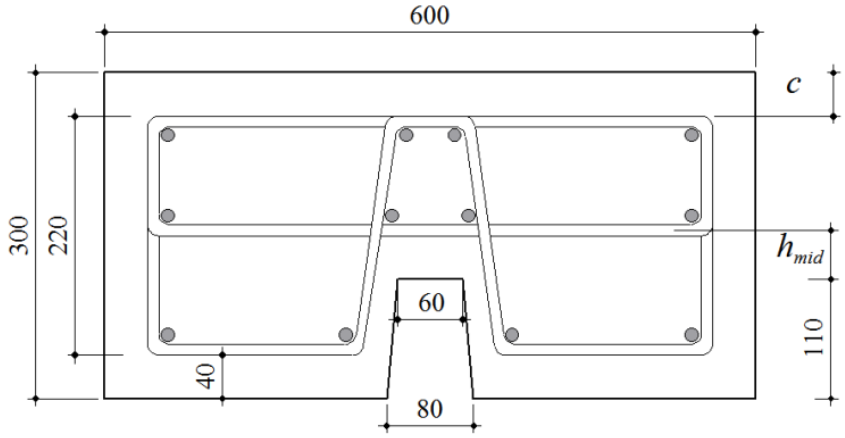

Fig. 5.13: Section of reinforced concrete block used in push-out specimens

As mentioned in the 3rd chapter, the concrete blocks of the tested specimens were submitted to diamond-cutting to check the failure interfaces. Besides, diamond-cutting has revealed that the distance h_{mid} of the center of the gravity of the middle transversal reinforcement from the edge of the inner rib was not always the same but varied between 30 mm and 50 mm, resulting consequently to a variation also of the covering of the upper reinforcement. The spacing of the reinforcement for each block of the push-out specimens was also revealed. The variation of the distance h_{mid} and of the reinforcement spacing have an influence in the ultimate resistance, as will be shown later in the parametric study, and can be used in the numerical model to explain the variance of the results of the push-out tests.

5.5.1 Static loading

The comparison for static loading is performed by using the prediction of the numerical model and the experimental values of the static tests of seven identical push-out specimens. Concerning the latter, the curves from final static tests following cyclic loading are also included since they provide information about the ultimate and the post failure resistance (figure 5.14).

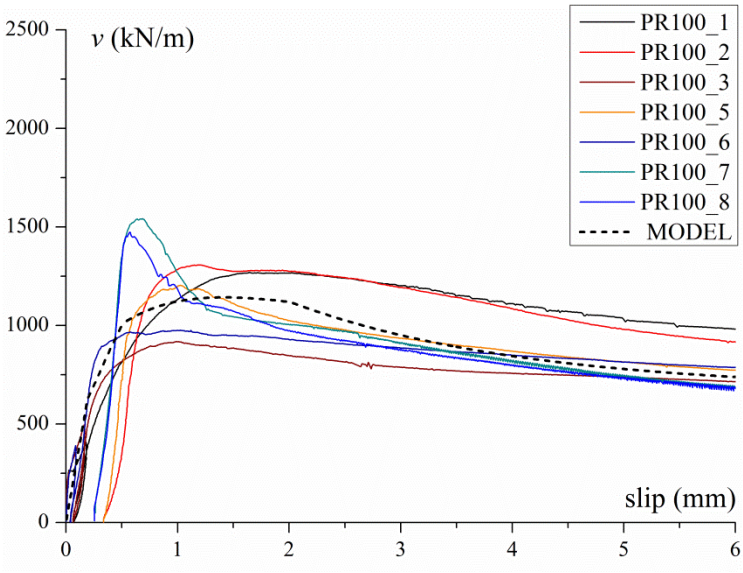

Fig. 5.14: Comparison between numerical model's prediction and push-out tests, using mean geometric parameters

Figure 5.14 presents the comparison between the structural performances of the push-out specimens and the numerical model's prediction for geometric parameters according to design of the section. The numerical model's prediction concerning the ultimate resistance is located in the middle of the variance of the performed tests which is expected since the model uses the mean values for the failure criteria and the other laws describing the behaviour of the interfaces. It is reminded that specimens PR100_7 and PR100_ 8 were tested several months after their fabrication due to the duration of the fatigue tests and their higher ultimate resistance could be attributed to the aging and increasing of the resistance of the cement grout. For the post-failure behaviour the numerical model's prediction stays about in the middle of the variation for slip up to 3 mm and for the rest it follows the convergence of the behaviour of the push-out specimens.

It was mentioned above that diamond-cutting of the push-out specimens allowed to reveale the precise values of the geometric parameters which may influence the connnection's performance such as the spacing of the rebars and especially the postioning of the middle reinforcement which is the main responsible for the confinement effect. Application of the precise geometric parameters can explain, together with the expected scatter for the resistance, the different performance of the specimens.

Figure 5.15 presents such a comparison between the specimen PR100_6 and the numerical model's prediction for a distance of the middle reinforcement form the edge of the rib, h_{mid}, equal to 50 mm as found after cutting of specimen. It is reminded that the less effective confinement of specimen PR100_6 was verified in the 3rd chapter by demonstrating the failure type of the embossed steel-cement grout interface which included areas with typical *bearing failure* corresponding to an inferior normal stress than the typical *shear failure* of the interface.

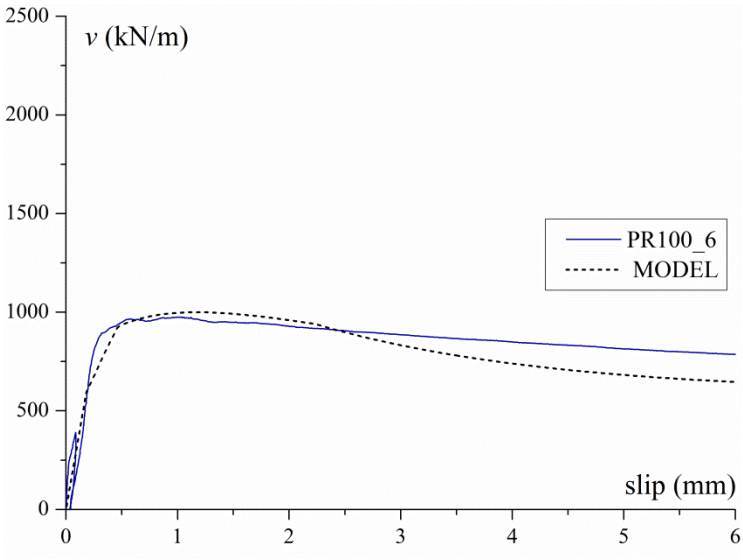

Fig. 5.15: Comparison between numerical model's prediction and push-out tests PR100_6, using precise geometric parameters

The comparison is satisfactory for slip up to 3 mm. For further slip the model underestimates slightly the connection's performance. This can be attributed to the fact that the real yielding stress of the steel reinforcement can be, as it is often the case in reality, higher than the characteristic yielding stress which was taken into account on the FEA performed for the confinement effect at section 5.3

The numerical model's prediction for the connection geometry of the push-out specimens presented in figure 5.14 provides some characteristics points A, B, C and D of the structural response (figure 5.16). These points are commentated hereafter. The numerical model provides in addition the evolution of the secant stiffness of each interface k_i as a function of the total slip s (figure 5.17) and the confinement effect (figure 5.18).

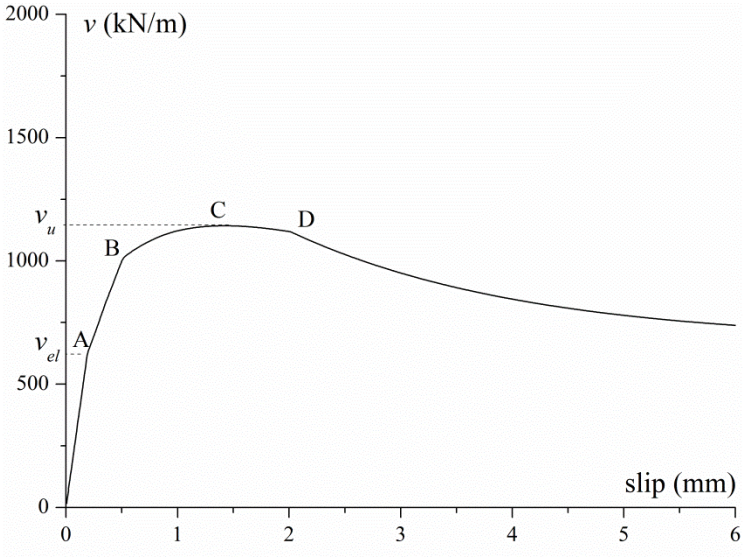

Fig. 5.16: Characteristic points on model's prediction curve

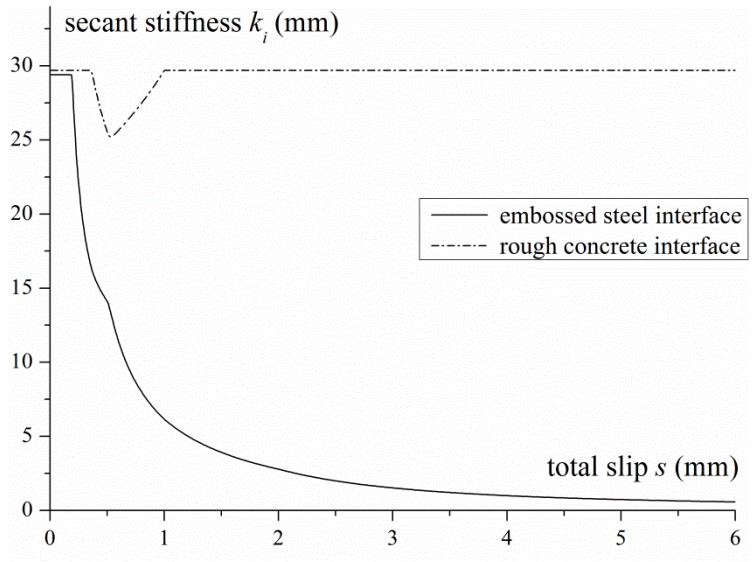

Fig. 5.17: Prediction of secant stiffness of interfaces

We notice in figure 5.16 several characteristic points:

- Point A (0.185 mm, 601 kN/m) corresponds to the end of an elastic behaviour. Till that point the stiffness of each interface is the elastic stiffness of their constitutive laws, as can be seen in figure 5.17. This point, in figure 5.18, is found to be located slightly after the end of the initial stiff branch of the curve of the confinement stress σ versus the uplift u which concerns the uncracked concrete section. The normal stress (figure 5.18), for this particular example, in point A, has increased to a value of 1.74 N/mm^2.
  From point A (end of the elastic behaviour of the interfaces) and after, the stiffness of the embossed steel-cement grout interface decreases (figure 5.17). The stiffness of the rough concrete-cement grout interface continues for a while to remain constant meaning that this interface continues to exhibit elastic behaviour (k_2=k_{el}=29.7 N/mm^3). This interface enters the plastic hardening domain of its constitutive law for a total slip between 0.35 mm and 1 mm, without however passing to the softening behaviour and finally it enters again the elastic domain for a total slip more than 1 mm, figure 5.17. Point A is of great importance for SLS and FLS as will be shown later on in section 5.5.2.
- Point B (0.50 mm, 100 kN/m) corresponds to the point at which the shear stress at the embossed steel-cement grout interface reaches the ultimate value τ_u, for that particular level of confinement stress σ = 2.33 N/mm^2. After that point the embossed-steel cement grout interface enters the softening behaviour, however the resistance of the connection continues to increase since the normal stress also increases forcing the softening behaviour of the embossed steel-cement grout interface to be developed at higher values. This is exactly the hardening effect that was noticed by Tassios [Tassios 1987] and Thomann [Thomann 2005] and was mentioned in the 4th chapter.
- Point C (1.33 mm, 1142 kN/m) is the first point where the resistance of the connection reaches the ultimate value (failure point) and for this particular example the normal stress at this point is equal to 3.55 N/mm^2. For a limited slip, after that point, the different combinations of the increasing normal stress and the developed shear stress in the embossed steel interface result to maintenance of the ultimate resistance.
- The decrease of the resistance becomes more abrupt at point D (2.01 mm, 1118 kN/m), where practically as we see in figure 5.18 point (4.11 N/mm^2, 0.58 mm), the confinement stress

stops to increase significantly. Consequently form that point and after the longitudinal shear force per unit length–slip relationship is similar to the softening part of the constitutive law of an embossed steel-cement grout interface with constant normal stress.

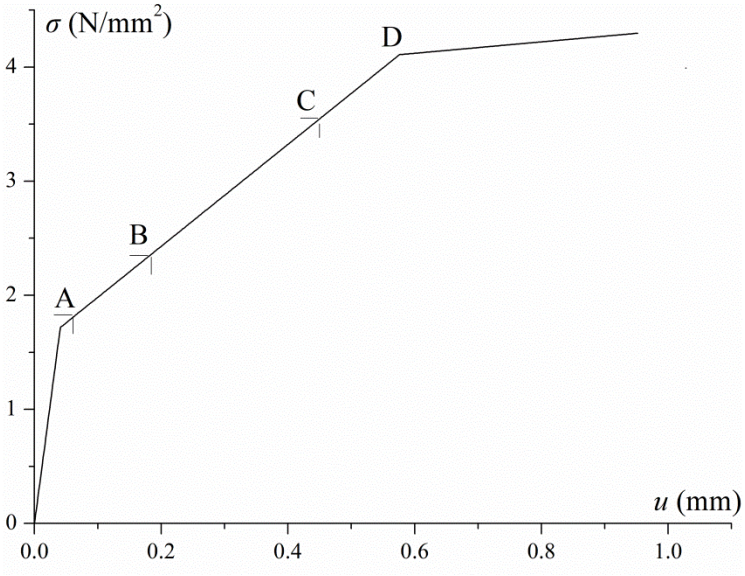

Fig. 5.18: Normal stress versus uplift form numerical model prediction
(Points A,B,C and D of figure 5.18 should not be confused with the points A,B and C of figure 5.7)

We may also recall in this point that the constant normal stress chosen for the direct shear cyclic loading tests in interfaces had a value of 1 N/mm^2 which corresponds about to the middle of the initial elastic branch of the curve from the push-out model prediction. Thus the initial hypothesis done for the level of the normal stress is justified.

Concluding as it concerns the static loading of the connection, the *numerical model* developed is validated. It provides for a given connection geometry, concrete type and reinforcement, the longitudinal shear force per unit length-slip relationship, the evolution of the stress state at each interface and the developed normal stress due to the confinement effect with very good accuracy.

The structural response of the connection as it concerns its ductility and deformation capacity depends on the availability of the system to provide increasing normal stress after failure. It is thus interesting to investigate the parameters that influence the connection's structural performance by a parametric analysis which will be presented in section 5.6.

5.5.2 Cyclic loading

In this section it is demonstrated how the behaviour of the connection at ULS following a cyclic loading can be predicted based on the curve from the numerical model for static loading and the conclusions from the analytical study in chapter 4 concerning cyclic loading of the connection. It is also presented in this section how the numerical model can provide a safe limit for cyclic loading of the connection.

The structural response of the connection at ULS after a cyclic loading with a defined maximum cyclic load for a certain number of cycles is provided by the model proposed in figure 4.20 in the 4th chapter. The model requires the curve of the longitudinal shear force per unit length versus slip for the connection for static loading, which is provided by the numerical model presented in this chapter. An application of such a prediction is presented with the following example.

Let us assume the connection detail of the push-out specimens, whose structural response is provided by the numerical model and presented in figure 5.16. Let us also assume that the connection is submitted to the same cyclic loading to that of specimen PR100_5, a total of 5 million cycles with amplitude v_{max}-v_u equal to 400 kN/m (v_{max} = 530 kN/m). From the prediction of the numerical model, figure 5.15, we obtain that the slip under a maximum cyclic load v_{max} = 530 kN/m for the first cycle becomes:

$$s_{V\,max,1} = 0.16 \text{ mm} \tag{5.19}$$

From equation (4.28) and for a mean value for the coefficient b_{con} equal to 0.072, table 4.9, we can then calculate the value for the slip under maximum load, $s_{Vmax,N}$, for 5 million cycles, equation (5.20).

$$s_{V\,max,N} = s_{V\,max,1} \cdot N^{b_{con}} = 0.16 \cdot \left(5 \cdot 10^6\right)^{0.072} \text{ mm} = 0.49 \text{ mm} \tag{5.20}$$

According to figure 4.20 the slip under maximum load, $s_{Vmax,N}$, can be used, instead of the residual slip of the previous cycle, as a threshold point (0, $s_{Vmax,N}$) for the longitudinal shear force per unit length-slip curve, figure 5.19.

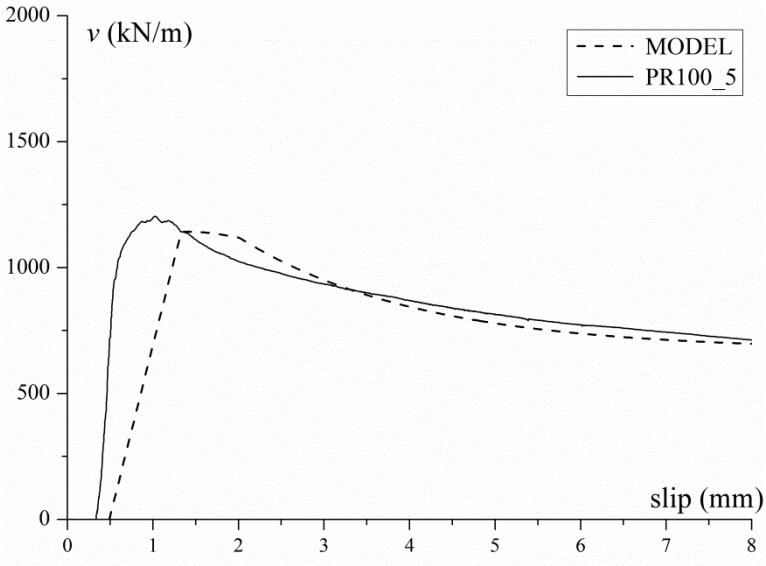

Fig. 5.19: Comparison between test and model for ULS following cyclic loading

Figure 5.19 presents the predicted behaviour for the connection of the push-out specimens at an ULS following a cyclic loading of a total of 5 million cycles with amplitude v_{max}-v_u equal to 400 kN/m (v_{max} = 530 kN/m). For comparison reasons the curve of the final static test, of the specimen PR100_5, is also presented in the same figure. As expected since the slip under maximum load, $s_{Vmax,N}$, is used instead of the residual slip of the last cycle, the model provides a more conservative behaviour than the real specimen for the ascending part.

Summarizing, as seen in chapter 4, the longitudinal shear force per unit length-slip relationship of the connection, at an ULS that follows a cyclic loading with maximum cyclic load lower than the elastic limit for monotonic loading, can be simulated for the behaviour prior to failure with a line connecting the point (0, $s_{Vmax,\,N}$) and the point (v_u, s_u). The term $s_{Vmax,\,N}$ is provided by equation (4.28), in which the term b_{conn} is given from the table 4.9. The value $s_{Vmax,\,1}$ and the point (v_u, s_u) are provided from the curve for static loading from the numerical model. For the post failure behaviour the post-failure part of the curve for static loading applies.

Safe limit for FLS

It was shown in section 5.5.1 that the initial elastic part of the curve in figure 5.16, up to the point A, corresponds to the domain in which the stiffness of each of the interfaces is equal to the elastic stiffness k_{el} of their corresponding constitutive law. In other words the developed stresses in the interfaces up to point A remain elastic. The increase of the normal stress in that part does not have an influence in the stiffness, since according to the proposed behaviour for the interfaces in the 4th chapter, the elastic stiffness k_{el} of the interfaces is independent from the normal stress. It was also found in section 5.5.1 that the concrete of the slab remains uncracked for the largest part of the curve up to the point A (figure 5.18). The longitudinal shear force per unit length at point A is equal to 601 kN/m, for the specific connection geometry of the push-out specimens, and represents a value equal to 0.53 times the ultimate resistance predicted by the numerical model.

$$v_A = 0.53 \cdot v_u \tag{5.21}$$

As we see in tables 3.5 and 4.8 for the push-out specimens submitted to cyclic loading for up to 2 or 5 million cycles without failure and with stabilization of the damage due to repeated loading, the ratio V_{max}/V_u varies from 0.41 to 0.55, including the limit proposed from equation (5.21). Thus based on this experimental verification for no failure for cyclic loading, and on the fact that the numerical model predicts elastic shear stresses in the interfaces up to point A, it can be assumed that the limit defined by point A, can be considered as a safe limit for cyclic loading of the connection. However parametric analysis is needed to define if this limit has always this certain value or varies in a specific range depending on the geometry of the connection, the concrete type, the reinforcement positioning and quantity. This parametric analysis is performed in section 5.6.

Application of equation (4.30) for the connection detail of the push-out specimens, considering as maximum cyclic load the value of the end of the elastic domain, 601 kN/m (the latter predicted from the numerical model, point A of figure 5.16) results in the following estimation of the number of cycles to failure.

$$N_f = \left(\frac{s_u}{s_{Vmax,1}} \right)^{1/b_{con}} = \left(\frac{1.33}{0.185} \right)^{1/0.072} \approx 792 \text{ billion cycles} \tag{5.22}$$

With such high number of cycles to failure, this means practically that the selected ratio $v_{max}/v_u = 0.53$ (v_{max} = 601 kN/m), for the specific connection geometry and steel reinforcement arrangement, is a safe limit to avoid fatigue failure at service life. It should also be noted that if instead of the mean value of the power index, b_{con}, we use the maximum experimental value of table 4.8, the number of cycles decreases to 28 billion cycles, yet this is of no importance for the expected service life of such a connection.

Concluding concerning the cyclic loading of the connection, the following statement is proposed:

The end of the elastic behaviour for static loading, as predicted for the connection by the numerical model, can be used as a safe limit for FLS (fatigue limit).

5.6 Parametric analysis

The parametric analysis is performed basically for the parameters presented in table 5.1. The geometric parameters of the table 5.1 are presented graphically in figure 5.3. Additionally to this parametric analysis, the 5% fractile values of the expressions of the failure criteria, for both interfaces simultaneously, are also used in order to investigate their influence and provide a conversion factor, n_v, needed to define the characteristic value of the connection resistance and a conversion factor, $n_{v,el}$, to be used for the characteristic value of the fatigue limit.

As a reference curve for comparison, the prediction for the connection geometry, the steel reinforcement arrangement and mechanical characteristics of the concrete block used for the push-out specimens will be applied for all cases.

Influence of the mechanical characteristics E_{cm} and f_{ck} of the concrete slab

The modulus of elasticity of the concrete E_{cm} presents different values for different concrete types. Moreover it varies within the same concrete type depending on the type of aggregates that are used for the mixture. The influence of different E_{cm} is studied within the same concrete type, for the actual case the type C50/60 that was used for the push-out specimens. The influence of the characteristic compressive strength of the concrete f_{ck} is studied simultaneously with a corresponding E_{cm}.

Figure 5.20 presents the influence of the mechanical characteristic of the concrete blocks. Figure 5.20_a shows three curves for concrete blocks with different values of the modulus of elasticity and figure 5.20_b shows three curves for concrete blocks with different characteristic compressive strength.

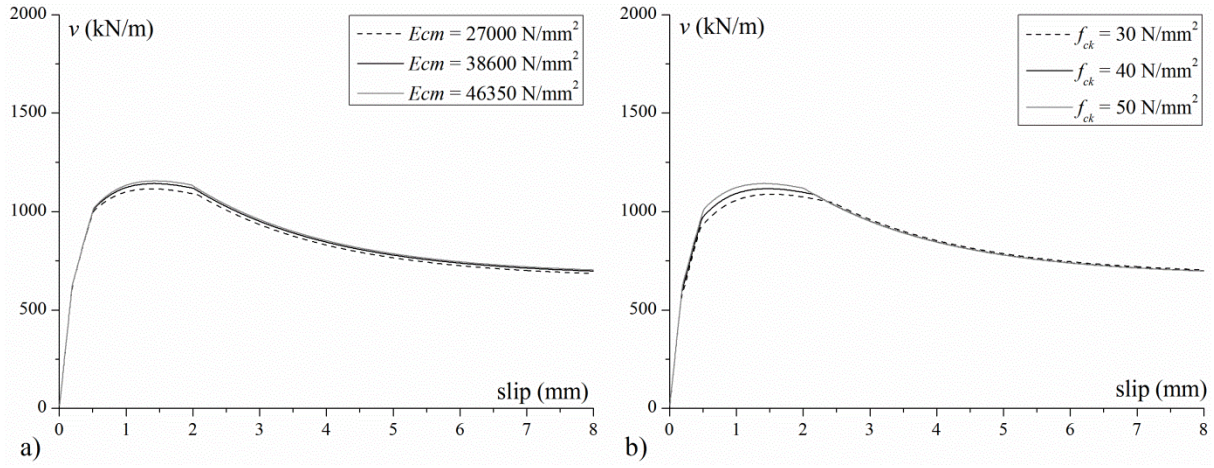

Fig. 5.20: Parametric analysis; a) modulus of elasticity of concrete E_{cm}, b) characteristic compressive strength of the concrete f_{ck}

The results of the analysis show that:

- The variation of the modulus of elasticity and of the characteristic compressive strength of the concrete result to minor changes on the normal stress-uplift relationship.
- Consequently there is not significant influence to the connection's behaviour. The benefit of the increased concrete mechanical characteristics is very limited.

Influence of the steel reinforcement and its positioning

Three different ratio of the area of the reinforcement versus the spacing of the rebars are checked. The positioning of the reinforcement is described, as in figure 5.3, by the distance h_{mid} of the middle reinforcement from the edge of the inner rib of the slab, and the covering c of the upper reinforcement which may vary due to different environments. Figure 5.21 presents the influence of the positioning and the influence of the ratio of the steel reinforcement versus spacing.

Analysis shows that:

- Increased covering leads to an increase of the contribution of the upper reinforcement to the confinement effect. However, the covering of the upper reinforcement has a minor influence on the ultimate resistance.
- The positioning of the middle reinforcement has an important influence from the moment that the shear stress in the embossed steel-cement grout interface enters the softening behaviour and thus depending on the normal stress. The closer is the middle reinforcement to the inner rib the higher is the achieved normal stress. This increase is though accompanied by a loss of ductility of the connection's performance.
- The ratio of the area of the reinforcement versus the spacing has a very significant influence once the shear stress in the embossed steel-cement grout interface enters the softening behaviour. Increased ratio causes a more effective confinement effect resulting to both increase of the ultimate resistance and the ductility of the connection. However it is not influencing the extent of the initial linear elastic domain prior to failure, used for FLS.

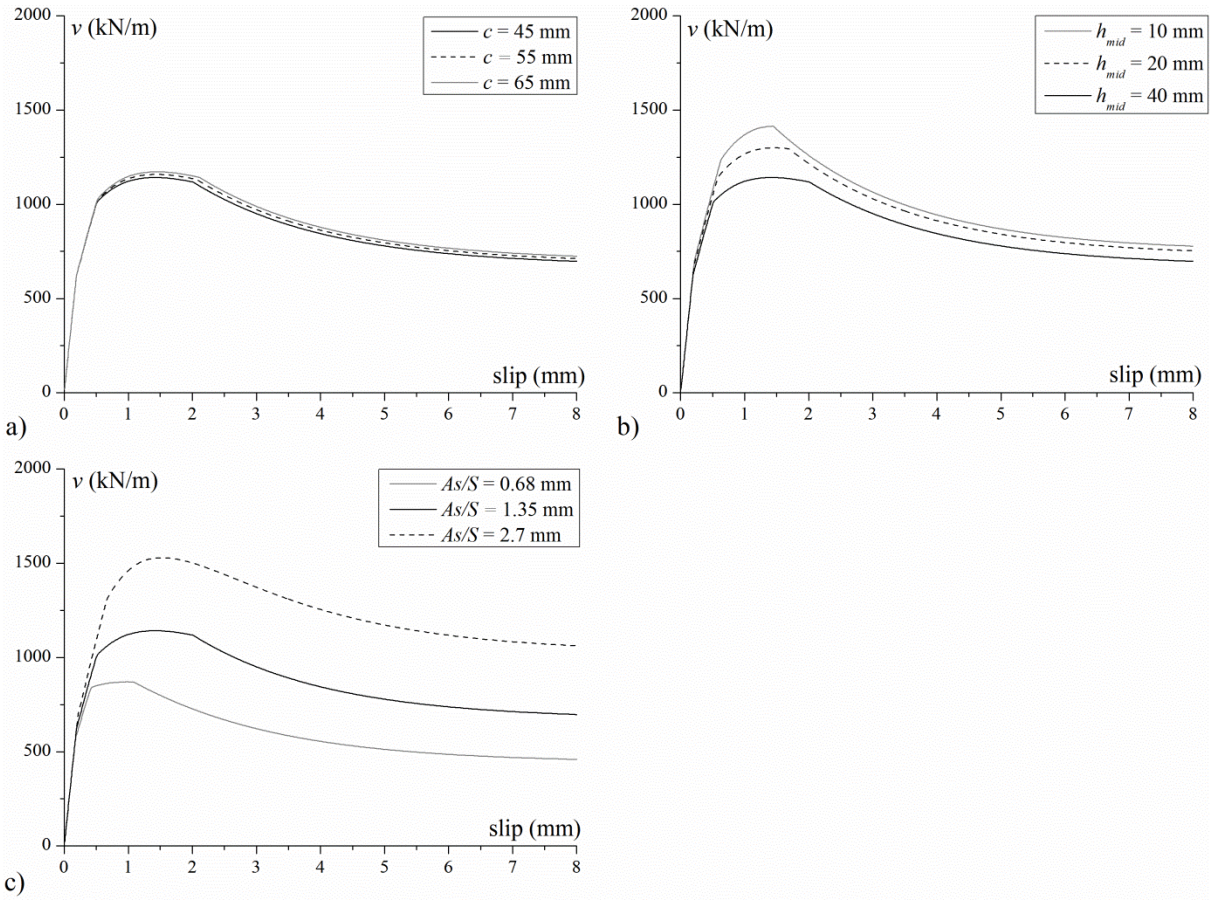

Fig. 5.21: Parametric analysis; a) Covering c of the upper reinforcement, b) positioning of the middle reinforcement and c) ratio of area of reinforcement versus spacing

Influence of the section geometry

The section geometry is described, as seen in figure 5.3, by the overall height of the slab *h* and the height of the inner rib h_{rib} the latter being equal to the height of the embossed steel plates used in the connection. The influence of these parameters is presented in figure 5.22.

Analysis shows that:

- The influence of the height *h* of the slab, figure 5.22_a, is active both in the elastic domain of the performance of the connection on the ultimate resistance and in the post-failure behaviour as well. In fact from the all the parameters investigated, the height of the slab is the only parameter which if increased moves also upward the end of the domain in which the shear stresses in the interfaces remain in the elastic part of their constitutive law. In other words an increase of the height of the slab results in a higher proposed fatigue limit (point A of figure 5.16).
- Concerning the height of the inner rib, h_{rib}, it was mentioned in the section 5.3 that it has a combined contradictory effect to the resistance, since from one part a diminishing in the height of the rib increases the normal stress, on the other side it diminishes the resistant area. For the parametric analysis for the height of the inner rib (and also height of the embossed steel plate) figure 5.22_b, it is shown that for a value of h_{rib} equal to 60 mm we obtain more or less the same ultimate resistance than with a rib with height 90 mm and slightly higher than a rib with h_{rib} equal to 110 mm for the same total height of the slab. This not apparent result is due to the very high values of the normal stress, more than 6.3 N/mm^2 at failure point, which is developed for this particular height h_{rib} equal to 60 mm. However, if the validity of the failure criteria is limited to the normal stress of the direct shear stress tests, this increased performance of h_{rib} equal to 60 mm would not be possible.

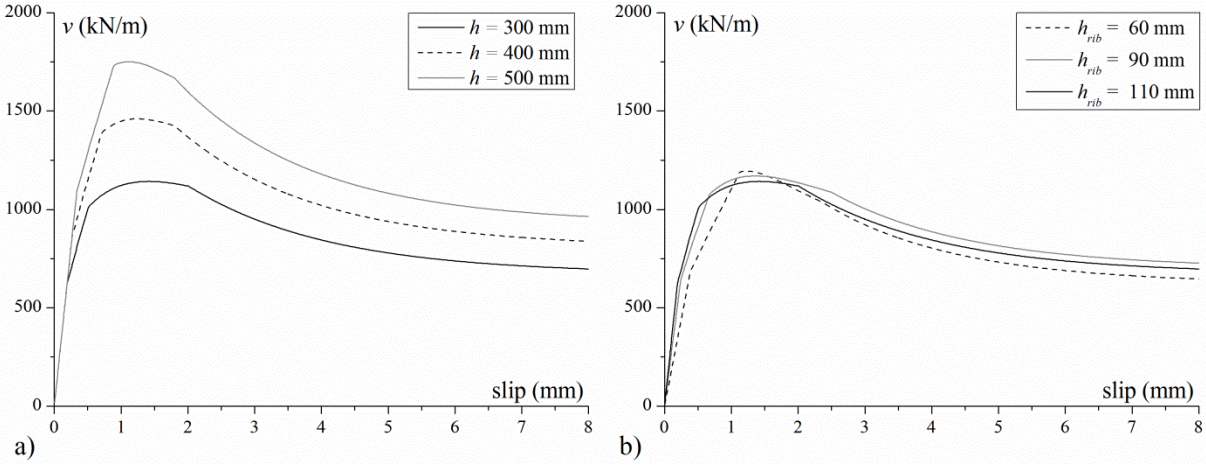

Fig. 5.22: Parametric analysis; a) height *h* of the slab, b) height h_{rib} of the inner rib

Parametric analysis is performed to investigate an optimum ratio of the height of the inner rib versus the total height of the slab, h_{rib}/h. These results are shown in figure 5.23. This figure shows that an optimum tends to be obtained for the value 0.2. Yet, the normal stress at failure point for those cases exceeds the normal stress of the direct shear stress performed. Consequently, if the linear increase of the ultimate shear resistance with the normal stress is limited to 5 N/mm^2 (the maximum normal stress applied at the direct shear tests) we obtain then that the optimum ratio of the height of the rib versus the total height of the slab, h_{rib}/h, translates form the value 0.2 to the value 0.25.

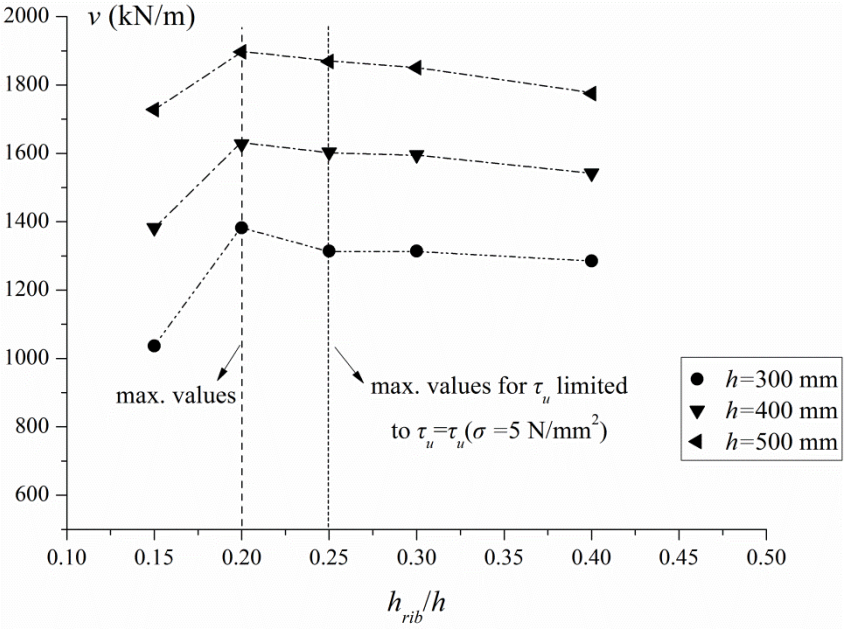

Fig. 5.23: Parametric analysis for the ratio h_{rib}/h. Concrete slab of type C50/60, with As/S = 1.35 mm^2/mm, c = 45 mm, h_{mid} = 40 mm

Similar optimum ratios to that of figure 5.23 are obtained for other possible combinations. In any case it should be controlled that the whole height of the connector remains in compression due to the transversal bending of the reinforced concrete deck, because in the opposite case the interfaces it is considered that they do not resist shear. In other words the height of the connector should remain in the compression zone for transversal bending.

Influence of the coefficients of the failure criteria

The numerical model proposed uses the mean values of the coefficients of the failure criteria of the interfaces. A comparison is made to investigate the use of the 5% fractile values of the failure criteria to the numerical model. This is performed simultaneously for both interfaces. The 5% fractile values of the failure criteria are calculated according to equation (5.23). With this comparison a conversion factor, n_v, can be defined to evaluate the characteristic value of the resistance, v_{Rk}, as well as a conversion factor, $n_{v,el}$, to evaluate the characteristic value of the fatigue limit, $v_{Rk,fat}$, (end of the elastic behaviour of the connection).

$$\tau_{u,k} = \tau_u - k_n \cdot s_X \Rightarrow \tau_{u,k} = (c + \mu \cdot \sigma) - k_n \cdot s_X \tag{5.23}$$

$\tau_{u,k}$: characteristic value of the ultimate shear stress in the interface

τ_u : mean value of the ultimate shear stress in the interface, calculated from the failure criterion for each interface, (c the adhesion-interlocking coefficient and μ the friction coefficient, provided from the table 4.4)

s_X : estimated sample standard deviation, provided from table 4.1 for each type of interface

k_n : characteristic, i.e. 5%, fractile factor, equal to 1.76 for the embossed steel-cement grout interface (20 sample values), and equal to 1.75 for the rough concrete-cement grout interface (24 sample values) [EN 1990:2002]

Using the characteristic values of the ultimate shear stress, for both interfaces simultaneously, which is the most conservative case, we obtain for the above studied cases of the parametric analysis the results presented in the table 5.2.

Table 5.2: Mean and characteristic values of the longitudinal shear force per unit length at failure (ultimate resistance) and of the fatigue limit (at the end of the elastic response of the connection)

Parametric analysis	v_u (KN/m)	v_{Rk} (KN/m)	$v_{Rk}/\ v_u$	v_{el} (KN/m)	$v_{Rk,fat}$ (KN/m)	$v_{Rk,fat}/\ v_{el}$	$v_{el}/\ v_u$
Push-out specimen	1142	1087	0.95	601	488	0.81	0.53
E_{cm}=27000 N/mm^3	1116	1058	0.95	601	488	0.81	0.54
E_{cm}=46350 N/mm^3	1156	1102	0.95	601	488	0.81	0.52
f_{ck}=30 N/mm^2	1088	1035	0.95	569	419	0.74	0.52
f_{ck}=40 N/mm^2	1117	1061	0.95	536	458	0.85	0.48
c=55 mm	1159	1105	0.95	601	488	0.81	0.52
c=65 mm	1173	1122	0.96	601	488	0.81	0.51
h_{mid}=10 mm	1415	1344	0.95	683	569	0.83	0.48
h_{mid}=20 mm	1300	1241	0.95	650	536	0.82	0.50
As/S=0.68 mm^2/mm	871	775	0.89	553	429	0.78	0.63
As/S=2.70 mm^2/mm	1529	1480	0.97	683	566	0.83	0.45
h=400 mm	1461	1380	0.94	845	722	0.85	0.58
h=500 mm	1750	1660	0.95	1073	946	0.88	0.61
h_{rib}=60 mm	1195	1163	0.97	674	612	0.91	0.56
h_{rib}=90 mm	1170	1113	0.95	625	535	0.86	0.53

A conversion factor for the connection resistance at ULS is defined from equation (5.24).

$$n_v = \min n_{v,i} = \min\left(\frac{v_{Rk}}{v_u}\right)_i = 0.89 \tag{5.24}$$

The conversion factor, n_v, is used to obtain the characteristic value of the connection resistance from the mean value of the resistance that provides the numerical model, equation (5.25).

$$v_{Rk} = n_v \cdot v_u \tag{5.25}$$

A conversion factor for the connection resistance at FLS and SLS, $n_{v,el}$, is defined from equation (5.26).

$$n_{v,el} = \min n_{v,el,i} = \min\left(\frac{v_{Rk,\,fat}}{v_{el}}\right)_i = 0.74 \tag{5.26}$$

The conversion factor, $n_{v,el}$, is used to obtain the characteristic value of the limit of fatigue, according to the equation (5.27).

$$v_{Rk,\,fat} = n_{v,el} \cdot v_{el} \tag{5.27}$$

The last column of the table 5.2 shows that the numerical model predicts that the limit for the elastic behaviour is lying in a range between 0.45 and 0.63 of the ultimate resistance.

Influence of the coefficient a ($a=\tau_{el}/\tau_u$)

The ratio $a=\tau_{el}/\tau_u$, ratio of the elastic shear stress versus the ultimate shear stress in an interface, limits the elastic domain in an interface. Hence it is expected that a variation of this ratio would influence the extent of the elastic behaviour of the connection as well and consequently the value of the conversion factor $n_{v,el}$. This influence can be investigated by a parametric analysis using the 5% fractile values of the ratio a.

The 5% fractile values of the ratio a for both interfaces, $a_{0.05}$, are obtained from their mean values and their estimated standard deviation according to code [EN 1990:2002] and are presented in the table 5.3.

Table 5.3: The 5% fractile values of the ratio a for the two interfaces; a) embossed steel-cement grout interface and b) rough concrete-cement grout interface

Interface: Cement grout-	$a_{0.05}$
Embossed steel	0.55
Rough concrete	0.54

However, it is has to be noted that in the experimental results the minimum values of this ratio are generally related to values of the elastic stiffness that are higher than the mean values. Thus using the $a_{0.05}$ values in a parametric analysis in combination with the mean values of the elastic stiffness of the interfaces would lead to too conservative design for the extent of the elastic response (the ultimate resistance is not affected). In fact, without presenting the corresponding table, such a parametric analysis results in a conversion factor for fatigue limit, $n_{v,el}$, half of that proposed by equation (5.26). Absence of a direct relation between the ratio a and the elastic stiffness, $k_{el,i}$, of the interfaces, due to limited experimental values, does not allow further analysis. Consequently the conversion factor proposed by the equation (5.26) will be considered in the design method presented in the next chapter.

5.7 Conclusions

The numerical model developed by Thomann [Thomann 2005] is used as a basis to propose a new model with updated and complementary interface laws and a new law for the confinement effect. The new model enables to calculate the longitudinal shear force per unit length-slip relationship at ULS for given connection geometry, mechanical characteristics of the concrete slab and steel reinforcement arrangement. This model provides the connection's ultimate resistance and deformation capacity. It can be used as a constitutive relationship for non-linear connector elements in order to simulate the structural behaviour of the composite beams when the slip should be taken into account.

The prediction of the ultimate resistance by the numerical model is based on the mean values of the constitutive and kinematic law and the failure criteria of the interfaces. Thus, in order to obtain the characteristic value for the ultimate resistance, v_{Rk}, a conversion factor n_v equal to 0.89 should be considered.

The numerical model enables to indicate a limit which can be used as a safe limit for FLS (fatigue limit). This limit (point A in figure 5.16) is the end of the initial linear part of the longitudinal shear force per unit length-slip relationship. It was found that in this part the shear stresses in both interfaces remain in the elastic domain of their constitutive laws. It was also found that the limit defined by the

point A, is located, as it concerns the normal stress-uplift relationship (figure 5.18) around the point of the change of the stiffness. Hence generally the concrete is uncracked for the domain defined by the fatigue limit. Defining of point A for each of the curves of the parametric analysis reveals that the limit for elastic behaviour is lying in a range between 0.45 and 0.63 of the ultimate resistance (last column of table 5.2), for mean values of resistance. Parametric analysis enabled to define also a conversion factor $n_{v,el}$ equal to 0.74 which is used to obtain the characteristic value of the fatigue limit, $v_{Rk,fat}$.

The parametric analysis has revealed the following results:

- The mechanical characteristics of the concrete slab have a minor influence on the connection's structural performance.
- The ratio of the reinforcement versus the spacing has a significant influence. An increase in this ratio provides a more effective confinement resulting to higher ultimate resistance and improved ductility of the connection by pushing the softening law to higher values which correspond to the increasing normal stresses.
- Positioning of the middle reinforcement closer to the inner rib of the slab causes a mobilization of the steel reinforcement for lower values of uplift and consequently resulting to a higher ultimate resistance. The ductility though deteriorates since the reinforcement yields sooner and the margin for the increase of the normal stress in the post-failure part is limited. Thus such a configuration should be used at regions where increased resistance is wanted without need for increased ductility, as it is the case for regions close to end supports.
- The height of the inner rib of the slab tends to present an optimum for the connection's performance when it is equal to 0.2 times the total height of the slab. This value translates to 0.25 if we limit the increase of the shear stress to the confinement level of the direct shear stress test on interfaces. Supplementary check should be performed to exclude part of the height of the inner rib being in tension due to transversal bending.
- The total height of the concrete slab at the vicinity of the connection has a favorable effect on the connection's ultimate resistance. In addition, the increase of the total height of the slab results in an increase in absolute values of the elastic limit which the numerical model suggests as a safe limit for FLS.

Based on the numerical model, the conclusions of the parametric analysis and on the state of the art in composite bridges, a design method for static and fatigue loading of composite bridges fabricated with the new connection will be presented in the next chapter. A design table of several characteristic sections for use in steel concrete-composite bridges will be provided, with a bearing capacity that satisfies the requirements presented in table 2.7 in the state of the art.

6. Design Method

6.1 Introduction

In this chapter a design method is presented for different limit states concerning steel-concrete composite beams in which the composite action is provided using connections by adhesion, interlocking and friction. The resistance of the connection to longitudinal shear is compared with the longitudinal shear acting in the connection. The connection's resistance to longitudinal shear force at FLS, SLS and ULS can be obtained by the numerical model presented in the 5th chapter. An elastic calculation of the longitudinal shear force distribution is suggested for FLS and SLS. Concerning ULS when the elastic method is used to calculate the cross-sectional bending resistance, an elastic calculation of the longitudinal shear force should be performed. For the cases that the plastic method is used to calculate the cross-sectional bending resistance the relationship between the applied moment and normal force has to be established in order to assess the maximum developed longitudinal shear for the sections that enter the elasto-plastic domain.

Finally a design table of several characteristic sections for use in steel concrete-composite bridges is provided with a resistance that satisfies the requirements presented in table 2.7 of the state of the art.

6.2 Design for FLS and SLS

6.2.1 Required resistance

The verification for the FLS can be performed with respect to fatigue limit. If for all cycles during the service life of the bridge, the longitudinal shear force per unit length in the connection remains lower than the fatigue limit, failure will not occur. As shown in the 2nd chapter in the state of the art, based on recordings from real traffic on eight bridges all over Switzerland, for the period 2003 to 2009, Meystre and Lebet [Meystre and Lebet 2011] calculated the 99% fractile values of trucks over 40 tones and propose a deterministic load model of two heavy trucks. According to that model, the two trucks are located the one next to the other in two fictitious lanes with a total load 780 kN and 540 kN correspondingly, including a dynamic amplification factor.

Application of that model to sections of twin-I girder composite bridges, from a database of Swiss highway bridges with spans from 30 to 120 meters, results to the maximum longitudinal shear per unit length expected for this type of bridges, $\Delta v(Q_{fat})$. Multiplying this value with a partial factor for fatigue strength γ_{fat} equal to 1.15, and adding the design longitudinal shear due to permanent loads, v_{long}, acting after the realization of the connection (v_{long} includes a corresponding partial factor γ_v) we obtain the required resistance to longitudinal shear per unit length for verification with respect to the limit of fatigue, presented also in table 2.7, equation (6.1)

$$v_{long} + \gamma_{fat} \cdot \Delta v(Q_{fat}) \leq 800 \text{ kN/m} \tag{6.1}$$

This value is higher than the value 530 kN/m obtained if we use the fatigue load model 1 of the code SIA 261. Consequently, for the design, the required resistance for fatigue limit should be considered according to the new model.

It is noted in table 2.7 that the required resistance to longitudinal shear per unit length for the occasional load case at SLS is 750 kN/m, inferior to the value needed for verification at FLS. Thus verification at SLS is covered by the verification for FLS.

6.2.2 Available resistance

It was found experimentally from push-out cyclic loading tests that connections submitted to cyclic loading with a ratio V_{max}/V_u between 0.41 and 0.55, for a total of 2 to 5 million cycles, developed an accumulated slip in the interface which stabilizes with the number of cycles, with an expectation of no further damage.

In the 4th chapter the analytical expressions of the evolution of the residual slip were developed which permit to precise the number of cycles to failure for such values of loading range. It was easily proven from a numerical application in the 5th chapter that the estimated number of cycles to failure goes beyond the service life of any bridge so that the above loading ratios can be considered as a fatigue limit for the corresponding connection geometry.

Defining a fatigue limit for connection geometry and steel reinforcement for confinement other than that of the push-out specimens was able with the help of the numerical model presented in the 5th chapter. It was found with the help of the numerical model that the shear stresses remain in the elastic domain and the concrete generally uncracked in the vicinity of the connection for loads between 0.45 and 0.63 of the ultimate predicted resistance. No fatigue failure is expected for shear stresses in the interfaces remaining elastic, as proven experimentally from cyclic loading direct shear tests on the interfaces.

Consequently, for the design of the new connection for FLS (which covers also the verification for SLS) the connection should present an elastic domain limited by the value v_{el}, which should be greater than the required shear resistance for fatigue, according to equation (6.2). The longitudinal shear force per unit length, v_{el}, is obtained by the numerical model (figure 6.1), and corresponds to the specific geometry, concrete type, steel reinforcement and positioning of the section.

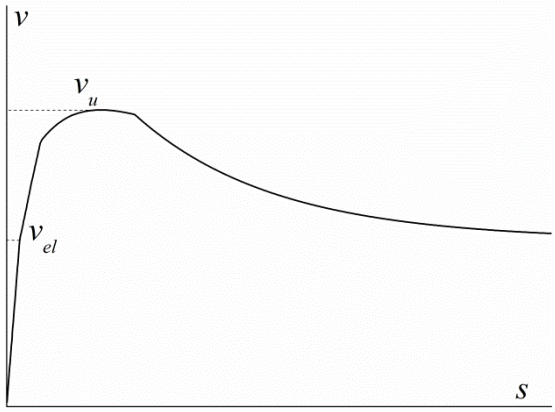

Fig. 6.1: Definition of end of the elastic behaviour for the longitudinal shear force per unit length-slip relationship for the connection, obtained by the numerical model

To obtain the characteristic value of the resistance we should take into account the conversion factor $n_{v,el}$. The latter is found from the parametric analysis performed in the section 5.6, by using the 5% fractile values of the failure criteria for both interfaces simultaneously. (The conversion factor does not consider any geometrical divergence of the connection detail). The characteristic resistance for FLS, $v_{Rk,fat}$, is defined by equation (6.2):

$$v_{Rk,\,fat} = v_{el} \cdot n_{v,el} \tag{6.2}$$

v_{el} : longitudinal shear force per unit length, at the end of the elastic behaviour of the connection's structural response as predicted by the numerical model

$n_{v,el}$: conversion factor for the connection longitudinal shear resistance at limit of fatigue, equal to 0.74

6.2.3 Verification

Summarizing, the design method for FLS (which covers also the verification for SLS) consists of the following steps:

- Step 1. Calculation of the required resistance to longitudinal shear for verification with respect to limit of fatigue. The value of 800 kN/m can be used, based on the state of the art presented in the 2nd chapter. However, for more precision and economic design it can be calculated in the following way. The fatigue model load of Meystre and Lebet [Meystre and Lebet 2001] should be applied in order to obtain the variation of the longitudinal shear force per unit length, $\Delta v(Q_{fat})$, for several sections along the beam, as would have be done also for the case of common connections with shear studs. The higher values are expected for the sections at the two extreme supports. In these values, obtained due to the traffic, should be added the design values of the longitudinal shear force per unit length, v_{long}, due to permanent loads acting on the connection (such as dead loads from coating, cornice and safety barrier).
- Step 2. Initialization of the connection geometry, mechanical characteristics of concrete, positioning, spacing and area of the reinforcement for the confinement effect.
- Step 3. Using the numerical model provided at the annex II, the designer structural engineer can obtain the corresponding curve, as the one illustrated in the figure 6.1, and from that curve the value of the resistance of the connection v_{el} at the end of the elastic behaviour of the connection's response.
- Step 4. Verification for FLS corresponding to the limit of fatigue is performed by using equation (6.3).

$$v_{Rk,fat} \geq v_{long} + \gamma_{fat} \cdot \Delta v(Q_{fat}) \leq 800 \text{ kN/m} \tag{6.3}$$

v_{el} : longitudinal shear force per unit length, at the end of the elastic behaviour of the connection's structural response

v_{long} : the design longitudinal shear force per unit length due to permanent loads acting in the connection after the realization of the connection, (v_{long} includes a partial factor γ_v)

γ_v : partial factor of the connection resistance equal to 1.25 [SIA-264 2003]

$n_{v,el}$: conversion factor for the connection longitudinal shear resistance at limit of fatigue, equal to 0.74

γ_{fat} : partial factor for fatigue strength equal to 1.15 [SIA-264 2003]

$\Delta v(Q_{fat})$: variation of the longitudinal shear force per unit length due to fatigue model load of Meystre and Lebet [Meystre and Lebet 2001]

If the control does not pass the designer should restart from step 1 and increase the height of the slab since, as it was found from the parametric analysis at section 5.6, this is the most effective solution to extend the elastic behaviour of the connection's performance and thus the fatigue limit.

Characteristic examples of arrangements that fulfill the verification proposed by equation (6.2) are presented in the design table in the section 6.4.

6.3 Design for ULS

6.3.1 Composite beams with elastic calculation of the cross-sectional resistance

In the case where an elastic calculation has been performed to assess the cross-sectional resistance of the composite beam for bending, the classic equation (6.4) based on the linearity between stresses and strains, can be used to calculate the longitudinal shear force per unit length, v_{Ed}, and consequently design the connection for each section x.

$$v_{Ed} = \sum \frac{V_{Ed,i} \cdot S_{c,i}}{I_{b,i} \cdot n_{el,i}} + v_{\Delta T} \tag{6.4}$$

v_{Ed} : design value of longitudinal shear force per unit length
$V_{Ed,i}$: design value of the shear force in the section caused by the design load i, acting after the realization of the connection
$S_{c,i}$: first moment of inertia of the slab calculated from the neutral axis of the composite section
$I_{b,i}$: second moment of inertia of the composite section calculated with the corresponding modular ratio $n_{el,i}$
$n_{el,i}$: elastic modular ratio for load i
$v_{\Delta T}$: longitudinal shear force per unit length due to thermal gradient ΔT

For the regions with negative moments, figure 6.2_b, cracking of the slabs implies a calculation of the first moment of inertia of the slab, $S_{c,i}$ and the second moment of inertia of the composite section, $I_{b,i}$, considering only the area of the reinforcement. However, such as a consideration, neglecting the tension stiffening effect, underestimates the developed longitudinal shear. For that reason, for the area of negative moments, the longitudinal shear can be calculated considering the concrete uncracked (stage I at figure 6.2, conservative approach) or taking into account the tension stiffening (stage II at figure 6.2). Such a method was proposed by Gomez [Gomez 2000] concerning spans between 30 to 80m. According to this method the concrete can be considered cracked and the tension stiffening effect is taken into account by multiplying the longitudinal shear obtained by a coefficient equal to 1.10.

The design value of the connection's resistance to longitudinal shear per unit length, v_{Rd}, is given by equation (6.5):

$$v_{Rd} = v_{Rk} / \gamma_v \Rightarrow v_{Rd} = v_u \cdot n_v / \gamma_v \tag{6.5}$$

v_{Rk} : characteristic value of the connection's resistance to longitudinal shear force per unit length
v_u : connection's ultimate resistance calculated with the numerical model (figure 6.1)
n_v : conversion factor for the connection longitudinal shear resistance, equal to 0.89
γ_v : partial factor of the connection resistance equal to 1.25 [SIA-264 2003]

The verification should fulfill the following equation:

$$v_{Ed} \leq v_{Rd} \tag{6.6}$$

Characteristic examples of arrangements that fulfill the verification proposed by equation (6.6), for v_{Ed} according to table 2.7 of the state of the art, are presented in the design table in the section 6.4.

6.3.2 Composite beams with plastic calculation of the cross-sectional resistance

Experimental investigation presented in the 3rd chapter and commentated in the 4th chapter, concerning the bending test of a composite beam, has shown that:

Ductile failure of a composite beam, fabricated with the new connection and developing its design plastic moment $M_{pl,Rd}$, despite the connection's limited deformation capacity, applies provided that the beam flexural resistance is reached before reaching the connection longitudinal shear resistance.

Figure 6.2 presents such a beam which is capable of developing its plastic moment at the span at the section where the load Q is applied.

For plastic calculation of the cross-sectional resistance, the longitudinal shear force per unit length does not follow the equation (6.4) because of the non-linearity between the stresses and the strains in the elasto-plastic domain. At plastification of the cross-section the normal force increases faster than the applied moment resulting, locally, in a peak of the longitudinal shear force per unit length, max_v_{Ed}. To achieve plastic behaviour of the beam the resistance of the connection to longitudinal shear force per unit length should be higher than the peak of the longitudinal shear force per unit length, max_v_{Ed}, for all sections, that enter to the elasto-plastic domain. This verification is expressed by the equation (6.7) and is imposed by the limited deformation capacity of this type of connections.

$$v_{Rd} \geq \max\_ v_{Ed} \text{ for all sections that enter the non-linear domain.} \quad (6.7)$$

The design value of the connection's resistance to longitudinal shear force per unit length, v_{Rd}, is given by equation (6.5).

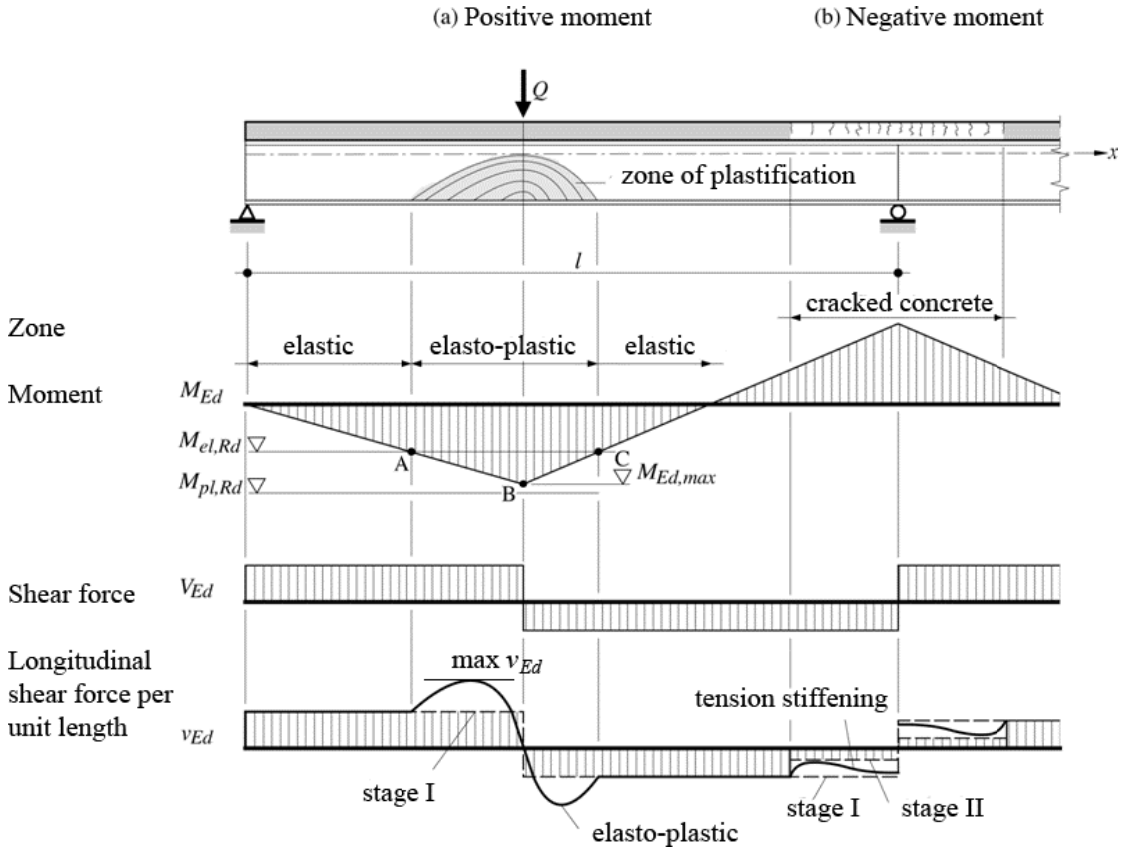

Fig. 6.2: Influence of the plastification of steel and of the cracking of concrete to the longitudinal shear force per unit length [Lebet and Hirt 2009]

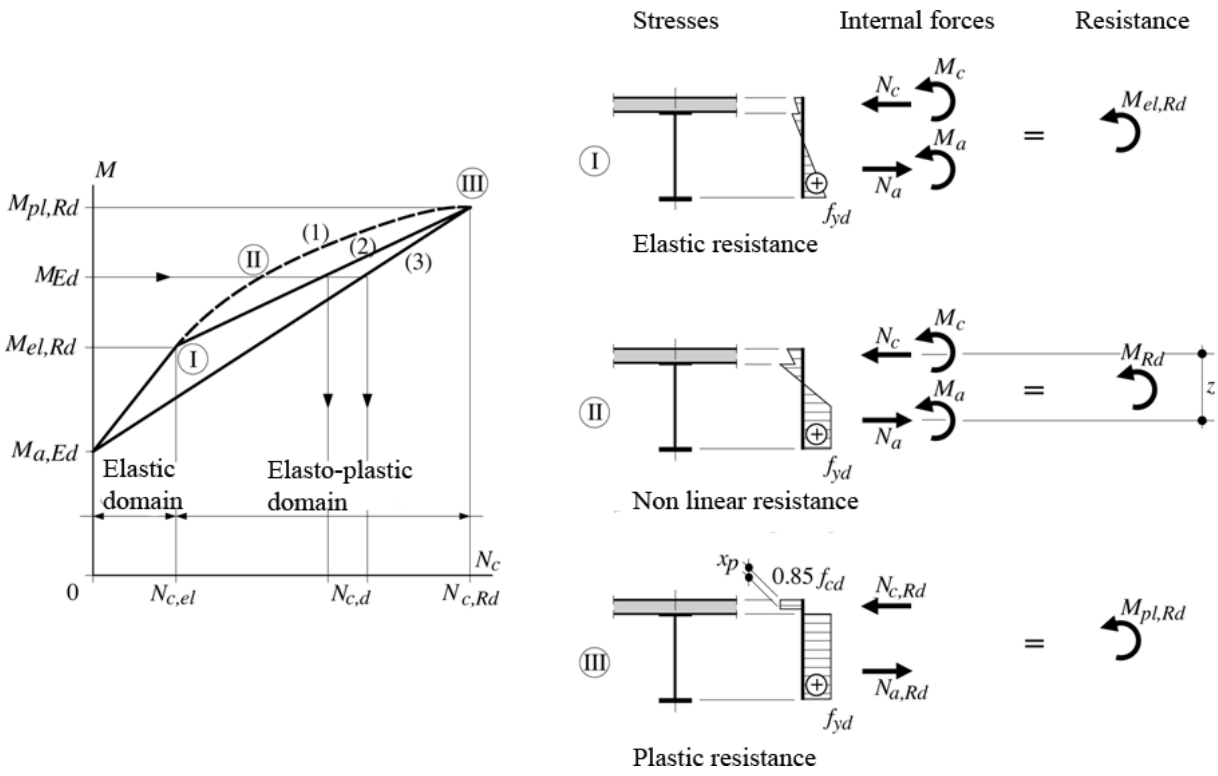

Fig. 6.3: Normal force in the slab of a composite section as a function of the positive bending moment [EC4 2004]

The longitudinal shear force per unit length, v_{Ed}(x), acting in a section can be expressed by the following equation (6.8):

$$v_{Ed}(x) = \frac{dN_{cd}(x)}{dx} = \frac{dN_{cd}(x)}{dM_{Ed}(x)} \cdot \frac{dM_{Ed}(x)}{dx} = \frac{dN_{cd}(x)}{dM_{Ed}(x)} \cdot V_{Ed}(x) \qquad (6.8)$$

In the equation (6.8) the tern $V_{Ed}(x)$ is the shear force at the section *x*. It is obvious from the equation (6.8) that in order to define the peak of the longitudinal shear force per unit length, max_v_{Ed}, the relationship between the normal force and the applied moment has to be established.

Such a relationship, for an unpropped beam during construction, is illustrated in the figure 6.3 in the diagram of the moment of the cross section versus the normal force in the slab [Lebet and Hirt 2009]. Concerning the elasto-plastic domain, the dotted line (1) in the diagram presents the "real" relationship between the moment and the normal force. The lines (2) and (3) present two possible simplified relationships. The simplified relationship presented by line (3) is proposed also by the Eurocode 4 part 2, for application in composite bridges.

For the beam in the figure 6.2 and for the part of the elasto-plastic zone between the sections A and B (respectively B and C), a mean value of the longitudinal shear force per unit length is given by equation (6.9):

$$\bar{v}_{Ed} = \frac{N_{c,d} - N^{A}_{c,el}}{l_{AB}} \qquad (6.9)$$

$N_{c,d}$: normal force acting in the slab at the point of the maximum moment (point B of figure 6.2)

$N^{A}_{c,el}$: normal force acting in the slab at the section where the plastification starts to occur (point A of figure 6.2)
l_{AB} : distance of sections A and B

The normal force $N^{A}_{c,el}$ at point A can be calculated by equation (6.10) , for neutral axis in the steel girder.

$$N^{A}_{c,el} = k \cdot \left(\frac{M_{b,Ed}(x_A) \cdot S_c}{I_b \cdot n_{el}} \right) \tag{6.10}$$

$M_{b,Ed}(x_A)$: bending moment at point A due to loads acting after the realization of the connection
S_c : first moment of inertia of the slab calculated from the neutral axis of the composite section at point A
I_b : second moment of inertia of the composite section at point A
n_{el} : elastic modular ratio for actions of short term
k : factor with value equal to 1 for section at point A

The normal force $N_{c,d}$ can be calculated assuming either the simplified relationship of line (2) in figure 6.3 and using the equation (6.11) or assuming the simplified relationship of line (3) in the same figure and using the equation (6.12)

$$N_{c,d} = N^{B}_{c,el} + \frac{\left(M_{Ed} - M_{el,Rd}\right)}{\left(M_{pl,Rd-}M_{el,Rd}\right)} \cdot \left(N_{c,Rd} - N^{B}_{c,el}\right) \tag{6.11}$$

$$N_{c,d} = \frac{\left(M_{Ed} - M_{a,Ed}\right)}{\left(M_{pl,Rd-}M_{a,Ed}\right)} \cdot N_{c,Rd} \tag{6.12}$$

M_{Ed} : bending moment at point B
$M_{el,Rd}$: elastic moment at point B
$M_{a,Ed}$: bending moment at point B for loads acting in the steel section only
$N_{c,Rd}$: normal force acting in the slab when section is fully plastified
$N^{B}_{c,el}$: elastic normal force acting in the slab for the section at point B
$M_{pl,Rd}$: design plastic moment of the composite section

However, verification by comparing the mean value of the longitudinal shear for the section l_{AB} with the connection's resistance v_{Rd} has a meaning only for ductile shear connections such as shear studs where a redistribution of forces is possible due to adequate deformation capacity.

Concerning connections by adhesion, interlocking and friction, the ductility and the deformation capacity is limited and varies. Thus the verification for the elasto-plastic zone should be performed necessarily using equation (6.7) which requires the peak of the longitudinal shear force per unit length, max_v_{Ed}. Assessing the latter is a difficult task and can only be solved by means of numerical methods [Bärtschi 2005].

Alternatively, when this is not possible, and if a minor redistribution is accepted due to a limited ductility of the new connection, a value close to max_v_E can be used. It comes out from equation (6.8) that such a value may be obtained if an increased term $dN_{Cd}(x)/dM_{Ed}(x)$ is considered. In figure 6.3 and from the diagram of the moment of the cross section versus the normal force in the slab it can be seen that from the two proposed simplified relationships, the term $dN_{Cd}(x)/dM_{Ed}(x)$ is higher for the simplified relationship indicated by line (2). Thus for the new connection, the verification of the longitudinal shear for the sections of the elasto-plastic zone can be performed by using the simplified

relationship indicated by line (2), provided that the deformation capacity would permit a minor redistribution. Use of the line (3) proposed by Eurocode 4, part 2, for composite bridges [EC4-part 2 2004] results in unsafe design for the new connection. (The use of the line (3) for connections with shear studs provides a mean value of the longitudinal shear, for the part of the span that enters the plastic domain, which is higher than the one if using the line (2). However this should not be confused with the above mentioned use of the line (2) concerning the new connection, because in this case, we are aiming at the peak value of the longitudinal shear, locally, which according to the equation (6.8) is provided when the term $dN_{Cd}(x)/dM_{Ed}(x)$ is higher).

For design practice, the imprecision by using the simplified relationship (line (2) at figure 6.3) for assessing a true peak of the longitudinal shear force per unit length, max_v_{Ed}, can be counterbalanced by performing a type of capacity design [Thomann 2005]. The *capacity design* consists of using in equation (6.11) instead of the design value of the normal force in the slab for plastification of the section at point B, $N_{c,Rd}$, the characteristic value, $N_{c,Rk}$, i.e. without using any partial resistance factor. In addition an increased concrete compression resistance could be taken into account due to aging of the concrete and realistic stress strain diagrams for the steel girder with hardening behaviour. Applying this method (commonly used in earthquake engineering for instance to provoke plastic hinge in the beam and not in the columns), can be guaranteed that the ductile bending failure of beam will occur before reaching the connection longitudinal shear resistance.

The uncertainties of assessing the redistribution of the longitudinal shear force per unit length, for sections at the plastic domain, due to the limited ductility of the connection orientate towards the choice of the elastic calculation of the cross-sectional bending resistance of the composite beam. However, as it will be shown in the design table presented in the section 6.4, the verification for FLS dominates the connection's design, resulting in high values of resistance for ULS that can be sufficient for a plastic calculation of the cross-sectional bending resistance of the composite beam.

6.4 Design table

This section presents characteristic examples of design of the connections by adhesion, interlocking and friction which can be used in engineering practice. The design is performed so that the connections fulfill the requirements presented at table 2.7, in the state of the art, concerning twin-I girder steel concrete composite bridges. In total nine sections for three concrete types are presented for different heights of the reinforced concrete slab. The modulus of elasticity of concrete for each concrete type is according to [fib Model Code 2010] for quartzite aggregates. The steel reinforcement is of type B500.

The table 6.1 provides all needed information concerning the connection geometry and the positioning of the steel reinforcement. The width of the lower part of the slab at the two sides of the connection is at least 300 mm. This distance was used during the FEA to investigate the confinement effect. The steel reinforcement that contributes to the confinement effect should have the appropriate anchorage length. The same area of reinforcement is considered for the upper, middle and lower steel reinforcement. It is noted that the steel reinforcement in the upper part of the slab is different from the transversal reinforcement positioned for the transversal bending of the slab. The latter is considered to be sufficient enough to prevent cracking of the slab due to transversal bending, for service loads. It is noted that the upper reinforcement initially has only a minor contribution to the confinement effect, and its contribution becomes significant for high values of uplift in the interfaces likely after failure of the connection, as it was verified by FEA and running of the numerical model.

The design table presents the characteristic value of the connection's resistance to longitudinal shear force per unit length at ULS, v_{Rk}, the slip at failure, s_u, and the characteristic value of the connection's

resistance at the end of the elastic domain, $v_{Rk,fat}$, which is used for the verification at FLS (limit of fatigue). For each section, the connection's resistance is provided for different level of normal stresses acting on the resisting interfaces, $\sigma_{ext,i}$, due to transverse prestressing or transverse bending of the slab and which range from 0 to 2 N/mm^2. These stresses are added to the normal stresses produced from the confinement effect. The connection's resistance to longitudinal shear force per unit length is calculated using the numerical model which was developed in the previous chapter.

The gray shadowed cells highlight the resistance values with corresponding $\sigma_{ext,i}$ = 0 N/mm^2 which is the basic value that can be considered as conception for a pre-design.

Table 6.1: Characteristic resistance to longitudinal shear force per unit length at ULS and FLS for connections by adhesion, interlocking and friction; a) C35/45, b) C40/50 and c) C50/60

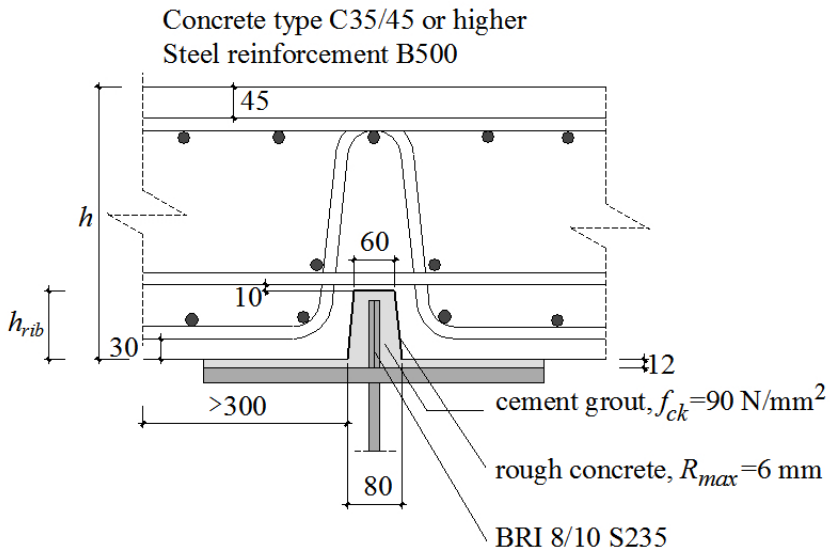

a) Concrete type C35/45

h (mm)	h_{rib} (mm)	As/S	$\sigma_{ext,i}$ (N/mm^2)	$v_{Rk} = v_u \cdot n_v$ (kN/m)	$v_{Rk,fat} = v_{el} \cdot n_{v,el}$ (kN/m)	s_u (mm)
525	125	Ø16/120	0	1770	820	1.16
			0.5	1895	900	1.20
			1	2030	1000	1.13
			1.5	2180	1090	1.14
			2	2340	1190	1.21
500	125	Ø16/100	0	1840	800	1.34
			0.5	1960	890	1.25
			1	2090	985	1.20
			1.5	2240	1080	1.19
			2	2420	1190	1.28
450	110	Ø20/100	0	2030	800	1.32
			0.5	2255	870	1.36
			1	2255	950	1.36
			1.5	2255	1045	1.36
			2	2255	1130	1.36

b) Concrete type C40/500

h (mm)	h_{rib} (mm)	As/S	$\sigma_{ext,i}$ (N/mm^2)	$v_{Rk}=v_u \cdot n_v$ (kN/m)	$v_{Rk,fat} = v_{el} \cdot n_{v,el}$ (kN/m)	s_u (mm)
525	125	Ø16/150	0	1670	805	1.20
			0.5	1890	900	1.13
			1	1940	1000	1.05
			1.5	2090	1090	1.09
			2	2250	1190	1.17
500	125	Ø16/120	0	1750	800	1.26
			0.5	1870	890	1.21
			1	2010	1000	1.16
			1.5	2160	1090	1.13
			2	2320	1190	1.20
450	110	Ø18/100	0	1910	800	1.33
			0.5	2025	865	1.27
			1	2255	960	1.36
			1.5	2255	1045	1.36
			2	2255	1130	1.36

c) Concrete type C50/60

h (mm)	h_{rib} (mm)	As/S	$\sigma_{ext,i}$ (N/mm^2)	$v_{Rk}=v_u \cdot n_v$ (kN/m)	$v_{Rk,fat} = v_{el} \cdot n_{v,el}$ (kN/m)	s_u (mm)
500	125	Ø16/150	0	1675	820	1.16
			0.5	1805	915	1.08
			1	1950	1010	1.04
			1.5	2110	1105	1.10
			2	2265	1200	1.17
450	110	Ø16/100	0	1805	805	1.29
			0.5	1925	890	1.21
			1	2055	975	1.21
			1.5	2255	1060	1.36
			2	2255	1155	1.36
425	100	Ø18/100	0	2050	810	1.36
			0.5	2050	885	1.36
			1	2050	960	1.36
			1.5	2050	1040	1.36
			2	2050	1115	1.36

The table shows that the design of the connection is governed by the requirement for the verification at FLS. This due to the fact that the conversion factor for the fatigue limit, $n_{v,el}$, is lower than the conversion factor, n_v, for the ultimate resistance, equations (5.24) and (5.26).

It also shows that if the designer chooses to decrease the height of the slab and consequently the height of the inner rib and of the connector as well, in order to achieve economy, the required confinement should be compensated by increasing the reinforcement ratio. Upgrading to a higher concrete type results often in reducing of the steel-reinforcement. It is also noted that the table presents few cases in which, for the same section, for different additional normal stresses, $\sigma_{ext,i}$, due to transverse prestressing or transverse bending of the slab, the same characteristic strength is obtained. This is due to the fact that the shear stresses in the interfaces reach the highest possible value, suggested by Eurocode 2 in paragraph 6.2.5 [EC2 2004], which is also adopted in this study and which for a cement grout with f_{ck}=90 N/mm^2 reach the value : τ_u=11.5 N/mm^2.

It is reminded that at the last year of this study, the company VSL, which was providing the material for the cement grout, proposed for the connection its new product, the cement grout VSL-HPI which is currently used in the prestressing tendons. As it was seen in the 3rd chapter in the table 3.5, the structural performance of the last two push-out specimens was superior to that of the previous one fabricated with the old type of VSL cement grout. The new product despite its lower compression resistance (66.8 N/mm^2 for the last two specimens and 75.5 N/mm^2 for the composite beam) presents a better performance due to its expansive agent that counterbalances the shrinkage and creates a kind of favorable pre-stressing in the interface. The design table 6.1 is based on the failure criteria, and the constitutive and kinematic laws obtained from analysis of tests with the old cement grout. However it can be assumed that is valid also for connections injected with the new cement grout since the latter results in better performance for the connection.

6.5 Conclusions

This chapter concludes the sequence of the study by proposing a design method for composite bridges fabricated with connections by adhesion, interlocking and friction.

- It was demonstrated that the developed numerical model in the previous chapter can be used to asses the ultimate resistance of the connection to longitudinal shear at ULS and predict the connection's structural performance including the post-failure behaviour.
- Concerning the verification at ULS, two cases were examined. Verification for the cases where the cross-sectional bending resistance is performed with the elastic method and secondly with the plastic method. Recommendations were made for both cases in order to apply a safe design. For a plastic calculation of the cross-sectional bending resistance the importance of considering the peak of the longitudinal shear force per unit length, max_v_E, was underlined. An alternative method was proposed, based on the Eurocode 4 [EC4 2004] for ductile connectors, combined with an approach of capacity design to avoid failure of the connection before the bending failure of the composite beam.
- It was also shown that application of the numerical model can help to define the end of the elastic behaviour of the connection. This limit, in which the shear stresses in the interfaces remain elastic, can be used as a fatigue limit for verification of the connection at FLS.
- Finally, using the numerical model, a design table was produced, for three different concrete types of the slab and for various connection geometry, so as to be used in design practice. The table shows that the verification for FLS dominates the design for the connection, resulting in reserve resistance for the ULS.

The following chapter summarizes the major conclusions of this study, proposing further work and final recommendations.

7. Conclusions

7.1 Objectives of the study and methodology

The new connection constitutes an alternative type of connection that is suitable for prefabrication and rapid execution while guaranteeing a durable solution. It can also serve as a solution where replacement of concrete decks is needed and where the steel girders are reused.

This study aims to complete the research performed at the laboratory concerning innovative connections by adhesion, interlocking and friction for steel-concrete composite bridges. The main objectives of this study, as presented in the introduction were:

- Development of a numerical model to predict the resistance of connections by adhesion, interlocking and friction for static loading. The model should be valid also for high level of confinement of the interfaces, predict the post-failure behaviour, and provide the deformation capacity of the connection.
- Study the behaviour of connections submitted to cyclic loading and to develop a method to predict the fatigue resistance of the new connection.
- Propose a design method for the connection of steel-concrete composite bridges, fabricated with the new connection and submitted to static and cyclic loading.

In order to fulfill the objectives, besides the study of the state of the art in interfaces and connections for steel-concrete composite bridges (chapter 2), the following work has been accomplished:

- *Experimental investigation* (chapter 3). A large number of direct shear tests, including both static and cyclic loading, were executed for three types of interfaces in order to investigate the interface behaviour. These interfaces are: a) embossed steel-cement grout interface, b) rough concrete-cement grout interface and c) UHPFRC-cement grout interface. Push-out tests under static and cyclic loading were performed to study the connection's behaviour.
  The static loading of interfaces has provided the experimental data which permitted the development of the laws that describe the behaviour of the interfaces. Static loading of push-out specimens have provided the data to validate the numerical model that was developed to predict the connection's structural performance.
  The cyclic loading of interfaces and connections has revealed the nature of the *damage* due to this type of loading, which is expressed by the development of a *residual slip* due to the repeated loading. Cyclic loading also provided a range of experimental values for determining the fatigue limit of the connection tested.
  Finally a composite beam, fabricated with the new connection, was submitted to high cycle loading to investigate the structural performance. A final static test was performed to prove the efficiency of the connection, at an ULS following the cyclic loading, and to prove the capacity of the composite beam to develop ductile bending failure before failure of the connection.
- *Analytical study* (chapter 4). Based on the experimental results, useful laws have been proposed to describe the interface behaviour. These laws are the *failure criteria*, the *constitutive* and the *kinematic laws*. The validity of the laws is up to 5 N/mm^2, the highest normal stress applied on the interfaces. The *post-failure behaviour* was studied in detail and expressions for the fracture energy were proposed.
  The analytical study helped to develop *analytical relationships* for the evolution of the residual slip in the interfaces and in the connection. These relationships help to establish a *safe fatigue failure criterion* for both the interfaces and the connection.

Concerning the composite beam, an analytical study considering slip in the connection at ULS has helped to demonstrate the capability of the composite beam to develop its design plastic moment.

- *Finite element analysis* (chapter 5). This tool was used in order to study and propose equations for the *confinement effect* which, together with the laws of the interfaces, determine the connection's resistance and structural performance. The proposed equations for the *confinement effect* account for the concrete mechanical characteristics, the connection geometry, and the steel reinforcement area and positioning, so to apply for *general use*.
- *Numerical model* (chapter 5). An existing model was updated and upgraded taking into account the analytical laws developed in the 4th chapter and a new more detailed and general expression for the confinement effect in order to predict the connection's resistance at ULS and the deformation capacity. The *numerical model* has also helped to define, scientifically, a *fatigue limit* for the verification at FLS of the connection. Using the numerical model a *parametric analysis* enabled to define the parameters that have a major role in the connection's performance.
- *Design method* (chapter 6). Based on the state of the art in steel-concrete composite bridges and the numerical model, a *design method* was proposed for verification of the connection at USL and FLS and a design table was provided for use in practice.

7.2 Major conclusions of the research

7.2.1 Interfaces

The studied interfaces subjected to shear stress, with simultaneous normal stress, present a failure criterion which is characterized by a linear relationship with normal stress and a constant contribution of adhesion and interlocking. The roughness of the interfaces has a favorable effect on the increase of resistance.

For static loading, the constitutive behaviour consists of an initial linear behaviour up to an elastic limit, τ_{el}, followed by a plastic branch towards the failure of the interface. In this part, prior to failure the uplift in the interface is limited to a value characteristic of each type of interface. Once failure occurs the resistance does not drop immediately but diminishes with an exponential decay. This interface behaviour, as proven by observations and analytical study, corresponds to a progressive degradation of the failure surface to a smoother one which obtains a final form when the resistance diminishes to the remaining frictional resistance. This degradation of the failure surface is described by the kinematic law after failure.

The analytical study combined the analytical expressions of the constitutive law for post-failure behaviour with the fracture energy release rate. The analytical expressions proposed can define the mechanical characteristics of interface layers which can be used for simulation of interfaces by means of FEA.

The elastic limit, τ_{el}, defined in static loading, is of great importance for cyclic loading. As long as the maximum cyclic shear stresses do not to exceed the elastic limit ($\tau_{max} < \tau_{el}$), the cyclic loading causes a kind of limited damage in the interface, expressed by the development of a residual slip which stabilizes with the number of cycles, practically after one to two million cycles. After a cyclic loading with the maximum cyclic shear stress $\tau_{max} < \tau_{el}$, further loading up to failure shows that the interface remaining resistance is equal to that of static loading, in other words no degradation of the resistance occurs in this case.

If the maximum applied shear stress of cyclic loading enters the plastic domain ($\tau_{max} > \tau_{el}$), the permanent slip is increased and after few cycles in the plastic domain, failure occurs when the slip under cyclic load reaches the value of the failure slip, s_u, for static loading. Once failure occurs, the constitutive law is that of the static loading.

7.2.2 Connection

The connection's behaviour both in static and cyclic loading results from the resistance of the interfaces that constitute the connection. An important factor is the confinement effect on the interfaces. The confinement effect is the increase of the normal stress applied on the interfaces due to the interaction of the kinematic law and the translational stiffness of the slab that encloses the connection. The confinement effect is responsible for extending the constitutive and kinematic laws to a higher level of normal stress. It defines the shear stress path of the developed shear stresses in the interfaces and determinates together with the behaviour laws of the interfaces the connection's resistance and deformation capacity.

The parametric analysis has shown that the confinement effect is generally more effective for high area of reinforcement located closer to the embossed steel plates and for increased height of the slab at the vicinity of the connection. An optimum ratio for the connection's resistance consists a ratio of the height of the inner rib versus the height of the slab between 0.2 to 0.25.

The connection's behaviour to cyclic loading is similar to that of the interfaces. For both apply the following *safe fatigue failure criterion*, equation (7.1):

$$s_{Vmax,N} \leq s_u \tag{7.1}$$

As long as the accumulated slip under maximum cyclic load, $s_{Vmax,N}$, does not exceed the failure slip for static loading, s_u, failure due to cyclic loading does not occur and the remaining capacity is equal to that obtained for static loading.

Cyclic loading of connections has reached up to 0.55 of the ultimate resistance without fatigue failure.

The numerical model was validated by the results from push-out tests. It predicts the connection's ultimate resistance and provides the deformation capacity. It also provides a limit, v_{el}, in which the stresses in the interfaces remain elastic. Cyclic loading under this limit causes a residual slip that stabilizes with the number of cycles. Hence this limit, v_{el}, can be used as a fatigue limit for the connection.

7.2.3 Steel-concrete composite beams

The verification at the FLS is performed with respect to the limit of fatigue, according to the equation (7.2).

$$v_{long} + \gamma_{fat} \cdot \Delta v(Q_{fat}) \leq v_{Rk,fat} \tag{7.2}$$

The verification for FLS with equation (7.2) implies that the characteristic value of the fatigue limit, $v_{Rk,fat}$, must be higher than the value which comes out from adding the design value of the maximum variation of the longitudinal shear, due to the traffic from the load model, $\gamma_{fat} \cdot \Delta v(Q_{fat})$, and the design value of the longitudinal shear from permanent loads acting after the realization of the connection, v_{long}.

The fatigue loading, can be calculated by applying a deterministic fatigue loading model of two heavy trucks based on the 99% fractile values from spectra of real traffic. This fatigue model enables to define the maximum variation of the longitudinal shear force, $\Delta v(Q_{fat})$, for the bridge types concerned.

Application of the fatigue model to a database of twelve typical twin-I girder steel-concrete composite bridges in Switzerland results in a value equal to 800 kN/m for the first part of equation (7.2), see equation (7.3).

$$\max\left(v_{long} + \gamma_{fat} \cdot \Delta v(Q_{fat})\right) = 800 \text{ kN/m} \tag{7.3}$$

The characteristic value of the fatigue limit of the connection, $v_{Rk,fat}$, is given by equation (7.4) as the product of the fatigue limit of the connection, v_{el}, and the corresponding conversion factor, $n_{v,el}$, the latter is equal to 0.74.

$$v_{Rk,\,fat} = v_{el} \cdot n_{v,el} \tag{7.4}$$

The fatigue limit, v_{el}, is provided by the numerical model for a given connection geometry, reinforcement area and positioning, and concrete type. It was found by parametric analysis that the fatigue limit, v_{el}, is lying in a range between 0.45 to 0.63 of the ultimate resistance, v_u.

Evaluation of the longitudinal shear in composite bridges has shown that verification at the FLS covers also the SLS, since the required resistance was found to be lower at the SLS.

The verification at the ULS shall be performed in two ways depending on the method chosen for assessing the cross-sectional bending resistance. For elastic calculation of the cross-sectional resistance, an elastic calculation of the longitudinal shear is performed. For plastic calculation of the cross-sectional resistance, the nonlinearity of stresses and strains should be taken into account and thus the peak value of the longitudinal shear resistance should be defined. For both cases the design value of the longitudinal shear acting in the connection must be lower than the design value of the connection's resistance. The latter is obtained from the numerical model also considering the corresponding conversion and partial factors of resistance.

7.3 Recommendations for practice.

- The design method presented in this study is subjected to the limitations presented in the section 1.4 for the type of steel-concrete composite bridges concerned.
- For the conception it should be taken into account that only the height of the interfaces which is subjected to normal compression stress is considered to participate in the shear resistance. If part of the interfaces is under normal tension stress, due to transversal bending of the reinforced concrete deck, the corresponding interface area should be considered inactive.
- Transversal prestressing, which is applied often in the cases of long cantilever deck, is expected to have a favorable effect on the connection's resistance and is also recommended so as to avoid any cracking on the upper part of the reinforced concrete slab when high negative moments develop transversally due to transversal bending from heavy trucks. Generally, since the reinforced concrete slab is considered uncracked on the top (hypothesis made in the study of the confinement effect) this should be guaranteed either by prestressing or by an appropriate conception detail of the cross section with a higher height, h, of the slab in the connection vicinity than the height, h', obtained from design for moment (figure 7.1); in that case any crack on top would occur on the place where the static height starts to diminish and not in the connection vicinity.
- It is generally suggested that composite bridges connections should prevent separation of the slab. A common proposed control is that the connection should resist a nominal ultimate tensile force, perpendicular to the plane of the steel flange, equal to 0.1 times the design of the ultimate shear resistance of the connection. For more about the resistance in tension one can

look up in the thesis of Thomann [Thomann 2005] where the resistance of the connection was investigated experimentally.

- The cement grout used for the connection should have similar characteristics to the one used in this study, such as a characteristic compressive strength of about 90 N/mm^2 and fluidity measured by performing the Marsh cone test less than 25 sec [VSL 2002]. Other types of cement grouts with high compression resistance, limited shrinkage and if possible with an expansive agent are also suggested for use, due to its expected enhanced performance (see section 7.4.1).
- Application of the design method, as seen in the design table in the previous chapter, leads to the conclusion that the design for FLS dominates the overall design of the connection, and may result in redundant resistance. A less conservative design would require further knowledge concerning the behaviour of the connection for cyclic loading that exceed the fatigue limit. This concerns further work which is discussed in the section 7.4.2.

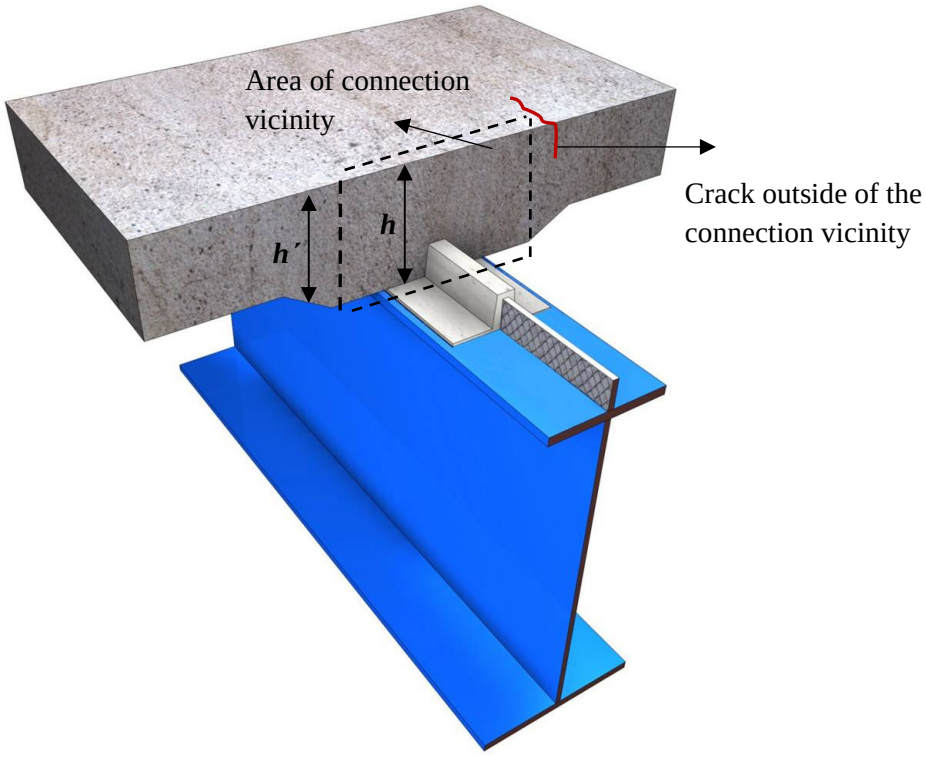

Figure 7.1: Conception detail to push the formation of any cracking at top of the reinforced concrete slab outside of the connection vicinity

7.4 Further work

7.4.1 Assessing laws for interface behaviour of a new type of cement grout

The failure criteria and the constitutive and kinematic laws for three interfaces correspond to a specific cement grout of the VSL company with a characteristic compressive strength about 90 N/mm^2. A new cement grout from the same company named VSL-HPI shows, as found experimentally by performing three direct shear and two push-out tests, an enhanced performance in comparison with the initial cement grout. This is due to an expansive agent that counteracts the loss of volume from shrinkage and creates a pre-confinement state in the interfaces. Use of this material can thus be suggested for practice; however the connection's resistance is likely to be underestimated. For a less conservative

design, meaning for a more accurate prediction of the connection's resistance from the numerical model, the failure criteria and the kinematic and the constitutive laws should be "updated" with new values corresponding to the new cement grout. This can be done by performing direct shear tests similar to those performed in the current study.

7.4.2 Fatigue verification with damage accumulation

The experimental investigation of the connection by means of push-out tests under cyclic loading did not establish a typical S-N curve for the connection. This is because either no failure occurred and tests were stopped, since no further damage was observed in the interface, or failure was reached from the first cycle (static loading). Consequently the definition of fatigue limit was chosen to be used in order to establish verification for FLS.

The question of what happens if few cycles, with higher amplitude than that of the fatigue limit, v_{el}, occur is always present and corresponds to a very rare but realistic situation. Accidentally, a situation like this occurred for push-out specimen PR100_4 (table 3.5), whose results concerning the slip were excluded from presentation due to that accident. As seen in the table 3.5 this specimen was subjected to cyclic loading with a variation of longitudinal shear V_{max}-V_{min}=1600-260 kN. After three million cycles a malfunction of the maintenance of the jack resulted to loading up to 2040 kN and an increase of the slip at about 1 mm. Afterwards the test was continued with the same variation of the longitudinal shear for one more million cycles without any increase of the residual slip which had stabilized. After four million cycles another error in the maintenance of the pumping system resulted in the destruction of the specimen. This accident demonstrated that it is possible to accept a limited loading over the fatigue limit for connections of that type. This phenomenon should be further investigated.

Damage accumulation method considering slip in the interface

A further work would consist of fabrication of push-out specimens with the cement grout of the same production. The specimens could be subjected to cyclic loading at different amplitudes. Few of them could be subjected with amplitude so that the maximum cyclic load is equal to the predicted fatigue limit from the numerical model. The rest could be subjected to cyclic loading with cycles that exceed the limit of fatigue ($v_{max,i} > v_{el}$) in order to provoke failure. In the same way as it was performed in this study, analytical expressions for assessing the damage, d_i, expressed by the accumulated slip $s_{Vmax,i}$, can be developed for each specific duration of the cyclic load, $v_{max,i}$. The verification of the connection could be then performed according to the damage accumulation method. This damage, d_i, for each specific duration of the cyclic load, $v_{max,i}$ can be expressed as a ratio with the failure slip, s_u, for static loading of the connection, equation (7.5):

$$d_i = s_{V\max,i} / s_u \tag{7.5}$$

The analytical expressions for the accumulated slip $s_{Vmax,i}$ should consider several matters such as the fact that damage may already be produced if previous cyclic loading periods have been applied. (For the same number of cycles, a load causes more accumulated slip when this number of cycles is closer to the beginning of the service life and less when it follows after other cyclic loading periods). The influence of the sequence of the application of the different cycle loading periods should also be taken into account.

The method should also fulfill the failure criterion presented in the 4th chapter according to which no failure occurs in the connection provided that the accumulated slip due to the cyclic loading is lower than the slip, s_u, which corresponds to failure for static loading. Finally considering all n loads applied during the service life of the bridge the verification can be done according to equation (7.6).

$$\sum_{i=1}^{n} d_i \leq 1 \tag{7.6}$$

Such a method may result in a less conservative design for FLS and consequently for ULS, since as it was shown in the previous chapter, the verification of the connection for FLS with respect to the fatigue limit dominates the design. Applying such a method, the higher loads should be considered to be applied first, since it is estimated by the equations presented in the 4th chapter that this results in more significant damage.

7.4.3 Connections between steel girder and UHPFRC deck

This experimental study proposes a way to produce an artificially rough interface, with the use of conical studs with 8 mm height, for an UHPFRC-cement grout interface. The failure criterion and the kinematic and constitutive law for such an interface were also presented. Three push-out specimens were fabricated with UHPFRC, in which two types of interfaces are developed; the embossed steel-cement grout interface and the UHPFRC-cement grout interface. Preliminary testing of the three push-out specimens has shown that such a connection generally presents higher ductility than the connection with the reinforced concrete blocks. Cyclic loading on direct shear specimens of an UHPFRC-cement grout interface resulted to conclusions similar to those of the other two types of interfaces. The resistance of such a connection in cyclic loading remains to be verified experimentally by means of cyclic loading on push-out specimens.

Concerning the use of the numerical model for the prediction of the structural performance of such a connection with a UHPFRC slab, the appropriate equations that describe the confinement effect for slabs made of such a material need to be developed. For this reason a finite element analysis should be performed, similar to the one executed in this study, for the case of reinforced concrete slabs. Such an analysis requires the knowledge of the UHPFRC fracture energy, which can be calculated experimentally [SIA-162/6 1999].

7.4.4 Study of the longitudinal shear between concrete slab and steel girder for long span steel concrete composite beams for plastic design of cross-section

It was found experimentally that a ductile failure and development of the design plastic moment of a composite beam, fabricated with the new connection, is possible provided that the beam flexural resistance is reached before reaching the connection longitudinal shear resistance. No experimental verification exists for composite beam with spans similar to that of real bridges. The theoretical investigation of this issue requires assessing the development of the longitudinal shear in the sections that are expected to be plastified and the possible redistribution depending on connection deformation capacity. This problem can be faced by performing a 3-dimensional finite element analysis for a real case. The connection between the steel girder and the reinforced concrete slab can be simulated by means of non linear springs connecting the nodes of the two structural elements. The constitutive law for these springs can be obtained from the numerical model developed in the 5th chapter. Such an analysis also provides accuracy with the normal stresses $\sigma_{ext,i}$ on the interfaces due to the transversal bending of the slab, from loads acting after the realization of the connection. Those normal stresses should be taken into account when running the numerical model to predict the force-slip relationship.

7.5 Use of obtained knowledge to other structural applications

The domain of confined interfaces has a wide range of applications in engineering practice. The application of an embossed steel-cement grout interface was studied by Menétrey and Brühwiler [Menétrey and Brühwiler 2008] for the connections between inclined prefabricated struts and

extensions of existing bridge decks. The UHPFRC-cement grout interface presented in this study could also be considered for the cases where inclined struts are fabricated from UHPFRC.

Another application could be a seismic damping/bracing system based on the cyclic behaviour of the confined interfaces. In the current experimental study the cyclic load does not change sign whereas in a seismic incident the sign changes. It would be interesting to investigate the low-cycle, high-amplitude, behaviour of such interfaces, especially concerning the energy absorbed during the cycles and for increased normal stress due to the confinement effect.

A possible seismic damping device could consist of two pairs of embossed steel plates welded with another steel plate perpendicular to them, likewise to the connector of the push-out specimens. This assembly (connector) is enclosed inside a steel tube, with indentations in its inner surface, filled with the high strength cement grout, section A-A in the figure 7.2.

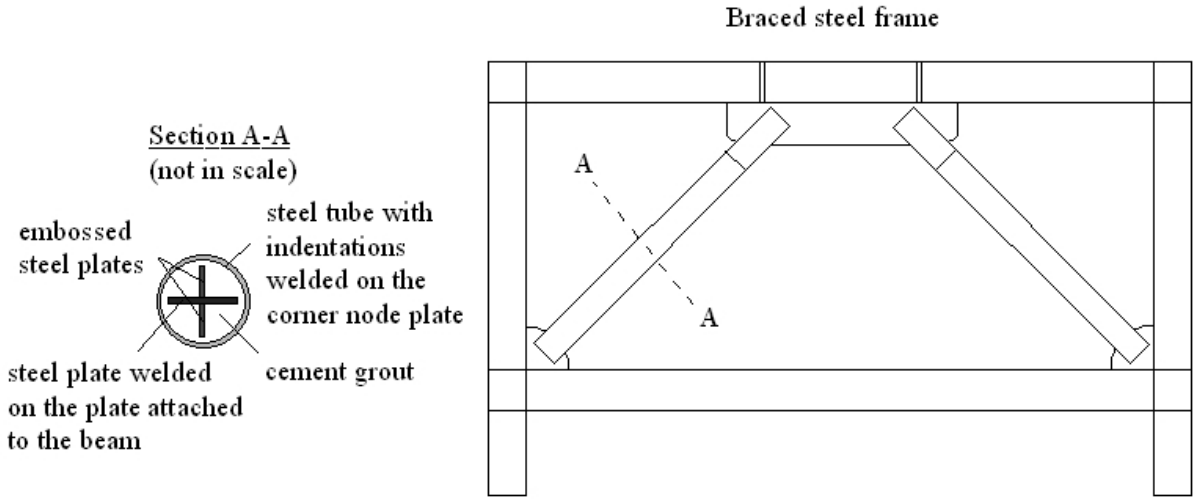

Fig. 7.2: Damping bracing system based on an embossed steel-cement grout interface

The whole structure could be a kind of a diagonal brace, with the steel tube starting from the corner node at the lower part, and the connector starting from the upper part, welded to the plate attached at the center of the beam. No other connection but the cement grout is applied between the steel tube and the connector. Such a structural element could be able to transfer normal force by means of shear in the confined interfaces. Furthermore due to its composite section it is likely to present sufficient resistance to buckling. Of course, basic economic and pre-dimensioning calculations are needed in order to justify such a research.

ANNEX I : Cement grout VSL-HPI

Procès-verbal

FO 3.5.120
26.11.2009

Rapport d'injection

Chantier : EPFL Dimitri Papastergiou
Lieu : Station 18
Etape : Poutre béton/métallique

Chantier N° 332 / 0030
Date d'injection : 25.11.2010
Feuille 1 de 2

Nombre de câbles injectés : 1 pc
Quantité de ciment injecté : 150 kg

Ciment marque : VSL-HPI®
Additif : (Premix)
Température °C (5°≤ cond. ≤35°)

Heure	Air	Câble	Ciment	Eau	Coulis
10:50	19.1	14.5	11.2	12.2	19.9

Charge N° / date de production : 10.05.2010
Norme : SN EN 445-446-447

Malaxage de base		Malaxage exécuté	
Ciment :	150 kg	150 kg	
Eau :	49.5 l	49.5 l	
Facteur E/C :	0.33	0.33	cond. ≤ 0.40

Malaxeur type VSL / N° 79'015 Caisse d'injection N° 1 Durée de malaxage : min. 3 minutes

Granulométrie / Fluidité

Fréquence d'essais [X] 1 x par 1/2 jour [ ] 3 x par jour, resp. chaque 4 heures

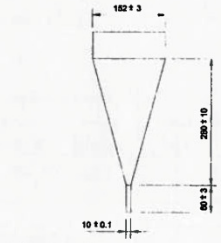

Test N°	Câbles Pos	Heure	Fluidité cond. ≤ 25"	Résidus sur tamis Oui / Non	Résidus sur tamis n ø mm
1	1	11:00	16.24	NON	0
2					
3					
4					
5					
6					
7					
8					

Essai à la mèche

Fréquence d'essais [ ] 1 x par 1/2 jour [X] 1 x par 1/2 jour - min. 3 tubes

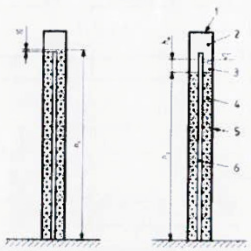

Légende
1 Etanchéité
2 Air
3 Eau
4 Coulis
5 Tube transparent
6 Toron, fils ou barre
h_0 Hauteur à t_0
h_n Hauteur à t_n

Tube N° 1 Heure	Mesures à	Hauteur Coulis mm	Hauteur eau mm	Variation de volume %	Ressuage eau %
11:00	t +0	100		cond. ≤ -1/+5	cond. ≤ 0.3
11:15	t +15	99	99	0.1	0
11:30	t +30	98	98	0.2	0
11:45	t +45	95	95	0.5	0
12:00	t +60	90	90	1	0
13:00	t +2.0 h	75	75	2.5	0
14:00	t +3.0 h	73	73	2.7	0
	t+24.0h				

VSL (Suisse) SA - rte Industrielle 2 - 1806 St-Légier - Téléphone 058 456 30 00 - Téléfax 058 456 30 95

Procès-verbal

FO 3.5.120
26.11.2009

Rapport d'injection

Chantier : EPFL Dimitri Papastergiou
Lieu : Station 18
Etape : Poutre béton/métallique

Chantier N° 332 / 0030
Date d'injection : 25.11.2010
Feuille 2 de 2

Essai à la mèche

Tube N° 2 Heure	Mesures à	Hauteur Coulis mm	Hauteur eau mm	Variation de volume %	Ressuage eau %
11:00	t +0	101		cond. ≤ -1/+5	cond. ≤ 0.3
11:15	t +15	100	100	0.1	0
11:30	t +30	98	98	0.3	0
11:45	t +45	96	96	0.5	0
12:00	t +60	90	90	1.1	0
13:00	t +2.0 h	74	74	2.7	0
14:00	t +3.0 h	73	73	2.8	0
	t+24.0h				

Tube N° 3 Heure	Mesures à	Hauteur Coulis mm	Hauteur eau mm	Variation de volume %	Ressuage eau %
11:00	t +0	100		cond. ≤ -1/+5	cond. ≤ 0.3
11:15	t +15	99	99	0.1	0
11:30	t +30	97	97	0.3	0
11:45	t +45	96	96	0.4	0
12:00	t +60	89	89	1.1	0
13:00	t +2.0 h	74	74	2.6	0
14:00	t +3.0 h	73	73	2.7	0
	t+24.0h				

Masse volumique à l'état frais

Fréquence d'essais [X] 1 x par projet [ ] 1 x par 1/2 jour, minimum 2x

balance de boue

	Heure	Câble Pos	Masse volumique entrée kg/dm3	Masse volumique sortie kg/dm3	Variation %	
1	1105	1	2.06	2.06	0.0	cond. ≤ 3
2						

Résistance à la compression

essai par

Fréquence d'essais [X] 3x 1 prisme 40x40x160 mm
[ ] Essai nécessaire

Eprouvette N°	Date d'essai	Age jours	Longueur mm	Largeur mm	Hauteur mm		Poids g	Masse volumique kg/dm3	Valeurs Moyennes kg/dm3	Charge de rupture kN	Résistance à la compression N/mm2	Valeurs moyennes N/mm2
1												cond. ≥ 30 (28j)
2												
3												
4												cond. ≥ 30 (28j)
5												
6												
7												cond. ≥ 30 (28j)
8												
9												

Remarque :

Spécialiste VSL :	S.Thomet	Exécuté le :	25.11.2010	Visa :
CDT VSL:	S.Thomet	Contrôlé le :	25.11.2010	Visa :

VSL (Suisse) SA - rte Industrielle 2 - 1806 St-Légier - Téléphone 058 456 30 00 - Téléfax 058 456 30 95

VSL (Schweiz) AG
CH-4553 Subingen
Industriestrasse 14
T 058 456.30.30
F 058 456.30.15

EPFL
Bâtiment GC - Station 18
Att. M. Dimitri Papastergiou
1015 Lausanne

Subingen, le 21.12.2010

Rapport d'essai

Coulis pour la précontrainte

Essai de la compression selon normes : SN EN 445 resp. SN EN 196-1

Projet Nr : 332'0030
Ouvrage : EPFL
Etape / Type de câble : Poutre béton et métallique
Essai : Premier essai
Entreprise de précontrainte : VSL (Suisse) SA Responsable : Adrian Gnägi VSL

Compression à 28 jours

Date de l'injection :	25.11.2010				Echantillons produit par :	VSL			
Date de l'essai :	21.12.2010				Essai réalisé par :	ST			
Désignation du prisme :	Hauteur (mm)	Largeur (mm)	Longueur (mm)	Poids (gr.)	Densité du coulis (kg/m³)	Essai sur demi-prisme			
						Charge de rupture (KN)		compression (N/mm²)	
P1	40.0	40.0	160.0	526.0	2.055	124.27	116.98	77.67	73.11
P2	40.0	40.0	160.0	529.0	2.066	124.24	119.02	77.65	74.39
P3	40.0	40.0	160.0	527.0	2.059	119.53	120.92	74.71	75.58
Moyenne								75.52	
Valeur								**≥ 30**	

Remarques :

Responsable du laboratoire : S. Thomet

ANNEX II: Visual Basic code for the numerical model

The numerical model predicts the relationship of the longitudinal shear force per unit length versus slip in the connection. It provides also the characteristic resistance, v_{Rk}, of the connection. Finally the fatigue limit, v_{el}, can be deduced from the point where the secant stiffness of one of the interfaces starts to decrease. (It is the point where the longitudinal force-slip curve changes stiffness).To obtain the characteristic value of the fatigue limit, $v_{Rk,fat}$, one has to multiply the value of the fatigue limit, v_{el}, with the conversion factor $n_{v,el}$ which is equal to 0.74.

The Visual Basic Code given, is related for visualization with a excel sheet named “connection”. Names referring to spreadsheet cells concern this specific excel sheet. All remarks and explanations are given in sentences starting with an apostrophe “ ' ” and in gray color. They do not have any contribution to the numerical model process. For visualization one can create charts on the excel file choosing the columns of his interest.

Visual Basic Code for the numerical model:

```
Sub ModConnexion_PR()
' version of 21 Nov 2011
' index 0 = interface embossed steel-cement grout , index 1 = interface rough concrete-cement grout
' cleaning of necessary space

Worksheets("connection").Activate
Range("Q6:Y33500").Select

Selection.ClearContents

Worksheets("connection").Activate
Range("B6:L33500").Select

Selection.ClearContents

'Variables and constants:
's variable stands for slip
'sigma variable stands for normal stress, σ, in the interfaces
'sigma_ext variable stands for existing normal stresses, σ_ext,i, in the interfaces, e.g. (transversal
prestressing)
'k variable stands for the secant stiffness, k_i, corresponding to slip s
'kel stands for the stiffness, k_el, of the elastic part of the constitutive law for each interface
'kpl stands for the stiffness, k_pl, of the plastic part of the constitutive law for each interface
'ksec stands for the secant stiffness corresponding to slip, s_u , at failure point of the constitutive law for
'       each interface
'htot variable stands for the total interface height, i.e.2 times the height of each interface
'a variable stands for the ratio a=τ_el/τ_u,
'htotkeq variable stands for secant stiffness of the connection for slip s
't variable stands for shear stress, τ, at each interface
'y variable stands for the addition of the uplifts of the embossed steel-cement grout interface and the
'       rough concrete-cement grout interface (a total uplift y develops at each side of the connection)
```

```
'v variable stands for the longitudinal shear per unit length, v
'vu variable stands for the ultimate longitudinal shear per unit length, v_u
'vrk variable stands for the characteristic resistance of the connection to longitudinal shear per unit
'       length, v_Rk
'tu variable stands for the ultimate shear stress, τ_u, related to failure criteria of each interface
'tf variable stands for the frictional shear stress,  τ_fr, related to residual resistance of each interface
'sel variable stands for the slip, s_el, which defines the end of the elastic part of the constitutive law of
'       each interface
'su variable stands for the slip, s_u, which defines the end of the plastic part of the constitutive law of
'       each interface
'after s_u ,the softening part of the constitutive law takes place
'sa variable stands for the coefficient s_a found in the kinematic and the constitutive law of each interf.
'u variable stands for the uplift, u, at each of the interfaces
'p variable stands for the increment of slip
'j variable is an integer with values 0 and 1 corresponding to each of the two interfaces
'n variable is an integer defining the number of repetitions

Dim si(1) As Double
Dim k(1) As Double
Dim kel(1) As Double
Dim kpl(1) As Double
Dim ksec(1) As Double
Dim htot(1) As Double
Dim a(1) As Double
Dim t(1) As Double
Dim tu(1) As Double
Dim tf(1) As Double
Dim sel(1) As Double
Dim su(1) As Double
Dim sa(1) As Double
Dim u(1, 100006) As Double
Dim j, n As Integer

' initialisation of variables
s = 0
n = 5
p = Application.InputBox("slip increment p =", , 0.005, , , , , 1)

For j = 0 To 1
   si(j) = 0
   t(j) = 0
Next

htotkeq = 0
y = 0
vu= 0
vrk = 0
sigma = 0
```

```
a(0) = 0.75
a(1) = 0.8
kel(0) = 29.4
kel(1) = 29.7
kpl(0) = 5.5
kpl(1) = 10.19
ksec(0) = 1 / (a(0) / kel(0) + (1 - a(0)) / kpl(0))
ksec(1) = 1 / (a(1) / kel(1) + (1 - a(1)) / kpl(1))
sa(0) = 2.07
sa(1) = 2.75
sel(0) = a(0) * 1.281 / kel(0)
sel(1) = a(1) * 1.837 / kel(1)
su(0) = 1.281 / ksec(0)
su(1) = 1.837 / ksec(1)

fc = Application.InputBox("compression resistance of grout fc [N/mm2] =", , 90, , , , , 1)
Ecm = Application.InputBox("modulus concrete Ecm [N/mm3] =", , 38600, , , , , 1)
h = Application.InputBox("slab height [mm] =", , 500, , , , , 1)
ha = Application.InputBox(" height of inner rib, hrib [mm] =", , 125, , , , , 1)
hb = Application.InputBox(" distance of middle bar from the lower edge of the inner rib, hmid
[mm]=", , 40, , , , , 1)
c = Application.InputBox("covering of upper reinforcement) c [mm]=", , 45, , , , , 1)
ast = Application.InputBox("area As [mm2] =", , 201, , , , , 1)
sbar = Application.InputBox("spacing of rebars [mm] =", , 100, , , , , 1)
fck = Application.InputBox("concrete characteristic strength, fck [N/mm2] =", , 50, , , , , 1)
nf = Application.InputBox("conversion factor for the ultimate resistance  nf =", , 0.89, , , , , 1)

'hrib stands for height of the connector which is also equal to the height of the inner rib of the slab
'hmid stands for distance of the center of the gravity of the middle reinforcement from the edge of the
'        inner rib of the slab
'nf stands for the conversion factor for the ultimate resistance, v_u,  so to obtain the v_Rk

ya = 0.043 * (33000 / Ecm) ^ 0.8 * (fck / 35) ^ 0.2
yb = (30000 / Ecm) ^ 0.1 * (ast / sbar / ha) ^ 0.3 * (ha / (h - ha - hb)) ^ 0.5 * 2.1 * (35 / fck) ^ 0.2 * (hb
/ 10) ^ 0.2
ka = (Ecm / 30000) ^ 0.7 * ((h - ha - hb) / ha) ^ 0.9 * (ast / sbar / ha) ^ 0.2 * 60 * (fck / 35) ^ 0.2
kb = (Ecm / 30000) ^ 0.2 * (ast / sbar / ha) * 1000 * (h - ha - hb) / h * (c / 6 / hb) ^ 0.2 * (35 / fck) ^
0.1

'ya, yb, ka , kb are the coefficients defining the relationship between normal stress and total uplift in
each side of the connection

For j = 0 To 1
   k(j) = kel(j)
Next

htot(0) = 2 * ha
htot(1) = htot(0)
```

```
sigma_ext = Application.InputBox("sigma ext =", , 0#, , , , , 1)

Worksheets("connection").Activate

While n < 100006
   s = s + p
   n = n + 1

   si(0) = s * k(1) / (k(0) + k(1))
   si(1) = s * k(0) / (k(0) + k(1))

      If si(0) < su(0) Then
         u(0, n) = 0.09 * (si(0) / su(0)) ^ 2
      Else
         u(0, n) = 0.09 + ((1.69 - 16.9 * sigma / fc) - 0.09) * (1 - Exp(-(si(0) - su(0)) / sa(0)))
      End If

   If u(0, n) < u(0, n - 1) Then
    u(0, n) = u(0, n - 1)
   End If

      If si(1) < su(1) Then
         u(1, n) = 0.16 * (si(1) / su(1)) ^ 2
      Else
         u(1, n) = 0.16 + ((2.18 - 29.2 * sigma / fc) - 0.16) * (1 - Exp(-(si(1) - su(1)) / sa(1)))
      End If

   If u(1, n) < u(1, n - 1) Then
   u(1, n) = u(1, n - 1)
   End If

   y = u(0, n) + u(1, n)

   If y < 2 Then
      If y > ya Then
         If y < yb Then
         sigma = sigma_ext + ka * ya + kb * (y - ya)
         Else
         sigma = sigma_ext + ka * ya + kb * (yb - ya) + 0.5 * (y - yb)
         End If
         Else
         sigma = sigma_ext + ka * y
      End If
      Else
      sigma = sigma_ext + ka * ya + kb * (yb - ya) + 0.5 * (2 - yb)
   End If
```

```
    tu(0) = 1.405 * sigma + 1.281
    tu(1) = 1.445 * sigma + 1.837
    tf(0) = 0.71 * sigma
    tf(1) = 0.845 * sigma

'Application of an upper limit of the shear stress for the 1st interface according to Eurocode 2
  If tu(0) > 0.5 * 0.6 * (1 - fc / 250) * fc / 1.5 Then
    tu(0) = 0.5 * 0.6 * (1 - fc / 250) * fc / 1.5
    tf(0) = 0.71 * (tu(0) - 1.281) / 1.405
    Else
    tu(0) = tu(0)
    tf(0) = tf(0)

'Application of an upper limit of the shear stress for the 2nd interface according to Eurocode 2
  If tu(1) > 0.5 * 0.6 * (1 - fc / 250) * fc / 1.5 Then
    tu(1) = 0.5 * 0.6 * (1 - fc / 250) * fc / 1.5
    tf(1) = 0.845 * (tu(1) - 1.837) / 1.445
    Else
    tu(1) = tu(1)
    tf(1) = tf(1)

  sel(0) = a(0) * tu(0) / kel(0)
  su(0) = tu(0) / ksec(0)
  sel(1) = a(1) * tu(1) / kel(1)
  su(1) = tu(1) / ksec(1)

  If si(0) > sel(0) Then
    If si(0) < su(0) Then
      k(0) = (kel(0) * sel(0) + kpl(0) * (si(0) - sel(0))) / si(0)
    Else
      k(0) = (tf(0) + (tu(0) - tf(0)) * Exp(-(si(0) - su(0)) / sa(0))) / si(0)
    End If
  Else
    k(0) = kel(0)
  End If

  If si(1) > sel(1) Then
    If si(1) < su(1) Then
      k(1) = (kel(1) * sel(1) + kpl(1) * (si(1) - sel(1))) / si(1)
    Else
      k(1) = (tf(1) + (tu(1) - tf(1)) * Exp(-(si(1) - su(1)) / sa(1))) / si(1)
    End If
  Else
    k(1) = kel(1)
  End If

  htotkeq = (htot(0) * htot(1) * k(0) * k(1)) / (htot(0) * k(0) + htot(1) * k(1))
```

```
    v = htotkeq * s

    ' printing of variables

    Worksheets("connection").Activate
    Cells(n, 2).Value = s
    Cells(n, 3).Value = v
    Cells(n, 4).Value = k(0)
    Cells(n, 6).Value = k(1)
    Cells(n, 7).Value = sel(0)
    Cells(n, 8).Value = si(0)
    Cells(n, 9).Value = su(0)
    Cells(n, 10).Value = sel(1)
    Cells(n, 11).Value = si(1)
    Cells(n, 12).Value = su(1)
    Cells(n, 17).Value = tu(0)
    Cells(n, 19).Value = tu(1)
    Cells(n, 20).Value = sigma
    Cells(n, 21).Value = y
    Cells(6, 22).Value = ya
    Cells(6, 23).Value = yb
    Cells(6, 24).Value = ka
    Cells(6, 25).Value = kb

    If v > vu Then
       vu = v
       vrk = vu * nf
     Cells(2, 7).Value = vrk

    End If

    If v < vu / 4 Then
       n = 100006
    End If

Wend
End Sub

'The cell (2,7) provides the characteristic resistance of the connection to longitudinal shear per unit
'       length, v_Rk
```

References

[ACI 318-83 1983] ACI Committee 318, *Building Code Requirements for Structural Concrete and Commentary*, American Concrete Institute, Farmington Hills, 369 pp.,1995.

[Anders 2007] Anders, S., *Betontechnologische Einflüsse auf das Tragverhalten von Grouted Joints.* Dissertation Leibniz Universität Hannover, Hannover, 2007.

[API 2000] American Petroleum Institute (Hrsg.): *Recommended Practice for Planning, Designing and Constructing Fixed Offshore Platforms*, Working Stress Design, 21st edition, Washington, 2000.

[Badoux 1985] Badoux, J. C., *L'évolution des ponts mixtes en suisse ces vingt-cinq dernières années*, Journal de la Construction de la Suisse romande, vol. 59, num. 10, p. 44-50, 1985.

[Bärtschi 2005] Bärtschi, R., *Load-bearing behaviour of composite beams in low degrees of shear connection*, Dissertation ETH No 15895, Eidgenössische technische Hochschule Zürich, 2005.

[Birkeland 1966] Birkeland, P.W., and Birkeland, H.W., *Connections in precast concrete construction*, ACI Journal, ProceedingsV. 63,No. 3, pp. 345-368, 1966.

[Bouazaoui 2006] Bouazaoui, L., Perrenot, G., Delmas ,Y., Li, A., *Experimental study of bonded steel concrete composite structures*, Journal of Constructional Steel Research, Vol. 63, pp. 1268-1278, 2007.

[Bouazaoui 2008] Bouazaoui L., Jurkiewiez, Delmas Y., Li A., *Static behaviour of a full-scale steel–concrete beam with epoxy-bonding connection*, Journal Engineering Structures, Vol. 30, pp. 1981–1990, 2008.

[Brozzetti 2000] Brozzetti, J., *Design development of steel-concrete composite bridges in France*, Journal of Constructional Steel Research, Vol. 55, No 1-3, pp. 229–243, Elsevier Science Ltd. Oxford, 2000.

[Brühwiler and Lebet 2010] Brühwiler, E, Lebet, J-P., *Updating of traffic loads on existing bridges*, 2010 Joint IABSE-fib Conference, 2010.

[BS 1134/1972] BS 1134:Part 1:1972, *Method for the assessment of surface texture. Method and instrumentation*, 1972.

[C5/05 SZS 2005] Centre Suisse de la Construction Métallique. *C5/05 steelwork. Tables de construction*. Zürich, 2005.

[Climaco and Regan 2001] Climaco, J.C.T.S. and Regan, P.E. *Evaluation of bond strength between old and new concrete in structural repairs*, Magaszine of Concrete Research, pp. 377-390, 2001.

[Collin et al. 2002] Collin, P., Stoltz, A., Möller, M., *Innovative Prefabricated Composite Bridges* Proceedings, IABSE SYMPOSIUM, Melbourne, 2002.

[COMBRI 2008] COMBRI, *Guide de conception. Partie II : Pratique actuelle et conceptions nouvelles des ponts métalliques et mixtes*, Stuttgart, 2008.

[Dauner 2002] Dauner, H.-G., Antille, S., *Ponts mixtes à construction rapide*, rapport OFROU 567,Office fédéral des routes, Berne, 2002.

[Dauner 2006] Dauner, H.-G., *Klebetechnik für den schnellen und wirtschaftlichen Bau von Verbundbrücken*, Stahlbau 75 (2006) pp. 552-557, 2006.

[Ducret 1997] Ducret, J.-M., *Etude du comportement réel des ponts mixtes et modélisation pour le dimensionnement*, Thèse EPFL No 1738, Ecole polytechnique fédérale de Lausanne, 1997.

[EC2 2004] EN 1992-1-1:2004 (E), Eurocode 2 : Comité européen de normalisation, Eurocode 2: *Design of concrete structures - Part 1-1: General rules and rules for buildings*, Bruxelles, 2004.

[EC4 2005] EN 1994-1-1:2004, Eurocode 4: *Design of composite steel and concrete structures –Part 1: General rules and rules for buildings*, Comité européen de normalisation, Bruxelles, 2005.

[EC4-part 2 2004] prEN 1994-2:2005, Final Draft, Eurocode4: *Design of composite steel and concrete structures - Part2: General rules and rules for bridges*, Comité européen de normalisation , Bruxelles, 2004.

[EN 10025-2] EN 10025-2:2003, *Produits laminés à chaud en acier de construction-Partie 2 : Conditions techniques de livraison pour les aciers de construction non alliés*, Comité européen de normalisation, 2003.

[EN 1990:2002] EN 1990:2002 (E), *Eurocode - Basis of structural design*, Comité européen de normalisation, Bruxelles, 2003.

[Feldmann et al. 2008] Markus, F., Oliver, H., Josef, H., and Sabine, R., *Fatigue Behavior of Shear Connectors in High Performance Concrete*, Proceedings of the 2008 Composite Construction in Steel and Concrete Conference VI, 2008.

[fib Model Code 2010] Fédération internationale du Béton (fib). *Model Code 2010. First Complete Draft*. Lausanne, 2010.

[Garbacz et al. 2005] Garbacza, A., Courard, L., Katarzyna, K. , *Characterization of concrete surface roughness and its relation to adhesion in repair systems*, Journal of Materials Characterization, Vol. 56, pp. 281-289, 2005.

[Ghoneim et al. 2010] Ghoneim, G., Perry, V.H., Carson, G., *Ultra high performance fibre reinforced concrete in footbridges*, Proceedings of the 8th International Conference on Short and Medium Span Bridges, Niagara Falls, 2010.

[Gomez 2000] Gomez, Navarro, M., *Concrete cracking in the deck slabs of steel-concrete composite bridges*, Thèse EPFL No 2268, Ecole polytechnique fédérale de Lausanne, 2000.

[Gonzalez e al. 2011] Gonzalez, A., Cantero, D., Obrien, E.J., *Dynamic increment for shear force due to heavy vehicles crossing a highway bridge*, Computers and StructuresVol. 89, pp. 2261-2272, 2011.

[Günter 2009] Günter, S., Braun, A.,*VFT-WIB-Brücke bei Vigaun- Verbundbrücke mit externer Bewehrung*, Stahlbau, Vo. 78, 2009.

[Habel 2004] Habel, K., *Structural Behaviour of Elements Combining Ultra-High Performance Fibre Reinforced Concretes (UHPFRC) and Reinforced Concrete*, Thèse EPFL No 3036, Ecole polytechnique fédérale de Lausanne, 2004.

[HBM 2000] HBM Mess- und Systemtechnik GmbH, *W1E, W5K. Inductive displacement transducers*, Technical Brochure, Darmstadt, 2000.

[Health & Security Executives: Pile/Sleeve Connections 2002] Health & Security Executives, *Pile/sleeve connections*. Offshore Technology report. Norwich. 2002

[Hieber et al. 2005] Hieber, D.G., Wacker, J.M., Eberhard, M.O., Stanto, J.F., *State-of-the-Art Report on Precast Concrete Systems or Rapid Construction of Bridges*, Final Technical Report,Seattle, 2005.

[Jaunin 1996] Jaunin, A., Lebet, J.-P., Boulanger, S., B*ase de donnée des ponts mixtes, document interne*, Laboratoire de la construction métallique (ICOM), Ecole polytechnique fédérale de Lausanne,1996.

[Jurkiewiez 2009] Jurkiewiez, B., *Study and cyclic behaviour of a steel-concrete composite beam with horizontal shear connections*, Journal of Constructional Steel Research, Vol. 65, pp. 2207-2216, 2009.

[Kitoh 1996] Kitoh, H., Sonoda, K., B*ond characteristics of embossed steel elements*, Composite Construction in Steel and Concrete III, Proceedings of an Engineering Foundation Conference, pp. 909-918, American Society of Civil Engineers, New York, 1996.

[Lamport 1988] Lamport, W. B., *Ultimate strength of grouted pile-to-sleeve connections*, Dissertation. University of Austin, Texas, 1988.

[Lebet and Hirt 2009] Lebet, J-P., Hirt, M., *Ponts en acier*, Traité de génie civil, Vol. 12, Lausanne, 2009.

[Lee et al. 2011] Lee, Y.-H., Joo, Y.T., Lee T., Ha. D.-H., *Mechanical properties of constitutive parameters in steel-concrete interface*. Engineering Structures, Article in press, 2011.

[Loov 1994] Loov, R.E., Patnaik, A.K., *Horizontal shear strength of composite concrete beams with a rough interface*, PCI Journal, Vol. 39, No 1, pp. 48-67, Precast/Prestressed Concrete Institute, Chicago, 1994.

[Lorenc et al. 2008] Lorenc, W., Ignatowicz, R., Kubica, E., Seidl, G., *Numerical model of shear connection by concrete dowels. Recent Developments in Structural Engineering Mechanics and Computation*, Millpress, Rotterdam, 2008.

[Menétrey and Brühwiler 2008] Menétrey, P., Brühwiler, E., *Design and experimental investigation of the joints of inclined struts for the widening of bridge deck slabs*, Structural Engineering International, Vol. 18, 2008.

[Meystre and Lebet 2011] Meystre, T., Lebet, J-P., *Modèle de charge de trafic actualisé pour les dalles de roulement en béton*, OFROU-AGB 2009/005. Provisoire du 10.10.2011.

[Naumann 2006] Naumann, J., *Aktuelle Entwicklungen im Straßenbrückenbau*, Stahlbau, Vol. 75, 2006.

[Oden and Martins 1985] Oden., J.T., Martins, J.A.C., *Models and computational methods for dynamic friction phenomena*, Computer methods in applied mechanics and engineering, Vol. 52, pp. 527-634, 1985.

[Oh and Kim 2007] Oh, B.H., Kim, S.H., *Realistic Models for Local Bond Stress-Slip of Reinforced Concrete under Repeated Loading*, Journal of Structural Engineering, Vol. 133, 2007.

[Orange 1999] Orange, G., Dugat, J., Acker, P., *A new generation of UHP concrete: Ductal. Damage resistance and micromechanical analysis*, Proceedings of the 3rd International RILEM workshop, HPFRCC3, Mainz, 1999.

[Papanicolaou et al. 2002] Papanicolaou, C.G., Triantafillou., T.C., *Shear transfer capacity along pumice aggregate concrete and high-performance concrete interfaces*, Materials and Structures, Vol. 35, pp. 237-245, 2002.

[Project MIKTI 2008] National Project MIKTI, *Steel-concrete bridges. A guide for novel structures*. 2008.

[Rauscher and Hegger 2008] Rauscher, S., Hegger, J., *Modern composite structures made of high performance materials*, International Conference on Composite Construction in Steel and Concrete, 2008.

[Schmitt et al. 2004] Schmitt, V., Günter S., Hever, M., Zapfe, C., *Verbundbrücke Pöcking – Innovative VFT-Träger mit Betondübeln*, Stahlbau, Vol. 73, 2004.

[SIA-162/6 1999] Norme SIA162 :1999, *Béton renforcé des fibres métalliques*, *Société suisse des ingénieurs et des architectes*, Zurich, 1999.

[SIA-260 2003] Norme SIA260:2003, *Bases pour l'élaboration des projets de structures porteuses*, Société suisse des ingénieurs et des architectes, Zurich, 2003.

[SIA-261 2003] Norme SIA261:2003, *Actions sur les structures porteuses*, Société suisse des ingénieurs et des architectes, Zurich, 2003.

[SIA-262 2003] Norme SIA262:2003, *Construction en béton*, Société suisse des ingénieurs et des architectes, Zurich, 2003.

[SIA-264 2003] Norme SIA264:2003, *Construction mixte acier-béton*, Société suisse des ingénieurs et des architectes, Zurich, 2003.

[Simulia 2011] Dassault Systèmes Simulia. *Abaqus 6.11-2 Theory Manual*, Providence, 2011.

[Sorelli et al. 2006] Sorelli, L.,G., Fanning, P., Toutlemonde, F., *Innovative bridge system of ultra high performance fibre reinforced concrete: experiments, modeling and design*. Proceedings, 7th International Conference on Short and Medium Span Bridges, Montreal, 2006.

[Tassios et al. 1987] Tassios, T.P., Vintzeleou, E.N., *Concrete-to-concrete friction*, Journal of Structural Engineering, Vol. 113, No 4, pp. 832-849, American Society of Civil Engineers, New York, 1987.

[Tateishi et al. 2003] Tateishi, K., Hanji, T., Shibata, K., *3-D shape measurement of corroded steel plate surface by digital stereography*, Proceedings of the 1st International Conference on Structural Health Monitoring of Intelligent Infrastructure (SHMII), pp. 699-704, Tokyo, 2003.

[Thomann 2005] Thomann, M., *Connexions par adhérence pour les ponts mixtes acier-béton*, Thèse EPFL No 3381, Ecole polytechnique fédérale de Lausanne, 2005.

[VSL 2002] VSL, *Grouting of post-tensioning tendons*, VSL Series No.5, Subingen, 2002.

[Walraven 1987] Walraven, J., Frénay, J., Pruijssers, A., *Influence of concrete strength and load history on the shear friction capacity of concrete members*, PCI Journal, Vol. 32, No 1, pp. 66-84,Precast/Prestressed Concrete Institute, Chicago, 1987.

[Wuest 2006] Wuest, J., *Comportement structural des bétons de fibres ultra performants en traction dans des éléments composés*, Thèse EPFL No 3987, Ecole polytechnique fédérale de Lausanne, 2006.

Dimitrios Papastergiou

Dipl.-Ing. NTU Athens
Nationality : Hellenic
Date of birth : 04 May 1974
Civil state: Married

CURRICULUM VITAE

Education

- 2008-present. PhD candidate in civil engineering, EPFL. Subject of the thesis: “Connections by adhesion, interlocking and friction for steel-concrete composite bridges under static and cyclic loading.”
- 2001-2002. Post-graduate diploma in structural design and analysis of structures, NTU Athens. Subject of the final project: “Assessing the ductility of eccentric braced frames using the push-over method.”
- 1993-1999. Master in civil engineering, NTU Athens. Subject of Master Thesis: “Etude du comportement mécanique d’une interface sol-structure sous sollicitations cycliques”. Executed, for the experimental part, in the geotechnical laboratory CERMES of the University ENPC-Paris and for the theoretical part in NTU Athens.

Professional experience

- 2008-present. Doctoral assistant in the Steel Structures Laboratory (ICOM), EPF Lausanne.
- 2007-2008 Civil Engineer. General Secretariat for Research & Technology-Greece
- 2002-2007 Civil Engineer. Structural studies and surveillance of construction of reinforced concrete earthquake resistance buildings and simple steel structures.
- 1999-2001. Military service. Second-lieutenant. Lieutenant.

Languages

- English (Level C2_Certificate of Proficiency in English)
- French (Level C1_Certificat pratique 1er Degré de l’université de Paris-Sorbonne)
- Greek (Mother language)
- German (Level A2)

Membership

- International Association for Bridge and Structural Engineering (Schweiz)
- Schweizer Gesellschaft für Erdbebeningenieurwesen und Baudynamik, SGEB
- Association of Civil Engineers of Greece
- Technical Chamber of Greece

Publications

- D. Papastergiou and J.-P. Lebet. *New steel-concrete connection for prefabricated composite bridges*, Stahlbau, vol. 80, num. 12, p. 894-903, 2011.
- D.T. Papastergiou and J.-P. Lebet. *New steel-concrete connection for composite bridges.* 8th International conference on Short and Medium Span Bridges, Niagara Falls, Canada, August 3-6, 2010.